THE UNIVERSITY OF SHEFFIELD

DEPARTMENT OF CIVIL AND STRUCTURAL ENGINEERING

PROJECTILE PENETRATION INTO FIBRE REINFORCED CONCRETE

by

Paul John Armstrong BEng (Sheffield)

A thesis presented to the University of Sheffield
for the degree of Doctor of Philosophy

July 1987

SUMMARY

A wide range of fibre reinforced concretes, potentially capable of sprayed application, and which could be used for protecting buildings, has been tested. Specimens 450mm square have been impacted by 7.62mm A.P. projectiles, and the damage assessed in terms of penetration path lengths within the specimens and the volume of the impact face spall crater. It has been found that inclusion of fibres does not increase the penetration resistance, but a small proportion of fibres significantly reduces the impact face spalling. The mechanisms of penetration and spalling have been examined using high speed photographic techniques and instrumented specimens.

ACKNOWLEDGEMENTS

This work was carried out in the Department of Civil and Structural Engineering of the University of Sheffield. The author is indebted to Professor T H Hanna both for the opportunity to carry out the research, and for the departmental facilities used in the production of this thesis.

The author is grateful to the Royal Armament and Development Establishment (Christchurch) for the award of the research contract upon which this study is based. The advice and information provided throughout the research period by the late Mr G M McNeil and Major W Port was much appreciated.

The supervision and ceaseless enthusiasm of both Dr W F Anderson and Dr A J Watson are acknowledged with great thanks, as is the substantial technical contribution of Mr A Hindle, both during and following the research period.

The typing ability and patience of Mrs J Cheetham, the draughtsmanship of Mr D A Maltby and the printing skills of Mr C J Clarke are all recognised with gratitude.

Several of the approaches documented in this thesis were enhanced by discussions with my colleagues, including; Dr B Archer, Dr P N Oldroyd, Dr A J Sanderson and Dr R G Brade. I am particularly beholden to the latter for his recent tolerance and understanding.

It is not possible to mention all of the people who have contributed to this work; my thanks and apologies are proffered to all of those not cited by name.

Finally, I wish to record my gratitude to Sue for her invaluable faith, assistance and encouragement throughout the writing of this thesis.

CONTENTS

LISTS OF TABLES

LIST OF FIGURES

LIST OF SYMBOLS

A	Projectile cross-sectional area.
$A(i),(ii),(iii)$	Independent quantitative primary variables.
A_c	Cross-sectional area of composite.
A_n	Functions of projectile and soil properties.
AP	Armour-piercing.
a	Constant.
B_1, B_2, B_3	Constants.
$B(i), B(ii)$	Independent qualitative primary variables.
b	Constant.
b_{jk}	Coefficients calculated from experimental test results.
C	Maximum coarse aggregate size.
C_D	Drag coefficient.
C_M	Material comminution.
CRH	Calibre radius head.
D	Normal penetration depth.
D_B	Burrow diameter.
D_C	Maximum crater diameter.
D_F	Final penetration depth.
D_H	Projectile calibre.
D_r	Relative density of dry sand.
d	Projectile diameter, fibre diameter.
E	Young's modulus of elasticity.
E_o	Initial kinetic energy at impact.
E_t	Strain-hardening modulus.

e	Concrete target thickness.
e_I	Elastic region volumetric strain (zero to finite stress)
e_P	Volumetric strain related to the jump from the elastic to the plastic region of the uniaxial stress-strain curve.
F	Uniaxial tensile load.
f	Fibre.
f'_c	Ultimate concrete compressive strength.
f_n	Function ( )
$f(\varepsilon)$	Multiplier function applied to p_I to allow for Projectile ogivity.
K	Number of primary independent qualitative variables.
k	Concrete penetrability factor = $15/f'_c$.
k_1, k_2, k_3	Constants.
L	Penetration path length.
L_I	Measured actual penetration path length.
L_P	Predicted penetration path length.
l	Fibre length.
m	Mass, matrix.
N	Nose performance coefficient.
N_1, N_2	Dimensionless shape factors.
N_3	Dimensionless shape factor, $0.72 < N_3 < 1.14$.
NL	Nose length.
n	$10.7(f'_c)^{\frac{1}{4}}$
p_I	Intertial pressure component.
p_s	Static pressure component.
$p(t)$	Compressive stress variation at the cavity surface at time t.
RQD	Rock Quality Designation.

R_s	Solid Reynolds Number.
r	Radius of spherical cavity at time t.
$\dot{r}$	Velocity of spherical cavity at time t.
$\ddot{r}$	Acceleration of spherical cavity at time t.
S	Soil properties constant.
T	Time for projectile to come to rest.
t	Time.
t_o	Time at initial impact.
U	Unconfined compressive strength for clay.
V	Volume.
V_A	Apparent Crater Volume.
V_B	Burrow Volume.
V_c	Total Composite Volume.
V_f	Volume fraction of fibre in composite.
$V_{f(crit)}$	Critical fibre volume fraction.
V_T	True Crater Volume.
v	Velocity at time t.
$\dot{v}$	Acceleration at time t.
v_o	Initial impact velocity.
W	Weight of projectile.
W_f	"Theoretical" Fibre Weight.
W'_f	"Practical" fibre weight (% weight by concrete weight).
x	Displacement in the direction of penetration at time t.
$\dot{x}$	v
$\ddot{x}$	$\dot{v}$
x_1, x_2, x_3	Coded values for A(i),A(ii),A(iii), Quadratic Response Surface Analysis.

Y	Target Yield Strength.
α	Positive constant.
β	Positive constant.
γ	Positive constant.
η	Fibre efficiency factor.
ρ	Density.
ρ_o	Initial target density.
ρ_p	Projectile density.
ρ_{LS}	Locking density of target material in snow region.
ν	Kinematic viscosity.
ε	Strain.
σ	Flow stress of target medium, standard deviation.
$\sigma_c, \sigma_f, \sigma_m$	Stress in composite, fibre, matrix.

GLOSSARY OF TERMS

"Actual/True" Crater: Further dissection of the "apparent" crater to the level defined by an internal cone of cracking below the impact face of a target. See Figure 3.13.

Actual (Penetration) Path Length: Distance, measured in three-dimensions, travelled by a penetrator within a target. Value measured to the projectile tip.

"Apparent" Crater: Depression formed in the front face of the specimen, caused by comminution and material displacement during the impact and penetration of a projectile.

Burrow: A narrow, elongated crater, normally of similar dimension to the projectile cross-section.

Penetrator: An object likely to penetrate a target as a consequence of its kinetic energy.

Penetration: Motion of a penetrator within a target.

Perforation: Penetration through to, and out of, the rear free surface of a target.

Projectile: Penetrator designed for efficient penetration.

Normal (Penetration) Path Length: Orthogonal distance from the target impact face to the projectile tip.

Scabbing: Tensile failure of the rear free surface of a target as a consequence of the impact stress wave and target characteristics. A shallow cone-shaped "scab" of target material may be released from the main body of the specimen.

CHAPTER 1

INTRODUCTION

A need to rapidly upgrade existing buildings likely to be subject to small arms fire, and also to quickly construct acceptably resistant new structures, had provoked some limited assessment in the late 1970s of the potential of sprayed concretes as projectile-resisting materials. At the same time, the use of discrete fibres of various types and materials was being promoted as a means of enhancing the toughness and tensile characteristics of plain concretes. It was suggested that a material combining both of these qualities, that is a fibre-reinforced concrete capable of sprayed application, had the potential to fulfil all of the envisaged requirements.

This thesis describes work carried out to optimise various plain concretes, of mix proportions suitable for sprayed application and reinforced with any one of several fibrous materials and fibre types. The aim was to reduce the effect of the impact and subsequent penetration of the materials when struck by a specific projectile.

Initially a detailed literature survey of penetration mechanics was performed, whilst the properties of both fibre reinforced and sprayed concretes were ascertained by reference to the published material. The obtained information was used to select the most promising overall approach for the study and further, the most appropriate composite constituents and proportions to use as a basis for actual trials. The literature survey, including a summary of subsequently published work, is included as Chapter 2.

A detailed review of the fibre market, considering both Europe and the USA, indicated that a large number of proprietary brands was available. Representative samples were chosen for preliminary trials, following which equipment for casting, curing and testing appropriately sized specimens was manufactured and assembled. As facilities were not available for the consistent production of specimens by the spraying process, standard procedures for the production and testing of poured targets, using sprayed concrete mix designs, were established. Specimen damage following impact was defined in terms of an "actual penetration path length" and a "true crater volume". Methods and equipment for measuring these were developed. Descriptions of both the experimental techniques and the tested materials are given in Chapter 3.

The experimental approaches used to pursue the optimum composite mix designs are described in Chapter 4. After some exploratory trials, a statistical method was adopted to simultaneously examine the influence of a number of variables, including fibre and aggregate types, concrete mix proportions and fibre content. An ambitious programme of testing at three days age was curtailed when very significant variability was observed. A second major test series, encompassing a smaller number of variables, was then carried out on seven day old concretes.

Examination of the impacted specimens indicated the existence of complex penetration and spalling (front cratering) mechanisms. Perusal of the available literature suggested that only very limited study of these mechanisms, for this specific target-penetrator combination, had been undertaken. Consequently, a study of the various aspects of the impact and penetration event was initiated. The work was concentrated on the development of several types of instrumented test, including both

high-speed and ultra-high-speed photography. These tests yielded some useful data, indicating the potential of the techniques for a future more rigorous study. The methods used and the results obtained are reported and discussed in Chapter 5.

Conclusions for all aspects of the study and recommendations for future work are listed in Chapter 6.

During the project a number of progress reports were produced and several facets of the work were published. Details are given in Appendix I.

CHAPTER 2

LITERATURE SURVEY

2.1 Penetration Mechanics and Analysis

The mechanisms of penetration of several materials, impacted by various projectiles, have been considered in this literature survey. Historically, several conceptually different approaches have been developed to predict the systems involved in projectile-target collisions. The following catalogues the various techniques before discussing the applicability of each to the specific projectile-target combination considered in this research.

It is generally accepted (Johnson,(1972)) that the first penetration equations were of the type;

$$-\frac{dv}{dt} = \alpha v^2 + \beta v + \gamma \qquad \text{...Eq.2.1}$$

where t = time

v = velocity at time t

α, β, γ = positive constants

Various specific forms of this equation were derived by Robins (c.1742), Euler (c.1750), Poncelot (c.1829/1835) and Resal (c.1895). Petry (1910) evaluated the constants in Poncelot's equation, publishing a penetration depth prediction equation. All equations of this type may be easily integrated, provided the boundary conditions are known. However the large amount of experimental scatter normally experienced in practical trials tends to indicate that such simple boundary assumptions are unrealistic.

Vanzant (1963) investigated the penetration of projectiles, of various weights and geometry, into cement and marble. Penetration as a function of impact velocity was expressed as;

$$D_F = k_1 v_o^a m^b \quad \text{...Eq.2.2}$$

where m = mass

a, b and k, are constants

Penetration was also related to initial kinetic energy at impact, E_o as;

$$D_F \alpha E_o^{2/3} \quad \text{...Eq.2.3}$$

Crater volume was considered in the same manner, the postulated relationships being;

$$V \alpha E_o^{4/3} \quad \text{...Eq.2.4}$$

For bullets of less than 25mm length, the power term of equation 2.3 was shown to reduce to ⅓, whilst that of equation 2.4 reduced to 5/4.

Young (1969) generated an empirical relationship from more than 160 full-scale penetration tests into earth, using penetrators of up to 2.6 tonnes. The developed formulae were presented as a penetration nomogram (Figure 2.1). Later work by Young (1972) lowered the minimum applicable value of projectile diameter from 75mm to 25mm and adapted the technique for use in layered homogeneous soils.

Austin and Pringle (1971) reviewed the available literature dealing with the effect of concrete constituent variation on projectile penetration. A penetration equation was presented;

$$D_F = 870/f'_c{}^{\frac{1}{2}} \; (W/D_H^2)(D_H/C)^{0.1}(v_o/1750)^n \quad \text{...Eq.2.5}$$

where f'_c = compressive concrete strength

W = projectile weight

D_H = projectile calibre

C = max.coarse aggregate size

$n = 10.7/(f'_c)^{1/4}$

The conclusions indicated that much of the preceding empirically-based military work was conflicting. It was suggested also that aggregate segregation and target stratification were to be avoided as they had a significant effect on penetration resistance.

Ross and Hanagud (1971) performed a theoretical analysis of the mechanics of penetration and perforation of a snow-covered Arctic Sea ice-sheet subjected to cylindrical, hemispherically-nosed projectile impact. Figure 2.2 illustrates the problem in a schematic sense, whilst Figures 2.3 and 2.4 show the assumed material properties during the two penetration phases. The basic premise was that the pressure on the spherical cavity boundary, at any time t, is equivalent to the resisting force acting over the surface of the projectile (i.e. by Newton, Force = pressure x projectile cross-section area = $m\dot{v}$). Hence, by modelling the compressive normal stress variation with time t, and integrating the resulting equation of motion, the exit velocity of the projectile at the snow-ice boundary may be calculated. This velocity is then used to repeat the procedure in the sea ice penetration phase, to yield a total penetration depth through the layered material.

Young (1972) revised his earlier empirical formulae. Utilising new test data the range of applicability of the equations was extended to 790m/s, with penetrators as small as 0.9kg being permitted. An accuracy of $\pm$ 20% was claimed for both depth and deceleration predictions, although correlation of results between natural and man-made targets was not attempted.

Murff and Coyle (1973) suggested an empirical function of the form;

$$m \frac{d^2x}{dt^2} = A_1 + A_2 + A_3 \frac{dx}{dt} + A_4 x^2 + A_5 \, x \, \frac{dx}{dt} \qquad \ldots \text{Eq.2.6}$$

where A_n are functions of projectile and soil properties

By integration, penetration depth formulae were established using appropriate data for both sand and clay targets. Important projectile and soil properties were;

U = unconfined compressive strength for the clay data.

d = projectile diameter

NL = nose length

D_r = relative density of dry sand

The equations yielded excellent correlation with the experimental data, though extrapolation outside the data field was not successful.

Zaid et al.(1973) studied the perforation of mild steel plate by flat-ended hardened steel cylindrical projectiles of 19mm to 75mm length. For 25mm mild steel plates, impacted at between approximately 50m/s to 300m/s, the kinetic energy required for containment of the penetrator within the target increased slightly with increasing projectile length. Both the homogeneity and material properties of the steel targets are fundamentally dissimilar to those of concrete. Any discussion of metal impact in this survey is included only to highlight particular methods and approaches.

Bernard and Hanagud (1975) documented the continuing development of spherical cavity expansion for use in dynamic stress conditions. The analysis was further developed for differing nose-shape, layered targets and oblique impact. The pressure model of a particular material was represented by a variable R_s, the "solid Reynolds Number";

$$R_s = \frac{\rho_o v_o^2}{Y} \qquad \text{...Eq.2.7}$$

where ρ_o = initial target density

v_o = impact velocity

Y = target yield strength

This value representing an order of magnitude index of the ratio of inertial forces to shear forces in the target material.

Butler (1975) used a computer code based on modifications of the Ross-Hanagud penetration theory to evaluate the accuracy and applicability of this rigid body approach when applied to rock impacts. Three rock targets were selected in the low-, medium- and high- strength categories of the Deere and Miller (1966) scheme. The projectiles had ogive noses with CRH (Calibre Radius Head - see Figure 2.6) values between 2-10 and weights of between 114-455kg. Impact velocities in the range 305m/s to 915m/s were recorded. In the accompanying parametric investigation a factor was presented to take account of the projectile ogivity (Figure 2.7), in the form of a multiplier function, $f(\varepsilon)$, applied to the inertial component of the pressure model. The required material properties used in the model enable this method to be used for a whole range of projectile-rock combinations, since no empirical penetration data is required.

Hadala (1975) attempted to evaluate the applicability of five existing predictive methods to the design of Earth Penetrating Weapons(EPW). This is the opposing direction from which penetration analysis is often approached. The requirement in this case is to investigate the action of the penetrated material upon the structure of the penetrator. This is the reason that obtaining deceleration-time histories (and especially peak deceleration) is often of such importance in ballistic studies. All five methods were compared with a single actual trial using a 182kg, 165mm diameter ogive projectile impinging normally at 152m/s. The five predictive approaches were;

i) Young's empirical formulae - discussed earlier.

ii) Spherical Cavity Expansion - discussed earlier.

iii) Cylindrical Cavity Expansion - uses the same approach as ii). However, the target medium is assumed to move horizontally to admit the projectile, thus generating an infinitely long cylindrical cavity.

iv) Force Law for Viscoplastic Solids (Allen, 1974) - a force law of the type;

$$-m\dot{v} = \alpha v^2 + \beta v + \gamma$$

where the target material is assumed to be viscoplastic; the generated equation is shown to be closely related to Young's empirical formulae.

v) Avco Differential Area Force Law - attempts to predict the normal and tangential stresses, at every point on the external surface of a penetrator, as a function of time during its impact with, and penetration into, a target material (Figure 2.9). By integration, the stresses over the whole projectile surface may be calculated, hence leading to the complete rigid body motion of the projectile. Figure 2.10 illustrates a calculated penetration-time history compared with actual data, for an oblique impact.

Unfortunately, this method is presently only suited to large penetrators impacting into homogeneous materials.

It was recommended by Hadala that methods i), ii) and v) should be further developed for EPW design.

An analysis of projectile penetration into rock and concrete was carried out by Rohani (1975). Simulations of impact were constructed by a computer code using the dynamic cavity expansion theory and an elastic-plastic compressible material assumption. A parametric study of the effects of concrete compressibility and concrete compressive strength on depth of penetration, at various velocities, was carried out for 880kg, 340mm diameter British Armour Piercing Bombs. For the range studied, penetration depth was shown to be only slightly dependent upon compressive strength; whilst compressibility appears to have a more significant

influence (Figure 2.11). For rock, the spherical cavity expansion solution was successfully compared with a finite-difference deformable body calculation, as shown in Figure 2.12. (The oscillatory path of the finite-difference code deceleration curve corresponds to particle motion within the deformable projectile). Parametric assessments of the effect of target yield strength (Y), Calibre Radius Head (CRH) and the ratio, projectile weight/area, on penetration depth prediction were also carried out. It was noted that a reasonable variation in Y had a more significant effect on the predicted penetration depth than did a reasonable change in any of the other relevant material parameters. Figures 2.13 and 2.14 summarise the remaining findings.

Chavez and Cassino (1975) studied the effect of pavement design on cratering damage from penetrating weapons. Both contact and buried explosive charges of up to 20kg were used. Steel fibre reinforced concrete slabs of 1300mm thickness comprised some of the trial specimens. However, although many photographs of the post impact condition of the slabs were presented, little useful information is given.

Bernard (1976) extended the work of Bernard and Hanagud (1975) to take into account deep penetration at very high impact velocities into homogeneous and layered targets. A more simple, though acceptable, way of approximating the actual shear stress-strain behaviour curve to a bi-linear function (Figure 2.15) is published. Penetration predictions into various materials, including concrete, are shown to correlate well with experimental data and empirical and finite-difference calculations, provided only that the target density and unconfined strength are known with reasonable accuracy.

A series of trials were carried out by Naus and Williamson (1976) to investigate the ballistic resistance of concretes reinforced with various fibres. Four types of impactor were used; small arms, mortars, grenades and explosives. For the specifically relevant trials, using small arms, a

number of weapons were employed including; M16 rifle, M37 (7.62mm) machine gun, 45-calibre pistol, 50-calibre machine gun and 20mm automatic gun. Ball ammunition was used in all cases, excepting that high explosive ammunition was included in the 20mm automatic gun trials. A number of 300mm square specimens, of between 25mm to 150mm thickness, were fired upon from ranges between 9m and 180m, with the great majority of the single shot M37 (7.62mm) machine gun trials being at 100m. In many cases, the selected targets were too small to remove the global effects (tensile rear face scabbing or gross specimen cracking) of the impact. Notwithstanding this limitation, the following information was presented;

i) Only a very slight trend for decrease in depth of penetration with increasing fibre content (0%-3% by concrete volume), for mild steel, drawn steel and glass fibre reinforced concretes impacted by small arm fire.

ii) A reduction in back face scabbing, under small arms attack, with increasing fibre content, at each specimen thickness. The more ductile steel fibres had superior performance to the glass fibres. These conclusions were also obtained with repeated impact trials.

iii) The relative magnitude of fragmentation, and probably the velocity of spalled particles, resulting from demolition charges or impact by small arms was significantly reduced with incorporation of fibres into the matrix.

iv) The effectiveness of each specimen to resist perforation was directly proportional to its thickness and inversely proportional to the projectile energy. Thickness in excess of that required to resist perforation did not reduce the depth of penetration, although the ability of the specimen to resist repeated impact was improved.

v) The effectiveness of the specimens in resisting penetration by small arms was directly proportional to range.

The Royal Ulster Constabulary (1976) carried out a series of preliminary trials to assess the potential of various thicknesses of fibre reinforced sprayed concretes for the protection of conventional cavity walls comprising 100mm concrete brick and concrete block. Steel fibres, 0.25mm x 25mm length, and polypropylene fibres, were each included in an unspecified concrete mix and sprayed on to cavity wall backings as 1", 2", 3" and 4" claddings. The weapons used were Garrand, SLR and Armalite rifles, handheld at 50m and 100m range. Both ball and armour piercing ammunition was used in the trials. Failure was defined as the penetrating, by the bullet, of a witness card placed in the wall cavity. The general conclusion was that between 2" and 3" of either steel or polypropylene fibre concrete was adequate to give complete protection to the inner skin of the cavity walls against the selected high velocity rifles. In these tests no compressive strength values were given for either brick or concrete nor was any plain concrete cladding assessed. At cladding thicknesses less than 2"-3", the likelihood of failure was significantly increased when armour-piercing, rather than ball, ammunition was used.

Backman and Goldsmith (1978) surveyed the general field of penetration-target interaction. Both target and projectile characteristics were considered; the former from semi-infinite media through to thin plates. A review was performed of the various approaches and the experimental methods for modelling penetration events.

Jonas and Zukas (1978) discussed the many approaches which have been used in the analysis of the mechanics of penetration. A concise section on the two different types of computer code was presented. Such numerical methods are the only way of solving the full equations of continuum physics, and thus providing as complete solution to an impact problem. A Lagrangian finite-difference code follows the motion of fixed elements of mass which have the computational grid fixed in the material. It has the ability to handle boundary conditions at free surfaces and material

interfaces, although inaccuracies arise when the grid becomes distorted due to shear and folding. For an Eulerian code, the grid is held fixed in space and the continuum passes through it, either as a set of discrete points or continuously. Hence large distortions can be accommodated although Lagrangian components may be necessary at material boundaries and interfaces. The overall advantages and disadvantages of finite-difference methods are discussed in Section 2.2.

Sedgewick et al.(1978) and Wilkins (1978) provided examples of the use of finite-difference codes into homogeneous metallic targets. The former presented Eulerian methods, whilst the latter used a Lagrangian approach.

Finch (1979) assessed the capability of various types of gravel armour against small arms fire. It was concluded that a 150mm thickness of loose gravel armour was adequate to defeat both armour piercing and ball 30-calibre projectiles.

As a development of the work carried out by the Royal Ulster Constabulary (1976), Port (1980) further considered the potential of sprayed concrete renderings to improve the penetration resistance of existing structures. Small arms weapons were used, with both armour-piercing and ball ammunition. A comparative test series indicated that, for practical purposes, the ballistic resistant properties of sprayed concretes are the same as poured concretes of similar specification. Whilst no specific information was presented regarding mix designs or actual experimental approach, it was reported that the sprayed concrete increased the ballistic resistance of masonry and similar construction materials and that the rendering, to have beneficial effect, should be of 100mm thickness or greater.

Various empirical formulae were assessed by Sliter (1980) for prediction of low velocity missile penetration into reinforced concrete structures. The National Defence Research Committee (NDRC) formula,

developed in 1946, was presented as;

$$D_F = \sqrt{0.45KN_3md(v_o/83.3d)^{1.8}} \qquad D_F/d \leqslant 2.0 \qquad \text{...Eq.2.8}$$

$$D_F = 4.41KN_3m(v_o/83.3d)^{1.8} + 0.025d \qquad D_F/d > 2.0 \qquad \text{...Eq.2.9}$$

where N_3 is a "missile shape factor"

$0.72 < N_3 < 1.14$

K is a "concrete penetrability factor" = $15/f'_c$

It is reported that no term for the quantity of reinforcement in the target is necessary in the formula as, at conventional percentages, it has been found to have no significant effect on local response up to and including the case of backface scabbing. A second formula, the CEA-EDF empirical perforation equation, is compared with the above, and was stated to generate more accurate results in the case of a solid cylindrical penetrator impacting a concrete target.

Degen (1980) has carried out a very similar review of available empirical formulae for the penetration of concrete slabs by rigid missiles.

Bernard (1980) presented an overview of earth penetration research in the United States of America. It was noted that the means of prediction had by this time turned full circle. For example, following the original development of Young's empirical formulae, cavity expansion theories had become popular. However, the limitations of these had since led to a resurgence in the use of empirical approaches. It was suggested that the more realistic contemporary approach was to use various separate empirical solutions for soils and rocks.

Hülsewig et al. (1982) discussed the impact of a 50g cylindrical steel projectile impinging, at velocities of 400m/s to 700m/s, 450mm x 450mm x 100mm thickness plain and fibre reinforced concrete specimens. The volume of the rear face "fragmentation zone" (tensile scabbing region) was the major damage parameter measured. It was located by sectioning the

target perpendicularly to the impact face. Two distinct angled cracks in the cross-section, running almost to the target rear surface, delineated the cone-shaped "zone". Fibre content was varied between 0 and 10%, by concrete weight, in 2% increments. Figure 2.16 shows the relationships noted between projectile kinetic energy and "fragmentation zone" volume, at each fibre content increment; the volume decreasing with increasing fibre percentage. Related tests indicated a decrease in fragmentation zone volume with increasing fibre aspect ratio (length:diameter).

Haldar and Miller (1982) compared 117 actual impact trials into concrete with penetration predictions generated by the NDRC formulae (Eq. 2.8 and Eq. 2.9). The NDRC equations greatly underestimated the actual penetration depths of bullet-type projectiles, whilst grossly overestimating for all other types of larger projectile. An alternative formula, based on the parameters of the NDRC formula, was presented, generating a series of relationships of the form;

$$D_F/d = -B_1 + B_2 I \qquad \text{...Eq.2.10}$$

where d = missile diameter

$$I = B_3 N W v_0^2 / d^3 f'_c$$

This approach is only, of course, valid for the data used in generating it, being essentially a curve-fitting exercise.

The originators of the CEA-EDF formula, Berriaud et al. (1982) reported further on a method for calculating the minimum concrete thickness to resist perforation under impact by various penetrators at up to 200m/s. The CEA-EDF equation, presented as;

$$v^2 = 1.7 f'_c \rho^{1/3} (de^2/m)^{4/3} \qquad 20<v<200\text{m/s} \qquad \text{Eq.2.11}$$

where e = concrete thickness

m = missile mass

ρ = concrete density

was compared favourably with a two-dimensional finite element analysis, the results being reasonably consistent for similar projectile/target combinations.

A review of literature concerned with the penetration resistance of concrete was published by Clifton (1982). The range of impact velocities was from quasi-static to shock loading; with the mechanisms of impact damage being considered. It was suggested that front crater volume varies approximately inversely with (compressive strength)$^{\frac{1}{4}}$. Stress wave propagation was discussed, with the contention that, due to mechanical impedance mismatch between the concrete and any large air voids or cracks, the stress waves may be almost totally reflected with a change in stress form and with the same stress intensity as the incident wave (assuming the gap to be sufficiently large). It was postulated that the artificial creation of a microcrack system in the concrete would lead to an improvement in its wave-damping capability, with a consequent reduction in damage from dynamic loading. It was claimed that air-entrainment has been proven to generate this beneficial effect. The impact strength of concrete was reported to be enhanced by the inclusion of discrete fibre reinforcement, although it was suggested that under shock-loading sufficient time may not be available to permit a redistribution of stresses via the energy-absorbing processes. At rates of 2.76GN/m^{2}s, the dynamic tensile strengths of fibre-reinforced and plain concretes had been shown to be very similar; possibly the main beneficial effect of fibres at high rates and intense loadings is to bridge cracks and thereby reduce fragmentation.

Forrestal and Longcope (1982) extended the cylindrical cavity expansion analysis of Hadala (1975), developing closed-form solutions for several elastic-plastic models to predict forces on conical-nosed penetrators into geological targets of constant shear strength.

Henager (1983) reported on a comparison of conventional reinforced concrete, with and without steel fibre inclusions, under explosive loading. The steel fibre added greatly to the continuing post-impact target integrity.

Clifton and Knab (1983) developed several impact test techniques from the work of Clifton (1982). Of relevance was the projectile penetration test equipment; a "Windsor Probe" gun explosively firing cylindrical steel missiles into concrete. This is a conventional non-destructive test used to assess in-situ concrete compressive strength. For the reported tests on discrete fibre reinforced, latex enhanced, expanded metal reinforced and plain concretes, the gun was adapted to allow a 102mm free flight before impact. The results indicated that the reinforcement type had no substantial effect on projectile penetration. Increases in compressive strength, however, generally resulted in decreases in the projectile penetration values.

Longcope and Forrestal (1983) developed the cylindrical cavity expansion analysis of Forrestal and Longcope (1982) to include targets exhibiting increasing shear strength with increasing pressure. A single trial, a 162kg steel penetrator impinging rock at 520m/s, was presented for comparison purposes. The theoretical and actual deceleration-time histories showed reasonable coincidence, with a significant increase in the rate of deceleration just prior to the penetrator halting.

During 1985, several important papers, in the increasingly studied area of penetration mechanics, were presented at a symposium entitled "The Interaction of Non-Nuclear Munitions with Structures". They are included in this literature review solely for information, since they were published too late to contribute to the research presented in this thesis.

Wolfe and Coltharp (1985) reviewed the commonly used methods to calculate backface scabbing in concrete slabs. It was suggested that the NDRC formulae were adequate, though conservative, predictors for minimum thickness to avoid scabbing under small missile impact.

Wolfersberger (1985) published the results of a database search to locate existing concrete breaching data, confirming that some of the important early research was no longer on record. An analysis of the NDRC formulae was presented, once more showing them to be significantly reliable. It was suggested that penetration depth had often been shown to be related to (target compressive strength)$^{-\frac{1}{2}}$. The normally observed wide scatter of concrete penetration data, regardless of the care exercised in performing the tests, was discussed in some detail. It was stated that; "Tests of identical projectiles at identical velocities against the same concrete target should produce identical penetrations; sometimes this occurs, but most of the time it does not", and on the same topic; "thus when seeking to demonstrate that some parameter or concrete variable has a small but predictable effect on penetration, somehow one must separate the signal from the noise; 'A graph of penetration versus one of the concrete variables does not necessarily imply a unique relationship'". This is why the study of concrete penetration is so intrinsically difficult. There is a necessity to statistically validate all data, including identical results obtained using identical targets, penetrators and methods, to obtain an adequate indication of its likely reliability. This implies that the satisfactory completion of any research in this area will depend very much upon the successful development of an original programme.

2.2 Applicability of Available Methods to Small Arms Penetration into Fibre Reinforced Concrete

As was documented by Rohani (1975), there are four distinct approaches available for penetration depth prediction;

a) Empirical

b) Assumed Force Law

c) Analytical Approach

d) Numerical Methods (computer codes)

One of the earliest tasks during this study was the selection of the most appropriate means of analysis from these alternatives.

The main advantage of the empirical approach is that a reasonably simple curve-fitting exercise may yield, under specific circumstances, the most accurate assessment of the penetration event. Unfortunately, the integrated equation of motion, which generates a deceleration-time history and depth prediction, may contain many parameters which are not defined explicitly in terms of the constitutive properties of the target material and/or projectile geometry, and which may only be determined from actual penetration data. As such, the accuracy of a conventional empirical method is limited to predictions within the data base from which it was developed. For fibre-reinforced concretes, the large number of different fibre types, material types and potential combinations implied that a very large number of trials would have to be carried out to obtain an adequate optimisation.

In the second approach, a force law is defined which is assumed to adequately model the impact and penetration events. Again, the empirical parameters must be defined from experimental data, limiting the range of applicability of the derived equations.

The Analytical approach c) consists of the initial definition of a constitutive law which adequately models the overall physical behaviour of the target material. A simple boundary-value problem is then used to derive the assumed force distribution corresponding to a simple field of motion. By integration, the force (which is assumed to be equivalent to the resisting force on the projectile)-motion equation yields a value for penetration depth and a complete deceleration-time profile. The spherical cavity expansion theory has, to date, been the most successful choice of boundary-value approximation. Using an analytical technique, all parameters appear in the penetration equations in terms of the particular projectile-target combination. As such, no limitation due to database

exists. However, the initial constitutive law may not be valid for materials of very different basic properties to those assumed. Whilst this approach may often be very arithmetical, it is normally relatively simple; as a result expensive computer runtime is used only sparingly.

At the time of the initiation of the study, analytical approaches were available only for homogeneous layered materials. Since the extent of effective homogeneity of fibre reinforced concrete was uncertain, this technique was discounted.

All of the above-mentioned techniques treat the projectile as a non-deformable rigid body; the fourth method however, allows for the elastic-plastic deformation characteristics of the penetrator. The computer code is currently the ultimate penetration study tool. Finite difference and finite element analyses can accurately model the penetration event by taking into account the entire set of field equations. They are approximate in that a set of discretised equations, corresponding to projectile-target interaction at points in space and time, are solved; but the inherent numerical errors present are of a much smaller order of magnitude than the errors introduced by approximating the target material properties, as carried out in the other procedures.

There are several disadvantages to the numerical approach, rendering them an impractical option for this study;

i) The computer codes are by no means "data in-results out" programs. Frequent interaction by an experienced operator is necessary.

ii) Such analyses are extremely time-consuming; generating very long mainframe computer run-times and consequent great cost. It is conventionally considered that computer codes are best used to establish the most important parameters of a particular projectile-target interaction. A constitutive analysis is then substituted to "fine-tune" the observed trends.

It was considered that the extreme cost, caused by the preliminary investigation of a very large number of relevant variables, made the use of a computer code assessment of fibre reinforced concrete impact completely unviable in this study.

iii) This type of program is presently valid only for homogeneous and, possibly, uniformly layered materials; a further reason for initially rejecting the approach when considering a material of uncertain effective homogeneity.

2.3 Properties and Applications of Fibre Reinforced Cements and Concretes

The use of fibres to improve the tensile resistance of otherwise brittle materials, for example in horsehair plaster, has long been an accepted process. However, much of this work has been qualitative; it is only within the last two decades that any real theoretical understanding has been attempted.

The following review chronologically catalogues the most quoted sources on both the development of fibrous concrete technology and the theoretical explanation of its behaviour. It is not a completely comprehensive library of published material; a vast number of papers have been published in the general area of fibrous concrete materials, as well as several state-of-the-art summaries, since the early 1970's.

Shah and Rangan (1971) investigated the mechanical properties of concrete and mortar reinforced with randomly distributed smooth steel fibres. Three-point bending tests were carried out on a series of 50mm x 50mm x 250mm beams reinforced with varying volumes and lengths of low-carbon steel fibres. The area under the complete load-deflection plot was taken as a measure of toughness (resistance to crack propagation) of the beam. Figure 2.17 shows the results for concretes with various volumes of 0.25mm x 0.25mm x 19mm fibre, in comparison to plain concrete of the same mix proportions. Whilst the toughness is greatly increased with increasing

fibre volume fraction, the flexural strength, although improved, does not exhibit such a striking trend. It was further shown that the increase in flexural strength and toughness is influenced by the fibre aspect ratio (that is the ratio length:diameter), an increase in l/d causing an increase in the measured composite properties. However, above an aspect ratio of, say, 100, great problems of mixability exist; this will be further discussed in Section 2.4. The effect of the orientation of the fibres with respect to the direction of applied load was investigated for samples under tensile conditions. It was indicated that following cracking, the closer the fibres were to a parallel direction with the load, the higher the load which could be sustained, and consequently the greater the measured composite toughness. An important conclusion of the work was that the reinforcing action of the fibres could be predicted using a composite materials approach based upon the material properties of the individual constituents.

Edgington and Hannant (1972) studied the effect of vibratory compaction on steel fibre orientation in concrete. It was concluded that when fresh concrete is externally compacted, as for example on a vertical vibrating table, then there is a tendency for the included steel fibres to align in planes perpendicular to the direction of vibration. Thus, the normal analytical assumption of three-dimensional random orientation is invalid should specimens be externally vibrated.

McCurrich and Adams (1973), listed several factors affecting the composite tensile strength of fibrous cements and concretes. Increases in strength may be generated by:

1 An increase in the modular ratio; E(fibre)/E(matrix).

2 An increase in fibre content.

3 An increase in the value of aspect ratio (l/d).

4 An increase in the degree of fibre alignment with stress direction.

All of the above apply to the limits of practicality. A simple rule of mixtures analysis was performed to illustrate the effect of increased volume fraction of fibres on strengthening in direct tension. It was also required to define the value $V_{f(crit)}$, the volume fraction of fibres required to carry the tensile load sustained by the concrete immediately before cracking occurs. The analysis was carried out as follows;

Assumptions;

i) Before cracking, the fibres are fully bonded to the matrix.

ii) Composite is under a uniaxial tensile load, magnitude F.

iii) Poissons ratio in fibre and matrix = 0

(i) and iii) being rather unrealistic possibilities).

Let cross-sectional area of composite $A_c = 1$

Let total volume of composite $V_c = 1$

where subscript c = composite

Fibre volume, V_f, is expressed as a fraction of the total composite volume

$$\frac{V_f}{V_c} = \frac{V_f}{1} \qquad \text{...Eq.2.12}$$

subscript f = fibre

Before cracking,

$$\varepsilon_c = \varepsilon_f = \varepsilon_m \qquad \text{...Eq.2.13}$$

subscript m = matrix

Under elastic conditions,

$$\therefore \frac{\sigma_c}{E_c} = \frac{\sigma_f}{E_f} = \frac{\sigma_m}{E_m} \qquad \text{...Eq.2.14}$$

σ = stress

E = Youngs Modulus

$$\text{Also, } F = \sigma_c A_c = \sigma_f A_f + \sigma_m A_m \qquad \text{...Eq.2.15}$$

$\therefore$ Since $A_m = A_c - A_f$ and $A_c = 1$

$$\sigma_c = \sigma_f A_f + \sigma_m (1 - A_f) \qquad \text{...Eq.2.16}$$

Considering a unit length of composite;

$$V_c = A_c.1 = 1, \quad V_f = A_f.1 = A_f$$

$$\therefore \quad \sigma_c = \sigma_f V_f + \sigma_m(1-V_f) \qquad \text{...Eq.2.17}$$

Introducing a fibre efficiency factor η, to take account of random orientation effects;

Composite tensile strength, $\sigma_c = \sigma_m(1-V_f) + \eta\sigma_f V_f$ ...Eq.2.18

A graphical representation of Equation 2.18 is given as Figure 2.18. The value of $V_{f(crit)}$ for strengthening in direct tension is noted at the intersection of the two plots $\sigma_c = \sigma_m(1-V_f)$ and $\sigma_c = \eta\sigma_f V_f$.

The problem of conglomeration of large volume fractions of high aspect ratio fibres in the mixing pan was also recorded in this paper. A large scale compressed air injection technique was cited as an efficient solution to the difficulty.

A state-of-the-art report, prepared by the American Concrete Institute Committee 544(1973), explained the ability of fibres to increase the toughness of concrete by suggesting that additional energy must be expended in order to de-bond ("pull-out") the fibres from the concrete matrix. Hence a considerable amount of extra work may be done before complete fracture of the material occurs. It was also stated that the phenomenon of fibre conglomeration is related to a number of factors, of which the most important appeared to be the fibre aspect ratio. Other contributory causes were held to be fibre volume percentage, maximum aggregate size, aggregate gradation and proportion, water-cement ratio and mixing method. A maximum aspect ratio of 100 was advised. According to this report, a wide range of unspecified tests, generating various rates and magnitudes of tensile and compressive dynamic loading, had recorded increases in dynamic strengths of fibre-reinforced concretes of between five to ten times that of plain concretes under the same test conditions. Once again, the greater energy requirement to pull out the fibres was given

as the reason for increased impact strength and resistance to fragmentation and spalling.

Pakotiprapha et al.(1974) investigated the mechanical properties of steel fibre reinforced cement mortar in flexure, torsion, axial compression and tension, by the application of the rules of mixtures. The use of this type of approach was validated using experimental data. The rupture strength results obtained supported the work of Shah and Rangan (1971), indicating little variation in flexural strength with increasing fibre volume; this contradicting a very early study by Romualdi and Mandel (1964).

Tattersall and Urbanowicz (1974) studied the effects of various chemical and physical treatments on the surface of short steel wires used as concrete reinforcement, in order to determine what factors most greatly influenced bond strength at the fibre-matrix interface. Their pull-out tests indicated that over the short term (i.e. 7 days), galvanised wires exhibited a marked improvement in bond strength over plain steel fibres. However, by 28 days, this situation had reversed, the interaction of the smooth steel fibres with the matrix becoming markedly stronger than the galvanised fibre-matrix combination. It was considered that the best way of improving bond strength in fibre reinforced concrete was to provide fibres with positive anchorages, by the use either of indented wires or alternatively wires with looped ends - although the latter would certainly exacerbate the already difficult random mixing procedure. With looped end steel fibres, tensile failure of the test specimen occurred due to yielding of the fibre, that is, any further increase in bond strength above this would be irrelevant. It was also noted that the extent and method of curing of the specimens appeared to have a significant influence on the subsequent bond characteristics.

Swamy (1974) gave detailed recommendations for the practical

use of steel fibre reinforced concretes. Amongst other aspects considered were mix design, fibre dispersion, batching, placing and finishing. An assessment of the likely properties of adequately produced steel fibre concrete was included in a very useful review. A suggestion was made that maximum coarse aggregate size should generally be limited to 10mm, whilst fine to coarse aggregate ratios of between 1:1 and 3:1 were cited as appropriate for concretes containing steel fibres.

An appraisal of the use of steel fibres in gunite (sprayed concrete) was presented by Ryan (1975). This indicated strongly that sprayed application was a feasible proposition and implied that the inclusion of fibres actually assisted the overall process. It was suggested that the "matting" structure formed by the fibrous inclusions during impact subsequently acted to absorb up to 50% of the normal quantity of rebound material. However, it was stated also that much of the remaining rebound would consist of fibrous inclusions. It was emphasised that adequate supervision and compliance testing was vital as a consequence of these limitations; recommendations were given with respect to the size and type of test cores to be taken.

Raouf et al.(1976) carried out several explosive tests on fibre-reinforced cement composites. Small explosive charges were glued on to one end of 25mm x 25mm x 210mm long fibre-reinforced cement paste bars. Carbon, steel, polypropylene and E-glass fibrous inclusions were tested (the last using High Alumina Cement, rather than OPC, in order to reduce the likelihood of alkaline attack upon the fibres). Plain cement bars were provided as controls. In this limited series of tests the effectiveness of each fibre type in holding together the impacted bars was listed, in descending order of effectiveness, as;

a) E-glass (in conjunction with High Alumina Cement Paste).

b) Polypropylene.

c) Steel.

d) Carbon.

It was considered that a more uniform distribution of fibres throughout the mix may have contributed to the greater impact resistance of the E-glass composite, the two types of cement pastes being assumed to have tensile strengths of the same order.

The rule of mixtures analysis, as used by McCurrich and Adams (1973), was developed by Mangat (1976) specifically for steel fibre reinforcement in concrete. An alternative approach, based on an effective fibre spacing concept, was also derived. Both theories appeared capable of predicting the direct tensile strength of fibre reinforced concrete, as evidenced by the experimental data included in the paper. The effective spacing concept takes into account both the imperfect bond characteristics of short fibres in addition to their geometrical distribution through the matrix. The relation between "effective spacing" and tensile strength was shown to be non-linear; strength decreasing with increasing "effective spacing". The particular relationship was stated to be unique for any particular fibre aspect ratio, in a particular concrete matrix.

Swamy and Stavrides (1976) carried out a statistical analysis of compressive and flexural strength results for both plain and steel fibre concretes. Using a mix design including 30% pulverised fuel ash and a water-reducing agent to improve workability, the authors found that the fibre concrete results for both types of loading exhibited larger standard deviations than the corresponding results in the plain concrete specimens. However, further analysis showed that, providing good quality control is ensured at all stages of manufacture and testing, there is no need to test a greater number of specimens than that conventionally used for plain concrete trials. A slight increase was observed in the compressive strength results of the fibre concrete specimens over their plain concrete equivalent. Detailed statistical analysis showed the observed difference was not due to chance but to the presence of the fibres.

Finch (1977), in a restricted document, reported upon the

effectiveness of fibre-reinforced sprayed concrete against small arms fire. A series of full-scale trials, using both 7.62mm ball and 30-calibre armour-piercing ammunition, fired at 50m range from handheld weapons was carried out. The targets were either rendered on to existing masonry or were made effectively free-standing by the use of backing materials with no significant resistance. Information on mix designs was not given, though a curing time of 14 days was quoted. Both monofilament polypropylene and steel fibre reinforced concrete targets were tested. A 75mm thickness of each type, on dense concrete block and brick walls, showed an encouraging amount of ballistic protection. Both of these materials, when applied as 150mm layers to thin skins of hessian, supported by wire mesh, produced a material of integrity; capable of resisting multiple rounds of 7.62mm ball penetrations. The targets also had the ability to withstand two rounds of 7.62mm armour piercing impactors at the same point of strike. These tests were not comprehensive, but did conclude that both materials show considerable promise for use in the reinforcement of existing buildings and structures subject to ballistic or blast attack, or for the rapid repair on a permanent basis of structural damage.

A report on Fibre Concrete Materials, prepared by RILEM Technical Committee 19-FRC (1977), attempted to prompt the development of appropriate test specifications, particularly with respect to material durability. A summary of much of the accumulated knowledge to date was included; both the composite and its potential constituents were discussed. A useful survey of fibrous inclusions, with predictions of the likelihood of successful future use, was a major feature of this work. The properties of many of these fibrous materials were also documented for comparison purposes.

Hannant (1978) published a major text on fibre cements and fibre concretes. An analysis was given of the postcracking flexural behaviour of fibre-reinforced concretes. Although a simplification, it served to show the likely improvement in the moment of resistance of a section as a result

of the extra ductility imparted by fibre pull-out or extension ("necking") across a crack. The critical fibre volume for flexural strengthening was shown to be less than or equal to, that for direct tension (derived by McCurrich and Adams (1973)). This book reported also that sufficient consistent data was by now available to confirm that the addition of fibrous materials was of significantly greater percentage benefit to the flexural strength of fibre-reinforced concretes than to the direct tensile strength. A theoretical treatment, related to the change in shape of the tensile stress block after cracking in flexure was presented. It was reported that the major factors affecting the flexural strength are the volume fraction and the aspect ratio of the fibres, an increase in either of these parameters leading to a higher flexural strength.

An attempt was made by ACI Committee 544 (1978) to define appropriate tests for the measurement of the properties of fibre reinforced concretes. Recommendations were made concerning specimen production; and the validity of standard plain concrete tests, when used for fibre concretes, was considered. New tests, designed to measure two of the more particular properties of fibre reinforced concrete, were proposed.

It was suggested that a specific means of evaluating energy absorption under load would be a valuable contribution. A "toughness index", basically of the type used by Shah and Rangan (1971), was proposed. Using a similar approach as that in a standard modulus of rupture test, third point loading is applied to a 4" x 4" x 12" (100mm x 100mm x 300mm) specimen and the load at first crack recorded. The test is allowed to continue until a mid-span deflection of 0.075" (1.9mm) has been reached. The toughness index is then defined as;

$$\frac{\text{Area under load-deflection curve to 0.075" midspan deflection}}{\text{Area under load-deflection curve to first crack}}$$

A dimensionless value results, with a reported range of 14 (for

fibrous concretes containing a low percentage of low strength, brittle short fibres) to 32 (for fibrous concretes with a high percentage of high strength, ductile long fibres). It was considered that this index is capable of showing the influence of fibre amount, length, configuration, strength and ductility. It was also reported to differentiate matrix factors such as cement content and aggregate proportions.

A further new drop-weight test was nominated, to demonstrate the amount of impact energy necessary first to start a visible crack in a fibrous concrete, and then to propagate that crack. A 2½" (63mm) by 6" (150mm) diameter fibre concrete specimen is centrally placed on a floor standing jig consisting of a base plate with four attached reference lugs. The sample is then subjected to centrally placed blows from a standard, hand operated 10lb (4.54kg) compaction-hammer, with a drop of 18" (457mm), via a 2½ (63.5mm) diameter hardened steel ball freely held on the target surface by a specially designed bracket.

A number of blows required to cause the first visible crack on the top surface of the specimen is recorded, as is the number of blows to ultimate failure. Ultimate failure is defined as the point at which the cracks in the specimen have opened sufficiently to permit the ensuing pieces of concrete to touch three of the four reference lugs, each of which was originally at a distance of 3/16" (4.8mm) from the specimen circumference. It was suggested that, using this test, a conventional plain concrete specimen may exhibit "impact strength" values of 30 blows to first crack and 32 blows to ultimate failure. A fibrous concrete may exhibit figures of say 45 blows, and at least 75 blows, for the same two failure criteria. (Later work by Henager (1981) and Swamy and Jojagha (1982) suggested values of about 100 and 500 respectively more correctly reflected the values likely to be recorded for fibre concretes).

It was emphasised that the techniques documented in this paper were intended to be the basis of standardisation, although it was recognised

that usage was likely to promote discussion and subsequent development. It was ultimately envisaged that the finalised standards would provide an adequate basis to produce design criteria.

An international symposium on "Testing and Test Methods of Fibre Cement Composites" was held during 1978. Verhagen (1978) discussed many practical methods developed to assess the impact resistance of various fibre concretes subjected to various types and magnitudes of impactors. Guidance was given on procedures, specimen dimensions, number of tests to be carried out and acceptable tolerances. For tests using bullets, the author suggested the results of five similar trials should not differ by more than 15%. It was stressed that this paper was to be used as an aid to development rather than as an established series of standards. At the same conference, Hibbert and Hannant (1978) reported on an instrumented Charpy-type pendulum impact machine designed to test 100 x 100 x 500mm specimens, over a span of 400mm, in flexure. the significant influence of the site and type of test machine on the obtained results was emphasised. Typical load-time curves for both steel and fibrillated polypropylene fibre reinforced concretes were given, along with similar data for a plain concrete sample. This design of machine provides a method of comparing specimens containing the various fibre types under identical test conditions. However, the results are not necessarily repeatable, even on another superficially identical machine, at a different site.

Walton and Majumdar (1978) provided some preliminary information on Kevlar-29 fibre reinforced cement paste specimens. It was suggested that the composite mechanical properties recorded were sufficiently encouraging to warrant further study. A reservation was noted with regard to the fire resistance of such composites. Kevlar fibres are organic and decompose at relatively low temperatures compared with say, glass or steel fibres. It was pointed out that full-scale tests would be necessary before the use of Kevlar in buildings could be recommended.

Denson and Monahan (1980) considered the use of fibre-reinforced lightweight concretes containing preformed foam or expanded polystyrene beads, giving a high degree of entrapped air, as construction materials for assault training villages. The concrete was required to absorb the impact energy of live small arms ammunition. In these tests preformed foam steel fibre concretes were most successful both in minimising penetration depth and also in prevention of ricochet and front-face spalling. Polypropylene and alkali- resistant glass fibres were also included in the trials.

Henager (1981) summarised the contemporary state-of-the-art of steel fibrous shotcrete design and production. An enduring problem had been the unacceptable quantity of fibre rebound. It was suggested, following a high-speed photographic study, that a large percentage of the rebounding fibre was blown away by the high pressure air stream; that is, the observed effect was not simply the result of the fibres bouncing from the work surface. A parametric study indicated that the most effective measures to reduce rebound seemed to be;

i) reduction of air pressure (air velocity or amount of air at the nozzle).

ii) use of a higher proportion of fine aggregate,

iii) use of smaller sized coarse aggregates,

iv) use of fibres of lower aspect ratio,

v) pre-dampening of aggregates to obtain the optimum moisture content,

vi) application of a shotcrete with the wettest possible stable consistency.

This review, and the dedicated issue of the journal containing it, is a useful starting point in obtaining a fundamental understanding both of the sprayed concrete process, and the more specific requirements of fibre-reinforced sprayed concretes.

In the same journal, Ramakrishnan et al.(1981) compared the performances of field-produced fibre shotcretes containing four different

types of steel fibres. It was shown that both collated fibres (i.e. bundles of fibre glued with water-soluble adhesive to create an artificially low aspect ratio) and hooked steel fibres could be successfully incorporated in conventionally produced sprayed concrete. Impact resistance was tested using a variation of the ACI Committee 544 (1978) procedure, differing only in the thickness of specimen used. Hooked fibre concretes showed a significant ability to control cracking and deformation under this type of impact loading, impact resistance increasing with increasing fibre content.

In a laboratory study, Morgan (1981) confirmed the practicality of using hooked end fibres in sprayed concretes, and observed mechanical properties results in accordance with those produced by Ramakrishnan et al.(1981).

Barr et al.(1982) advanced an alternative version of the toughness index suggested by ACI Committee 544 (1978). This new test removed the restrictions on specific specimen type and prescribed deflections; instead a specimen is loaded until the load-deflection graph extends to twice the measured deflection at first crack. Figure 2.19 illustrates a typical response for a polypropylene concrete, and defines the proposed toughness index. It was documented that this toughness index varies from 0.25 for plain concrete up to a maximum of unity for very tough fibre reinforced materials.

Narayan and Kareem-Palanjian (1982) considered the factors influencing the workability of steel-fibre reinforced concretes. Standard slump and Vebe consistometer tests were used to assess the workability of several concrete mixes, containing varying volume fractions of several different steel fibre types and aspect ratios. It was concluded that the most likely way to achieve a workable mix, whilst incorporating a large volume fraction of fibres, was to set the fine aggregate content of the mix to as high a value as possible.

The limitations of the ACI Committee 544 (1978) impact resistance test method, applied to lightweight fibre concretes, were investigated by Swamy and Jojagha (1982). It was reported that extremely large variations, up to more than 1200% in one test, could occur in the number of blows recorded to first crack of identical specimens. It was suggested this reflected the randomness of cracking in concrete, the occurrence of weak sections as in all concrete elements, the non-uniformity of fibre distribution and also the inherent limitations of "drop-weight" type tests. Such large variation was not recorded in the number of blows required to produce ultimate failure; further, a low impact resistance to first cracking did not necessarily indicate low impact resistance to ultimate failure. It was reported that the test adequately reflected the influence of all the major material parameters, including aggregate strength, aggregate-matrix bond, fibre shape and fibre geometry. It was concluded that a high fibre length and aspect ratio, with surface deformations enabling extensive debonding, appeared to be essential characteristics for high impact resistance.

Bijen (1983) carried out a direct comparison of several commercially available glass-fibre reinforced cements, including a number of alkali-resistant glass fibres. It was stated that these latter materials nevertheless suffered deterioration, with time, as the interfilament spaces of the glass fibre bundles gradually filled up with calcareous compounds under moist conditions. A polymerised cement matrix had been used to ameliorate this condition. However, it was concluded, on the basis of accelerated ageing tests, that all of the tested glass fibre composites were still liable to brittleness in the long term, with a consequent reduction in impact resistance.

A fracture model to generate the crack growth resistance curve (R-curve) of fibre reinforced cementitious composites was developed by Visalvanich and Naaman (1983). It was documented that, using the

experimentally obtained tensile load-displacement relationship for the material, and an adequate model for the propagating crack shape (assumed to maintain the same shape with time), the entire plot of energy demand per unit crack extension could be generated. The model was compared with experimental data and showed good correlation. A similar approach was presented by Wecharatana and Shah (1983), using the concept of crack opening displacement (COD) to define the influence of the propagating crack shape. That is, a given crack in the matrix was considered to propagate when the COD reached a critical value at the boundary between the fibre bridging zone and the matrix zone - which provides some pre-cracking resistance as a result of aggregate interlock and microcracking. It was emphasised that this value was based only on an approximate analysis which required further refinement. Again good correlation with experimental data was observed.

Raouf and Hussain (1984) discussed various properties of steel fibre concretes at early ages. Ultrasonic pulse velocity testing was used to assess the unconfined compressive strength of fibre concretes at between 3 and 24 hours. It was evident that the presence of the fibres was greatly significant in terms of the evaluated percentage increase in unconfined compressive strength at very early ages; this influence reducing with time. At all of the tested ages, the percentage increase in unconfined compressive strength was found to be linearly related to the volume fraction of fibre.

2.4 Limitations in Sprayed Fibre Reinforced Concrete Constituents

Fibre reinforced and sprayed concretes are specialised materials, the successful production of each of which is dependent upon the selection of an appropriate mix design. The problems are compounded when the material is both to contain fibres and be potentially suitable for sprayed application.

Attempting to produce a sprayable fibre reinforced concrete constrains the final composite in a number of related ways;

i) The matrix parameters are dependent upon the quantity, shape and type of fibre used.

ii) The matrix parameters must reflect the requirements of the spraying process(es).

iii) The limitations of the spraying process has an influence upon the fibres incorporated in the composite.

The various parameters used in mix design are discussed below, taking into account these related aspects.

Water:cement ratio

In order that sprayed concrete should not have excessive flowability, a low w/c ratio, compared to ordinarily placed concrete, is desirable. The Concrete Society Code of Practice for Sprayed Concrete (1980) suggests values in the range 0.35 to 0.5 are necessary for the successful placing of sprayed concrete. The addition of fibres, however, substantially alters the composite workability and may promote variation from these values.

Henager (1981) suggested that fibre and coarse aggregate rebound, a major problem with sprayed concretes, is reduced by applying the concrete at the wettest stable consistency.

Aggregate:cement ratio

The Concrete Society Code of Practice for Sprayed Concrete (1980) recommends, for dry-mix processes, a range of 3:1 to 4:1 for this value. For the wet-mix process it is further suggested that an upper limit of 6:1 may be acceptable. (See Section 4.4.5 for definition of the "dry-mix" and "wet-mix" processes).

Fine-coarse aggregate ratio

Hannant (1978) documented that, by experience, a satisfactory mix for fibre concrete should contain a mortar volume of about 70%, the remainder being coarse aggregate.

Swamy (1974) observed that the fine:coarse ratio generally varied between 1:1 to 3:1 in successful mixes, whilst Henager (1981) recommended the use of an increased proportion of fine aggregate as an appropriate means of reducing rebound.

Aggregate size

The Concrete Society Code of Practice for Sprayed Concrete (1980) specified the nominal maximum sizes of coarse aggregates to be 20mm, 14mm and 10mm. It advised against the use of the larger sized aggregates as they were stated to cause excessive rebound, a view echoed by Henager (1981).

Swamy (1974) recommended that, for successful steel fibre concretes, a maximum aggregate size of 10mm was appropriate. Hannant (1978) agreed with this view, providing diagramatic evidence that uniform fibre dispersion is more difficult to achieve as the aggregate size increases from 5mm to 10mm to 20mm. Figure 2.20 shows this effect, indicating the increase in fibre interaction with increasing aggregate size.

Fibre Aspect ratio

Many researchers, for example, McCurrich and Adams (1973), have confirmed the increasing improvement of composite material properties with increasing fibre aspect ratio (length:diameter).

Swamy (1974) reported that an aspect ratio of 80-100 appeared to be optimum in terms of strength, mixing, placing and compaction requirements.

Hannant (1978) recommended that an upper limit of 100 should be defined, in order to avoid fibre conglomeration.

Fibre Length

Hannant (1978) suggested that fibres of a length greater than half the specimen thickness should be avoided, since such fibres tend towards a two-dimensional alignment.

The Concrete Society Code of Practice for Sprayed Concrete (1980) suggested that fibre lengths must be compatible with transporting hose

diameters (normally 50mm) to reduce the possibility of blockages.

The above recommendations were used as a basis for the preliminary mix designs of this study. The later experimental programmes were then further influenced by the information obtained in the foregoing tests.

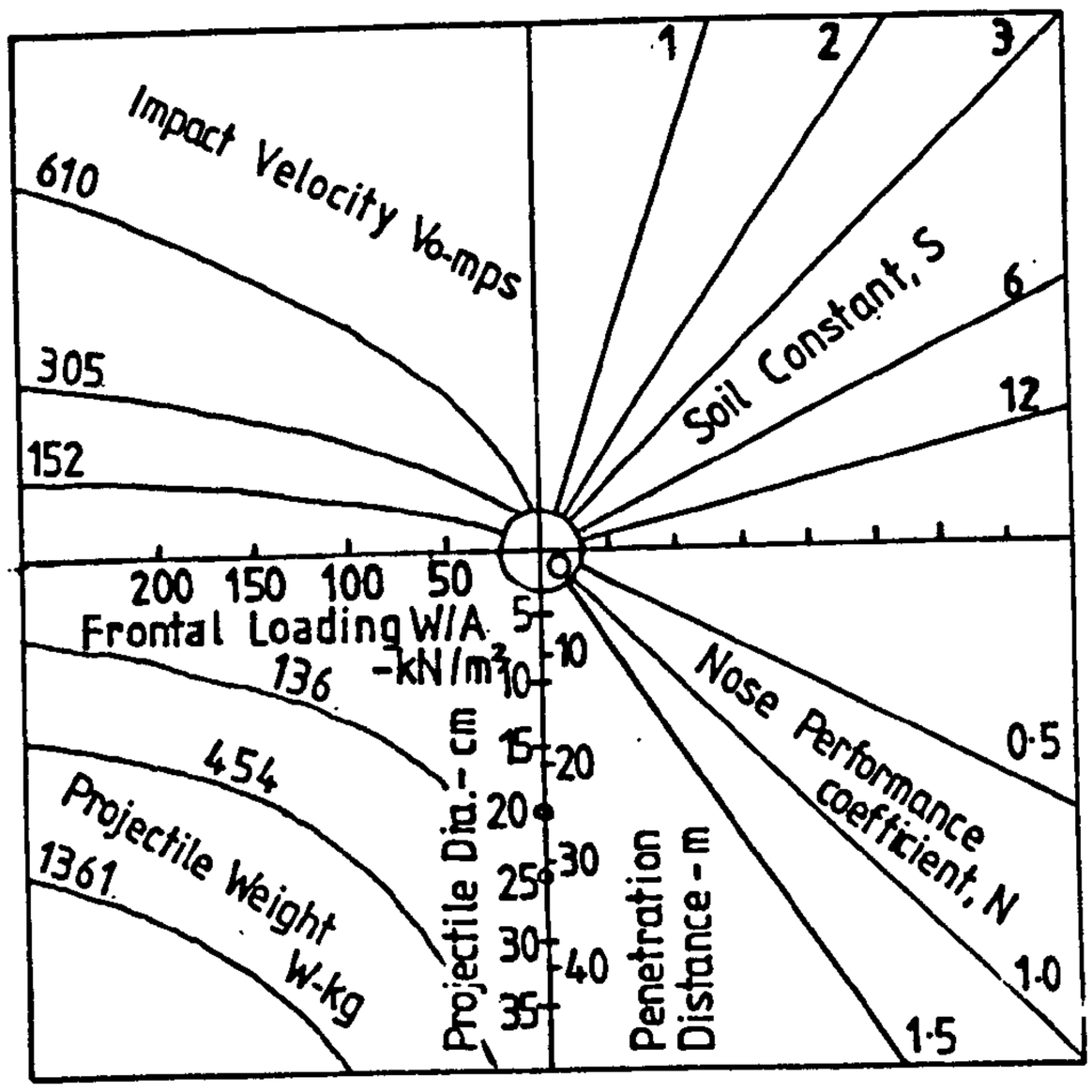

Figure 2.1 Penetration Nomogram (SI Units)
(Young 1969)

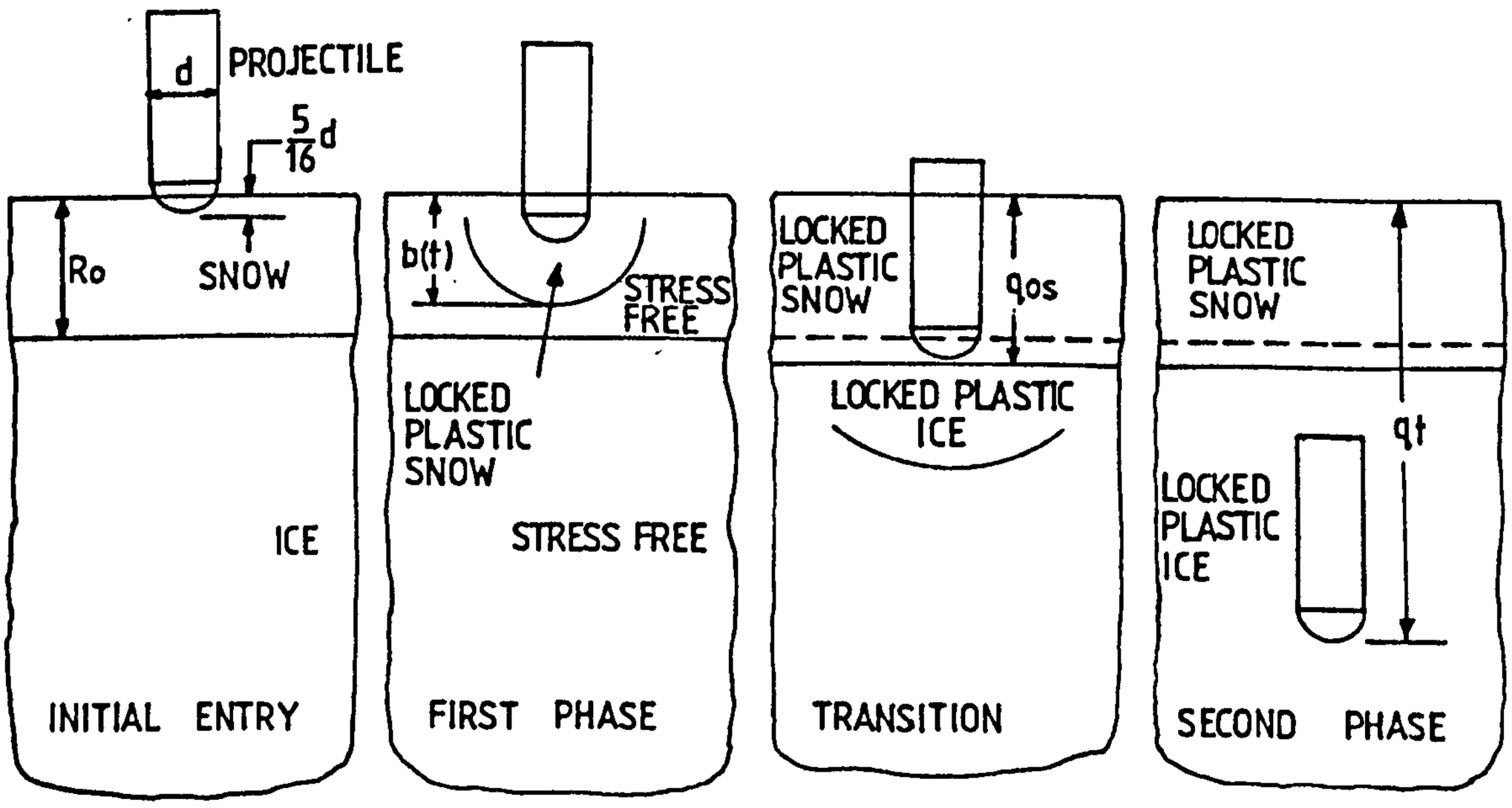

Figure 2.2 Schematic Representation of Penetration Process in Snow Covered Arctic Ice Sheet
(Ross and Hanagud, 1971)

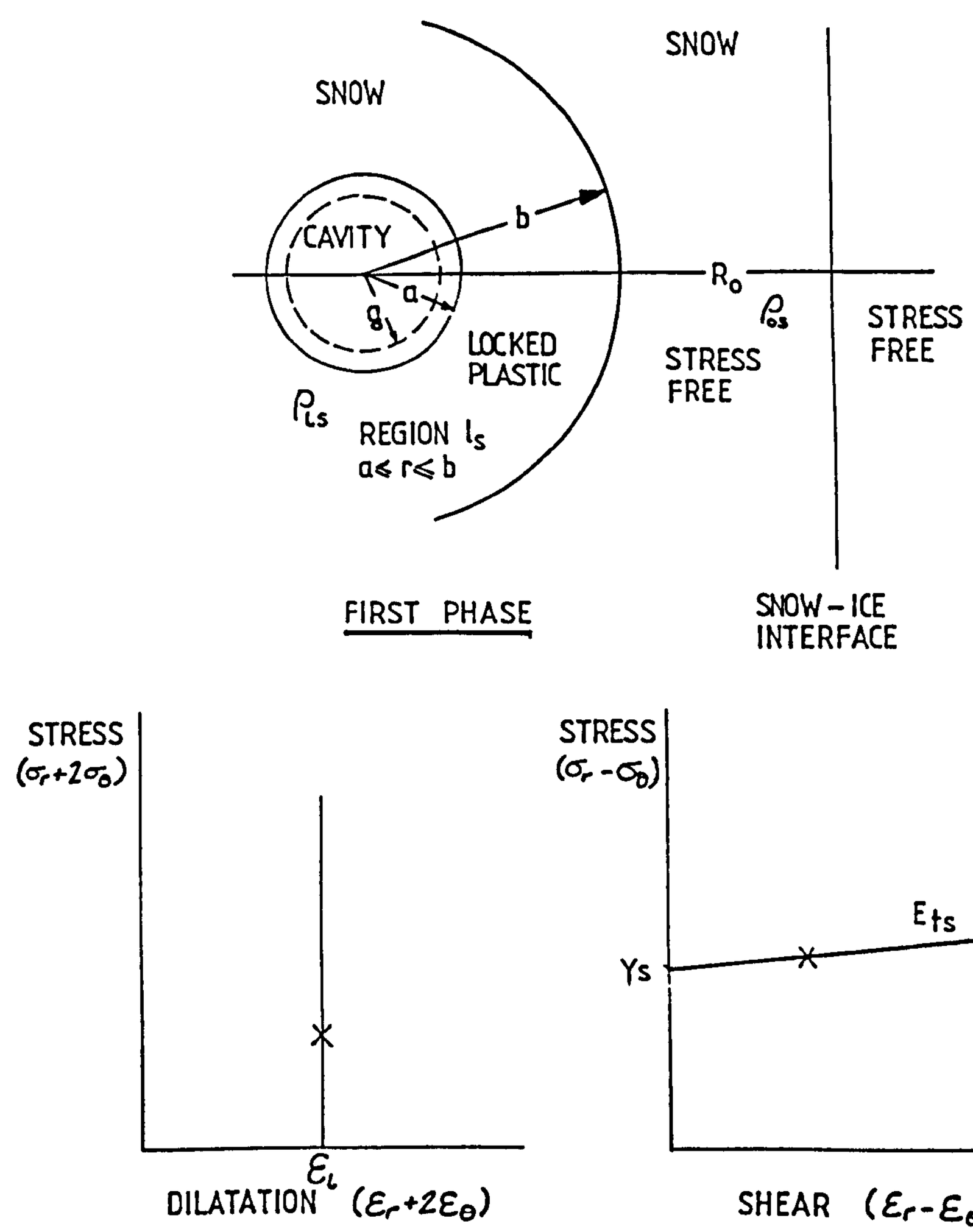

Figure 2.3 Dynamic Cavity Expansion Problem and Idealized Stress-Strain Curves for a Rigid Plastic, Ideal Locking Material with Linear Strain Hardening (Ross and Hanagud, 1971)

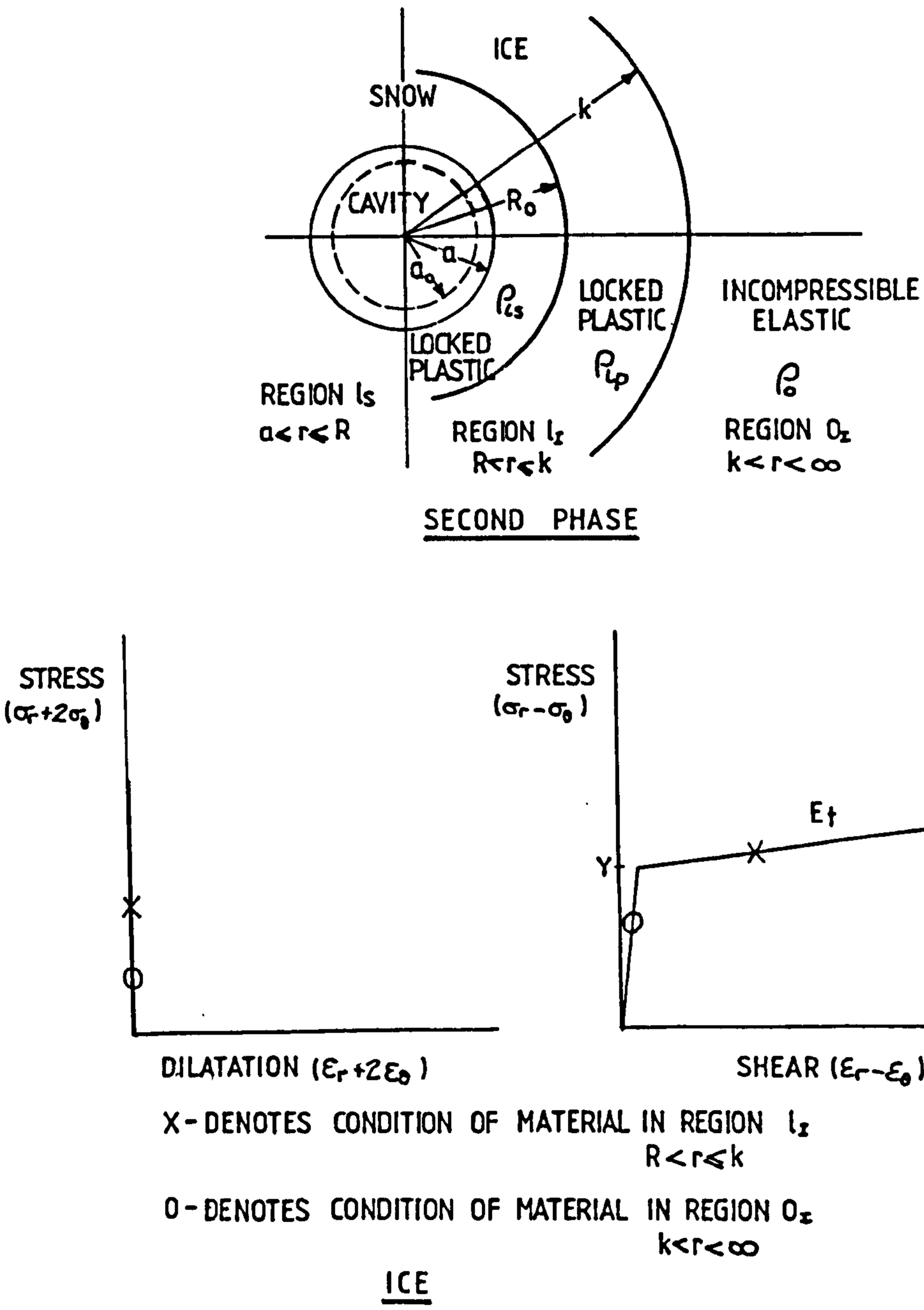

Figure 2.4 Dynamic Cavity Expansion Problem and Idealized Stress-Strain Curves for an Elastic-Plastic, Incompressible Material with Linear Strain Hardening (Ross and Hanagud, 1971)

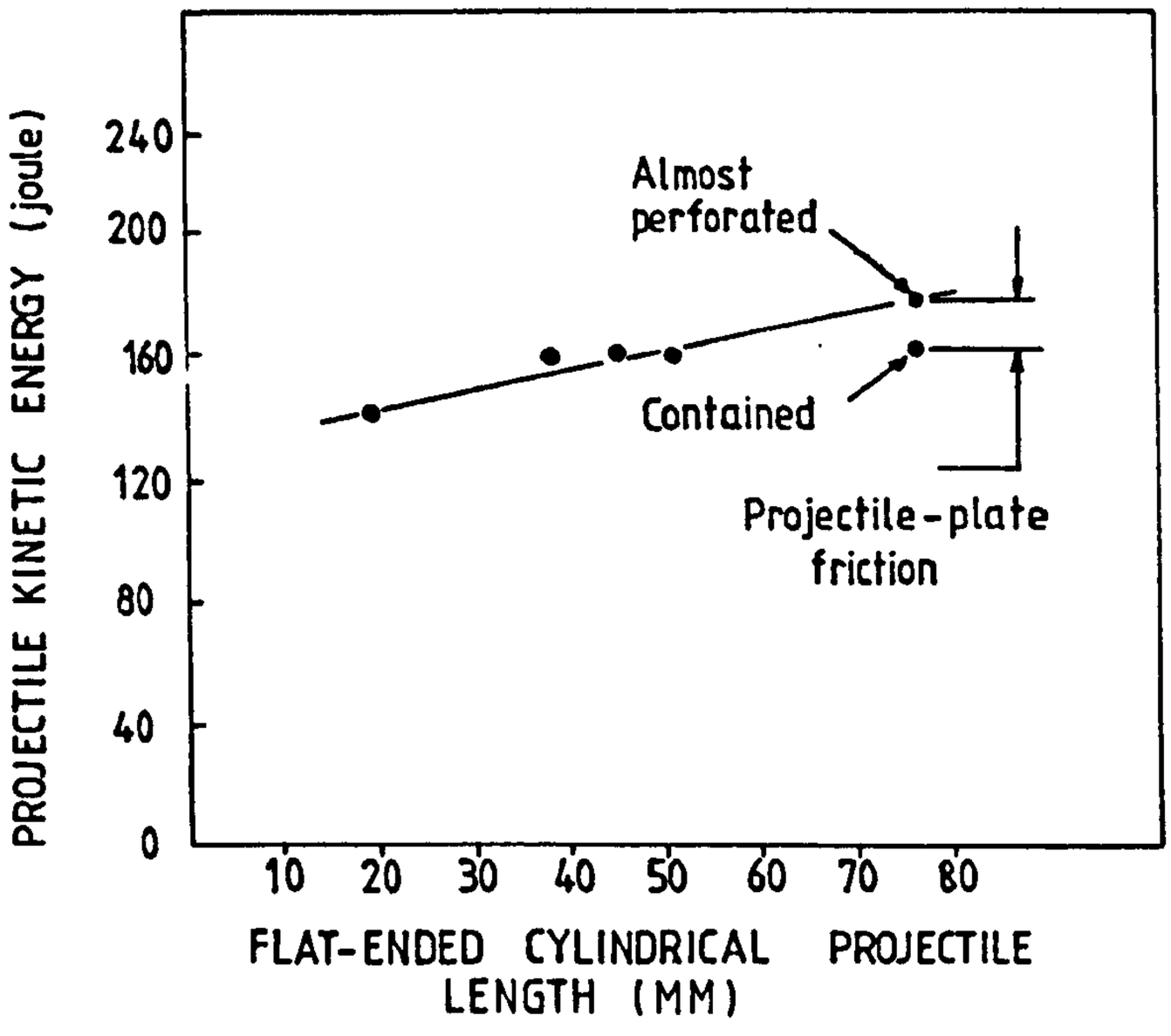

Figure 2.5 Kinetic Energy for Containment versus Projectile Length for Impact of Mild Steel Plate (Zaid et al, 1973)

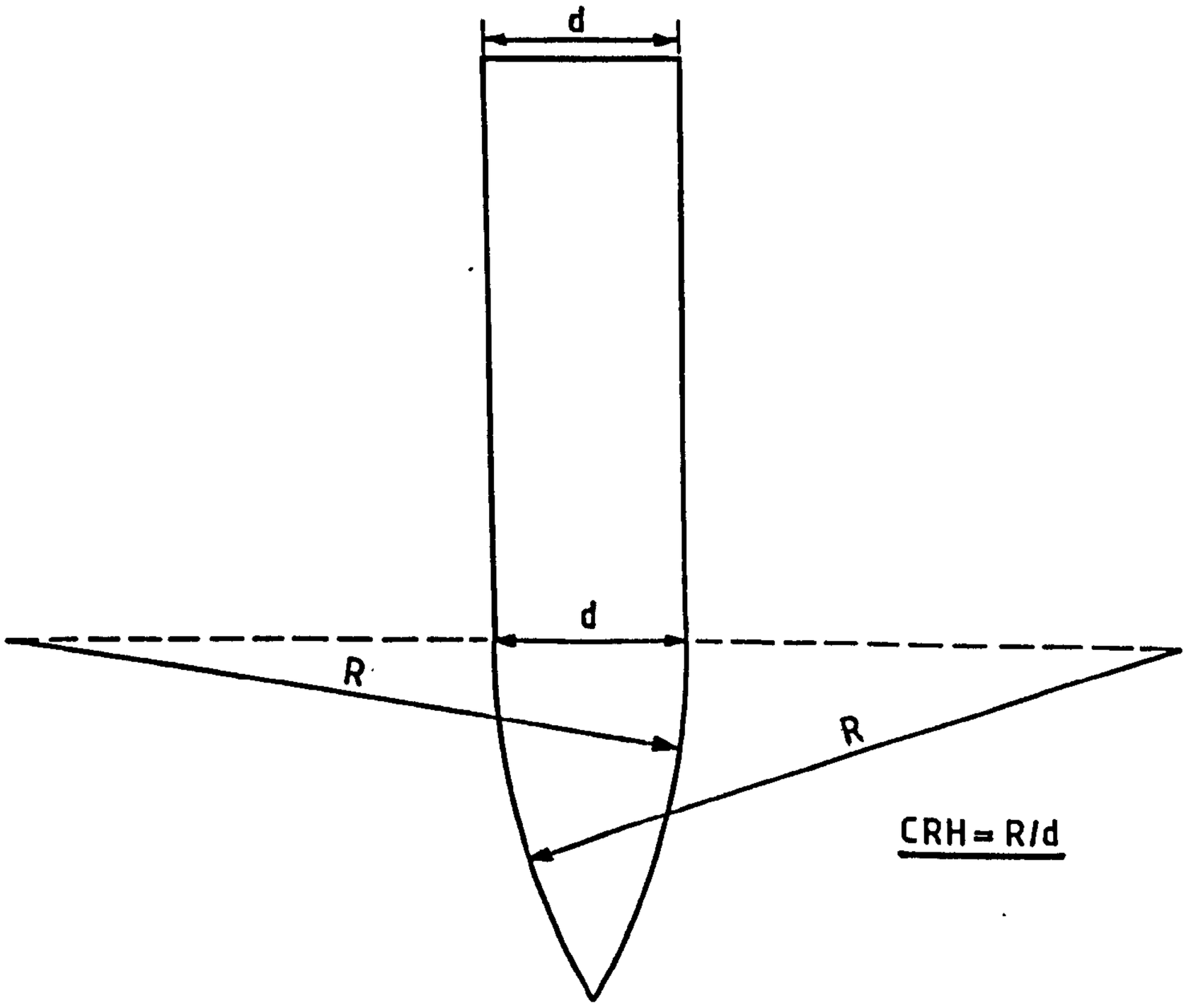

Figure 2.6 Definition of CRH (Butler, 1975)

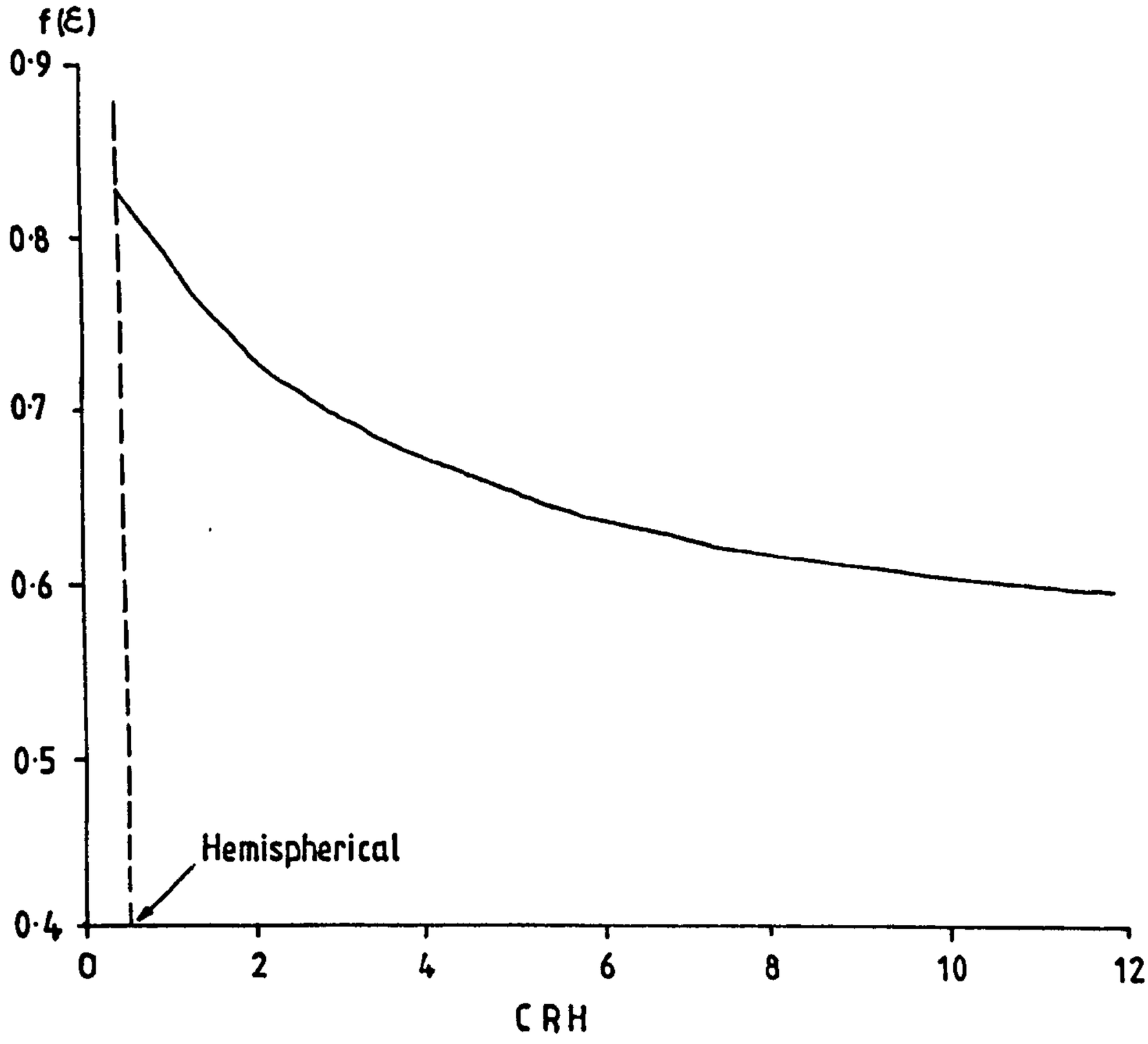

Figure 2.7 Ogive Nose Factor, f (ε) vs. CRH (Butler, 1975)

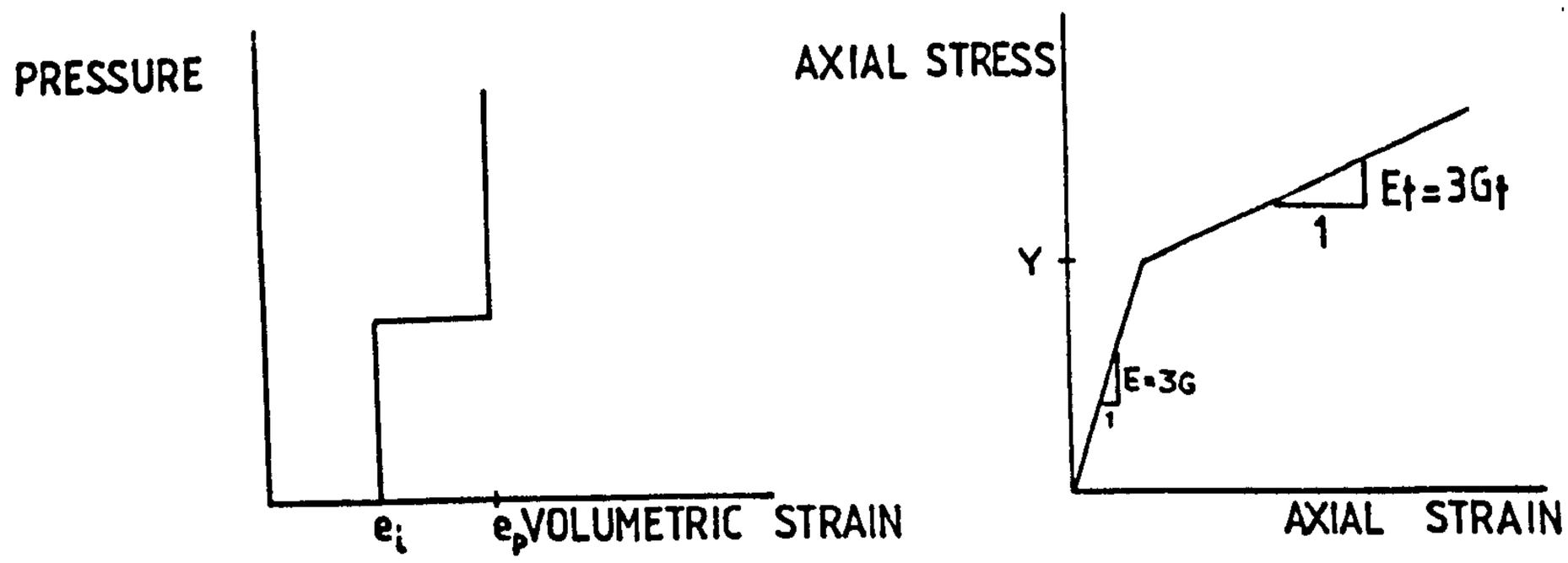

Figure 2.8 Idealized Stress-Strain Curves for a Locking Elastic-Plastic Material (Butler, 1975)

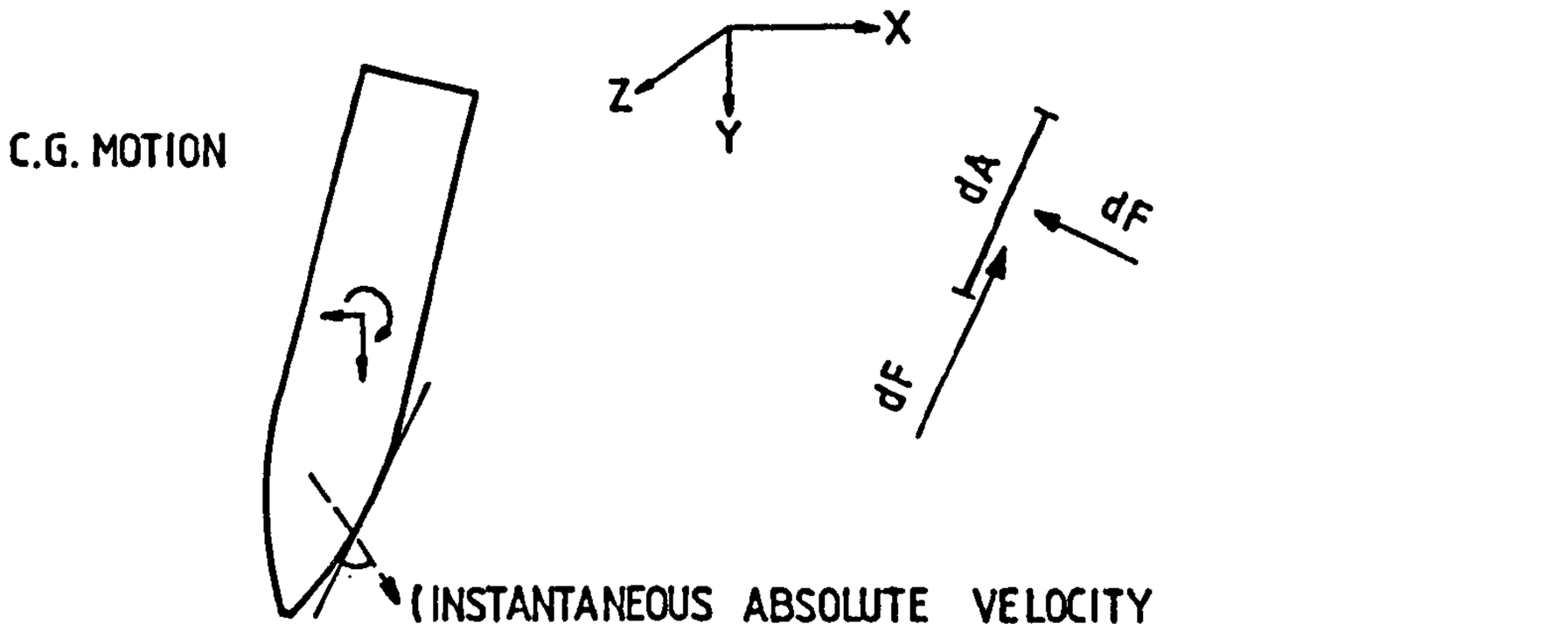

Figure 2.9 Configuration for AVCO Differential Area Force Law Equation
(Hadala, 1975)

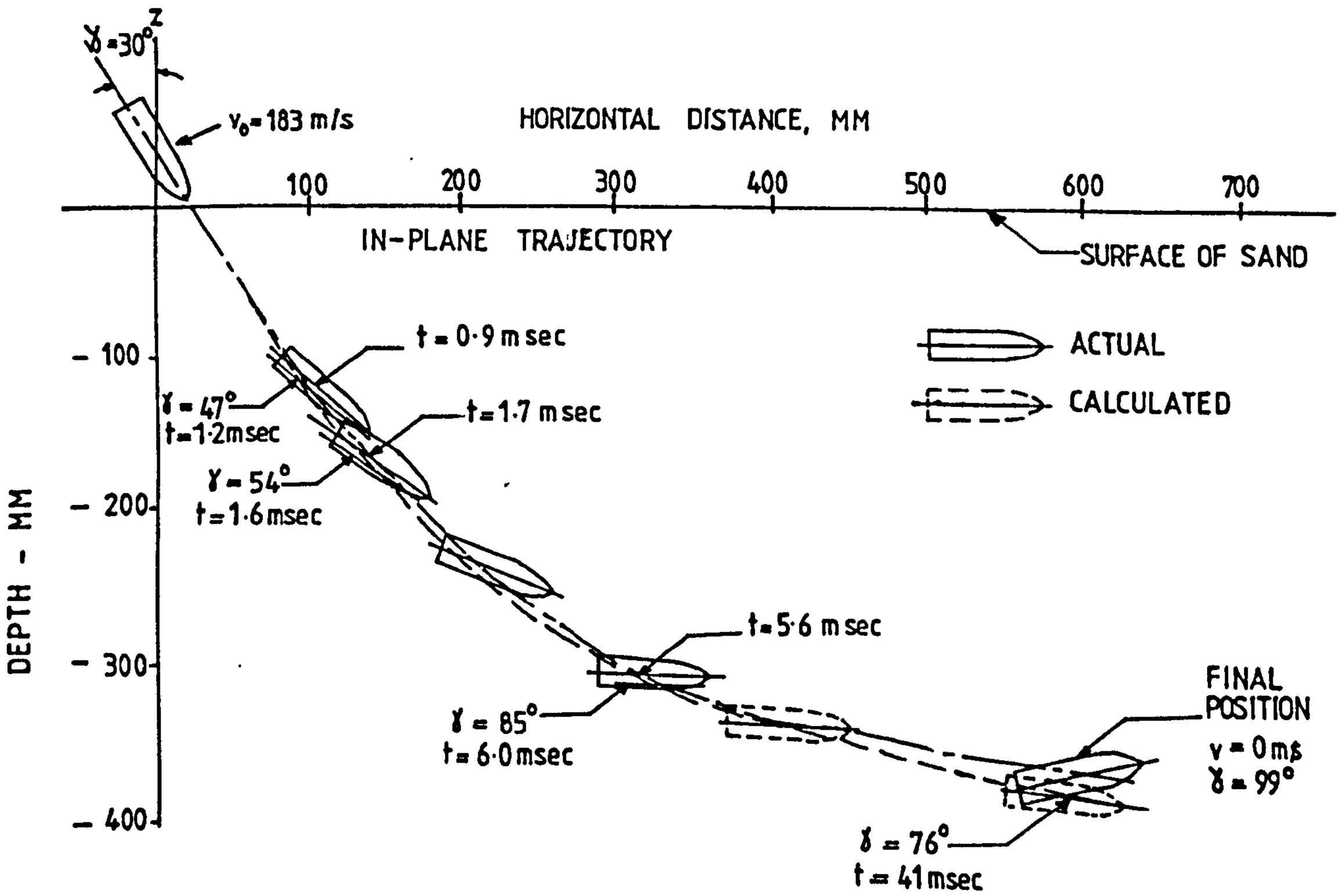

Figure 2.10 The Trajectory of a 20mm Projectile Impacting a Dry Sand Target: A Comparison of Experimental Data and an AVCO Differential Area Force Law Calculation
(Hadala, 1975)

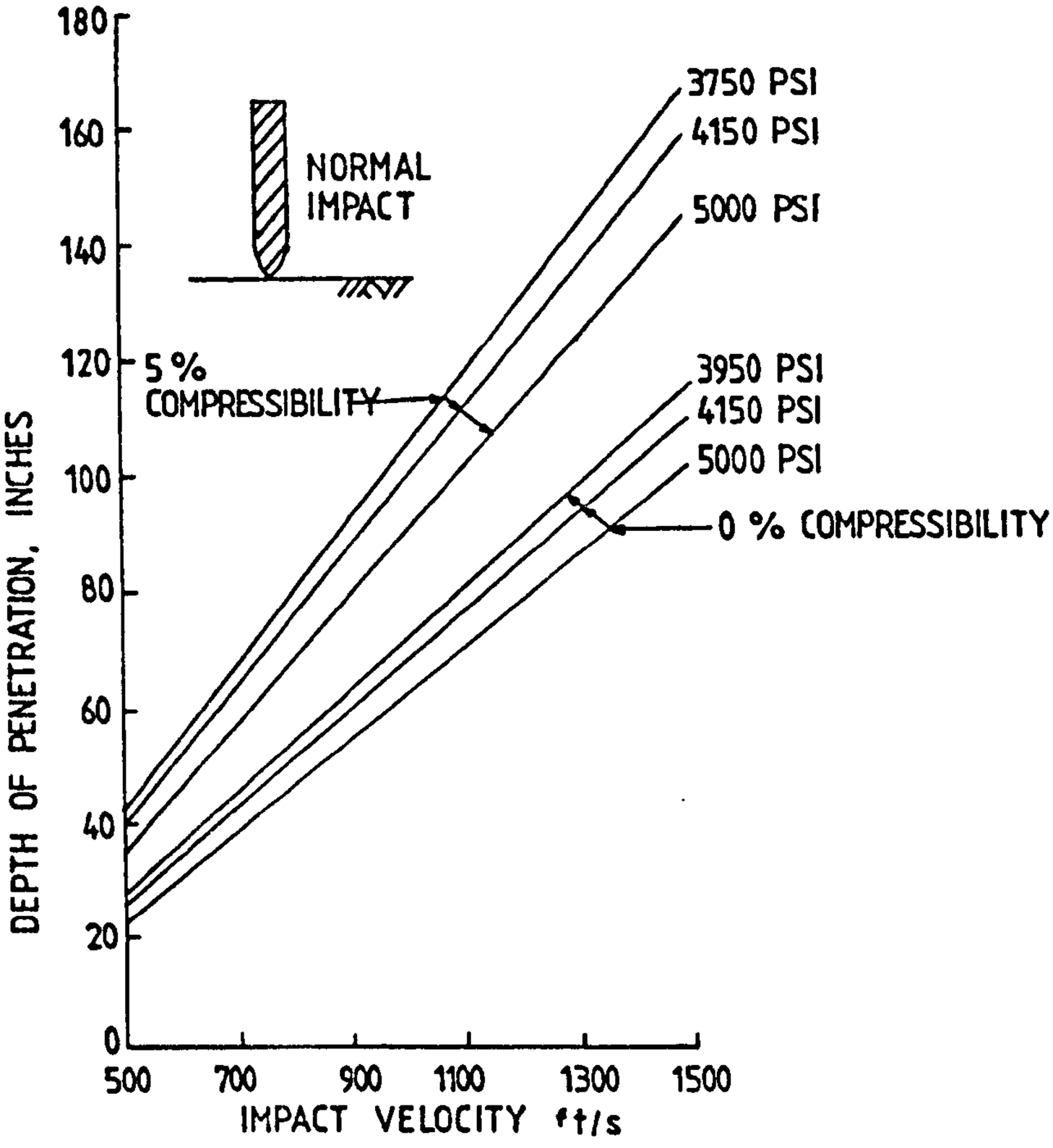

Figure 2.11 Calculated Depth of Penetration Against Impact Velocity for 0- and 5-percent Compressible Concrete Targets of Varying Strengths (Rohani, 1975)

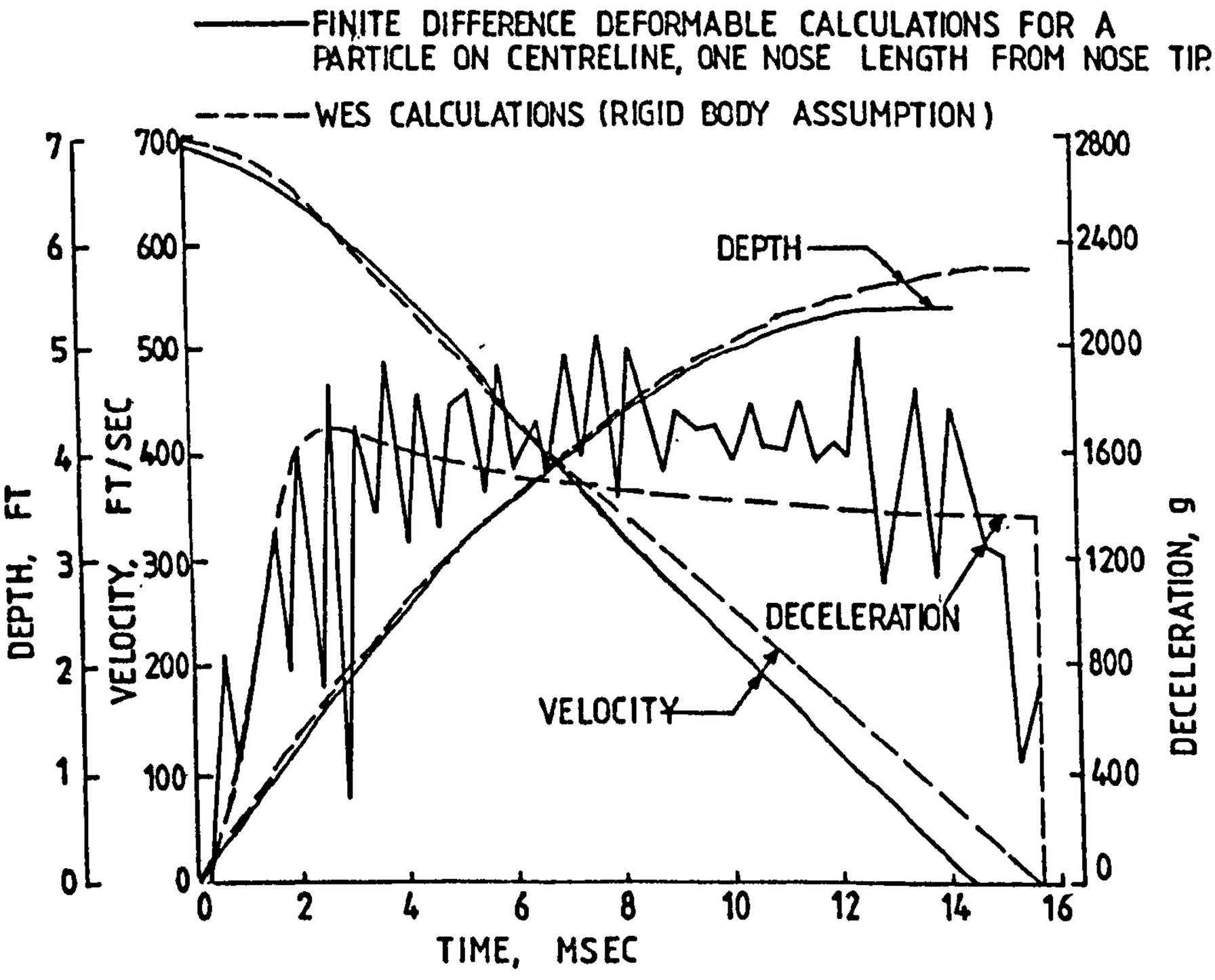

Figure 2.12 WES Rigid Body Motion-Time Histories Superimposed on Finite-Difference Deformable Body Calculations for Large-Scale (9in. 1000lb) Penetration of Rock (Welded Tuff) (Rohani, 1975)

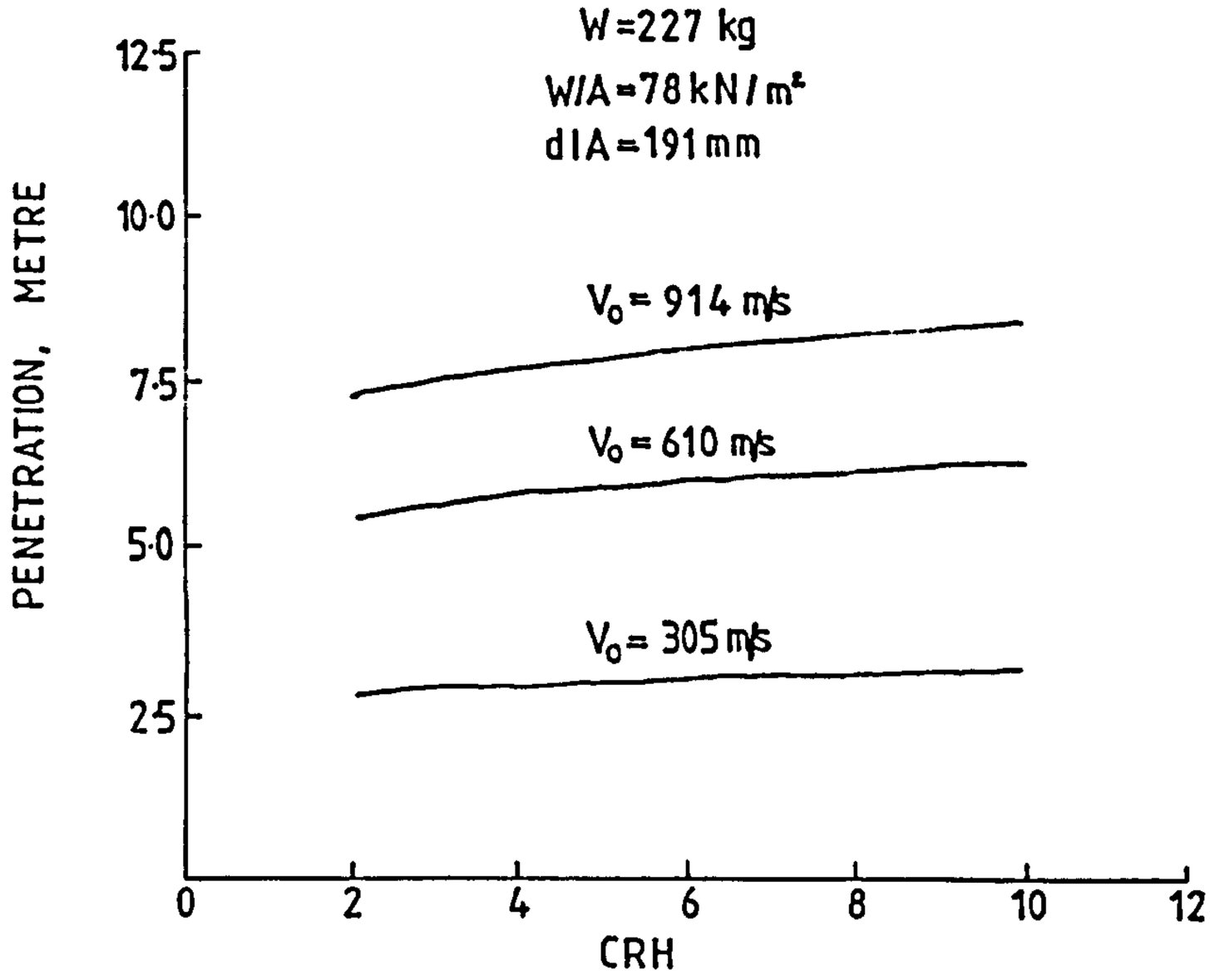

Figure 2.13 Effect of CRH on Predicted Penetration into Low-Strength Rock
(Rohani, 1975)

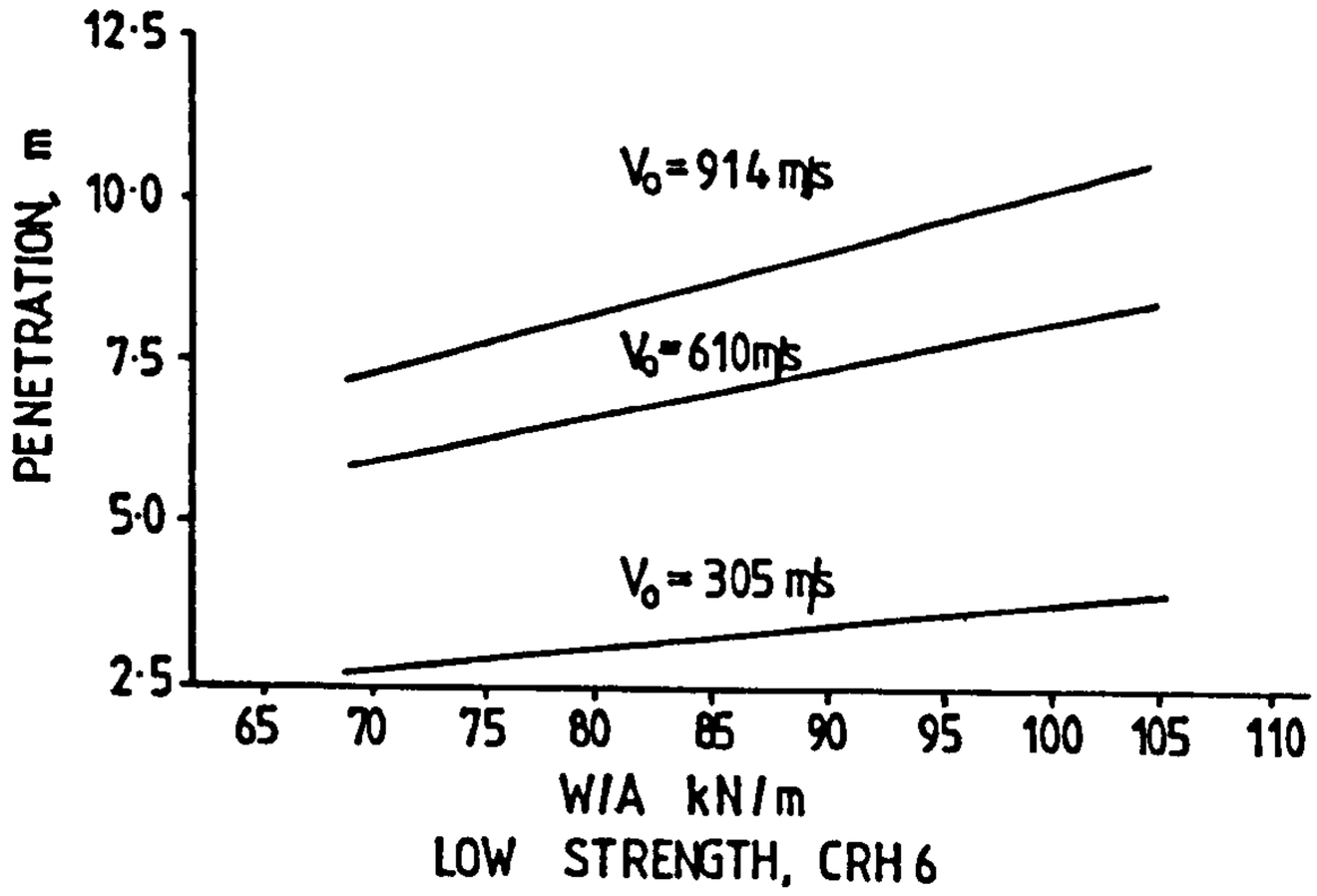

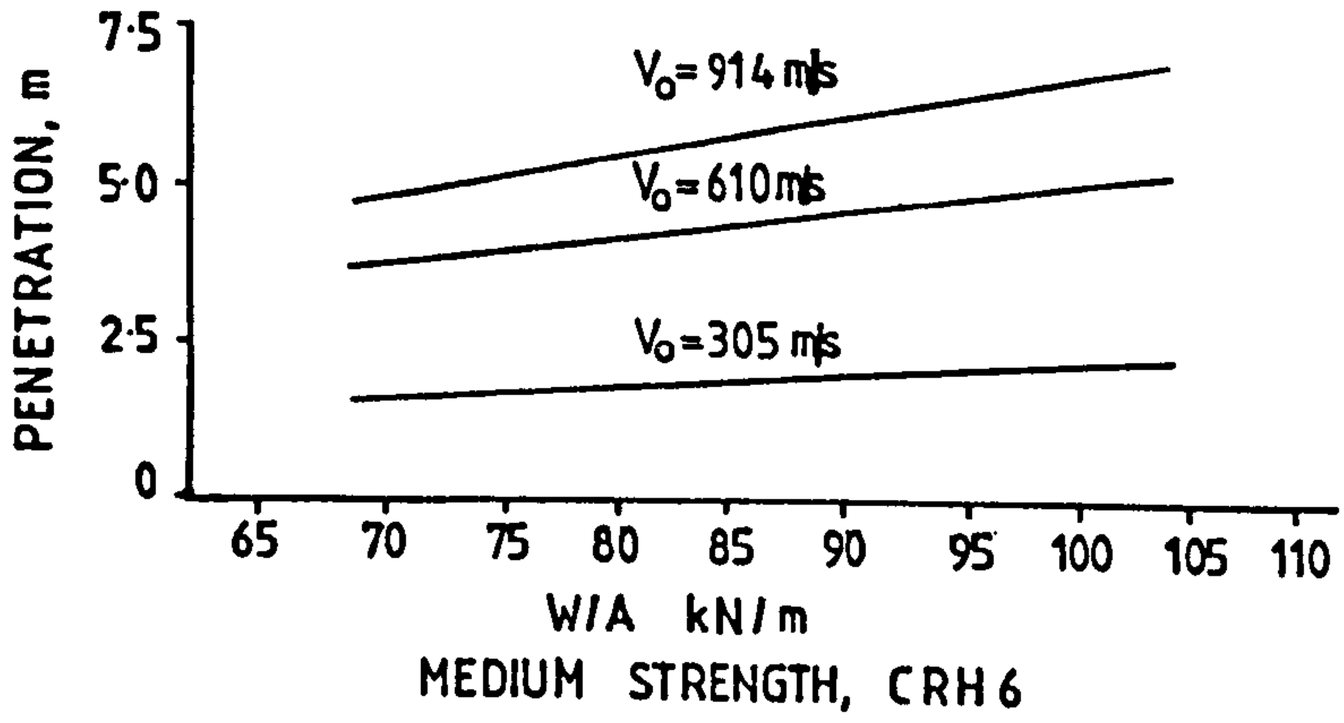

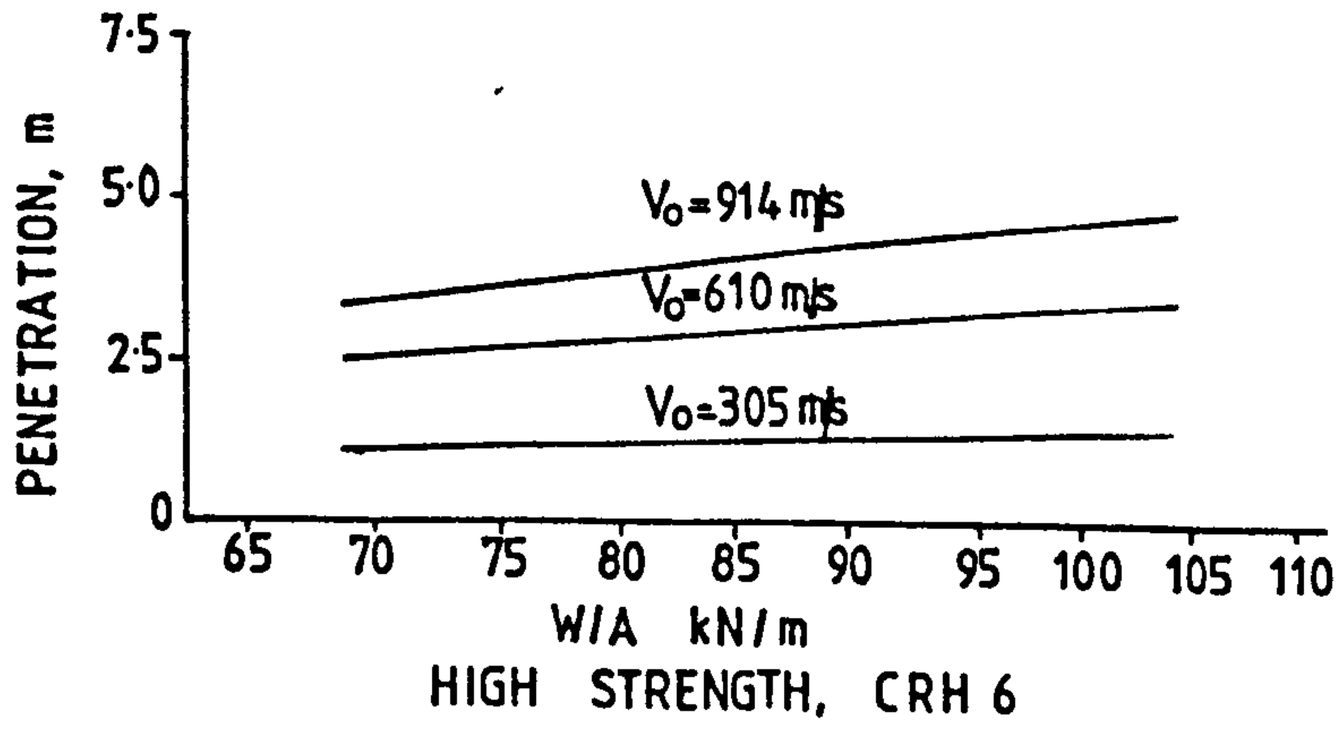

Figure 2.14 Curves Showing the Effect of Weight-Area Ratio, W/A on Predicted Penetration into Various Rock Types (Strengths)
(Rohani, 1975)

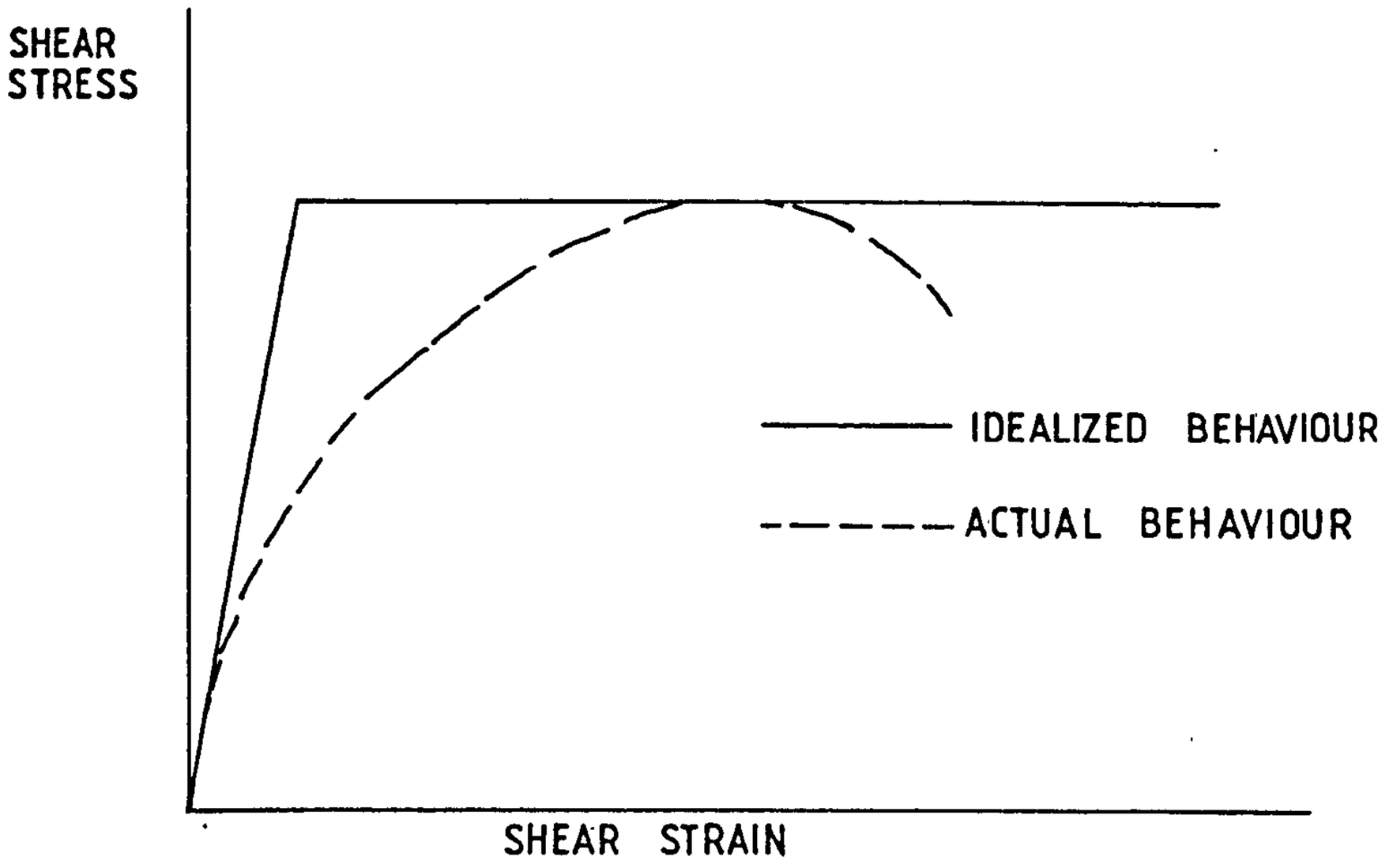

Figure 2.15 Plot Showing Idealization of Actual Stress-Strain Curve (Bernard, 1976)

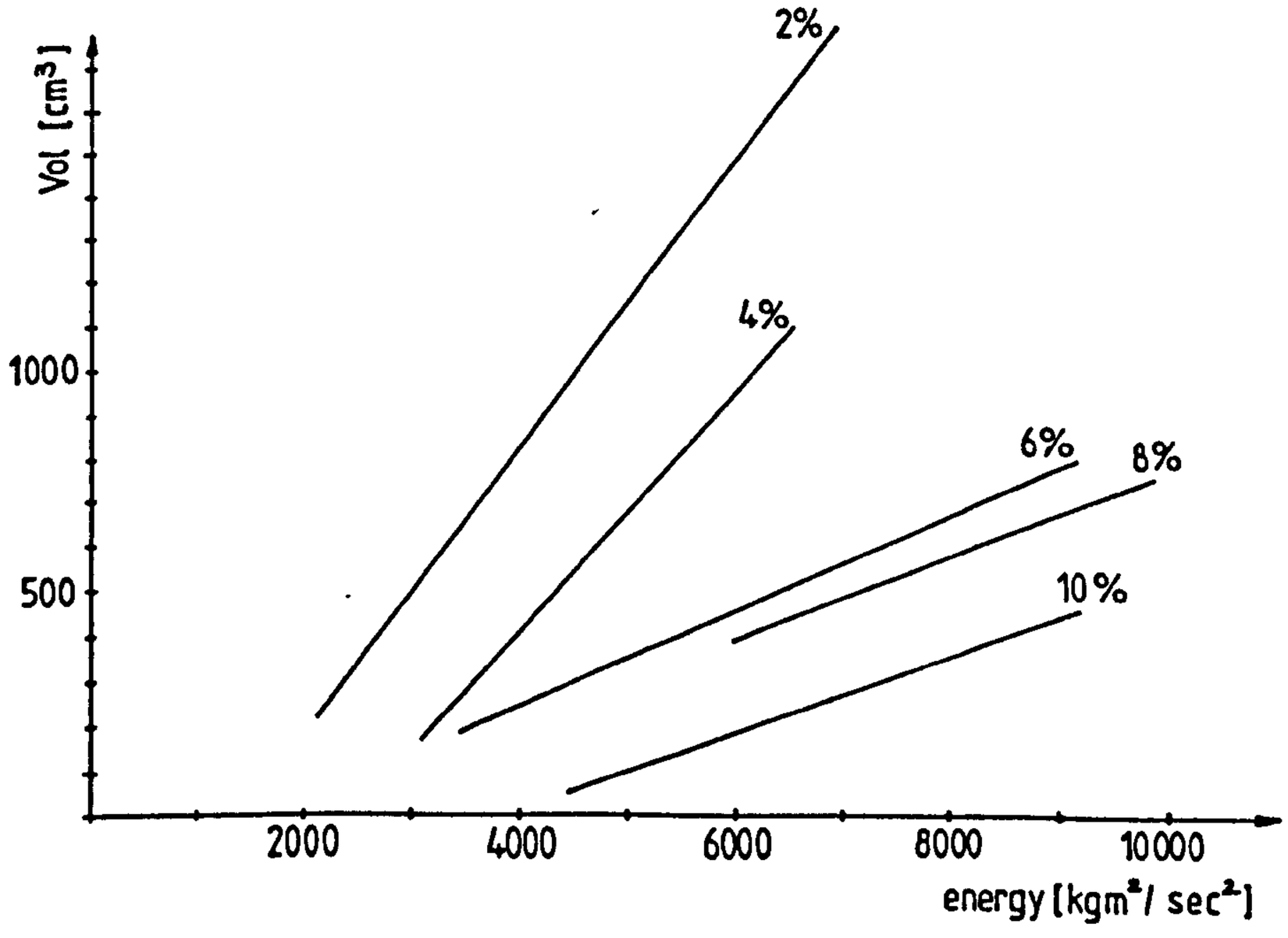

Figure 2.16 Fragmentation Zone Versus Energy for Different Degrees of Reinforcement
(Hulsewig et al, 1982)

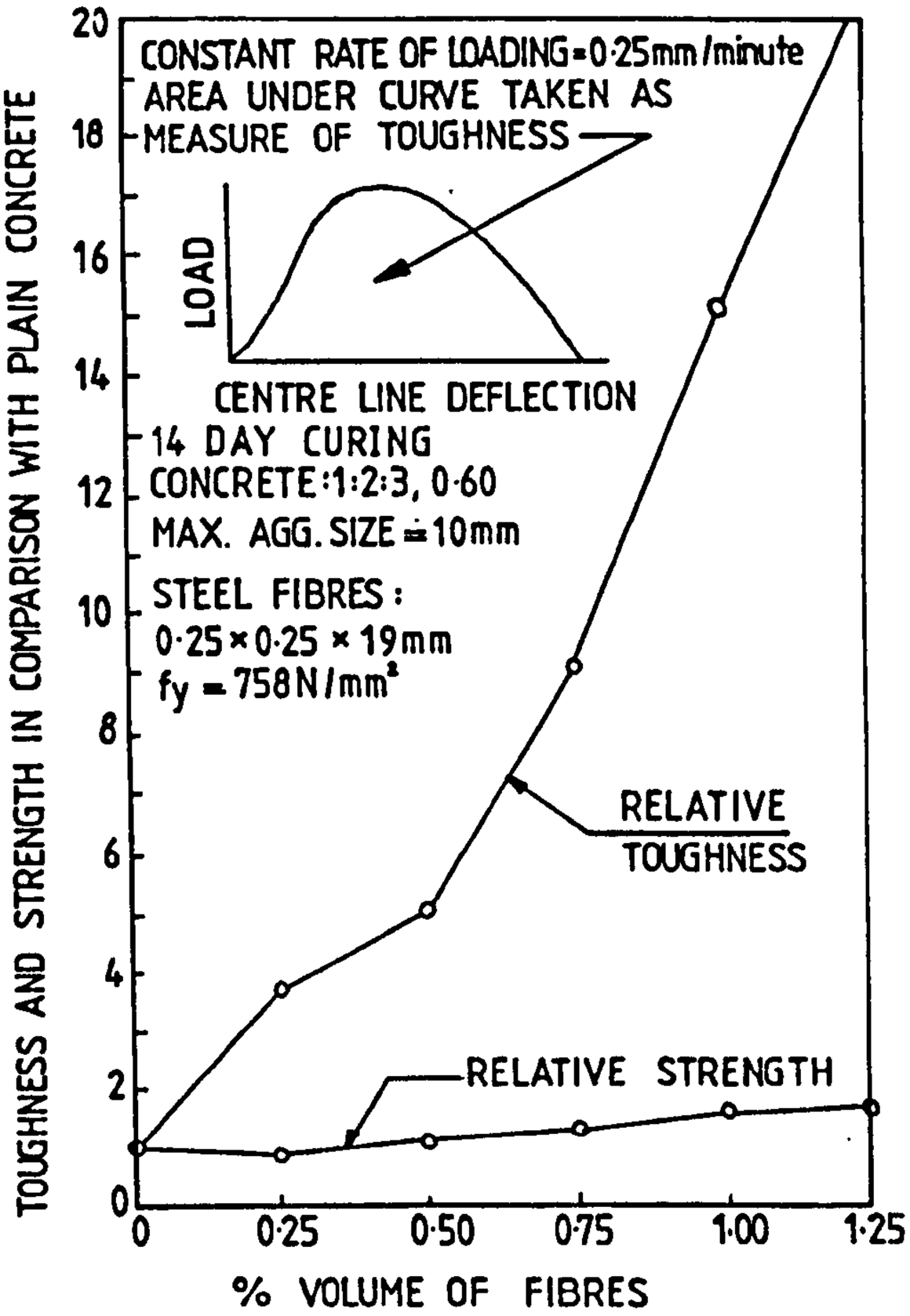

Figure 2.17 Effect of Fibre Volume on Composite Toughness and Strength in Flexure
(Shah and Ranagan, 1971)

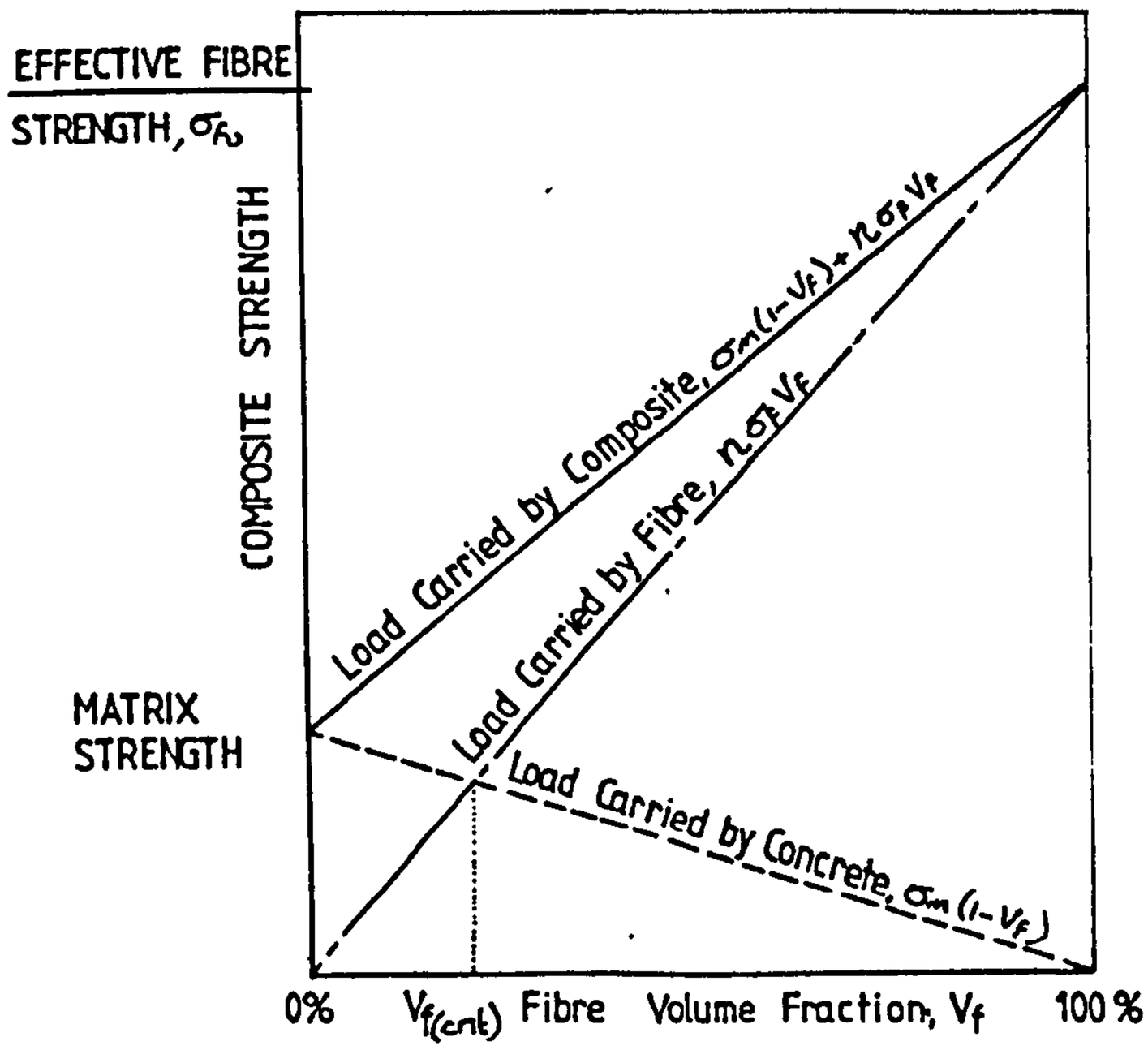

Figure 2.18 Variation in Fibre Concrete Strength with Volume Fraction of Fibres as Predicted by the Rule of Mixtures
(McCurrich and Adams, 1973)

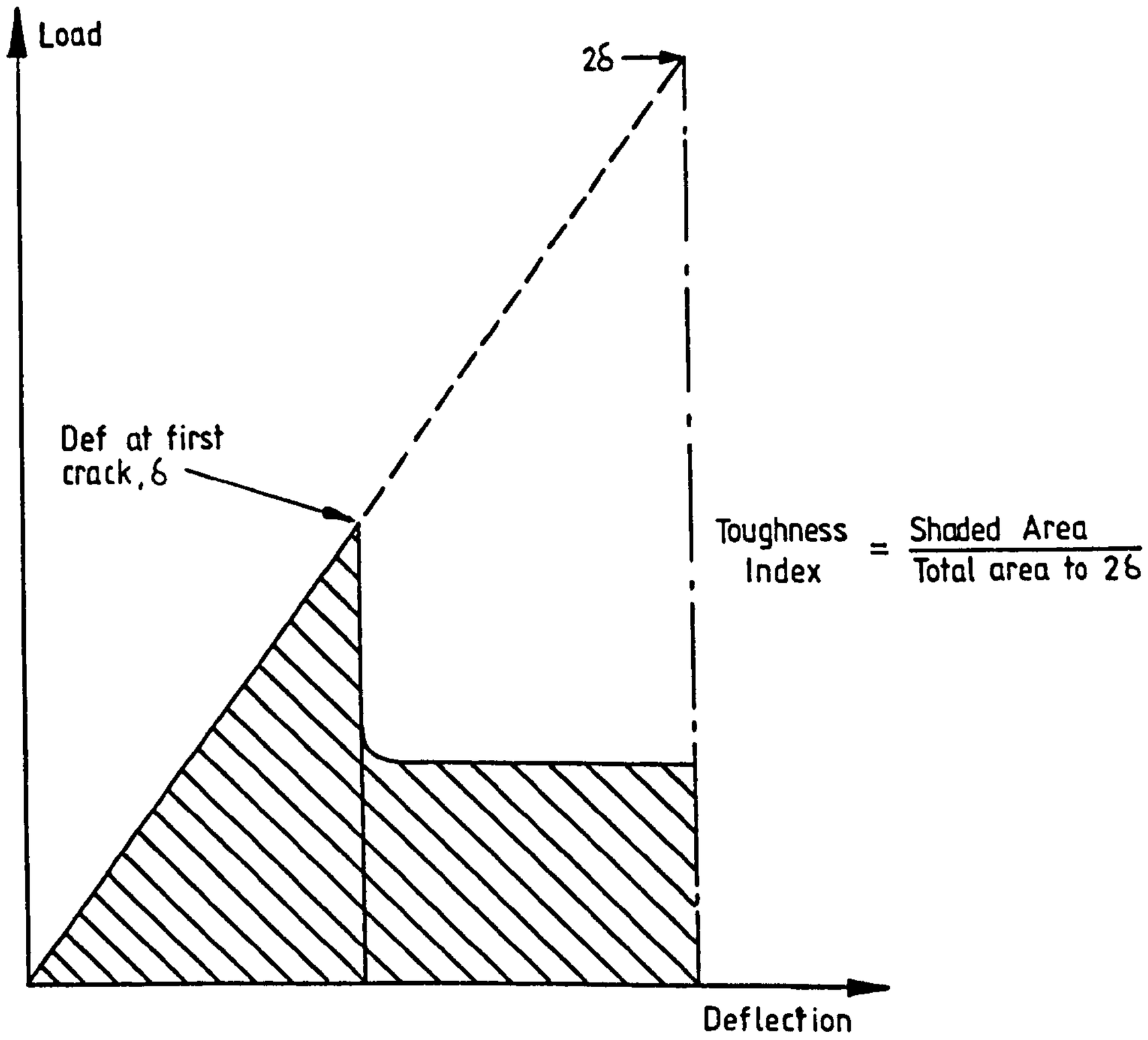

Figure 2.19 Proposed Definition of Toughness Index
(Barr et al, 1982)

5mm Aggregate

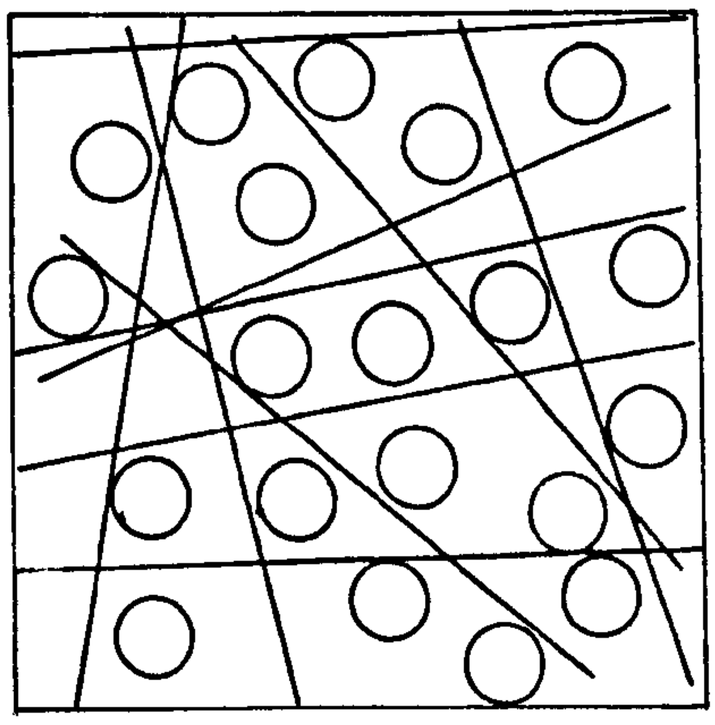

10mm Aggregate

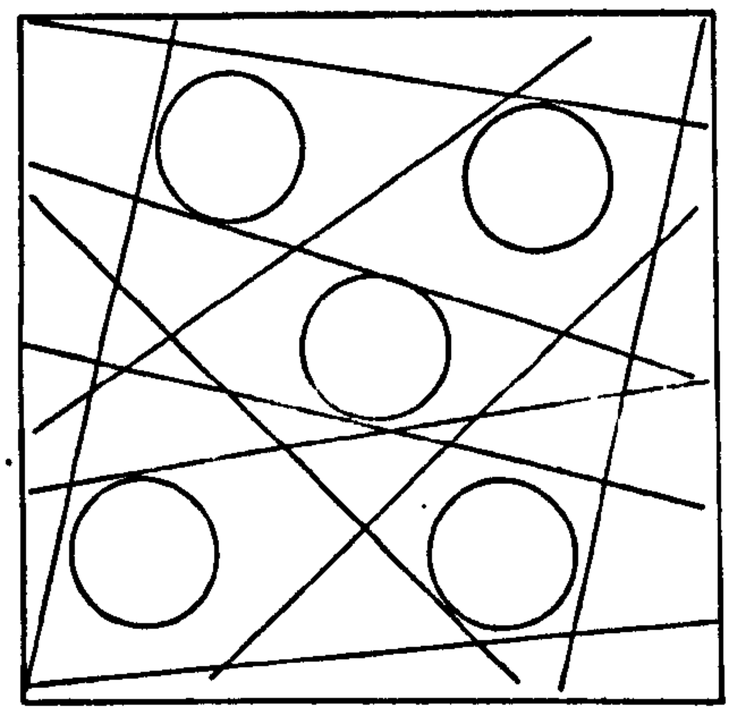

In all cases Fibre Length =
Square Side Length = 50mm

20 mm Aggregate

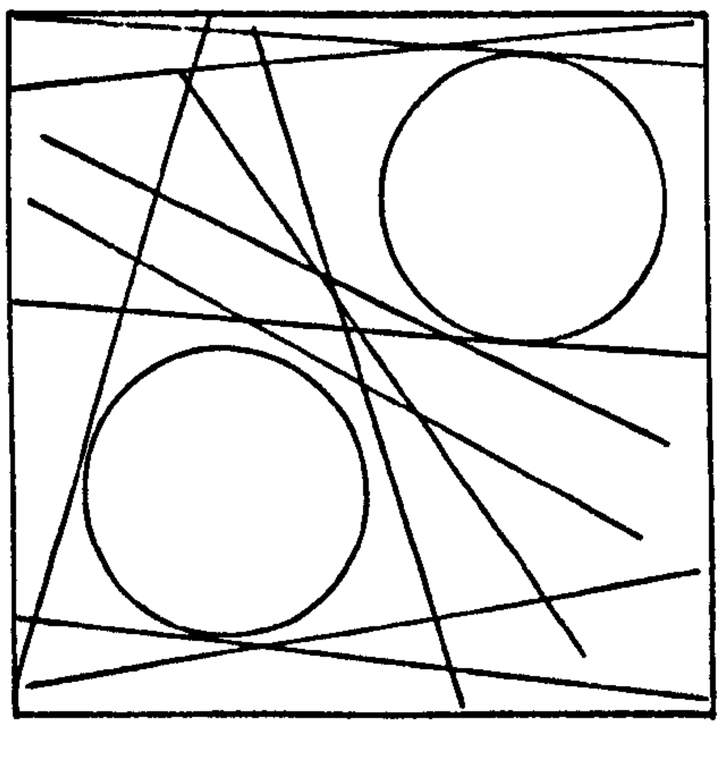

Figure 2.20 Effect of Aggregate Size on Fibre Distribution and Interaction (Hannant, 1978)

CHAPTER 3

MATERIALS, SPECIMEN PREPARATION, EQUIPMENT AND DAMAGE ASSESSMENT

3.1 Materials

Plain concrete has been used extensively in the construction industry for many years. It consists of a cementitious material capable of hardening progressively with time in the presence of water, and fine and coarse aggregates which act as filler and provide stability and strength to the cement paste.

The relative proportions of the cement, aggregate and water dictate the properties of the concrete. The tensile strength of concrete is only 10-20% of the compressive strength and to improve tensile behaviour, discrete fibres may be added to the mix.

This investigation has examined the value of using fibre reinforced concretes to defeat high velocity penetrators and the materials used are described in the following sections. Details of all material suppliers and equipment manufacturers may be found in Appendix II.

3.1.1 Mix Design

The design of the concrete mixes was difficult because the resultant material had to be suitable for sprayed application and had to include discrete fibres.

Available literature indicated an upper aggregate size limit of 10mm to ensure a random fibre distribution in an unconglomerated manner. For pumpability, a relatively cement rich paste is required, whilst the ratio of coarse to fine aggregate inclusions should be less than in a conventional concrete.

The proportion of the constituent materials differed as work progressed; however, in all cases, mixes were developed assuming a target density of 2400kg/m^3 and adopting "by weight" mix ratios.

3.1.1.1 Cement

Ordinary Portland Cement to B.S.12:1978 was selected as the standard basic constituent. Admixtures were not considered since these would not be readily available in some field situations.

3.1.1.2 Aggregates

Zone 2 or Zone 3 sands to B.S.882:Pt.2:1973 have been used as fine aggregates.

Three types of coarse aggregates were used: rounded river gravel, crushed limestone and crushed basalt. All of these complied with the requirements of B.S.882:Pt.2:1973 for 10mm single size aggregate and details of their properties are given in Table 3.1

3.1.1.3 Fibres

During the last two decades, many different fibrous materials have been incorporated into cementitious materials. Each material may be placed in one of two distinct groups, those which have a modulus of elasticity less than the host matrix, such as nylon, polypropylene, cellulose and vegetable fibre, and those of a greater modulus including steel, asbestos, glass, Kevlar and carbon. Low modulus materials generally suffer from a high rate of creep under load, such that they cannot maintain high stresses over a period of time without gross deformation of the cracked composite. They may also have a high value of Poissons Ratio, such that any extension in length will be reflected by a significant reduction in the fibre diameter, this leading to a lowering of bond strength with increasing load so that composite failure will occur by fibre pull-out. In order to improve the bond characteristics of these fibres, mechanical aids have been considered, for example, using a fibrillated polypropylene (much like parcel string) to allow interaction between matrix and fibre, or producing fibres with surface irregularities. High modulus fibrous materials do not normally creep much, but, due to the smooth nature of some types, e.g. drawn steel wire, it is often considered necessary to improve the bond

characteristics by either producing fibres with an indented shape, an irregular surface profile, or by changing the fibre shape, e.g. adding hooked ends or forming a sinusoidal profile.

Initially, no constraints were placed upon the choices of fibrous materials for this study. However, to reduce the experimental study to a manageable size, a number of fibrous types were rejected either before testing or in the early stages of the experimental work. These fibres are listed in Table 3.2 and the reasons for rejection stated.

Since for impact resistance it was felt that the greatest possible local energy absorption would be necessary, fibrillated polypropylene was chosen as representative of the low modulus group in an attempt to avoid fibre pull-out.

The choice of fibres with a higher modulus than the matrix material was even more difficult, since there is a very large variety of such fibres, particularly steel based ones. Several different methods of manufacture are applied to a number of grades of steel, the intention being to improve the mechanical bond between fibre and matrix, so that more of the impact energy is expended in fibre pull-out or, for fibres where an effective anchorage is generated, in fibre yielding. Both stainless and carbon steels with typical tensile strengths of 400 to 2100N/mm^2 are used in the manufacture of fibres, which may be produced in circular section by drawing, or as by-products of scrap sheet steel, this giving rise to rectangular or square section inclusions. Alternatively a melt extract process exists by which a spinning notched disc produces fibres from molten steel held in an induction furnace. The disc is just in contact with the metal surface and flicks off irregularly edged crescent-section fibres, the length being defined by the disc thickness. Drawn fibres may be mechanically deformed by crimping, bending or die-stamping, in order to improve the bond characteristics of the composite material.

Another high modulus fibre used was Kevlar, which is the trade name of a group of organic fibres, having very high strength. These fibres are produced as a large number of very fine (12μm) filaments in various lengths. Two types were suggested for use in concrete, PRD-29, a fibre with a modulus of 58kN/mm² and a tensile strength of 2760N/mm² and PRD-49, a higher modulus material (133kN/mm²) with the same strength. The lower modulus material was selected as it was considered adequate for inclusion in a matrix whose modulus was around 33kN/mm².

The types of fibre tested in the major part of this study are listed in Table 3.3 with an indication of their dimensions, costs and extent of usage. Further information about the manufacture of fibres and their use in concrete may be obtained from Hannant (1978).

3.1.1.4 Ammunition

At the selected size of projectile, 7.62mm, there was a choice of two conventional types of impactor. The first, and generally more common, of these was the standard ball type; whilst the alternative was the armour-piercing projectile. The core of the ball penetrator is formed of soft lead alloy, whereas the armour-piercing penetrator core is of hardened steel.

During the very earliest trials, the relative penetrability of the two projectile types was considered. A few comparative trials, using typical concrete mix designs, were carried out. These decisively indicated that the armour-piercing missiles generated significantly greater path lengths, since total core disintegration at impact did not occur, as it did with the softer lead alloy centres of the ball projectiles. This finding was in accordance both with earlier work on fibre reinforced sprayed concretes (RUC(1976), Finch (1977)) and also with studies carried out on rock/elastomer composites by Anderson et al.(1980). Since it was proposed to establish the limits for safety of the fibre-reinforced concretes, the 7.62mm armour-piercing projectile was selected as the standard impactor for

all subsequent trials. Details of both ammunition types are given in Table 3.4.

3.2 Specimen Preparation

3.2.1 Mix Production

A Creteangle Type ME pan mixer with a diameter of 900mm and a capacity of 0.113m³ was used. This enabled three standard sized specimens (450 x 450 x 125mm) and three 100 x 100 x 100mm cubes to be cast as a single batch. Composites containing a high percentage of fibre tended to bulk so it was not usually possible to cast all the specimens from one mixer load. Two equally sized half-mixes were then used. The included fibre contents were expressed in terms of percentage weight of plain concrete weight. See Appendix III for details of the relationship between fibre volume, theoretical fibre weight and practical fibre weight.

3.2.2 Moisture Content Measurement

During this work, all of the concrete material has been cast by pouring under site conditions. As such, it was not possible to completely dry the aggregate constituents. It was thus necessary to make an allowance for the free water content of the aggregate in calculating the weights of the various concrete constituents.

To have a reasonably quick measuring technique a 2kg sample of aggregate was tested in a standard siphon can as described in B.S..812:Part 2:1975. The siphon can measures moisture content relative to a known condition. In this case, the required constants were obtained for each aggregate in an oven-dry state, hence all moisture content values are given as percentage moisture content by aggregate dry mass. In analysing the results initially only a percentage (between 50-80%) of the measured value was assumed as aggregate surface water, the rest being taken as absorbed water. It was later decided that a more consistent result was obtained by assuming all aggregate moisture was available for combining with the cement during hydration. Although this is not a strictly valid assumption, its

consistent adoption meant that it was not necessary to estimate the actual values of absorbed moisture.

3.2.3 Material Mixing Technique

A standard mixing method was maintained throughout the project;

1 Charge mixer with fine and coarse aggregate, mix for one minute or until thoroughly combined.

2 Add Ordinary Portland cement and mix to a consistent material.

3 Add water, mix for one minute or until a consistent matrix exists.

4 Add fibre whilst mixer is rotating. The method dependent upon the characteristics of the material:

i) With steel and polypropylene fibre, the material was already in a reasonably separated state and was added to the matrix directly sieving through a 50mm mesh on to the moving surface. The action of the mixer paddles then ensured that a random distribution occurred, up to the practical limit of fibre inclusion.

ii) With the Kevlar materials each filament had a diameter of approximately 12 micron, and these clustered together and were extremely difficult to separate. To reasonably distribute the fibres, it was necessary to separate them into smaller clusters (approximately 50mm diameter) and then to pneumatically transport them, via a 50mm internal diameter hose, to the surface of the material. Whilst it was impossible to disperse the fibre as completely discrete inclusions, this led, with the lower fibre contents, to a reasonably uniform mixture. With higher fibre contents a significant amount of fibre clustering did occur.

3.2.4 Concrete Casting Moulds

After the preliminary testing, special timber units were manufactured. The first of these was a large mould, as shown in Figure

3.1, designed to hold nine 450 x 450 x 125mm slabs, whilst allowing them to be stripped by one person, if required. Later, two other five slab units, similar to Figure 3.1, were constructed and used in conjunction with the original one. All formwork was treated with Shell MRO, a standard mould release agent, before concrete casting.

Twelve standard 100mm cube moulds were also used.

3.2.5 Vibration Technique

A three-dimensionally random distribution of fibres through the concrete matrix was considered desirable for all specimens. It has been found that external vibration may lead to a non-three-dimensional distribution (Edgington and Hannant(1972)), whilst poker vibration, if not carried out properly may lead to a non-random distribution because the fibre originally close to the poker may be dispersed from it, leaving a zone of unreinforced material. A compromise of a Kango 950 electric percussion hammer fitted with a 140mm x 100mm rectangular plate was adopted to compact the concrete to a constant state, after which a plastic float was used to level and finish the surface.

3.2.6 Curing Method

Immediately after casting the specimens were covered with polythene sheeting and allowed to cure for 24 hours before the formwork was removed. The slabs and cubes were then placed in a high humidity room operating to B.S.1881:Pt.3:1970 requirements. The specimens were cured until immediately before testing when they were transferred, as a batch, to the firing range.

3.3 Penetration Tests

3.3.1 Gun, Gun Mounting Frame and Solenoid Firing System

Projectiles were fired from a number 3 pressure housing fitted with 7.62mm routine proof barrel. For the tests carried out up to 13:05:81, a barrel which had previously fired almost 12,000 rounds was used. After

this date a new barrel which had fired only 35 proofing rounds was substituted.

The gun was connected with its solenoid firing system and trigger linkage to a sturdy box section frame and rawl-bolted to the range floor (Fig.3.2). A D.C. solenoid, Philips Control type 32. was connected, via a stiff linkage, to the trigger mechanisms of the weapon. During testing, this connection was made just prior to the release of the trigger safety catch. Figure 3.3 shows the equipment in place, whilst Figure 3.4 shows the electrical firing circuit. The 11.4kgf, 18mm stroke length solenoid, rectified for A.C. mains connection, was itself triggered by a remote firing box comprising a safety lock-out switch and an off-biased firing switch. In order to reduce current fluctuation and electrical interference, all connections were co-axial and a large capacitor was placed across the live side of the two-pole switch. For several of the high speed photographic tests it was necessary to rectify the mains supply at the firing box rather than the solenoid. For this reason, the connectors at the solenoid were changed so that the bridge rectifier could be isolated without difficulty.

3.3.2 Target Specimen Holder and Mounting Frame

Preliminary tests carried out to assess typical target damage, indicated that a relatively large (450 x 450 x 125mm) and heavy (approximately 65kg) standard sample would be required to prevent gross cracking and tensile (back face) scabbing. A target stand which held the slab perpendicular to the bullet path whilst providing only edge restraint was manufactured from rectangular hollow section steel. Ease of positioning of the target was ensured by using a sloping frontal area, as shown in Figure 3.5. The frame was rawl-bolted to the range floor and the tight-fitting slabs were located by a series of rubber straps. The target face was 20m down range from the end of the gun barrel.

3.3.3 Projectile Velocity Measurement Equipment and Mounting Frame

Variations in projectile mass, amount to propellant, propellant temperature, barrel wear and mounting frame stiffness all have an effect on the projectile velocity. In order to detect "rogue" rounds, an optical velocity measurement rig as shown in Figure 3.6 was designed and constructed. Three identical bases were manufactured. Figure 3.7 shows the details, each station consisted of a 3V light source supplied from a constant power supply and a train of 50mm focal length bi-convex lenses incorporating a 2mm slit to provide a congruent beam of light. The light was focussed on a photodiode, part of an electronic circuit yielding a positive on-off triggering system as the light beam was momentarily broken. Each photodiode circuit was powered by an 18v battery pack, though output to the timing devices (initially a Racal-Dana 9903 electronic timer and a Racal-Dana 9904 electronic timer) was limited to approximately 13V, dropping to 1.2V as the light beam was broken by the passing projectile. Figure 3.8 illustrates the sharpness of the falling voltage profile, this making it eminently suitable as an electronic trigger.

The three stations were placed 1.5, 2.0 and 2.5m from the target front face, so that mean velocities 1.75 and 2.25m from the target could be obtained, both as a check on the timing equipment and also to give a value for the projectile deceleration. The stations were mounted on a 50mm x 30mm box-section steel frame at the 1m height of the bullet path. The first station was connected to the "start" channel of the first timer, the middle station to the "stop" channel of the first timer and the "start" channel of the second timer. Finally, the third station was connected to the "stop" channel of the second timer. In use cross-interference was encountered. Isolating the wiring gave very little improvement, so only two stations and the Racal-Dana 9904 timer were used for the majority of measured velocities. The stations were placed at 1.5 and 2.5m from the target face, leading to a mean velocity value at 2m from the target.

3.4 Penetration Test Procedure

The target was located in its holder, the gun loaded, the bolt replaced, the trigger-mechanism screwed down, the trigger-solenoid ,linkage connected and finally trigger mechanism safety catch released. The range door was secured and warning sirens sounded. If transient recording equipment was in use, this was armed, as were the electronic timers. The interlock key was then placed in the firing box and the off-biased switch was tripped.

In some cases, for example whilst using high speed cameras, the firing event was triggered by the instrumentation. In these cases an alternative interlock system was built into the firing sequence in order to maintain personnel safety.

3.5 Assessment of Damage

Preliminary tests showed that target damage consisted of several facets, present to differing degrees in different material combinations. Figure 3.9 illustrates the various characteristics. Basically, a crater was formed on the front face, a burrow dimensionally similar to the projectile diameter was generated through the material also occasionally a back face crater was caused by the removal of a "scab" of composite. Since this study was mainly concerned with the reduction of penetration and target damage for hard impact, a specimen was selected of sufficient thickness to ensure that scabbing never occurred. The two major failure characteristics were therefore, penetration path length and front crater volume. Techniques were developed to measure these in a consistent and repeatable manner.

3.5.1 Measurement of Projectile Penetration

For the very early tests, utilising the more consistent composites, a projectile path very nearly perpendicular to the target impact face (i.e. along the same line as the initial projectile flight path) was observed. This led to a decision to measure path length as normal penetration depth

from the target surface. When some of the other types of fibre and aggregate were incorporated, the projectile experienced a significant deviation from its initial line, in either a straight or curved direction in three-dimensions. Consequently normal penetration depth measurement became of limited value, since the actual path length could be much greater than the normal distance from target surface to projectile tip. An alternative measurement was recorded to take account of this effect. Immediately after testing crater volume was measured as described below. Then the specimen was positioned under a concrete coring machine fitted with a 100mm diameter bit, and a 125mm long cylindrical core encompassing the complete projectile path was removed from the specimen. This was placed in a Clipper concrete saw and 10mm thick slices were removed from the rear surface until the projectile tip was located. Using this point and the point of entry, it was possible to estimate a "most-likely" path for the projectile. The core was then sectioned along this path, normal to the target front surface, to expose the burrow and penetrator. In cases where a three-dimensional (rather than a planar) deviation had taken place, a further step was required. This involved the "joining up" of the exposed sections of the burrow by removing small amounts of concrete using a 4mm width cold steel chisel and small hammer. After the path was fully exposed it was measured as distance travelled using an appropriate method (Figure 3.10).

3.5.2 Measurement of Crater Volume

The impact and subsequent penetration of the projectile, coupled with effects generated by the stress wave motion, caused the formation of a front face crater in the specimen. The actual dimensions of this crater were dependent upon the composite constituents and properties. Initially it was considered that stereometric photography, coupled with computer analysis to generate a three-dimensional "ground-model" would be the most appropriate measurement method, since it allowed a maximum of information

to be recorded and stored before the specimen was dissected to expose the projectile path. However, after preliminary investigation, it was realised that the very large number of samples required to carry out a valid statistical or parameter study precluded the use of such a time-consuming approach. It was decided to develop a mechanical version of this optical procedure.

Figure 3.11 shows the general approach, a 125mm stroke length Linear Variable Displacement Transducer (LVDT) was placed accurately, relative to a known datum, in a perspex frame. This was situated on a perspex base-plate which could be accurately positioned on the specimen front face. The base-plate carried a central grid of 40 x 40 holes, spaced at 5mm intervals, giving an area large enough to cover the biggest crater. The LVDT was connected, through an 8-bit μMac PETSET 1 analogue-digital converter, to a Commodore 3032 Microcomputer, itself coupled to a printer and disk-drive. Thus, at grid spacings dependent upon the accuracy required, a series of three-dimensional coordinates (i.e. a depth reading at known plan coordinates) could be developed by placing the LVDT probe on the crater surface at each point in turn and transmitting the voltage (as a digital value) to the microcomputer. The computer was programmed to accept a complete set of data, to store it on disc if required, and then to calculate the crater volume using the standard trapezium rule, first in a "rows" direction and then in a "columns" direction, giving an arithmetical check for the computer program. It was also possible to generate a series of crater profiles using the collected data, again in two orthogonal directions. Figure 3.12 gives details of the connections between the various components of the system. Appendix IV contains more details of the computing approach and a full program listing.

Several points are worthy of further comment.

i) An 8-bit Analogue-Digital converter allows for a resolution of 0-255 in 256 intervals.Using this in conjunction with a 125mm LVDT therefore, a resolution of 125/256mm approximately 0.5mm was possible for depth measurements. Due to the limitations of accuracy as discussed in ii) below, this was considered a reasonable compromise, since the maximum aggregate size was 10mm and the alternative type of A-D converter would have been a much more expensive 12-bit version capable of a resolution of 125/4096 (.03)mm.

ii) Early sectioning of post impact specimens showed the kind of effect recorded on Figure 3.13. That is, a zone of obviously damaged material below the visible crater. The initially present void was therefore defined as an "apparent crater". the "true crater" was exposed by removing the damaged concrete using a 4mm cold steel chisel and small hammer, cutting the restraining fibres when necessary. The volume of this "true crater" was then measured. This approach was deemed appropriate as it was considered that the extensively damaged zone could contribute little to the continuing integrity of the specimen. That is, under further attack, the loose and fractured areas would add little or nothing to the overall material resistance.

iii) An important advantage of this approach was the recording of the data on disk, since this permitted further manipulation. For example, contour plans of the craters are possible using the stored data, whilst a digital ground model may also be developed. Since the subsequent coring and sectioning procedure caused a great deal of irreversible damage to the crater areas (particularly if the largest crater diameter was

more than the 100mm core bit diameter), it was valuable to retain the maximum possible information.

10mm single size Aggregate type	Description	Oven dry specific gravity	Saturated surface dry specific gravity	Aggregate crushing value	Aggregate impact value
Limestone	Angular light grey crushed rock	2.67	2.68	23	23
Basalt	Angular dark grey-green crushed rock	2.75	2.82	17	17
River gravel	Mixed quartzite quartz, flint, sandstone, limestone	2.57	2.60	19	25*

* Quartzite component only.

Table 3.1 Details of B.S.812:1975 Properties for Coarse Aggregates Used.

Fibre Material Type	Reasons for exclusion from test programme
Asbestos	Hazardous material
Carbon	High capital cost for full parametric study.
Cellulose	Hygroscopic, dimensions vary with the moisture content, material rots.
Glass	Alkaline attack causing brittleness in OPC matrices. Alkaline resistant glasses [e.g. cem-FIL] available only for non-structural applications.
Nylon	Polypropylene had similar properties at a more economic price.
Rock Wool	Difficult to produce consistently in a form useful for incorporation into concrete.
Vegetable	Sensitive to moisture changes, often difficulties with congolmeration during mixing.

Table 3.2 Fibre Types considered but not used, with reasons for rejection.
(Ref: Hannant (1978), RILEM Tech.Com.19FRC(1977))

Fibre Type	Dimensions (mm)	Cost/kg	Used for tests in sections
Mild steel circular	38 x 0.3dia	N/A	4.2.1
Mild steel circular	27 x 1.0dia	N/A	4.2.1
Melt extracted carbon steel	35 x $\overline{0.3}$dia	N/A	4.2.2, 4.2.3
Cold-drawn circular steel	30 x 0.3dia	N/A	4.2.3
(ME) Melt extracted carbon steel	25 x $\overline{0.3}$dia	183p at June 1983	4.3.1,
(DRA) Circular drawn brass-coated carbon steel	25 x 0.25dia	82.5p at January 1982	4.3.1 4.4.1
(DUO) Circular drawn brass-coated indented carbon steel (Duoform)	25 x 0.25dia	82.5p at January 1982	4.2.3,4.3.1, 4.4.1
(13K) Kevlar-29 (Type 970) polyamide	13 x 12μm	US$13.85 at January 1982	4.3.1
(37K) Kevlar-29 (Type 970)	37 x 12μm	US$16.23 at January 1982	4.3.1
(POL) FORTA FIBRE latticed bundled polypropylene	37mm length	US$13.09 at January 1982	4.3.1

Table 3.3 Fibres used during optimisation procedures

a) 7.62mm NATO armour-piercing (AP) P80 ammunition	
General description	Cartridge comprising: case, bullet, lead alloy sealant, percussion cap and propellant charge. Total assembly length = 71.1mm
Bullet (i.e. object in flight)	Bullet jacket made from 90/10 gilding metal. Bullet length = approximately 33mm Bullet mass = 9.6 - 9.9g.
Core of bullet	Hardened steel, Length = 23.8mm, Diameter = 6.10mm Core mass = 3.74g
Stated Mean Velocity	825m/s @ 20m @ 21°C
b) 7.62mm NATO ball ammunition	
General description	Cartridge comprising; case, bullet, percussion cap and propellant charge. Total assembly length = 71.1mm. Total assembly weight = 24.4g.
Bullet (i.e. object in flight)	Bullet jacket - 90/10 gilding metal Lead alloy core Bullet length = approximately 29mm. Bullet mass = 9.3g.
Stated Mean Velocity	849m/s @ 5m.

Table 3.4 Details of projectiles used for testing (Manufacturers specification)

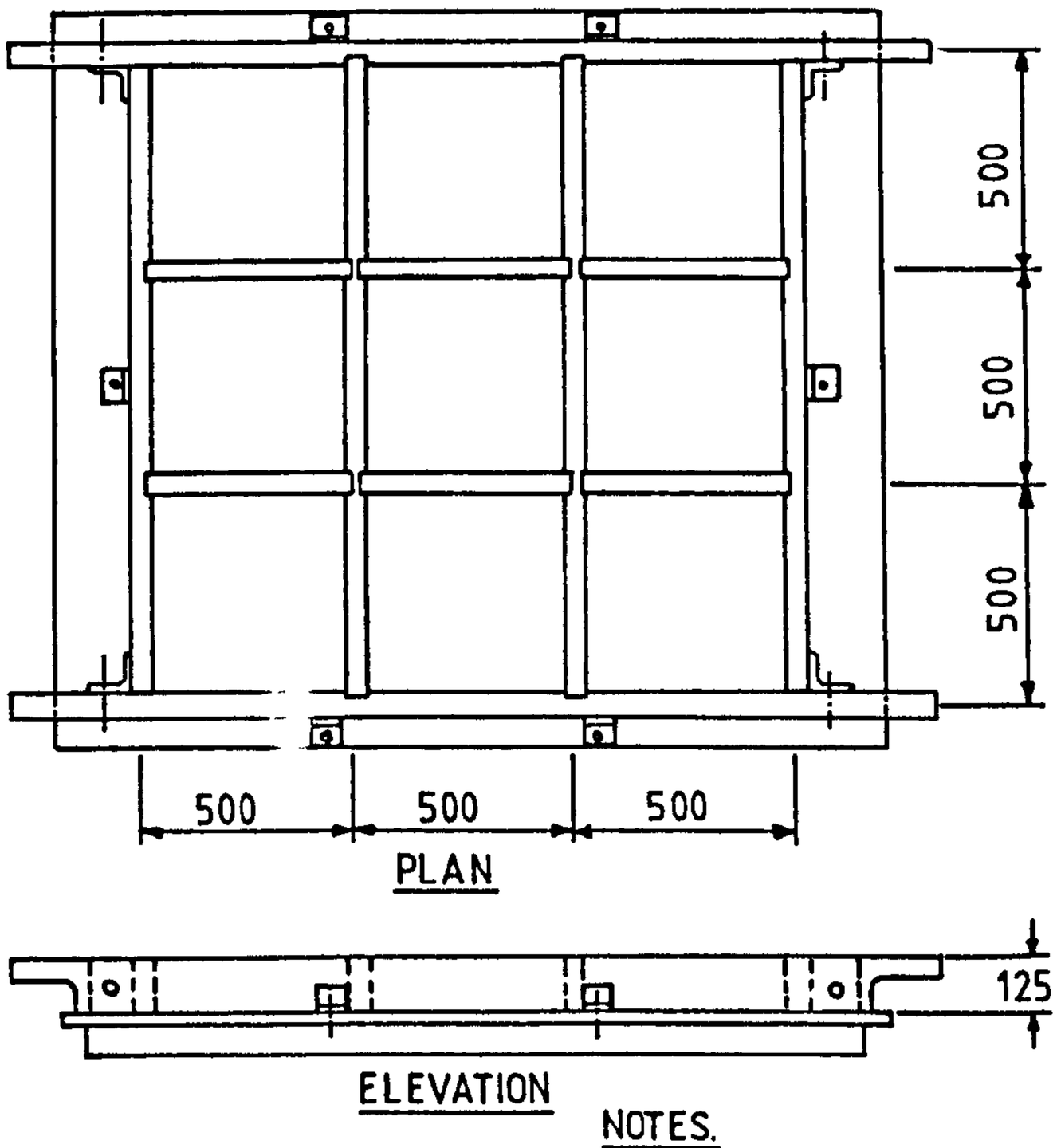

NOTES.

1. All main timbers 125 × 50 mm
2. Base 25 mm blockboard
3. Base Angle sections 60 × 60 mm
4. Corner Angle sections 100 × 100 mm
5. All bolted connections incorporate wing nuts

Figure 3.1 Timber Form to Cast 9 No 450mm x 450mm x 125mm Concrete Slabs

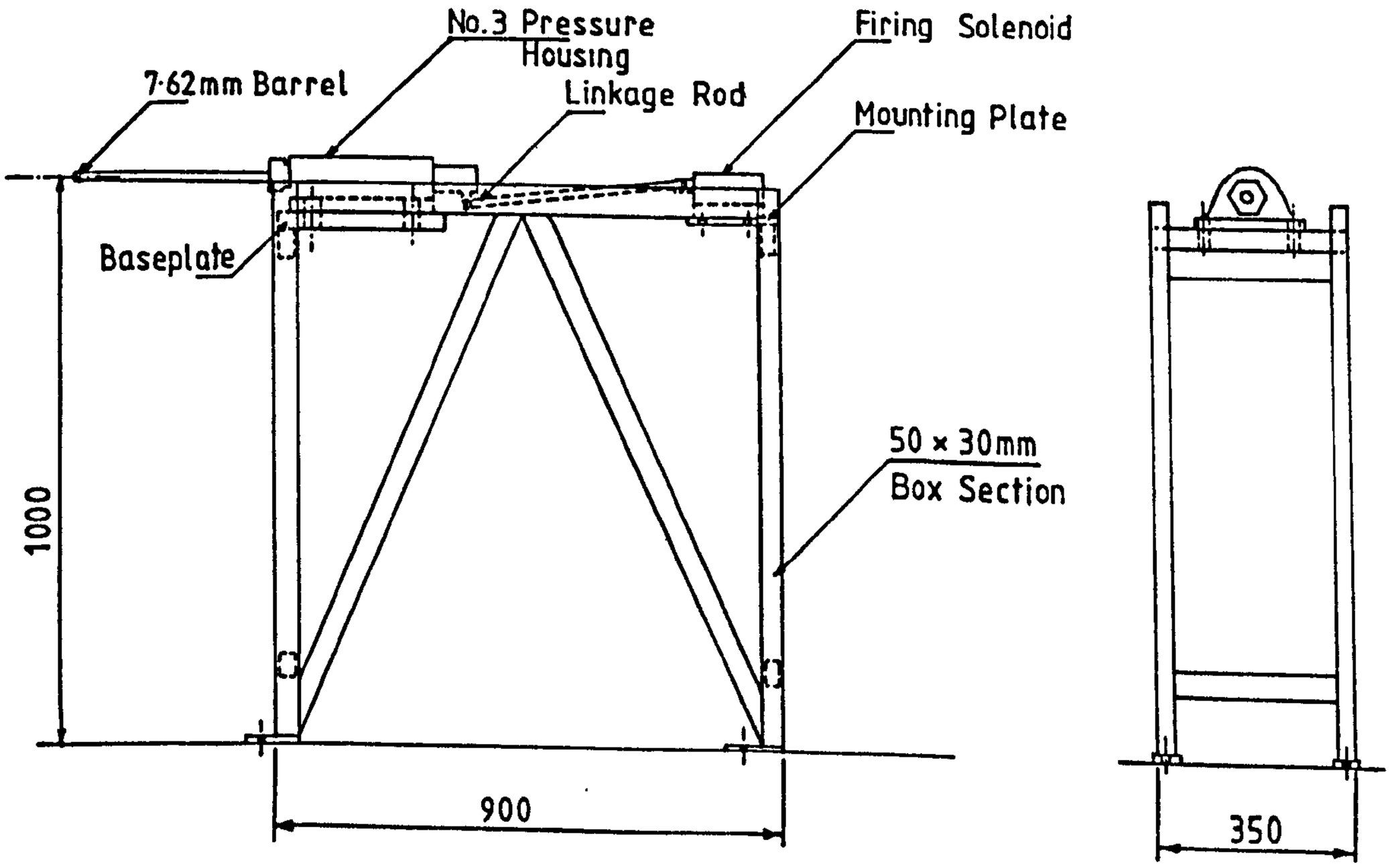

Figure 3,2 General Arrangement of Gun and Solenoid Activated Firing System.

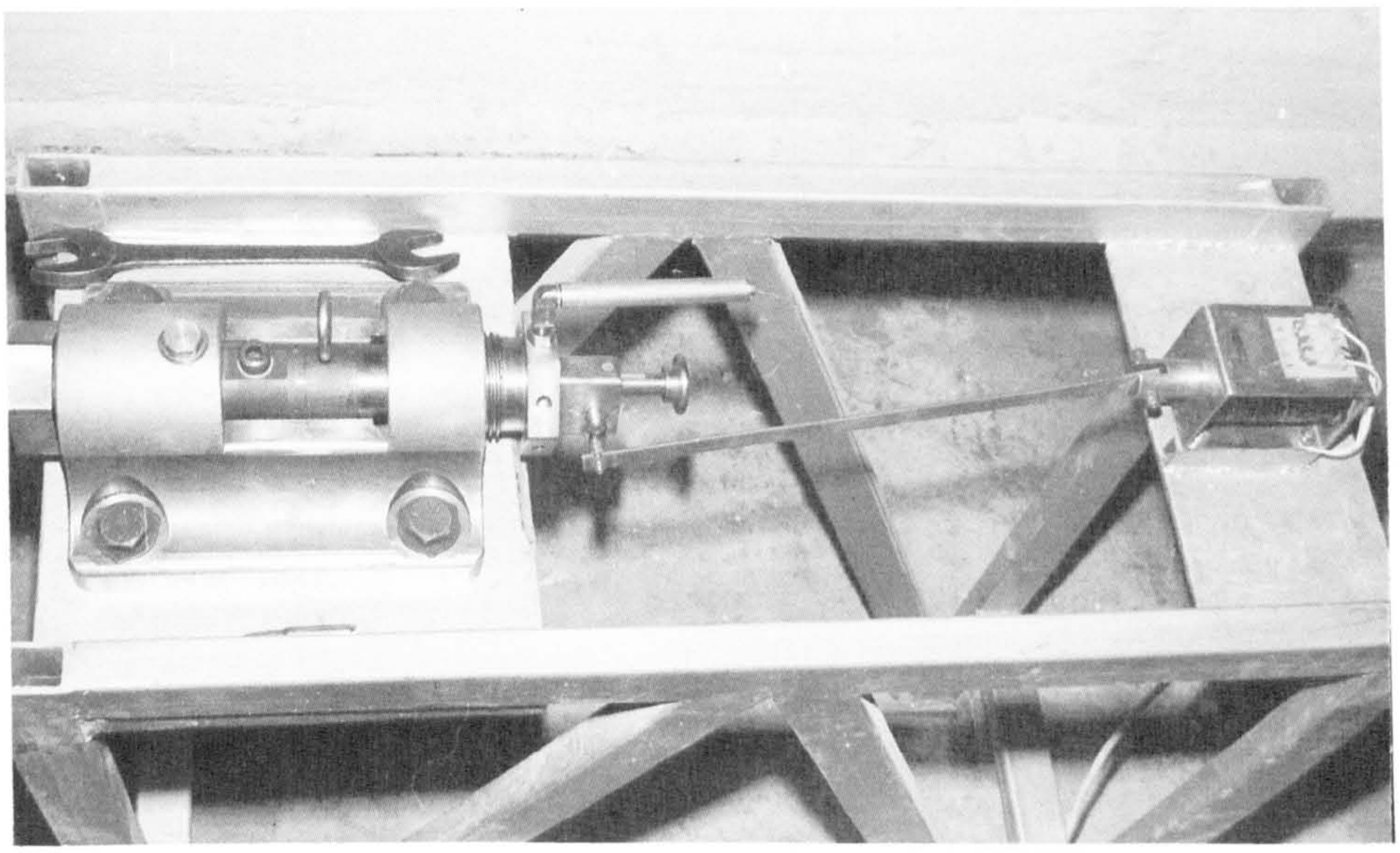

Figure 3.3 Detail of Gun, Breech and Solenoid Linkage

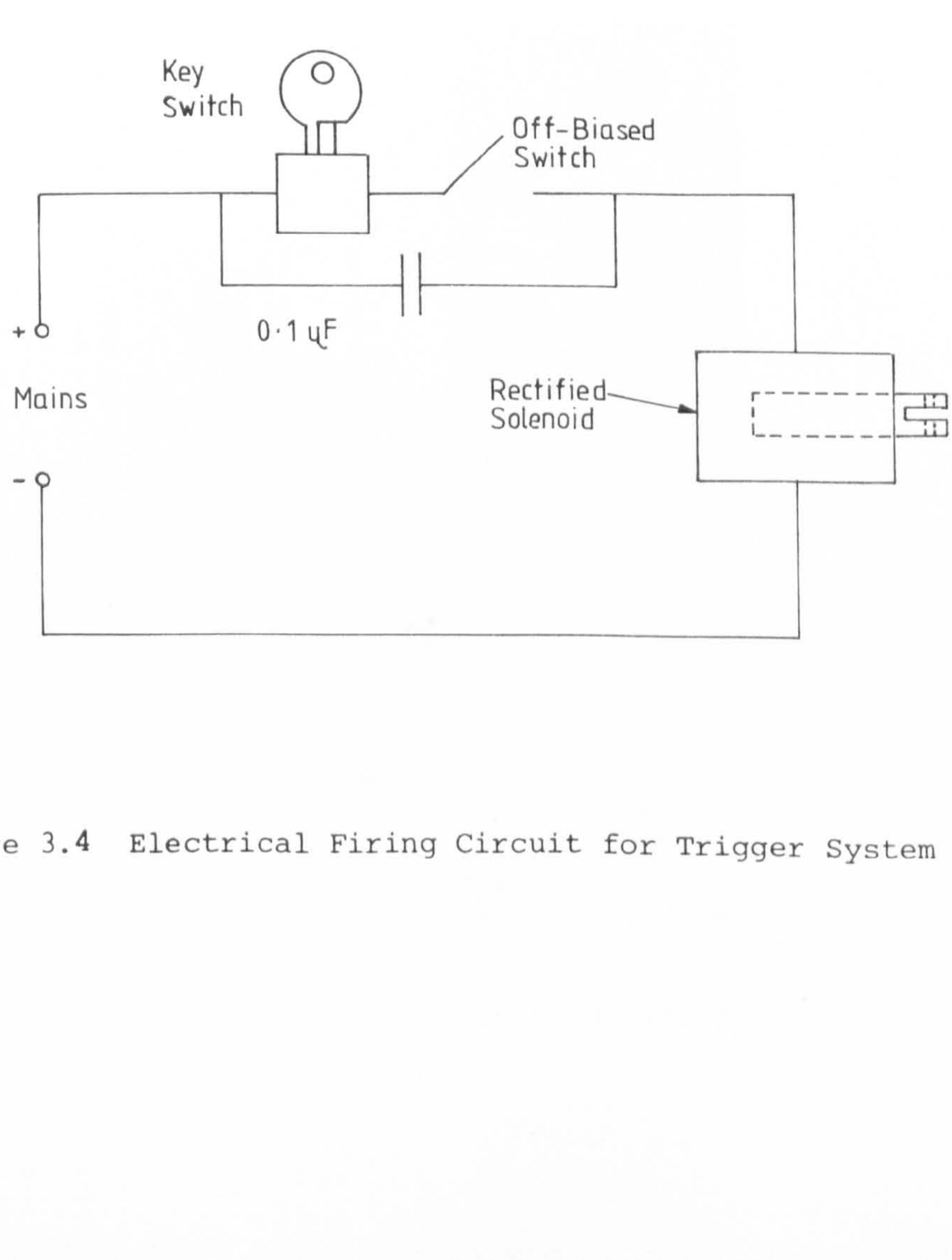

Figure 3.4 Electrical Firing Circuit for Trigger System

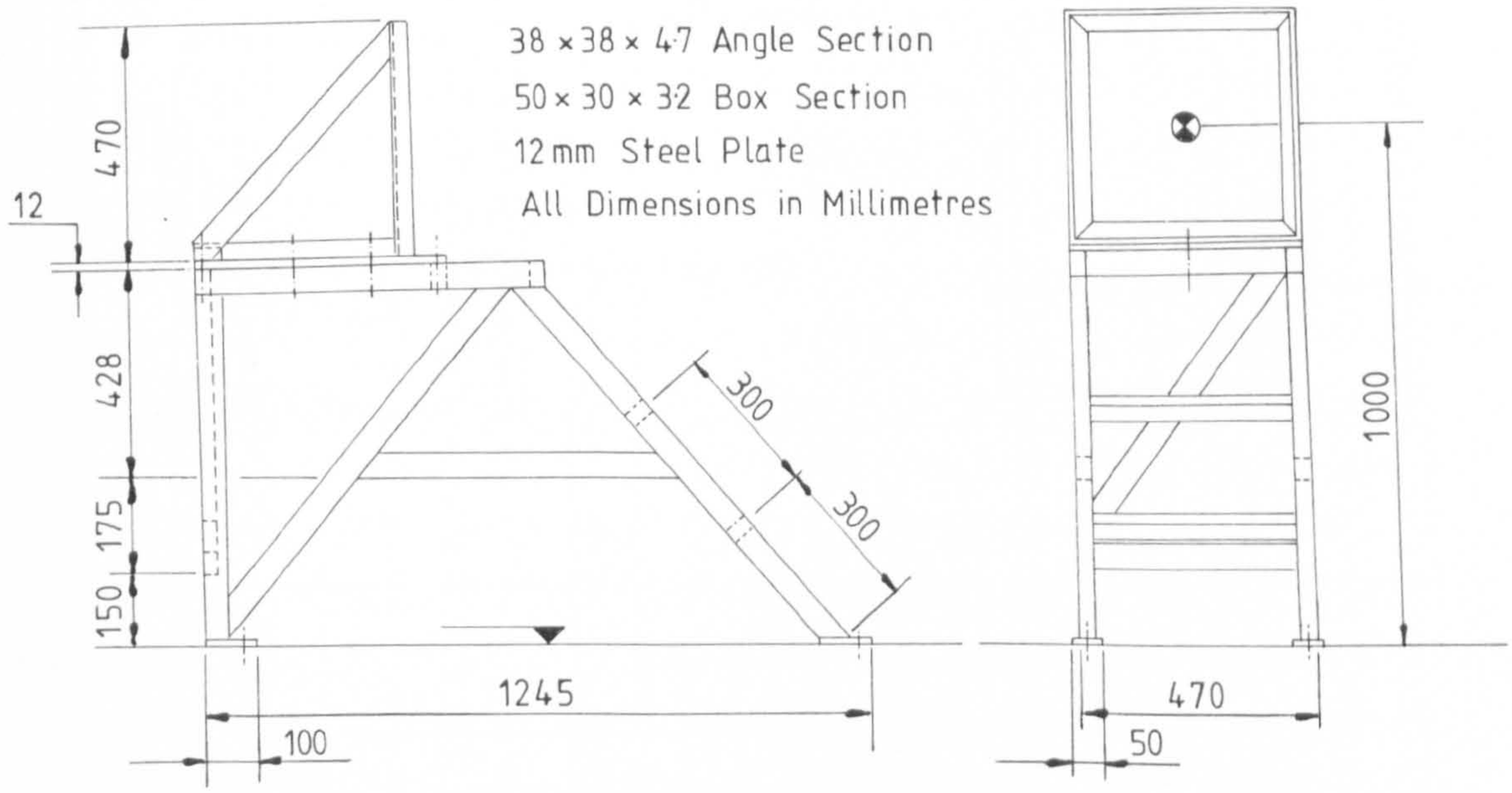

Figure 3.5 Target Frame for 450 x 450mm Specimens

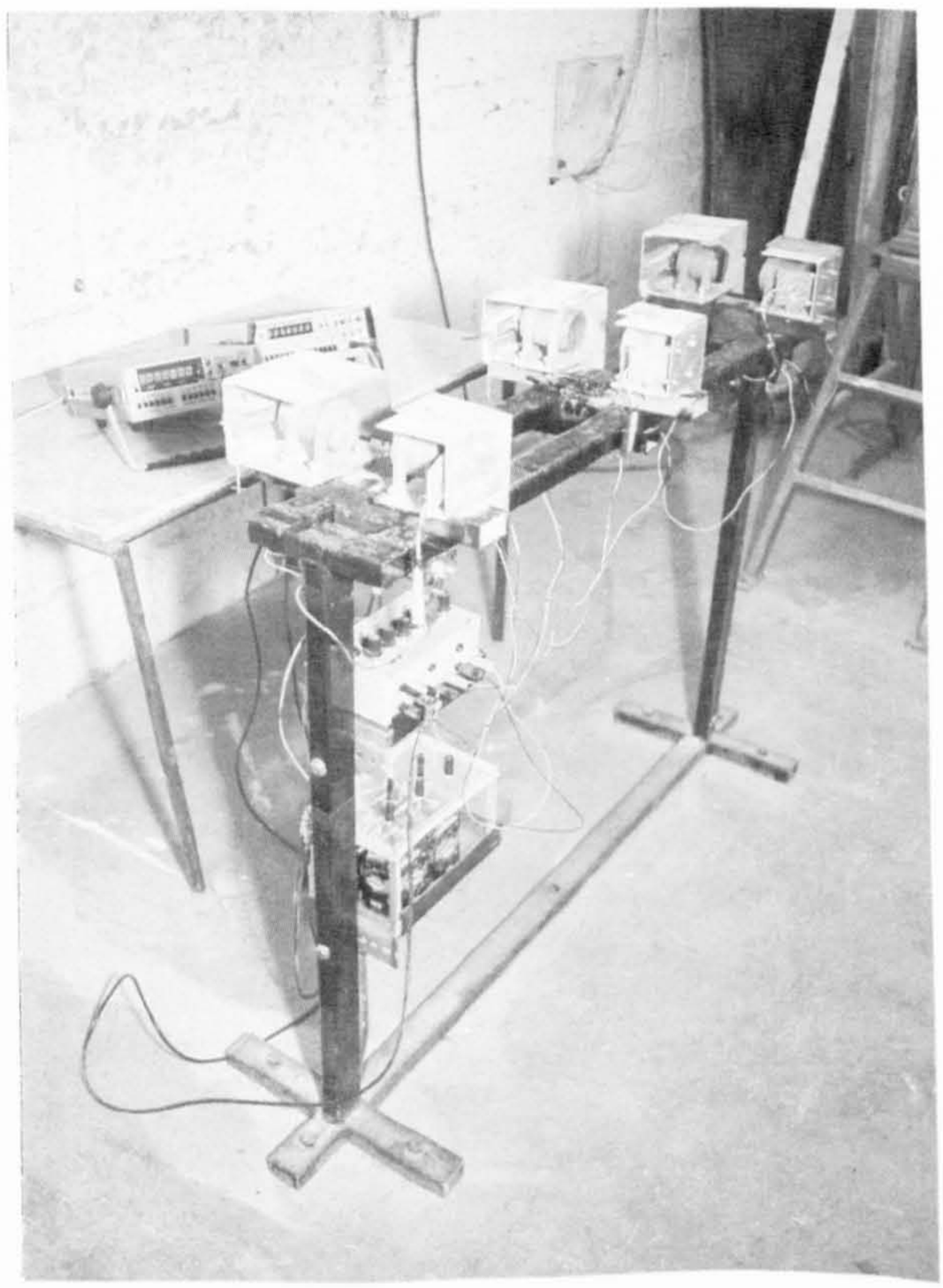

Figure 3.6 Projectile Velocity Measurement Equipment

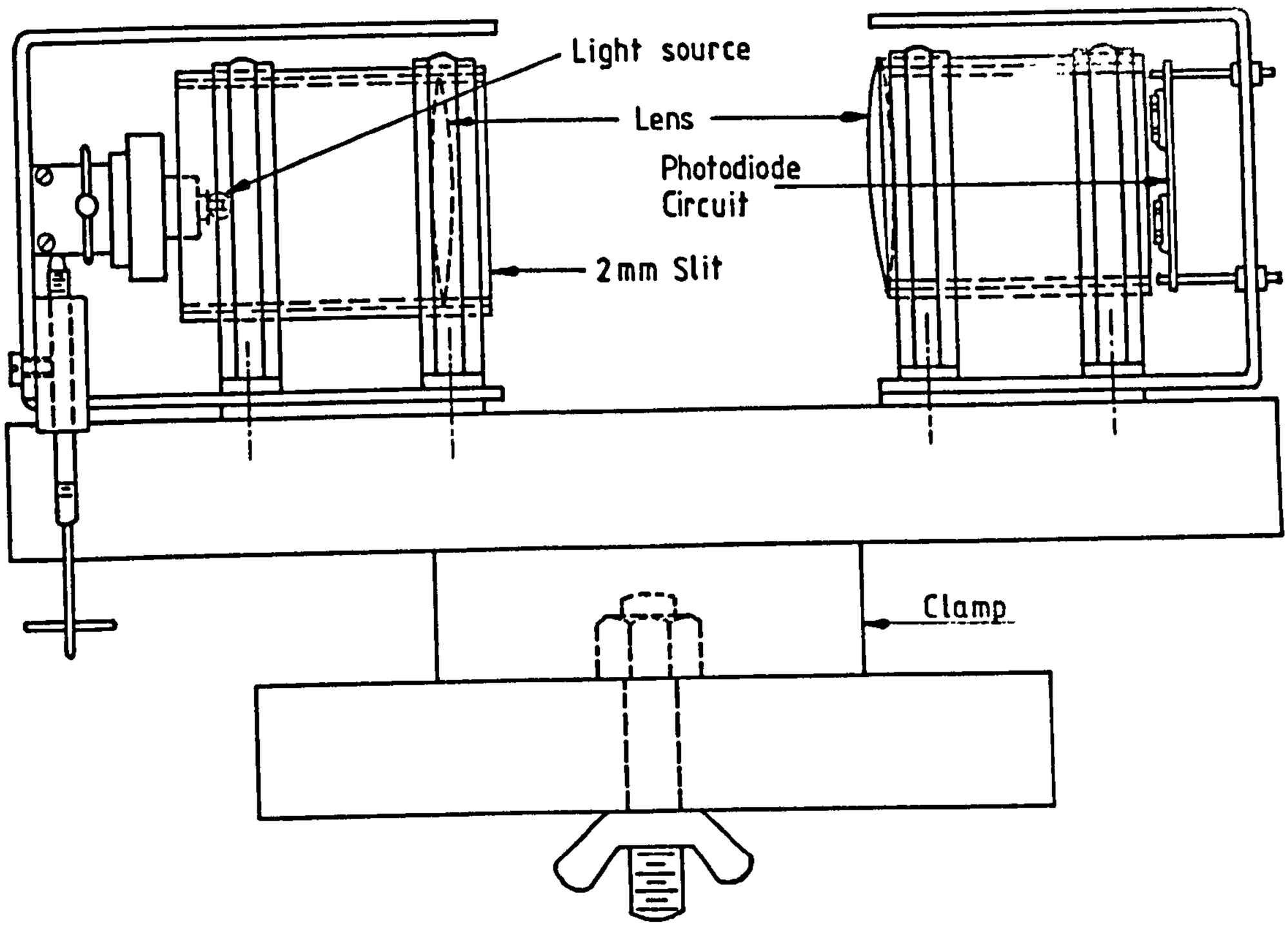

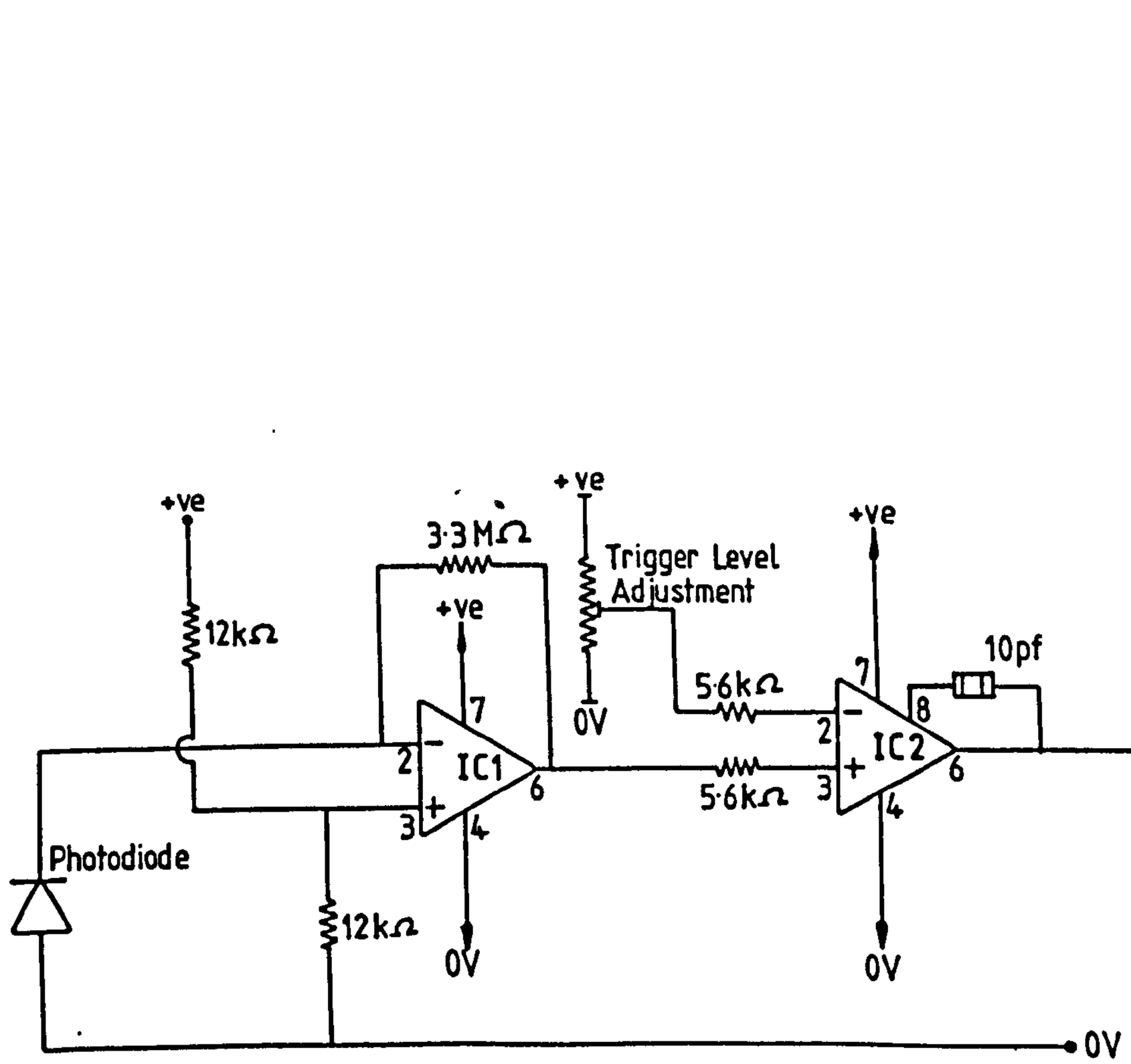

IC1 - 741 Operational Amplifier
IC2 - 531 Operational Amplifier

Figure 3.7 Elevation of Single Optical Velocity Measurement Base and Electronic Circuit Details

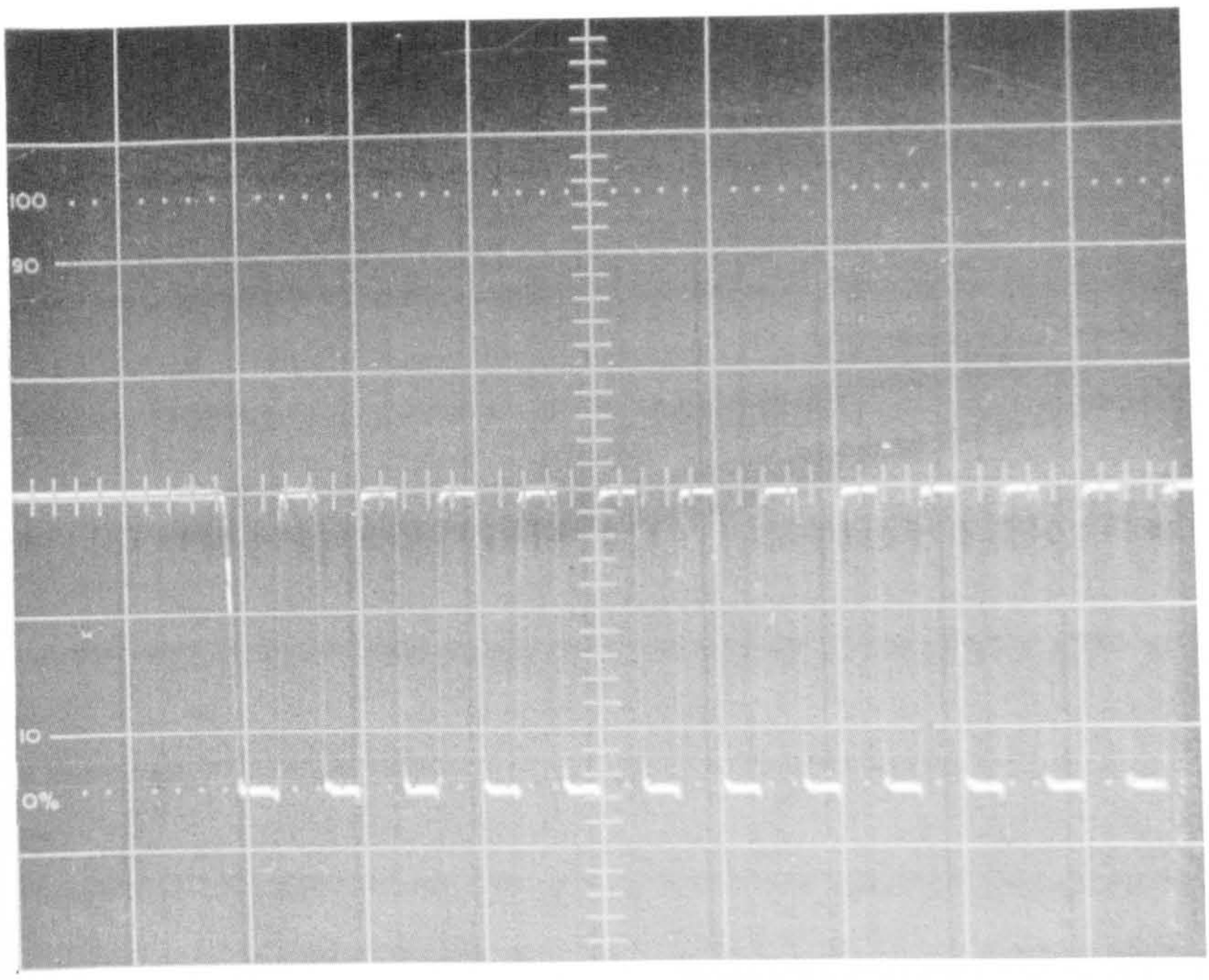

Figure 3.8 Oscilloscope trace illustrating trigger profile

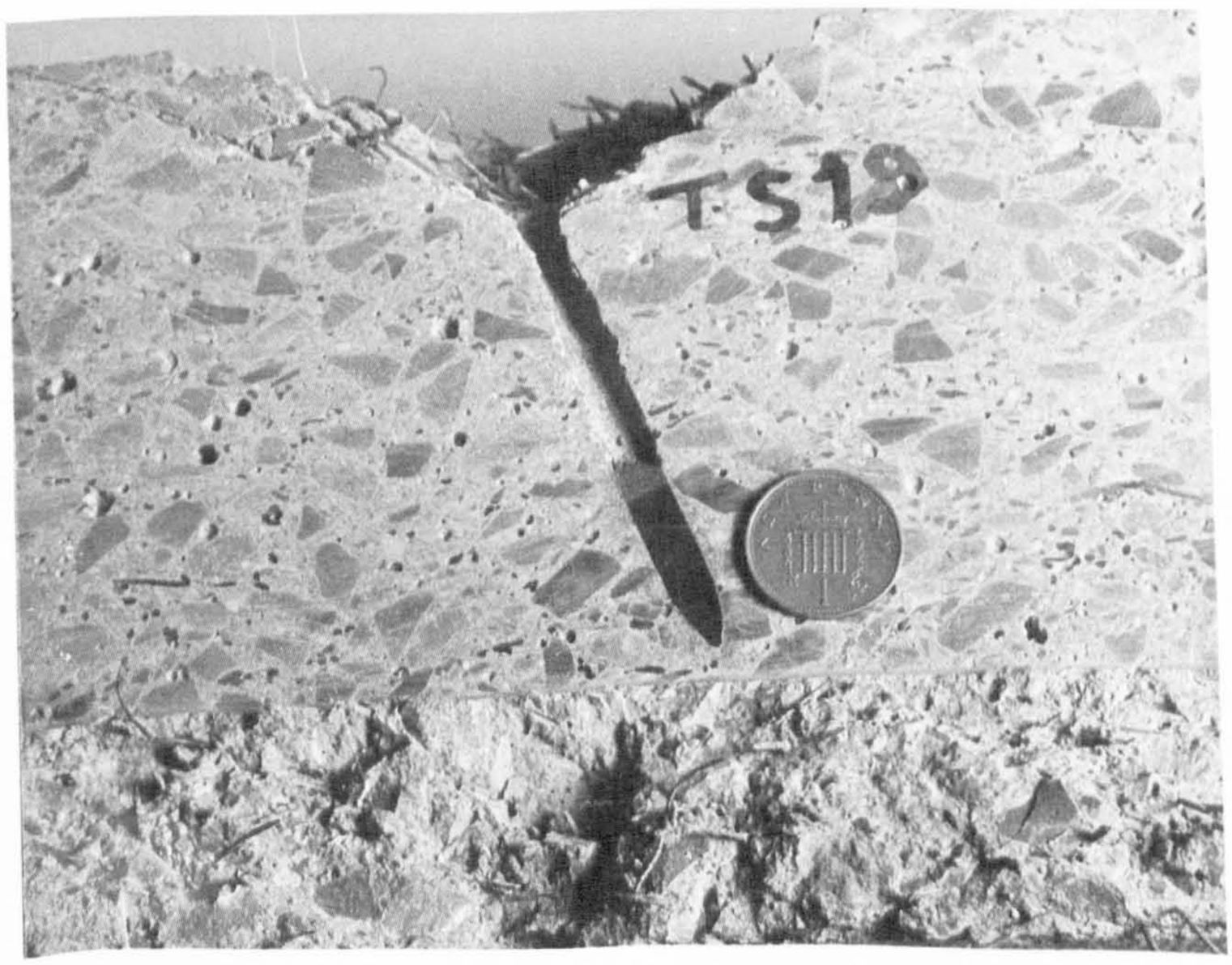

Figure 3.9 Typical Post-impact target damage

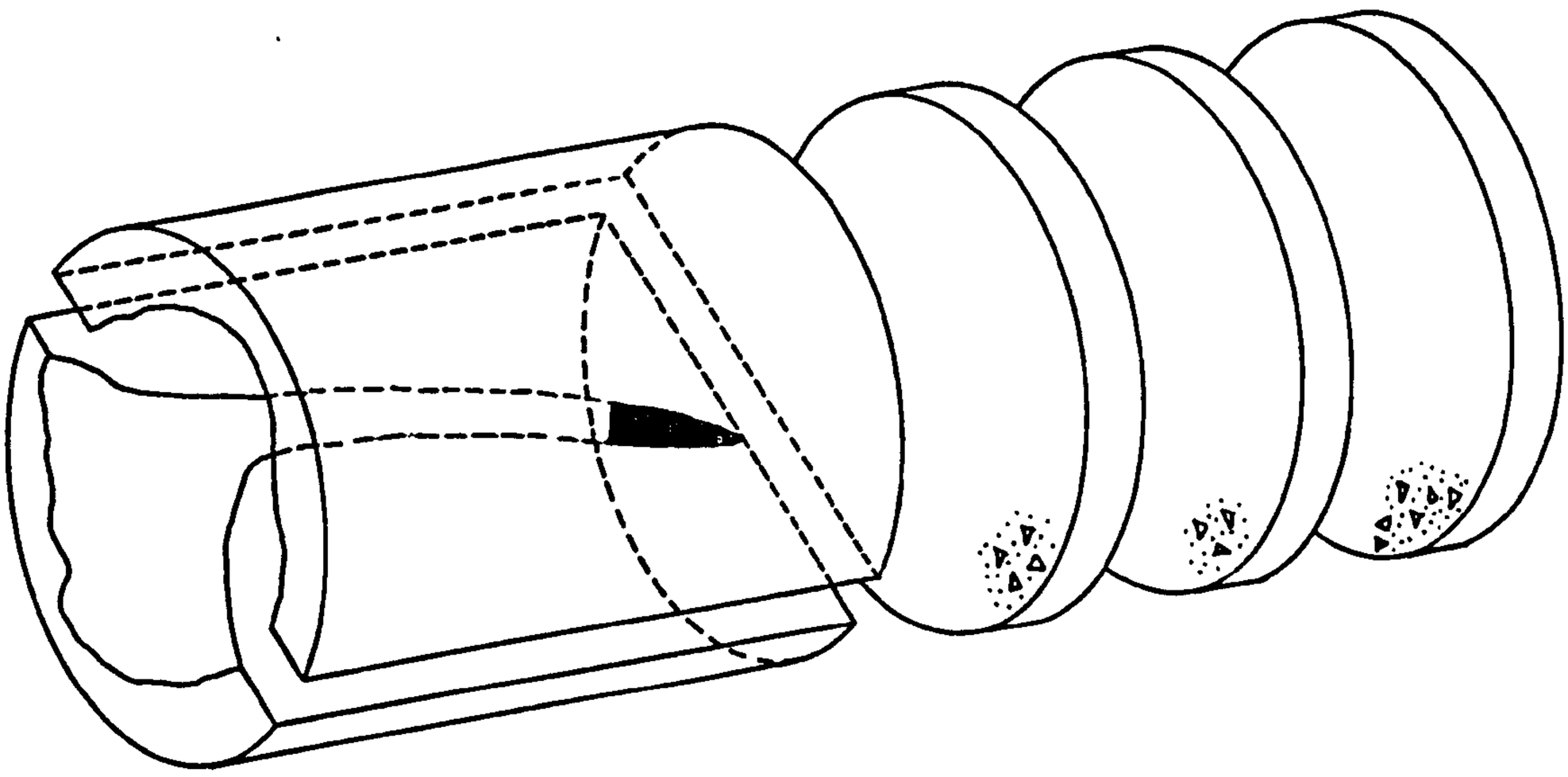

Figure 3.10 Definition of Actual Path Length

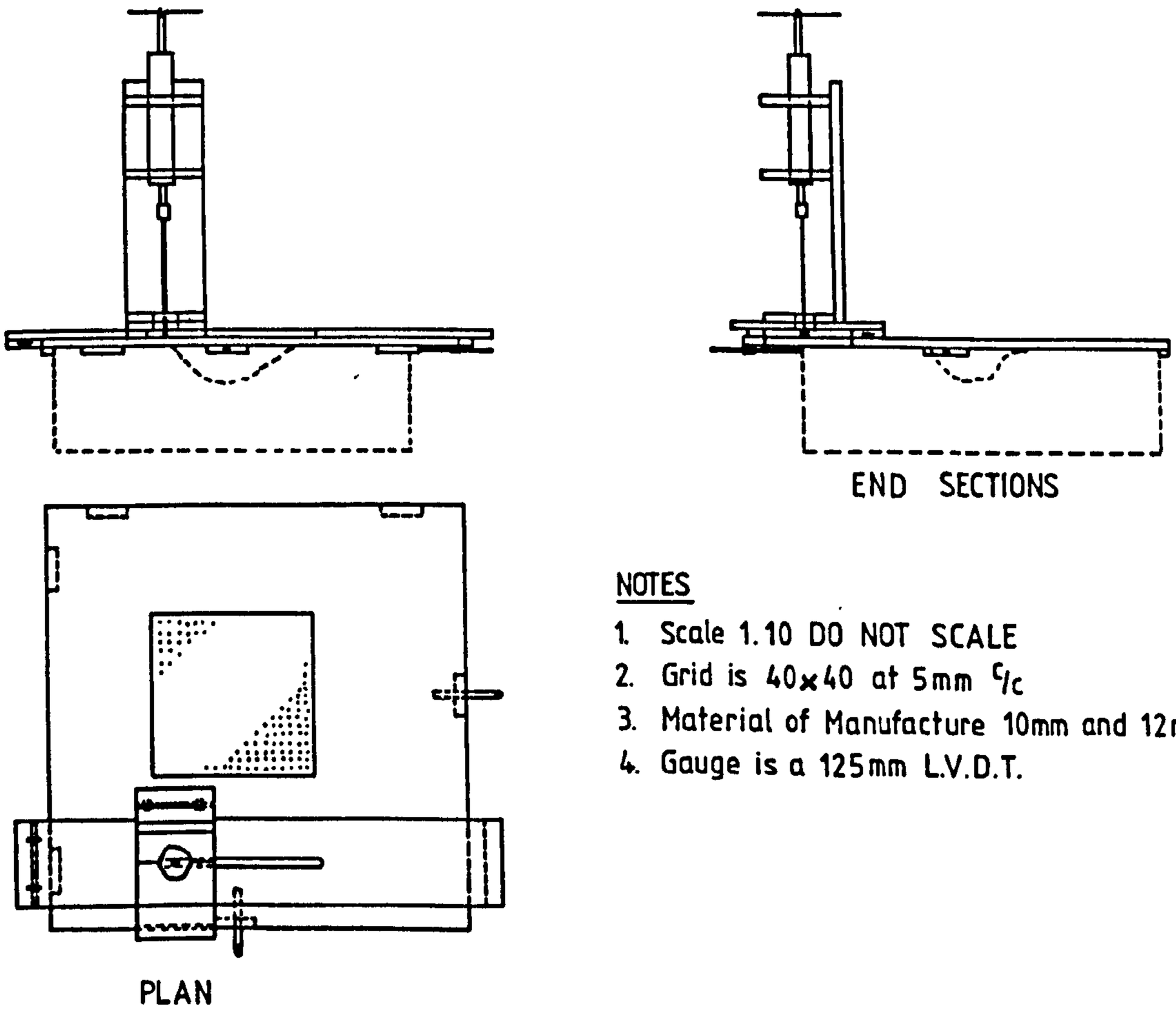

Figure 3.11 Crater Volume Analysis Equipment

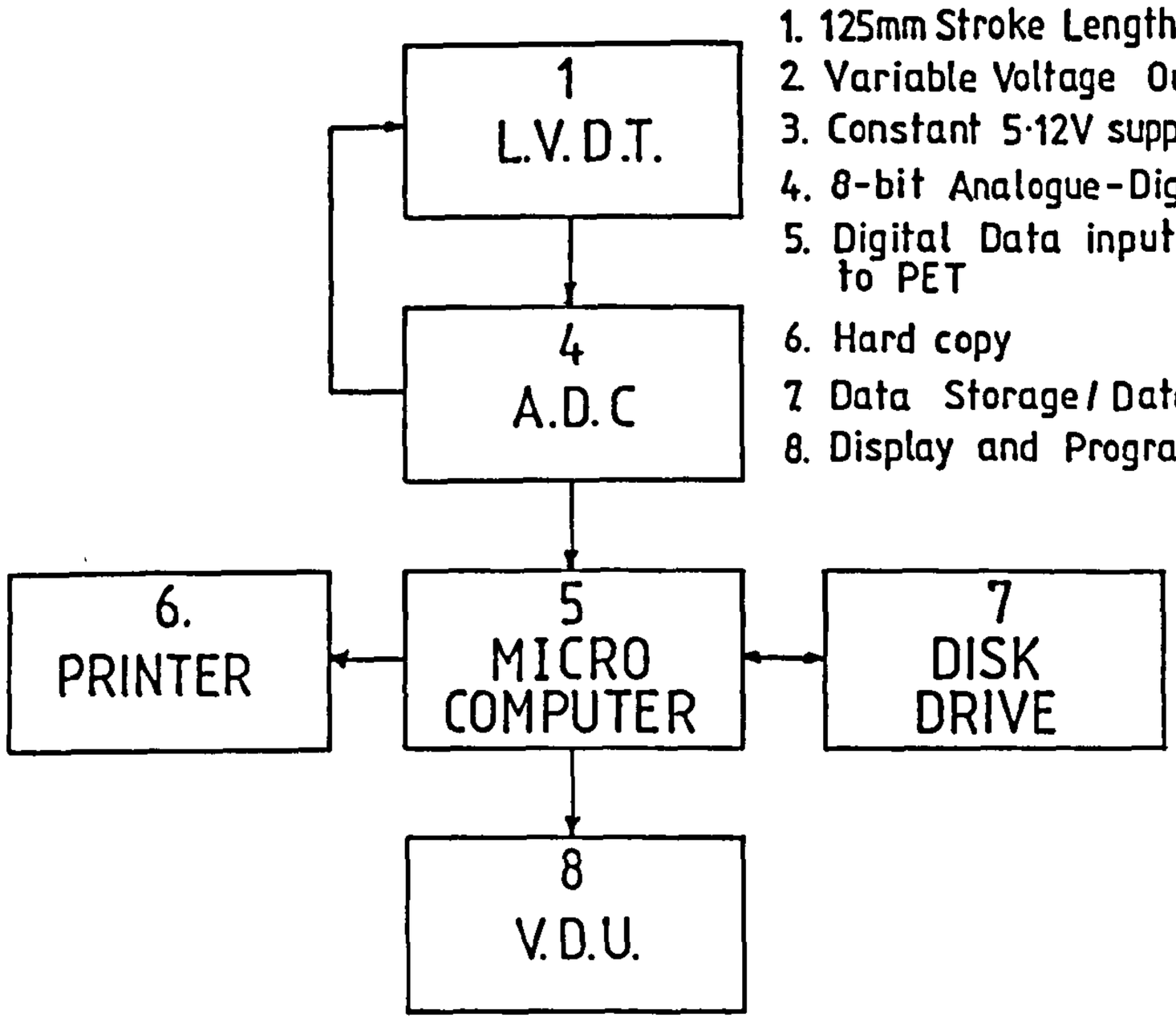

Figure 3.12 Crater Volume Measurement - Computer Interaction

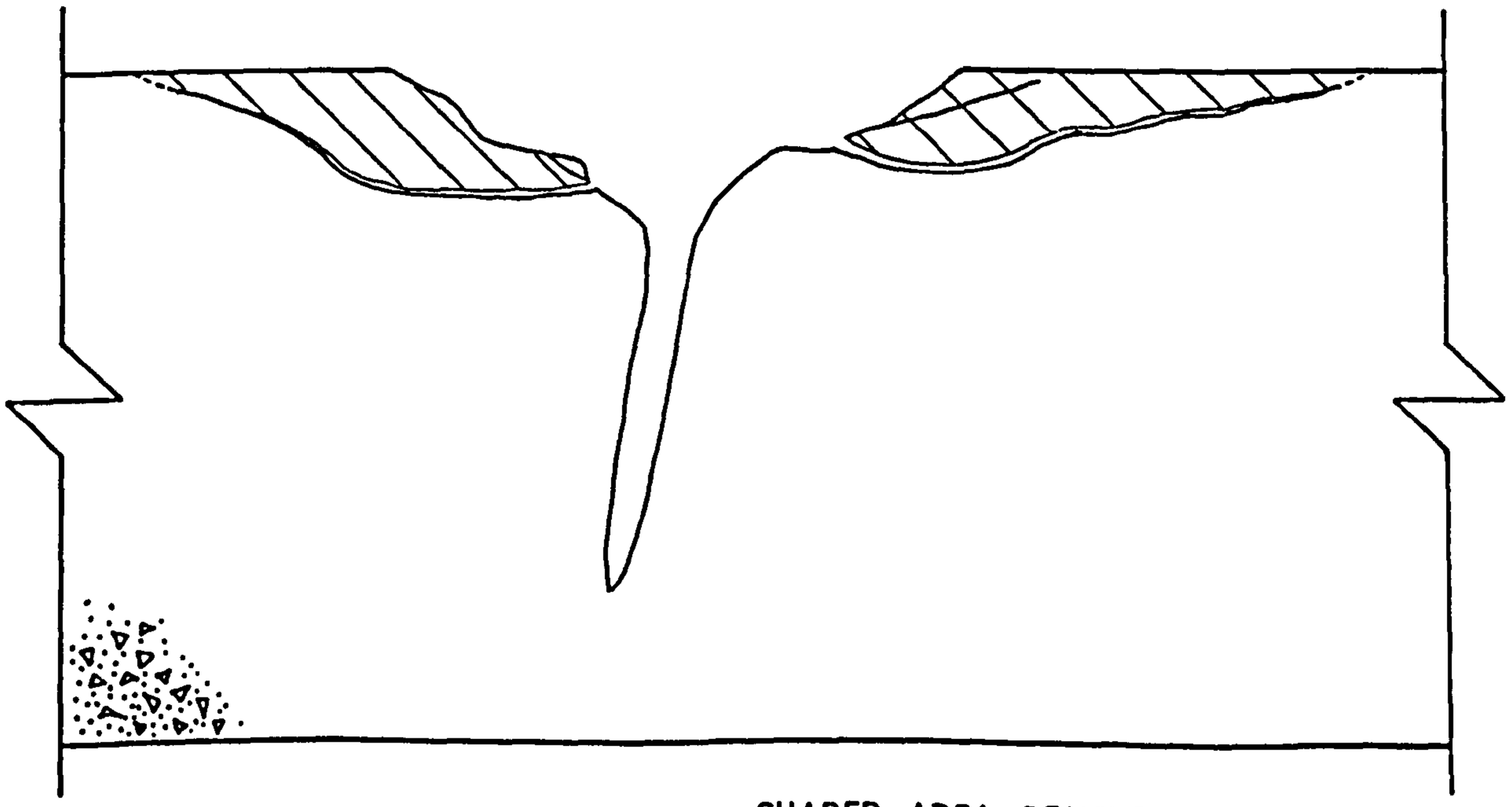

Figure 3.13 Illustration of Relationship Between "True" and "Apparent" Crater

CHAPTER 4

EXPERIMENTAL STUDY OF FIBRE REINFORCED CONCRETE VARIABLES

4.1 Introduction

4.1.1 General Approach

The literature shows that various approaches have been developed to define the displacement-time history of impact and penetration events. It was concluded that an empirical approach, neither requiring the definition of an accurate constitutive model of physical behaviour, nor employing large amounts of expensive computer time, was potentially the most useful analysis tool in the case of a specific penetrator impacting a material which was to be optimised in terms of minimum penetration path length and, possibly, front face spall damage. Earlier work, carried out by Anderson et al. (1980), had used a limited series of tests to fit an approximate mathematical model with a statistically valid result. This approach, known as surface response theory, was adopted and developed, allowing the statistical analysis to be performed by microcomputer. As a consequence of the variability observed in the completed early series however, the statistical technique was suspended and replaced by a more limited experimental programme. Subsequently, a conventional parametric study, varying coarse aggregate type, fibre type and fibre content was successfully completed. Each of the two approaches are discussed in this chapter. However, the choice of appropriate variables for the empirical studies and the results of some preliminary trials used to assess the influence of various factors of the event are reported first.

4.1.2 Variables Considered (Materials and Measurement)

The static properties of a plain concrete are dependent on the type and proportion of the material constituents and also upon the age at testing. For a fibre-reinforced concrete, the proportion, aspect ratio and

type of fibrous inclusion has a further effect upon the post-cracked properties of the composite.

In this study, as it was not possible to accurately vary the impact energy, a standard impact was assumed and the effect of controlled change in various of the qualitative independent variables was monitored. The potentially measurable characteristics of damage, the "quantitative dependent variables" are listed as Table 4.1. It was initially recognised that the penetration resisting characteristics of a particular specimen could be defined in one of two ways, either as a true path length through the target, or as an orthogonal distance travelled into the target, measured from the impacted face. However, as was also found in similar rock/elastomer studies carried out by Anderson et al.(1980), significant deviation from the original orthogonal path was observed on sectioning the concrete targets. In a few cases this path deviation caused the penetrator to reverse its original direction completely, inducing a reduction in the measured value of orthogonal path length. As a consequence, and to ensure a limiting condition for safety, actual penetration path length was selected as the prime indicator of penetration resistance for the main test series. A specific, though laborious, exposure technique was developed to obtain this measurement to an accuracy of $\pm$ 2mm, as described in Section 3.5.1, at the cost of the less significant normal path length value.

As the study was developed, the near surface effects of the impact and subsequent penetration were noted to change with variation in target materials, the size of the crater formed during the impact was considered the most reliable indicator of the overall local damage being caused by both penetrator presence and stress wave propagation in the target. As discussed in Section 3.5.2, the "true" volume of this crater was established and measured by a microcomputer-based method.

Of the other characteristics given in Table 4.1, burrow diameter and volume were deemed to be of lesser importance, whilst burrow length was

adequately allowed for as a component of the actual penetration path length (though not as part of a normal path length measurement). It was initially believed that the maximum surface diameter of the crater formed would be of significance. However, following the realisation that the vast majority of impacted targets exhibited unsymmetrical actual crater plan shapes, this measurement was not pursued, as it gave no insight into the general material response. In a homogeneous material, such as steel or wax, this value is of importance and, where appropriate in these studies, was measured.

In ideal circumstances, the quantity of comminution of the various matrix constituents could possibly be a useful indication of the amount of projectile energy expanded in the penetration of a particular component. However it was impractical to consistently obtain such information during this work.

The intention of this research was to examine the effect of changes in both the qualitative and quantitative independent variables defining the event on the damage parameters considered to be of most significance. In all parametric studies, to minimise the number of trials required it is desirable to hold constant as many independent variables as is deemed possible. The relevant quantitative independent variables are given in Table 4.2, whilst the qualitative variables included fibre type, coarse aggregate type, fine aggregate type, cement type and projectile type.

For the surface response theory approach, the primary independent variables (i.e. those not held constant) included quantitatively; water/cement ratio, aggregate/cement ratio and fibre content and qualitatively; fibre type and coarse aggregate type. The remaining (secondary) independent variables were held, or assumed, constant.

In the case of the "limited variable" analysis, a single primary quantitative independent variable was selected, fibre content, and two primary qualitative independent variables, coarse aggregate type and steel

fibre type, were considered. The other (secondary) independent variables were then held, or assumed, constant.

4.2 Preliminary Tests

There are several difficulties in producing small quantities of sprayed concrete, not least being the lack of material consistency likely to be generated. As a consequence, poured concrete specimens were used throughout these trials. It is of interest to consider the possible effect of this decision upon the subsequent findings of the research.

When the concrete is sprayed into wooden moulds a large quantity of coarse aggregate and fibre is initially lost by rebound, until a sufficiently thick cement paste cushion has been established on the formwork base and sides. This mortar layer tends to be more apparent at the corners of the mould. The resulting panel has significant inconsistency throughout its depth and width. The Concrete Society Code of Practice for Sprayed Concrete (1980) instructs that, where cores are required for compliance testing, test panels of plan dimensions no less than 750mm x 750mm should be used; with the subsequent cores not being taken within 125mm of the edges of the panel. Such a panel size would not be a practical proposition for manual handling, notwithstanding the remaining difficulty of unknown material inconsistency with depth and width.

As a compromise, the search for an individual specimen size of sufficient dimension to successfully isolate local effects such as penetration and spalling from global effects, such as gross cracking to the edge of the specimens and consequent target break-up, was initiated. Each of these slabs was to be held in a vertical position by the frame discussed in Section 3.3.2 and illustrated as Figure 3.5. In this orientation, the slab was effectively two-way spanning under impact. However, so as to approach the same support condition as in a free-standing, and potentially quasi-semi-infinite, field situation, the selected target and frame

combination was to be sufficiently stiff to avoid significant elastic motion of the target and holder. (This was later confirmed as a by-product of the high speed photography trials (Section 5.2.1)). The target selected would, by virtue of its relatively small boundaries compared with any realistic field usage of the material, tend to generate a significantly more concentrated stress wave field. This, exacerbated by a lack of the pre-compression normally available to an actual structural unit, would, at first sight, imply a more damaging overall effect. However, this process was deemed to be unlikely to effect the parameter of prime concern, the overall penetration path length. Further, the selected square plan shape of the target meant that the effects of the edge reflected stress waves tended to cancel each other out at their point of intersection. Such a specimen could thus be considered to generate overall limiting conditions for safety and to be a valid means of comparing different target materials. During the parametric studies (Sections 4.3 and 4.4) only a single specimen suffered from gross target cracking and break-up, whilst potentially injurious tensile scabbing was not generated in any such target. Hence the sizes selected below fulfilled both the experimental and ergonomic requirements.

4.2.1 Slab Frontal Area

To establish the plan area of specimen required to ensure that only local effects were suffered by the slab (rather than "global" effects such as gross cracking to slab edges), a series of specimens of various mix types and proportions were cast and impacted centrally at 7 days. As this testing was carried out at a very early stage, available materials were used; the mixes given in Table 4.3 were selected after reference to the literature. All of the specimens were cast using rapid hardening cement, 10mm single size river gravel and zone 2 (B.S.882:Pt:1973) limestone sand. Several of the large slabs were initially impacted centrally and then

attacked at other points on the face in order to define the "edge-distance" at which gross cracking could be expected.

Table 4.4 gives a summary of the projectiles used and the results obtained. As a result of these tests, a target plan area of 450mm x 450mm was selected.

4.2.2 Specimen Thickness

As it was not considered practical to attempt to measure the residual energy of a projectile perforating a specimen, tests were carried out to determine the minimum thickness at which perforation was unlikely to occur in an average fibre concrete mix. Specimens of various thicknesses of steel fibre reinforced concrete were manufactured and impacted at 14 days by a 7.62mm armour-piercing (AP) projectile. Table 4.5 gives the details of the mix designs used, the basic constituents being Ordinary Portland Cement, zone 2 (B.S.882:Pt.2:1973) limestone sand and 10mm single size limestone, in conjunction with 2.5% by concrete weight of 35 x $\overline{0.3}$mm (nominal) melt extract carbon steel fibre. In order to examine the sensitivity of the material to changes made in compensating for aggregate moisture content, half of the specimens were cast assuming that all of the siphon can moisture content value (by dry mass) was available as free water to the concrete matrix, whilst the second half were cast assuming only 50% of the measured value was available. This led to a much weaker matrix (higher water-cement ratio) in the latter case, reflected in the compressive strength values obtained.

Table 4.6 gives a summary of the results obtained, the major conclusion being that a slab of 450 x 450mm p[lan area and 125mm thickness was sufficient to contain a 7.62mm armour-piercing projectile without global cracking occurring,.

4.2.3 Variation in Fine Aggregate Type

Initial indications were that the type of fine aggregate incorporated into the material had an insignificant effect on the measured damage

phenomena. Since it was attractive to use a single fine aggregate type for all specimens in order to reduce the required number of combinations tested, a small comparative series was carried out using a similar mix design and three different sand materials, i.e. i) zone 2 limestone sand, ii) zone 3 grit (sharp) sand, iii) zone 4 building sand, all zones defined by B.S.882:Pt.2:1973.

The mix design consisted of Ordinary Portland Cement (1 part), 10mm single size limestone (3 parts), fine aggregate (3 parts), water (0.55 parts) and 6.7% by concrete weight of 25 x 0.3mm (nominal diameter) melt extracted carbon steel fibre. Three similar 450 x 450 x 125mm specimens were cast for each combination. The slabs were stripped from the moulds at one day and cured until impacted by a 7.62mm AP projectile at three days. This short period of time was chosen in order to highlight any differences present. The moisture contents, by dry mass, of the limestone sand and 10mm single size limestone were derived using a standard siphon can test (B.S.812:Pt.2:1975). However, constants for the other two fine-grained materials were not available and an oven-dried sample was used to derive the moisture content values by dry mass. This led to an inconsistency in the materials strengths, as shown in Table 4.7. The results (Table 4.7) obtained for mean penetration path length values of the three show only a 20% reduction even though the mean strength value of the limestone sand based material was twice that recorded for the other two materials. As the scatter of the results is within the range of random variation usually experienced in this type of dynamic testing, it is reasonable to conclude that the type of sand used was of little significance.

4.2.4 Variation in Steel Fibre Type

For several of the fibrous materials, the choice and number of different types used was very much dependent upon limited availability (for example, Kevlar-29). However in the case of steel fibres it was necessary to carry out a preliminary study of more readily available fibres to

observe whether a measurable difference in damage parameters occurred with the different lengths and cross-sectional designs; in an attempt to reduce the number of combinations to be tested. The single concrete mix design selected consisted of 1 part O.P.C., 2.36 parts 10mm limestone, 2.33 parts zone 2 sand and 0.49 parts water to which 5% of fibre by concrete weight was added. This mix has the same basic material ratios as those used for the majority of the earlier dimensional evaluation tests (Sections 4.2.1 and 4.2.2), although in this case 75% of the measured aggregate moisture content by dry mass was assumed to be available as free water. This requires an adjustment to the stated ratios to give a true comparison with the other presented designs, for which all moisture content was considered as free water. The slabs were cast, stripped from the moulds at one day and stored until immediately before central impact by a 7.62mm A.P. projectile at three days of age. Three similar specimens were cast for each of three different steel fibre types;

i) 25 x 0.25mm brass-coated indented mild steel fibre (Duoform).

ii) 35 x $\overline{0.3}$mm melt extract mild steel fibre.

iii) 30 x 0.3mm cold-drawn circular steel fibre.

The results obtained for mean normal penetration depth given in Table 4.8 indicated that none of these fibres had an obviously superior performance in terms of penetration resistance. Hence, the fibres for the quadratic response surface analysis and later empirical approach were selected for each of casting and availability.

4.3 Initial Statistical Approach

4.3.1 Description of Method:Quadratic Polynomial Fitting

The preliminary tests carried out indicated that, of the quantitative dependent variables given in Table 4.1, penetration path length was the most reasonable parameter by which to judge ballistic resistance, whilst the crater volume gave the most useful assessment of overall impact damage. As penetration resistance was considered of prime importance, it was

necessary to devise an experimental series to monitor the effect on penetration path length of variation in both types and proportions of constituent materials. Given the large number of qualitative and quantitative independent variables (Table 4.2), it was advantageous to hold as many as possible constant, thus reducing the overall number of material combinations to be tested. In this study, three independent quantitative primary variables were selected.

A (i)Water cement ratio (w/c) - Designated x_1 (coded value)

A (ii) Aggregate cement ratio (a/c) - Designated x_2 (coded value)

A(iii) Fibre content (W_f') - Designated x_3 (coded value)

These values were varied whilst the other variables given in Table 4.2 were held, or assumed, constant.

In considering which of the qualitative independent variables were to be constant, it was recognised that the number of combinations of this group dictated the total number of individual series to be carried out; thus it was advantageous to minimise the number of these variables. After the preliminary tests given in Section 4.2 it was decided to vary only:

B (i) Fibre type

B(ii) Coarse aggregate type

In the light of earlier experiments and literature study, six fibres were selected as usefully representative of the available sources:

i) ME-25 x $\overline{0.3}$mm nominal diameter melt extract carbon steel fibre.

ii) DUO-25 x 0.25mm indented circular drawn brass-coated carbon steel fibre (known as DUOFORM).

iii) DRA-25 x 0.25mm circular drawn brass-coated carbon-steel fibre

iv) 13K-13mm length KEVLAR-29 (Type 970), 12μm diameter, polyamide fibre.

v) 37K-37mm length KEVLAR-29 (Type 970), 12μm, polyamide fibre.

vi) POL-37mm FORTA fibre, latticed bundled polypropylene fibre (see Figure 4.1)

Table 4.9 gives the material properties for all of the selected fibrous materials. Three coarse aggregate types described in section 3.1.1.2 were chosen to give a contrast in hardness and particle shape.

i) L-Limestone-low strength, angular.

ii) B-basalt-medium strength, angular.

iii) RG-river gravel-high strength, rounded.

Hence in order to cover all combinations of qualitative independent variables, 6 x 3 = 18 series were required.

The usual approach to a parametric study is to select one of the quantitative independent variables and vary it through a relevant range whilst holding the other variables constant, and monitoring the effect on the damage parameters. Each variable is treated in this manner in order to locate the most significant factors and the approach may then be repeated for the most important variables, using a more sensitive range of values. In this particular case, a range of five values for each variable was considered necessary in order to sensibly cover the possible material mix designs. Hence, if a standard parametric study had been used, $5^3 = 125$ combinations would have been required for a full experimental plan. The results would only be valid for the particular combination of coarse aggregate type and fibrous material type considered. A full study of all aggregate and fibre combinations would therefore have necessitated the investigation of 3 x 6 x 125 composite designs, some 2250 tests, each specimen consisting of a single 450 x 450 x 125mm slab of approximately 62kg weight, a total of approximately 140 tonnes ($58m^3$) of concrete material, all cast by hand. As this was considered an unreasonable proposition, it was decided to adopt a statistical method developed by Anderson, Watson and Johnson (1980) from work recorded by Cochran and Cox (1957). A mathematical model, or response surface, was generated for each fibre aggregate combination to prescribe an estimated value for penetration path length to any particular combination of water/cement ratio,

aggregate/cement ratio and fibre content. In this particular study, it was considered that as quadratic response surface approximation would yield sufficient accuracy. Thus a prediction equation of the form:

$$Lp = b_o + b_1x_1 + b_2x_2 + b_3x_3 + b_{12}x_1x_2 + b_{13}x_1x_3 + b_{23}x_2x_3 + B_{11}x_1^2 + b_{22}x_2^2 + b_{33}x_3^2 \quad \text{... Eq. 4.1}$$

L_p = predicted penetration path length

b_{jk} = coefficients calculated from experimental tests

X_k = values for A(i), A(ii), A(iii)

was used. It is attractive to develop a model which is symmetrical and closed, since this reduces the number of points required for a reasonable approximation. In an experiment with three primary quantitative independent variables:

A (i) Water/cement ratio (x_1)

A (ii) Aggregate/cement ratio (x_2)

A(iii) Fibre content (x_3)

the actual response surface generated by the infinite number of possible combinations may be represented as a sphere, centred at the origin, on the three axes x_1, x_2, x_3 (see Figure 4.2). A model must be selected which approximates to this surface.

The explanation of the model is simplified by discussing the concept of coded levels. As an example, the fibre content of a particular test series may vary between 0% and, say, 7.0% weight by concrete weight. A series of coded levels is used, the values dependent upon the number of primary quantitative independent variables, i.e.

$$X_3 = -2^{k/4}, -1, 0, +1, +2^{k/4}$$

where K = number of primary independent quantitative variables = 3.

In the case discussed above,

0% by weight is equivalent to $-2^{3/4}$

7% by weight is equivalent to $2^{3/4}$,

the values -1, 0, +1 being correctly proportioned between these. This same proportioning procedure is also carried out for x_1 and x_2. Then, the sphere is initially approximated by a cube of 8 points:

(-1,-1,-1) (1,-1,-1) (-1,1,-1) (1,1,-1)

(-1,-1,1) (1,-1,1) (-1,1,1) (1,1,1)

(points ABCDEFGH in Fig. 4.2).

This first estimate is improved by adding the points on the sphere which lie on the radii carrying the centre of each face of the cube, that is the 6 points;

$(-2^{3/4},0,0)$ $(2^{3/4},0,0)$ $(0,-2^{3/4},0)$

$(0,2^{3/4},0)$ $(0,0,-2^{3/4})$ $(0,0,2^{3/4})$

(points JKLMNP in Fig. 4.2).

Then, so as to give a roughly equal precision to all of the predicted values of the response surface within a sphere of radius 1 (at coded scale), 6 more points are added at the origin, i.e.

6 points at (0,0,0).

Thus a total of 8 + 6 + 6 = 20 combinations are required to give a potentially reasonable estimate of the actual coded response surface. This estimate can be shown to be the polynomial given as Eq. 4.1, where it can now be seen that the relevant coded values for x_1, x_2 and x_3 will yield a particular value of Lp, predicted path length, for any one of the 125 combination alternatives, providing that the b_{jk} coefficients are known. The coefficients are calculated using the actual penetration path length values measured from the twenty combinations tested. Whilst the derivation of the coefficient equations may be found in Appendix V the results are given below:

$$b_o = 0.166338 \left[\sum_{i=1}^{20} L_i\right] - 0.056791 \left[3 \sum_{i=1}^{8} L_i + 2^{3/2} \sum_{i=9}^{14} L_i\right] \quad \text{... Eq. 4.2}$$

$$b_1 = 0.073224 \left[\sum_{i=1}^{8}(-1)^i L_i + 2^{3/4}\sum_{i=9}^{10}(-1)^i L_i\right] \quad \text{... Eq. 4.3}$$

$$b_2 = -0.073224 \left[(L_1 + L_2 + L_5 + L_6)-(L_3 + L_4 + L_7 + L_8) + 2^{3/4}\ (L_{11}-L_{12})\right] \quad \text{... Eq. 4.4}$$

$$b_3 = -0.073224 \left[\sum_{i=1}^{4} L_i - \sum_{i=5}^{8} L_i + 2^{3/4}\ (L_{13}-L_{14})\right] \quad \text{... Eq. 4.5}$$

$$b_{12} = 0.125000 \left[(L_1 + L_4+L_5 + L_8)-(L_2 + L_3 + L_6 + L_7)\right] \quad \text{... Eq. 4.6}$$

$$b_{13} = 0.125000 \left[(L_1 + L_3+L_6 + L_8)-(L_2 + L_4 + L_5 + L_7)\right] \quad \text{... Eq. 4.7}$$

$$b_{23} = 0.125000 \left[(L_1 + L_2 + L_7 + L_8)-(L_3 + L_4 + L_5 + L_6)\right] \quad \text{... Eq. 4.8}$$

$$b_{11} = 0.062500 \left[\sum_{i=1}^{8} L_i + 2^{3/2}\sum_{i=9}^{10} L_i\right] + 0.006889 \left[3\sum_{i=1}^{8} L_i + 2^{3/2}\sum_{i=9}^{14} L_i\right]$$

$$- 0.056791 \left[\sum_{i=1}^{20} L_i\right] \quad \text{... Eq. 4.9}$$

$$b_{22} = 0.062500 \left[\sum_{i=1}^{8} L_i + 2^{3/2}\sum_{i=11}^{12} L_i\right] + 0.006889 \left[3\sum_{i=1}^{8} L_i + 2^{3/2}\sum_{i=9}^{14} L_i\right]$$

$$-0.056791 \left[\sum_{i=1}^{20} L_i\right] \quad \text{... Eq. 4.10}$$

$$b_{33} = 0.062500 \left[\sum_{i=1}^{8} L_i + 2^{3/2}\sum_{i=13}^{14} L_i\right] + 0.006889 \left[3\sum_{i=1}^{8} L_i + 2^{3/2}\sum_{i=9}^{14} L_i\right]$$

$$-0.056791 \left[\sum_{i=1}^{20} L_i\right] \quad \text{... Eq. 4.11}$$

The values of L_1 to L_{20} are actual path length measurements coinciding with particular coded value combinations, as shown in Table 4.10. In testing

each of the 18 qualitative independent variable combination sets, the full statistical procedure was as follows:

1 For each of the three primary quantitative independent variables, select the limits for the range levels e.g. water/cement ratio 0.35-0.55, aggregate/cement ratio 1:3-1:7, fibre content 0%-7% by concrete weight.

2 Proportion these limits to give five values equivalent to $-2^{3/4}$, -1, 0, +1, $+2^{3/4}$

3 Cast twenty 450 x 450 x 125mm specimens with the coded level combinations of Table 4.10.

4 Cure at 20 $\pm$ 1°C, 90% + relative humidity.

5 At three days, test each specimen with a single central impact of a 7.62mm armour piercing projectile .

6 Measure the actual penetration path lengths L_1-L_{20} (Table 4.10).

7 Calculate the response surface coefficients b_o-b_{33} (Eqns.4.2-4.11).

8 Using the quadratic response surface equation 4.1 calculate the predicted path lengths for the twenty tested combinations.

9 Compare the actual and predicted path lengths, for the required level of significance, using a standard χ^2 test, to check whether the lack of fit is significant.

Then, assuming 9 is acceptable -

10 Either -

i) Differentiate the response surface Eqn. 4.1 with respect to each x-variable in turn, giving three simultaneous equations, which are solved to yield, if possible, a minimum value for the predicted penetration path length. Usually a complex result is derived, however, which is invalid as a minimum value estimation.

or,

ii) Substitute all 125 alternative combinations into the response surface Eqn. 4.1 to locate the combination generating the smallest predicted penetration path length. This procedure may not give an accurate result, as extrapolation outside the bounds of the "star" defined by the analysis is taking place. The results are used to show trends for more sensitive experimentation.

Following the collection of the experimental data, the above, with the possible exception of 10(i), is very suited to microcomputing techniques.

Programs were written to;

i) Calculate the values of b_o-b_{33} using the measured penetration path length values.

ii) Calculate the predicted path lengths for the twenty actual path length combinations and carry out the χ^2-test at any required significant level.

iii) Fit all of the 125 combinations of the 3 x-variables into the prediction equation to locate the minimum value.

The programmes are listed in Appendix V.

A useful feature of this approach is that the coefficient formulae and response surface equation may be used in terms of any of the quantitative dependent variables (Table 4.1), simply by measuring the actual values of the particular phenomenon of interest (e.g. crater volume) from the twenty specimens tested in the series, and inputting them to the various computer programs in order to generate the necessary coefficients, statistical verification and minimum value. Thus the particular combination giving, for example, minimum true crater volume could be calculated using existing specimens and existing software.

4.3.2 Selection of Material Variable Ranges

The variable ranges correlated to the coded values were selected after referring to the relevant available literature and in the light of the preliminary tests.

i) Water/cement ratio

The material was to be suitable for placing using the sprayed concrete process. The Concrete Society Code of Practice for Sprayed Concrete (1980), recommends that the water/cement ratio the material will be in the range 0.35-0.50 by weight in order that a dense impermeable concrete is produced. Early experiments had shown 0.35 to be a very low figure for fibre concrete, as the inclusions greatly reduced the material workability. The top limit was defined as 0.55 for the first series of tests, so as to raise the values of the intermediate (-1,0,+1) coded levels.

For later series, as the problem of workability became more obvious, the upper limit was raised further and the coarse:fine aggregate ratio reduced to improve pumpability.

ii) Aggregate/cement ratio

The Concrete Society Code of Practice for Sprayed Concrete (1980), suggests that the aggregate/cement ratio should normally be within the range 3:1 to 4:1 for the dry mix process up to perhaps 6:1 for the wet mix process for pumpability and high durability. In the first series of tests, an aggregate/cement range of 3:1 to 7:1 was used to generate a response surface envelope containing the most acceptable values. It was later realised that including a value as high as 7:1 meant that the +1 and $+2^{3/4}$ coded values (6.2:1 and 7.0:1) in the statistical analysis were both below the minimum cement content required by the Code of Practice for the Structural Use of Concrete (1972),

assuming conditions of severe exposure in plain concrete. The upper limit of the aggregate/cement ratio range was then altered to 5.0:1. According to Hannant (1978) a satisfactory mix for fibre-concrete should contain a mortar volume of about 70% with only about 30% consisting of particles greater than 5mm. However, preliminary mechanism tests had suggested projectile path length to be very much dependent upon the amount of coarse aggregate hit during the penetration process. As a compromise, the fine:coarse aggregate ratios were held at 1:1 for the first series cast. For later series the ratios were changed to 2:1 (fine:coarse) when it was recognised that the pumpability of the first series was doubtful. This change brought designs more in line with Hannant's recommendation.

iii) Fibre content

Although much research has been carried out on the static properties of fibre-reinforced concretes and a more limited amount on the dynamic response of the material to explosive and drop hammer type loading, no literature was found which detailed the type of effects to be expected for this particular impactor/target combination. Hence the range of fibre proportions by concrete weight was selected mainly on the basis of published work with modifications made in the light of results obtained during the main test series. The actual ranges by weight vary with the particular density of each of the fibrous inclusions. For steel fibre, 0%-7.0% by concrete weight was used in the first series. After casting the first series of 20 slabs, it was considered that, in order to ensure the guaranteed response surface enveloped the potential optimum combinations, a higher upper limit should be used as it was clearly possible to include more fibre in the composite

without causing a non-random distribution. From the Kevlar-29 reinforced concrete preliminary tests, which were carried out to explore potential mixing methods and acceptable fibre concentrations, a value of 2.0% by concrete volume (equivalent to 1.23% by concrete weight) was selected as a high upper limit so as to cover all likely combinations.

4.3.3 Results of Statistical Analysis

Each of the eighteen planned series combinations was given a two-week turn-round time between casting and gathering of penetration event data. However, a delay in coring the slabs later led to a number of series being analysed almost simultaneously. Only when six of the envisaged eighteen combinations had been completed and analysed was the unacceptably random nature of the results fully appreciated. Also, more perforations of the specimens were observed than was expected. Since residual energy of the projectile had not been measured, an allowance on actual path length travelled was necessary for each perforated specimen in the statistical analyses. The microcomputer analysis was run several times, the perforated slabs being given a total path length value of actual length +0 to 30mm in 5mm increments, so as to locate the best fit.

The following sections confirm the details of the results and generated model for each fibre type/aggregate type combination tested. The specific information concerning mix designs, aggregate moisture contents, concrete compressive strengths, measured path lengths and the appropriate calculated path lengths may be found in Appendix VI.

i) Series ME/B/1-20

Three of the twenty slabs in this series perforated and were given incremental values, as discussed above. For all analyses, the chi-squared test between predicted and actual path lengths generated a confidence level of <0.5% (chance of

error >99.5%). Table VI.1 gives details of the statistical analysis.

ii) Series DUO/B/1-20

Quadratic response surface analysis again gives a model with a confidence level of <0.5%. Four perforations were recorded with this series, for which the incremental procedure was adopted without any improvement to the model generated. The analysis uses a centre-weighting of six similar specimens of a mean mix design, $(x_1, x_2, x_3) = (0,0,0)$. In this series, although the density and compressive strengths of the 100 x 100 x 100mm cubes, taken from these identical mixes, was reasonably uniform, path lengths ranging from 27mm to 120mm were measured for the six supposedly identical specimens. The target yielding a 27mm path length contained neither projectile or burrow after impact, implying either a ricochet or very rapid change in projectile direction on impact, although velocity measurements indicated a normal round. For this specimen, the 27mm crater depth was thus assumed to be the path length. Removing this value from the statistical analysis gave no improvement in correlation between the model and the actual response surface. Table VI.2 has details of the incremental statistical analysis.

iii) Series 13K/B/1-20

Many perforations occurred in this series, due possibly to the difficulty of adequately separating and mixing the 12μm diameter Kevlar-29 filaments into the concrete matrix giving a non-homogeneous concrete containing fibre bunches. As shown in Table VI.3, the best statistical fit when the incremental technique was used for perforations was when path length

equalled actual length + 0mm, giving a 25% confidence level.

Indications were that a combination of:

x_1: water/cement ratio = 0.35

x_2: aggregate/cement ratio = 5.0:1 (fine:coarse. 2:1)

x_3: fibre content = 1.22% by concrete weight

would yield the minimum penetration path length (104mm) at the stated confidence level.

iv) Series 13K/RG/1-20

Two of the twenty specimens were perforated. The statistical "best fit" at 50% confidence level was generated at a path length = actual + 0mm for these two slabs. The minimum valid path length was indicated at:

x_1: water/cement ratio = 0.35

x_2:aggregate/cement ratio: 5.0:1 (fine:coarse, 2:1)

x_3:fibre content = 0.98% by concrete weight

The minimum path length for this combination was predicted at an unrealistic value of 1mm, all other predictions being negative. This is illustrated in Table VI.4.

v) Series 37K/RG/1-20

A single slab of this series perforated, for which the technique of incremental additions was used; whilst another slab showed no trace of burrow or projectile, necessitating a best estimate of path length equal to crater depth. As shown in Table VI.5, a "best fit" of 0.5% confidence level was calculated for the generated response surface models. With a Kevlar fibre of this length, many conglomerations of significant size occur, notwithstanding the pneumatic injection technique employed, so that a non-uniform material with obvious zones of weakness is produced.

vi) Series 37K/B/1-20

The difficulty of adequately distributing the fibrous material through the concrete matrix was again encountered. A single perforation was dealt with incrementally in the statistical analysis. However, a confidence level of <0.5% was generated at all levels as shown in Table VI.6.

vii) Tests POL/B/1-5 and POL/B/10

A standard statistical plan consisting of twenty tests was initiated using this 37mm length lattice bundled fibre. Unfortunately, only a small quantity was eventually received from the manufacturers, limiting the tests to an incomplete series. It was qualitatively observed that the polypropylene bundled lattice fibre has great potential in terms of its mixability in a standard concrete mixer, although its use in a dry-mixed sprayed concrete application would certainly require further investigation. The fibre did not appear to enhance matrix ballistic resistance to any greater degree than the other inclusions tested. Hence because of its cost and import difficulties, its use was discontinued.

4.3.4 Discussion of Statistical Approach

Although the approach described has been used successfully in the past, it was shown to be of very limited value in investigating fibre-reinforced concretes under the conditions employed. Possible reasons for this are:

i) Variation in curing conditions during the first 24 hours,whilst the concrete was still held in the moulds, could be significant since testing is at only three days.

ii) Use of only a single slab at each selected point in the mathematical model, potentially leading to a non-representative value being input to the model.

iii) A larger number of perforations occurring than initially expected.

iv) Several alternative types of projectile path development with different effects on path length, were observed.

Although the optimisation of the fibre-reinforced composites has not been possible, some useful conclusions were drawn from these series:

i) The very fine fibrous material Kevlar-29, consisting of 12μm diameter fibres, initially in bunches of 600 filaments, is not particularly suitable for uniformly random dispersion into a concrete containing coarse aggregate. Whilst it may be possible to develop specialised equipment to aid in the injection and dispersion of this material, its high cost and lack of availability make it an unattractive proposition at the present time.

ii) Polypropylene lattice bundled fibre is an easily distributed material which may add to the post-impact structural integrity of a concrete material, but it is not readily available and its use for sprayed concrete application requires further study.

iii) Steel fibrous materials are the most suitable for sprayed concrete application since their inherent stiffness encourages separation during mixing, assuming a length/diameter ratio of not greater than 100 is used.

iv) The mechanisms involved when a projectile impacts and penetrates into fibre reinforced concrete are very complex. A better understanding of these may aid design of protective barriers. Therefore, in addition to the further studies to optimise fibre reinforced concrete (Section 4.4) some tests to examine impact and penetration mechanics were initiated (Chapter 5).

4.4 Limited Variable Approach

Following the failure of the relatively complex statistical approach, in which the interaction of five primary independent variables was examined, a conventional parametric study was initiated. As discussed in Section 4.3.4, significant lack-of-fit of the generated mathematical models had been observed, due possibly to target inconsistency and non-typicality. The replacement approach reduced the likelihood of such difficulties by lowering the number of primary independent variables considered and increasing both the number of specimens at each particular material combination and the specimen age at testing. Such an emphasis made the microcomputer-based statistical analysis redundant, since neither aggregate/cement ratio nor water/cement ratio was varied to provide the appropriate model points. It was felt that this significant change in approach was necessary to produce data with an acceptable level of statistical confidence. It was further recognised that the quadratic response surface technique could, depending upon the results of the limited variable approach, possibly be used to fine-tune the obtained information in a further experimental programme.

4.4.1 Description of Method

On the basis of published information on sprayed concrete (for example, Concrete Society (1980), and Hannant (1978)) and on the preceding experimental studies, a single concrete mix design, detailed in Table 4.11, was selected for all tests using 10mm single size limestone, basalt and river gravel respectively as coarse aggregates.

Fibre choice was governed by low unit cost, each of uniform mixing and availability. The earlier work had suggested fibrous inclusions had little, if any, effect on penetration resistance, so those fibres which had appeared to have the most significant effect on spall resistance were chosen, i.e. 25 x $\overline{0.3}$mm nominal diameter melt extracted carbon steel fibre,

25 x 0.25mm brass-coated indented circular drawn steel fibre (Duoform) and 25 x 0.25mm brass-coated circular drawn fibre.

Five levels of fibre content from 0% to 10% by weight, were chosen for each of the nine possible aggregate/fibre type combinations. The upper limit, equivalent to 3.0% fibre volume, which is very high, was chosen because some of the earlier work had shown that penetration path length could be greatly reduced if the projectile encountered less dense composite pockets, which are a result of fibre balling during mixing with high proportions of fibre.

Three similar specimens were cast for each aggregate/fibre content combination. There were nine series of fifteen specimens, a total of 135 tests. All tests were carried out using a single central impact of a 7.62mm A.P. projectile after seven days curing, the first 24 hours in the mould and the remainder in a constant humidity room. Damage was assessed using the methods described in Section 3.5.

4.4.2 Test Results

The complete set of results are listed in Appendix VII, but in this section they are presented in graphical form for each coarse aggregate type in turn. At each fibre content there are three points, one for each slab cast. Occasionally, for reasons stated, not all three points have been used to find the mean value. The figures in brackets at each fibre content are the mean values for the experimental points actually used. The best fit lines through the mean points have been fitted by regression analysis. Graphs comparing the concrete compressive strength and density have only one point for each fibre content, as a single set of three cubes was taken for each series of three slabs and generally tested at 7 days. On a few occasions cubes were tested at 8 days and in two cases at 12 days. Neville (1981) suggests that the increase in cube strength from 7 to 28 days is of the order of 50%. Hummel (1959) has suggested a linear relationship between strength and logarithm of age within the range 3 days to 2 months.

As the 8 day and 12 day strengths would therefore be expected to be about 5% and 20% respectively higher than the 7 day strength, they have been reduced by these amounts. This reduction caused a negligible change in the observed trends.

4.4.2.1 Limestone Series

Figure 4.3 shows penetration path length variation with fibre content for concretes cast using limestone aggregate. For melt extract fibres there is a trend for decreasing penetration with increasing fibre content. However, two specimens, one with no fibre and the other with 10% fibre had very low penetration path lengths due to no definite burrow being formed. When these two low values are disregarded, the rate of reduction in path length with increased fibre content remains the same, but the intercept with the path length axis is increased.

A similar slight reduction in path length with increasing fibre content was noted for the Duoform fibres. One low penetration at 7.5% fibre content was disregarded in establishing the mean value because the projectile had glanced off the velocity measuring station before impact.

For drawn fibres there was a large variation in penetrations for the 0%, 7.5% and 10% fibre contents as a result of no projectile burrows being apparent in three specimens after sectioning. Including these low points gives a trend for reduction in path length with increasing fibre content, but the trend is less apparent if they are excluded.

Figure 4.4 shows true crater volumes plotted against fibre content. The addition of 2.5% melt extract or Duoform fibres to plain concrete results in a very significant decrease in crater volume and a smaller decrease with the addition of more fibre, the minimum volumes being at 10% and 7.5% fibre contents for melt extract and Duoform respectively. The variability of the crater sizes when these fibres are included is much less than those found with plain concrete. For drawn fibres the effect of

increasing fibre content on crater volume was more gradual, with a minimum volume being recorded at 7.5% fibre content.

Figure 4.5 is a plot of cube compressive strength against density for all of the limestone concrete. This shows the expected trend of increasing strength with density. The figures beside the experimental points are the percentages of fibres in the mix. Close examination will show that when melt extract fibres are included in the concrete, increasing fibre content gives an increase in concrete compressive strength and density. This corresponds with the trend for decrease in penetration path length and crater volume with increasing percentages of melt extract fibres shown in Figures 4.3(a) and 4.4(a).

Figure 4.5 shows that for concrete with 7.5% and 10% Duoform fibres and 10% drawn fibres, low densities and strengths were measured. This is due to the higher percentages of these fibres preventing thorough mixing of the concrete/fibre composite and giving non-uniform voided specimens. Figures 4.3(b) and (c) and Figures 4.4(b) and (c) would suggest that, in terms of penetration path length and crater volume, these are good mixes though the relatively low values of the material properties at 7 days are such that they could be considered unsuitable for structural use, either on strength or durability grounds.

4.4.2.2 Basalt Series

Figure 4.6 shows penetration path lengths plotted against fibre content for concretes cast using basalt aggregate. For melt extract fibre concretes (Figure 4.6(a)) there appears to be a trend for actual path lengths to increase slightly with fibre content, more consistent results being obtained at higher fibre contents. One specimen with 2.5% fibre content had a low penetration path length of 30mm because there was no evidence of a projectile burrow on sectioning. Omitting this value in the analysis does not change the overall trend.

Figure 4.6(b) shows that for Duoform fibre concrete although a minimum mean penetration path length was measured at 5% fibre content, the variation in mean path length over the range of fibre contents was small. The regression analysis indicated a very slight trend for increasing path length with fibre content.

For concrete containing drawn fibres (Figure 4.6(d)) there appears to be a slight trend for decreasing penetration path length with increasing fibre content. It should be noted that one of the specimens containing 5% fibre was perforated, and although the actual penetration path length through the specimen was measured, this will be an under-estimation because of the residual energy in the projectile leaving the specimen. Omitting this value does not significantly alter the gradient of the linear regression.

Figure 4.7 shows the relationships between true crater volume and percentage fibre for the three fibre types. For melt extract fibre concretes (Figure 4.7(a)) the inclusion of 2.5% fibre results in a very significant reduction in the mean crater volume. Only two values were available to find the mean for the 0% fibre content specimen as the third specimen split completely on impact. Increasing fibre content leads to further, but much smaller, reduction in the measured crater volumes.

For Duoform fibre concretes (Figure 4.7(b)) there is a more gradual decrease in crater volume with increasing fibre content, the most significant reduction being measured when the fibre content was increased from 2.5% to 5.0%.

In the case of the drawn fibre concretes (Figure 4.7(c)) a significant decrease in volume was noted when the fibre content increased from 0% to 2.5%. The general trend is for decrease in mean volume with increase in fibre content, although the minimum mean volume was actually obtained with 7.5% fibre.

Figure 4.8 is a plot of cube compressive strength against concrete density for all the basalt concretes, all values being adjusted to a seven-day equivalent. The trend for increased density and strength with increasing percentage of melt extract fibres, although apparent, is not so marked as with limestone concrete. Again, inclusion of higher percentages of Duoform and drawn fibres has led to mixing problems and yielded low densities and strengths making the concretes probably unsatisfactory for structural use.

4.4.2.3 River Gravel Series

Figure 4.9 shows penetration path length variation with fibre content for concretes cast using river gravel aggregate. Figure 4.9(a) shows that using melt extract fibres there was a large range of measured penetration path lengths for each fibre content, possibly due to the number of tests in which the projectile core was fractured. One of the 0% fibre specimens had no projectile burrow; however ignoring this specimen only slightly alters the apparent trend for path length to increase with increasing fibre content.

Gross difficulties were encountered in trying to incorporate 10% Duoform fibres in the river gravel concrete so these three specimens were not cast. The results for the other four fibre levels are shown in Figure 4.9(b). There is an indication of path length increasing slightly with fibre content. If the low value, due to lack of penetration burrow, at 2.5% fibre content is ignored, the same trend is observed with a reduced correlation coefficient. Again in a number of tests the projectile core fractured during penetration and the measured path lengths are therefore probably on the conservative side.

Two of the experimental points giving low values of path length in Figure 4.9(c), which shows the results for drawn fibre contents, have been disregarded because the projectiles glanced off the velocity rig shrapnel guard before impacting the targets. The remaining points indicate a trend

for reduction in path length with increasing fibre content. One of the values obtained using 10% fibre content is low due to the absence of a projectile burrow. If this point is ignored, then the general trend becomes less significant and the minimum mean penetration path length is recorded at 7.5% fibre content.

Figure 4.10 shows the variation in true crater volumes with fibre content for concretes cast with river gravel aggregate. Figure 4.10(a) shows that for melt extract fibres there is a reduction in crater volume with fibre content up to 5% fibre. Increasing amounts of fibre results in slightly larger crater volumes being measured. It is noticeable that the reduction in crater volume from 0% to 2.5% fibre content is much less marked than with the other aggregates.

The results for Duoform fibre concrete containing river gravel (Figure 4.10(b)) were inconclusive. Although the largest craters were formed with 0% fibre, there was no definite trend with increasing fibre content.

Figure 4.10(c) shows a distinct decrease in crater volume with increasing percentage of drawn fibres, the most significant reduction occurring when the first 2.5% fibres were added. Two low points at 0% and 5% fibre content should be ignored for reasons stated above.

Figure 4.11 shows that as with other aggregate types there is a trend for increasing compressive strength with increasing density which is more marked for the melt extract type fibre concretes than the others. Again problems in mixing higher percentages of Duoform and drawn fibres are apparent with low strength being observed for the 7.5% and 10% drawn fibres. The 10% Duoform fibre mix was not cast because of its gross heterogeneity. It should be noted that for those specimens which could be considered adequately mixed, lower strengths were measured on river gravel cubes than those from cubes with the other two aggregates.

4.4.3 Discussion of Limited Variable Approach

4.4.3.1 Variability of Results

Before discussing the results of the limited variable approach further, it is worth considering the variation in the results from similar specimens so that the reliability of the trends may be appreciated. Examination of Figures 4.3, 4.4, 4.6, 4.7, 4.9 and 4.10 shows that for any set of three similar specimens there may be considerable variation in penetration path length and crater volume. In a few cases, as detailed in Section 4.4.2, low penetration values were obtained because no projectile burrows were found on sectioning the specimens. Possible reasons for this are discussed in Section 5.3.3 but in the following discussion these low penetration values have been omitted from the analyses. The crater volumes in these cases have, however, been included, since it is considered that these will be fairly representative. Some indication of the inherent scatter in the results of projectile penetration into concrete test data may be seen in Table 4.12. This shows the range, means and standard deviations of values obtained from tests on sets of nominally similar specimens which contained no fibres. The considerable scatter shown is similar to that found in penetration studies on rock/elastomer composites (Anderson et al. 1980)). Wolfersberger (1985) in a data base search of concrete penetration found that rarely did identical projectiles impacting identical concrete targets product identical results. In the present study the scatter may be due also to slight variations in some of the secondary variables listed in Table 4.2. The introduction of fibres into the concretes is likely to increase the variability, particularly when the inclusion of large amounts of fibre creates mixing difficulties and leads to non-uniform concretes.

Figures 4.5, 4.8 and 4.11 give plots of '7 day corrected' compressive strength against density for the limestone, basalt and river gravel concretes respectively and these highlight some of the mixing problems.

Linear regression analyses of these plots gave percentage fits of 82.5%, 85.9% and 81.2% for limestone, basalt and river gravel concretes respectively, indicating highly significant relationships between increasing compressive strength and increasing density. However, more detailed examination of the plots shows that density and strength did not always increase with increasing fibre concentrations.

For concretes cast with melt extract fibres there is a trend for increasing density with increasing fibre content, the trend being most marked for the limestone/melt extract fibre concretes as shown in Figure 4.5. The increase in density in this case also leads to an increase in compressive strength with increasing fibre content. However for the other two aggregate types there is little increase in compressive strength with density increase due to increasing fibre content (Figs. 4.8 and 4.11).

Melt extract fibres have a non-circular cross section and this provides them with an extra stiffness which reduces their effective aspect (length/diameter) ratio. This reduction aids the incorporation of the fibre into the concrete since there is little tendency for the fibres to bunch during mixing. For the limestone/ melt extract fibre concretes the strengths and densities would indicate a homogeneous material at all fibre content levels. For the basalt/melt extract fibre concretes it was concluded that the specimens were homogeneous up to 5% fibre content, but there was some heterogeneity probably due to air voids in the 7.5% and 10% fibre content specimens, as indicated by a slight decrease in compressive strength from the 5.0% fibre content value. The increase in density with fibre content in Figure 4.11 would indicate that the river gravel/melt extract fibre concretes were fairly homogeneous at all fibre content levels, although strength did not increase significantly.

The trends for concretes cast with Duoform fibres were not so apparent as those for melt extract fibre concretes. Figure 4.5 shows that the addition of 2.5% Duoform fibres to the limestone concrete gave an

increase in both density and compressive strength, indicating a homogeneous mix. Addition of 5% fibres increased the density slightly but led to a strength decrease, perhaps indicating that the specimens were becoming non-homogeneous. As more fibre was added the density and compressive strength reduced considerably indicating a non-uniform voided concrete. For basalt/Duoform fibre concrete (Figure 4.8) the density and compressive strength increased when 2.5% fibres were added indicating a homogeneous material. Addition of 5.0% and 7.5% fibres led to a slight increase in density but with a corresponding slight decrease in strength indicating slight non-homogeneity. The addition of 10% fibres led to a significant drop in both density and strength values as a result of the specimens being voided. Figure 4.11 shows that, as with the other two aggregate types, and increase in both density and compressive strength, indicating homogeneity, was observed when 2.5% Duoform fibres were added to river gravel concrete. The addition of 5.0% and 7.5% fibres, whilst leading to density increases, gave compressive strengths lower than that found with a 2.5% fibre content, thus indicating that the specimens were beginning to show signs of non-homogeneity. The considerable mixing difficulties encountered when 10% Duoform fibres were introduced into river gravel concrete meant that this series of specimens was not cast.

The combined results from the Duoform fibre test series would suggest that a homogeneous material can only be cast using 2.5% fibres. At 5% fibre content there may be slight non-homogeneity but this should have little effect on the strength or structural behaviour of the material. However, including 7.5% or 10% fibre content led to gross non-homogeneity and materials which are unsuitable for structural purposes.

The trends for all concretes cast with drawn fibres are similar to those for the Duoform fibre composites. As shown in Figure 4.5, up to 5% fibre incorporated in limestone concrete gives slight increases in density and strength indicating homogeneous specimens, but a decrease in strength

is noted with 7.5% fibre indicating the onset of non-homogeneity. With 10% fibre a low density and strength are recorded indicating a voided specimen. Figures 4.8 and 4.11 show that for basalt and river gravel concrete with up to 5.0% drawn fibre content, density increases, although there is little strength improvement between 2.5% and 5.0% fibre content suggesting that at the latter level a little voiding may be occurring. Very low values of density and strength were recorded from those specimens containing 7.5% and 10% drawn fibres confirming the difficulty of obtaining homogeneous mixes at these high fibre contents.

Both Duoform and drawn fibres, although having nominally the same aspect ratio (100) as the melt extract fibres, are more flexible and tend to bunch during mixing. The density and strength measurements would suggest that although it may be possible to obtain satisfactory concretes containing up to 10% melt extract fibres, an acceptable upper limit for Duoform and drawn fibres would appear to be about 5% fibre content. There were also signs that it was more difficult to cast fibre concretes using the rounded river gravel aggregate than the more angular limestone and basalt aggregates. Figure 4.11 shows that trends with increasing fibre content are less marked and the slope of the strength/density regression line is much shallower than with the other two aggregates.

Because of the inherent variability of penetration test results and the effects of non-homogeneity of some concretes cast with high fibre contents, statistical analysis of the results has been left at a fairly elementary level, and when examining trends in the following results, the variation should be considered before drawing any conclusions.

4.4.3.2 Penetration Path Lengths

Figure 4.3 shows the results for the concretes cast with limestone aggregates. With all fibre types the regression lines have a slight negative slope indicating a slight decrease in penetration path length with increasing fibre content, but it should be noted that in no series was the

minimum mean penetration path length associated with the maximum fibre content.

In Figure 4.6 penetration path lengths are plotted against fibre content for the concretes cast with basalt aggregates. the regression line through the basalt/melt extract fibre results has a slight positive slope indicating a slight increase in penetration path length with increasing fibre content. At the higher fibre contents there is surprisingly little scatter of results. The regression line through the basalt/Duoform fibre results is almost horizontal indicating that penetration path length is independent of fibre content. In one of the tests in the basalt/drawn fibre series a target perforation occurred. The path length in the target was measured as 131mm and since the projectile will have had some residual kinetic energy when exiting the specimen, this figure will be an under-estimation of what the actual path length would have been if perforation had not occurred. This path length of 131mm is 14% higher than the next highest path length recorded in any of the nine test series. Including this point in the analyses has no significant effect on the regression line as shown in Figure 4.6(c), the trend being for a slight decrease in penetration path length with increasing fibre content. Figure 4.9 shows the penetration path length with increasing fibre content for the river gravel concretes. For melt extract and Duoform fibres there were slight positive slopes to the regression lines indicating a slight increase in penetration path length with increasing fibre content. The opposite trend was found for the river gravel/drawn fibre series. Significant amounts of scatter may be observed in these series, particularly for the river gravel/melt extract fibre tests.

Table 4.13 lists the coefficients in the regression equations and the percentage fit of each regression line. The conflicting trends of positive slopes in some series and negative slopes in others suggests that increasing fibre content has no significant effect on penetration path

length. The low values of the slope coefficients and the low values of percentage fit confirms that the penetration path length is independent of the amount of fibre included in a concrete composite. It could be argued that only results from those specimens which appeared homogeneous should be considered in this analysis. However, some of the tests described in Section 4.3.3 indicated that non-homogeneities could destabilise the projectile and reduce its penetration path length. Results for the complete range of fibre levels were therefore included in the analysis.

All the results for each aggregate type can be grouped together to give a sufficiently large population to examine the influence of aggregate type on the penetration resistance. Figure 4.12 shows histograms of penetration path lengths for each aggregate type. It can be seen that the shortest mean penetration path length of 78mm was found in concretes cast with river gravel aggregate, although there was a wide range of values as indicated by the standard deviation of 20mm. Limestone concretes gave a mean value of 84mm with a standard deviation of 12mm and basalt concretes yielded the largest mean value of penetration path at 89mm with a standard deviation of 16mm.

Similar penetration studies of rock/elastomer composites (Anderson et al.(1980)) showed that the harder the rock and the denser the aggregate packing, the better the penetration resistance. For these rock/elastomer composites best performance was achieved with river gravel which gave a mean normal penetration depth of 51mm for the optimum composite mix. For limestone and basalt composites the mean normal penetration depths were 75 and 81mm respectively.

Comparison of the results with the present study shows that although the performances of the limestone and basalt aggregate fibre concretes are only slightly inferior to the rock/elastomer composites, and that best performance was achieved in both cases using the river gravel aggregates,

the improvement in performance using river gravel concretes was not nearly so marked as in the rock/elastomer composite study.

In the rock/elastomer study it was found that the best performance was achieved using large size aggregate (26.5 to 37.5mm), and it was argued that the enhanced performance was due to the harder river gravel particles fracturing the cores of the armour piercing projectiles and thus reducing their efficiency as penetrators. Because the fibre reinforced composites were designed for sprayed application, maximum aggregate size was only 10mm. These particles are therefore less likely to break up the projectile cores than the larger ones used with the elastomer composite. However, in a number of tests using river gravel/fibre concretes, broken cores were found and these were generally associated with the lower values of penetration path length.

Comparison of the mean values and standard deviations in Table 4.12 for the fibreless concretes and Figure 4.12 for all the specimens shows a great similarity between results, a further indication that inclusion of fibres leads to no significant improvement in reducing projectile penetration. Examination of the standard deviation in Figure 4.12 shows that considerable scatter was found in the river gravel tests, probably indicating a variation in performance depending on whether the projectile collided with a number of aggregate particles and possibly fractured, giving a low penetration value, or travelled mainly through matrix material giving large penetrations. Examination of the compressive strengths of those mixes which were considered fairly homogeneous, i.e. all melt extract fibre composites and those containing up to 5% Duoform and drawn fibres, shows that the river gravel concretes were the weakest with a mean compressive strength of 45N/mm^2 compared with values of 54N/mm^2 and 49N/mm^2 for limestone and basalt concretes respectively. Thus projectiles which did not fracture on impact with hard gravel particles were likely to penetrate further through the specimen than in other aggregate concretes,

so giving the high values of penetration path length. The mean penetration path length found for basalt concretes was slightly greater than the mean value for limestone concretes. This may be due to the slightly lower mean compressive strength of the basalt concretes, as indicated above.

Least scatter of results was found with limestone concretes where the nature of the aggregate led to a very homogeneous composite when combined with cement paste.

The significance of the range of variations found for each aggregate type is indicated in Table 4.14. On the basis of the calculated mean values and standard deviations from the tests, the penetration path lengths have been predicted for certain degrees of confidence.

It can be seen that although river gravel gave the lowest value of mean penetration path length in the test series, the predicted path length for 99% confidence is the largest because of the scatter of test results. The more homogeneous nature of the limestone concretes means that at the 99% confidence level these concretes give the shortest predicted penetration path length.

It is interesting to note that the penetration path length (131mm) measured when the one perforation occurred in the basalt test series is just marginally greater than the path length (129mm) predicted for 99% confidence in this series.

It should be stressed that all measurements in this study are in terms of penetration path length, and as discussed in Chapter 5 of the report the projectile burrows are rarely straight and perpendicular to the impact face. If fibre reinforced concrete is cast to a thickness of 130mm this will be on the conservative side, particularly with limestone aggregates where there would appear to be a superior bonding between concrete matrix and aggregate due to the chemical nature of the latter.

Reference to Table 4.6 will show that in the preliminary tests to determine suitable specimen thicknesses, none of the 125mm nor 150mm thick specimens were perforated.

4.4.3.3 True Crater Volumes

Figures 4.4, 4.7 and 4.10 show true crater volumes plotted against fibre content for each combination of aggregate and fibre type. In all test series the largest craters were found in specimens without any fibres, and there was considerable variation in the crater volumes for these specimens, as shown in Table 4.12. The addition of fibres reduces the variability of the results up to the 5% fibre content level i.e. the range over which all specimens can be considered fairly homogeneous. This is demonstrated in Table 4.15 which gives the maximum percentage variation from the mean value in a set of three results from similar specimens for each test series. The effect of adding greater percentages of fibre to produce non-homogeneous specimens is reflected in the increased percentage variations at the 7.5% and 10% fibre concentration.

Although the non-homogeneity of these higher fibre content specimens leads to more variation in the results, there is still a tendency for the true crater volume to decrease with the inclusion of more fibres. This may be due to the fact that front face spall is partly caused by the tensile stress waves which are reflected from the back face of the impacted specimen, and the non-homogeneities are likely to affect the transmission of these stress waves through the specimen. This is further discussed in Chapter 5.

The trends for decreasing crater volume with increasing fibre content shown in Figures 4.4, 4.7 and 4.10 are such that the use of linear regression analysis was not considered appropriate. To obtain an impression of the overall trends, the mean crater volumes for each fibre content level have been expressed as percentages of the mean crater volume at zero fibre level, and plotted against fibre content in Figure 4.13.

This shows that crater volume reductions varying between 16% and 78% are found at the 2.5% fibre content level. At the 5% fibre content level one very large crater volume recorded in the river gravel/Duoform series is greatly influencing this result. The difficulties of incorporating rounded river gravel and the Duoform fibres gave a lower than expected strength at this fibre level, as indicated in Figure 4.11, suggesting a non-homogeneous mix which may be responsible for this anomalous result. Ignoring this series, Figure 4.13 shows that at the 5% fibre content level the total crater volume reduction varies by between 52% and 70% of the 'no fibre' crater volume.

Ignoring the anomalous river gravel/Duoform series results, the maximum crater volume reduction occurred on increasing the fibre content from 2.5% to 5.0% in the basalt/Duoform fibre series and river gravel/melt extract series. and on initially adding 2.5% in all other series.

The severity of the front face spall in an unreinforced concrete will be dependent on the tensile strength of the concrete. Although tensile and compressive strengths cannot be precisely related, it is interesting to look at the relationship between the mean true crater volume and the compressive strength of the fibreless specimens, as shown in Figure 4.14. There is a definite trend for decrease in crater volume with the increase in compressive strength, the percentage fit of the best straight line through the points being 52%. Although the addition of fibres may only increase the compressive strength of concrete by up to about 25%, a much more significant increase in tensile strength may be achieved, and this will greatly enhance the spall resistance as shown in Figure 4.13.

An indication of the relative performance of the different aggregates and fibre types with respect to spall resistance may be obtained by looking at the mean true crater volumes for each aggregate and fibre type in turn. The values for the series with no fibres have been excluded because of the large variation in results (Table 4.12). In Table 4.16 mean values are

only listed for the 2.5%, 5.0% and 2.5% + 5.0% combined because at higher fibre concentration heterogeneity is such that comparisons would not be valid. The table would suggest that within the ranges of variability found in this testing, limestone and basalt concretes are fairly similar, but fibre concretes cast with river gravel aggregate may be susceptible to greater front face spalling. Table 4.16 also indicates that at a 2.5% fibre content it is irrelevant which fibre type is used, but at 5% fibre content a slightly better performance may be obtained with melt extract fibres or Duoform fibres.

4.4.4 General Discussion

The major objective of this study was to examine the use of fibre reinforced concretes, suitable for application by a spraying process, as penetration resistant structural materials. The spraying techniques impose constraints on the mix, as do the requirements of a fibre concrete, and maximum aggregate size has been limited to 10mm. The relatively low water/cement ratios required by sprayed concretes produce a higher than "conventional" 7-day strength; a figure of 40N/mm^2 is a reasonable estimate for the fibreless concretes used in this parametric study. This is an adequate value for most structural purposes. Addition of fibre, up to the limit of homogeneous mixing, will enhance this strength. The basic mix design of Table 4.11 has been found satisfactory. Depending on the type of spraying process used it may be difficult to control the water content and for any mix suitable compliance testing should be used at the point of application of the material.

The tests carried out using the "limited variable" approach have shown that the addition of fibres does little, if anything, to improve the penetration resistance of the concrete. Addition of fibres does however considerably reduce the front face spall damage and so may improve the performance of the material against repeated fire.

Although an addition of 2.5% fibre significantly improves spall resistance, examination of Figure 4.13 will show that, overall, more consistent improvement will be achieved by incorporating up to 5.0% fibre by concrete weight into the mix. However, at this fibre content, signs of non-homogeneity are becoming apparent. The 2.5% and 5.0% figures should thus be considered as minimum and maximum values respectively.

Although there was little difference in the performance of concretes containing the different steel fibre types, the homogeneity produced in targets manufactured with the easily mixed melt extract fibres suggests that these should be used wherever possible.

Of the aggregates, rounded river gravels should be avoided if possible since they produce a fibre concrete which is slightly more difficult to uniformly mix, causing lower compressive strengths and, unless the projectile core is fractured in the early stages of penetration, larger actual penetration depths. Such concretes also appear to generate larger front face "true" craters than either of the other two aggregates. Better performances are achieved with the more angular aggregates, particularly limestone which combined well with the cement matrix to give better penetration resistance with less variation in performance.

For the materials tested, the optimum combination in terms of reliable performance would be the inclusion of 5% melt extract steel fibres in a 10mm limestone aggregate concrete mix.

It is of interest to compare the results of this study with previously published work. However, as only a single projectile type at a single velocity has been used in these trials, there is no possibility of either definitively validating or disproving the available empirical formulae. Only general comment may be made for these existing approaches, which were actually produced from trials using much larger missiles. The relevant penetration prediction equations from the literature survey (Chapter 2) are:

i) Austin and Pringle (1971) - Equation 2.5

ii) NDRC formulae (1946) - Equations 2.8 and 2.9

iii) Berriaud et al. (1982) - Equation 2.11

In each case, the penetration depth is inversely proportional to the concrete compressive strength. Such a result has not been found in these studies, where the obtained compressive strength was very much dependent upon the homogeneity of the composite, this being influenced by the fibre content of the target; whereas penetration path length was not greatly influenced by fibre proportion. A further factor may be the similarity of projectile to aggregate size, this aspect is worthy of further study for plain concretes which are not required to have a sprayed application.

A comparison may qualitatively be made between this study and the few published researchers who have considered the particular projectile-target material combination. In general, these have been basic field trials, carried out by the military, and do not contain very much detail of material design and experimental procedure. Naus and Williamson (1976), for single shot 7.62mm ball ammunition fired from a M37 machine-gun at mainly 100m range, perceived "only a very slight trend toward a decrease in depth of penetration with increase in fibre content". The coarse aggregate used in the tests was described only as "3/8" gravel" and is not further specified. In this thesis, river gravel concretes showed the greatest scatter of results; any such trends are thus likely to be only tentative at best. It was also reported that back face scabbing reduced with increasing fibre content, at each specimen thickness between 25mm and 150mm. This is in line with the findings of Hüslewig et al. (1982); it is however not directly comparable with this study, where back face scabbing was specifically disallowed.

The Royal Ulster Constabulary (1976) considered the use of unspecified steel and polypropylene fibre concretes sprayed as between 1" to 4" thickness claddings on to conventional brick/block cavity walls. The

results obtained are not directly synonymous with this study but did indicate that, at lower cladding thicknesses, the likelihood of failure increased when armour-piercing rather than ball ammunition was used. Such a finding was noted from the very preliminary tests of this study.

Other researchers, such as Finch (1977) and Port (1980) concluded that (sprayed) fibre concretes, incorporating both steel and polypropylene fibres, showed potential for overall ballistic resistance enhancement of existing structures. Such findings are in general agreement with this thesis; the extent and volume of "true" crater formation was reduced with increasing fibre content for all concrete and fibre combinations tested. However, the previously intimated improvement in penetration resistance was not confirmed by the research reported here.

4.4.5 Field Use of Fibre-Reinforced Sprayed Concretes Against Small Arms Fire

The basic mix used for the "limited variable" approach to testing was selected to permit the composite to be placed by either of the two commonly available sprayed concrete techniques.

The first of these is known as the "wet-mix" process. It involves the transporting of ready-mixed concrete to the point of application through lengths of hose, the material being moved by a displacement type pump. On reaching its destination, compressed air is used to break up the composite and project it on to the structure or formwork. The advantages of this method are;

i) The proportions of the concrete constituents are totally defined at the batching and mixing stage.

ii) A smaller amount of aggregate (and fibre) rebound occurs than with the alternative dry-mix system.

iii) Less dust is raised than with the dry-mix system.

iv) Samples can more easily be taken for concrete compliance testing than with the dry-mix system.

In the alternative "dry-mix" process, a mix consisting of all of the concrete components (except water and, where appropriate, fibres) is charged into a mechanical feeder and carried pneumatically along the delivery hose. At the nozzle, water is injected into the dry-mix before its projection on to the work surface. The quantity of water added is left to the discretion of the nozzle operator. This approach means it is impossible to quantify the water/cement ratio of the as-placed concrete. Consequently, test panels must be manufactured at the site of the work to produce samples for compliance testing. The system, nonetheless, has several advantages over the wet-mix process;

i) The dry mix may be carried over significantly greater distances by compressed air than it is practicable for a displacement pump to transport a wet mass.

ii) Production may be temporarily halted without any need to clear the feeder and delivery hose.

iii) The capital cost of dry-mix equipment is low compared with wet-mix.

iv) Equipment is simpler, leading possibly to less maintenance and down-time.

Both of these processes have been used for successful fibre concrete placement. In the wet-mix system fibres may be added either in the mixing hopper or at the delivery hose nozzle. A third possibility is to project the fibres on to the finished work before its initial set occurs.

It is more difficult to add fibres without conglomeration during initial batching of dry-mixed materials. It is thus preferable to use a separate pneumatic feed for the fibres. This is normally a delivery hose tapped into the concrete feed at a point immediately before the water is added to the mix. Alternatively, fibres have been sprayed on to freshly placed concrete, the main problem being the impossibility of establishing a

truly random three-dimensional distribution of the fibre throughout the concrete.

Various references are available discussing the area of sprayed concrete production. Undoubtedly, one of the most useful starting points is the American Concrete Institute Special Publication No 14: "Shotcreting", whilst the American journal "Concrete International", in January 1981, devoted a complete issue to an assessment of the then contemporary state-of-the-art. The proceedings of a Symposium on Sprayed Concrete (C180) held in London (1980) is a further source of information. Short courses, regularly organised by the Cement and Concrete Association, permit the detailed discussion of specific facets of the techniques.

For the materials of this project, it is recommended that the wet-mix system be adopted wherever possible. The quality and consistency of the composite are more easily controlled and tested, as they are outside the influence of a nozzle operator. Also, personnel safety is greatly enhanced by employing a less rebound-prone technique to place a composite containing potentially dangerous steel-fibre inclusions. In either case the operatives should undergo supervised training and be supplied with adequate safety equipment, specifically suited to this very specialist procedure.

Batching of the material should be by weight, converted perhaps into proportions equivalent to full bags of Ordinary Portland Cement. In ideal circumstances,a fully dry aggregates should be used. Otherwise, a standard moisture content test may be used to assess the aggregate free water content.

The material should be placed in accordance with the recommendations of the Concrete Society Code of Practice for Sprayed Concrete (1980), complete with any later addenda or amendments. Areas particularly worthy of comment include;

i) **Rebound**

Sprayed concrete suffers from an initial inconsistency upon application due to the rebound of coarse aggregate and fibre until a sufficiently thick 'cushion' of adhesive cement paste has built up on the host surface. The thickness of this fine aggregate composite must be accurately assessed by producing test panels for any particular mix and formwork construction. The indications of this work are that mortar-type material should not be considered to contribute any significant resistance to projectile passage. The selected thickness of protection must reflect this finding; the overall value being increased as required.

For work which includes construction details such as internal wall returns and/or reveals, further operatives must be made available equipped with compressed air lances. The lances are used to remove any build-up of rebound material from potential "blind corners". Failure to remove the rebound will lead to a non-homogeneous voided construction of greatly reduced integrity and durability.

ii) **Flash Coating**

On completion of the sprayed application of a steel-fibre reinforced concrete, the finished surface will have numerous potentially injurious fibres projecting from it. These should be covered by the application of a flash coat of sprayed plain concrete.

iii) **Curing**

In large-scale use, one of the many liquid-based proprietary curing agents should be sprayed on to the finished work to avoid premature drying-out.

iv) **Formwork**

Used as a cladding material, the composite will be sprayed on to an existing structure and will not require any formwork or supporting falsework. However the surface must be clean, sound and roughened before treatment. Dry surfaces should be thoroughly wetted.

As a free-standing material adequate backing and support must be supplied. The falsework aspects of this will be very much dependent upon the structure being constructed. However, it is worth noting that both mesh-reinforced hessian, Finch (1977), and thick polyurethane sheeting have been successfully used as permanent formwork; the latter also being appropriate as insulation. In many cases it would be attractive to spray either side of the polyurethane in turn generating a filled-cavity construction. The use of inflatable structures, temporarily fixed in plan position, is becoming more common. The (often hemispherically shaped) pneumatic formwork is sprayed with concrete and deflated once the material has achieved adequate structural integrity. The mould may be re-used many times, with a rapid production cycle dependent only upon the strength-gaining characteristics of the concrete.

4.5 Other Experimental Studies

4.5.1 Use of X-Ray Photography to Monitor Fibre Distribution

During this project a limited opportunity arose to have access to X-Ray photographic equipment. It was used on a number of occasions to confirm that the mixing methods employed were providing a random three-dimensional distribution of fibre throughout each specimen, consistent with the accepted assumptions. Figure 4.15 is one such photographic plate; it shows the distribution of 25mm length melt extract steel fibres through a

150mm diameter core taken from specimen number TS89. The random distribution of the fibre is clearly seen, as is the resting position of the projectile (at 138mm penetration path length). The impact crater, burrow and rear face crater are also readily apparent in the photograph. In future studies, the use of this type of equipment would remove the need to section and/or core the concrete specimens thereby ensuring that the tested material was not damaged during analysis. This would prove especially useful with significantly fractured targets, particularly if they contain various types of detector (see Section 5.2.9).

4.5.2 Use of Electron Microscopy to Examine Projectile Target Adhesion

Throughout the study it was occasionally noted that cementitious material would adhere to the metallic projectile core during the penetration event, the resulting attachment being very difficult to break. Whilst it was not possible to accurately assess when this adhesion was occurring it was nevertheless of interest to observe it more closely.

Back Scatter Electroscopy was used to examine a single hardened steel core, Figure 4.16. At 80X magnification with the major axis of the core laying NNW to SSE in the photograph there is a clear indication of the surface indentations caused by the spinning of the projectile within the material. The implication is that the core itself retains some of the rotational force imparted by the rifling even after detachment from the projectile sheath. This effect may also be observed in Figure 4.17 where the impacted material is mild steel. At higher magnification, 390X, the adhered cement paste can be seen to have bonded within the scoring to a significant degree (Figure 4.18). It would thus seem reasonable to assume that the fusing has taken place as the projectile has come to rest. At this time the steel would be at a high temperature hence any bond generated would be likely to become more powerful as the materials cooled and contracted.

Quantitative Dependent Variable	Symbol (units)
Normal penetration depth	D (mm)
Penetration path length	L (mm)
Crater volume - apparent	V_A (mm^3)
Crater volume - true	V_T (mm^3)
Burrow diameter	D_B (mm)
Maximum crater diameter	D_C (mm)
Burrow volume	V_B (mm^3)
Material comminution	C_M

Table 4.1 Quantitative dependent variables for fibre reinforced concrete penetration event.

Quantitative Independent Variable	Symbol (units)	Status
* Water/cement ratio	w/c (-)	Variable/constant+
* Aggregate/cement ratio	a/c (-)	Variable/constant+
* Fibre content (% weight)	W_f (kg)	Variable
Age at testing	t (days)	Constant 3 days/7 days+
Fibre aspect ratio	L/d (-)	Constant-100
Bullet velocity	v_o (m/s)	Assumed constant-820
Specimen size	- (mm)	Constant-450x450x125
Maximum aggregate size	- (mm)	Constant-10
Angle of impact obliquity	- (degrees)	Constant-90
Aggregate moisture content	- (% by dry mass)	Adjusted to dryness

* Primary variables in quadratic response surface generation.
\+ For "Limited Variable" Approach

Table 4.2 Quantitative independent variables for fibre reinforced concrete penetration event.

Spec. No	Specimen Dimensions (mm)	Fibre Type	Fibre Dimensions (mm)	Coarse Aggregate Cement Ratio	Fine Aggregate Cement Ratio	Water Cement Ratio	Fibre Content (%wt)	Mix Design Source
PS1	250x250x75	Mild Steel Circ. Sect.	38 x 0.3	2.15	2.15	0.55	2.7	M10 Overlay Design
PS2	500x500x75			2.15	2.15	0.55	2.7	
PS3	610x610x75			2.15	2.15	0.55	2.7	
PS4	250x250x75	Mild Steel Circ. Sect.	27 x 1.0	2.15	2.15	0.55	2.7	
PS5	500x500x75			2.15	2.15	0.55	2.7	
PS6	610x610x75			2.15	2.15	0.55	2.7	
PS7	500x500x75			2.36	2.36	0.45	5.0	National Standard Design
PS8	610x610x75			2.36	2.36	0.45	5.0	

Table 4.3 Summary of mix designs for slab frontal area tests.

Specimen No	Compressive Strength (N/mm^2)	Density (kg/m^3)	Projectile Type	Impact Point (mm) ((0,0) is top left-hand corner	Results and Comments
PS1	36	2390	A.P.	(120,140)	Perforated, gross cracking to two nearest edges.
PS2	36	2390	A.P.	(230,260)	Perforated,no gross cracking.
PS3(1)	36	2390	Ball	(305,310)	Normal path length= 40mm, no gross cracking.
PS3(2)	36	2390	Ball	(410,430)	Gross cracking to nearest edge.
PS3(3)	36	2390	Ball	(200,405)	Normal path length= 40mm, no gross cracking.
PS4	32	2400	A.P.	(105,140)	Perforated, gross cracking to two nearest edges.
PS5	32	2400	A.P.	(235,275)	Perforated, gross cracking to two edges (possibly handling)
PS6(1)	32	2400	A.P.	(285,325)	Perforated, no gross cracking.
PS6(2)	32	2400	Ball	(410,210)	Perforated, gross cracking to nearest edge.
PS7	45	2480	A.P.	(250,285)	No gross cracking, rear crater present.
PS8(1)	45	2480	A.P.	(285,345)	Perforated, no gross cracking.
PS8(2)	45	2480	Ball	(470,460)	Gross cracking to two nearest edges
PS8(3)	45	2480	Ball	(490,410)	No gross cracking to edges.

Table 4.4 Summary of specimens tested and ammunition used for slab area selection.

Specimens No	Coarse Aggregate Cement Ratio	Fine Aggregate Cement Ratio	Water Cement Ratio	Comments and Mix Design Source
TS1-TS8	2.36	2.36	0.45	National Standard Design
TS9-TS16	2.35	2.30	0.52	Initially National Standard Design, however moisture content taken as 50% free water, requiring adjustment for comparison

Table 4.5 Summary of mix designs used for specimen thickness determination.

Specimen No	Specimen Thickness (mm)	Compressive Strength (N/mm^2)	Density (kg/m^3)	Perforation
TS1	75	60	2450	Yes
TS2	100	60	2450	Yes
TS3	125	60	2450	No
TS4	150	60	2450	No
TS5	75	61	2450	Yes
TS6	100	61	2450	No
TS7	125	61	2450	No
TS8	150	61	2450	No
TS9	75	37	2340	Yes
TS10	100	37	2340	Yes
TS11	125	37	2340	No
TS12	150	37	2340	No
TS13	75	46	2350	Yes
TS14	100	46	2350	Yes
TS15	125	46	2350	No
TS16	150	46	2350	No

Table 4.6 Summary of perforation test results.

Fine Aggregate Type	Mean Density (kg/m^3)	Mean Compressive Strength (N/mm^2)	Mean Penetration Path Length (mm)
Zone 2 Limestone	2560	44	103
Zone 3 grit (sharp)	2340	21	127
Zone 4 Building	2400	18	121

Table 4.7 Summary of results obtained for fine aggregate type investigation.

Steel Fibre Type (Aspect Ratio=100)	Mean Density (kg/m^3)	Mean Compressive Strength (N/mm)	Normal Penetration Depth (mm)
Duoform	2430	38	106
Melt extract	N/A	N/A	108
Cold-drawn circular	2440	31	109

Table 4.8 Summary of results for tests to investigate variation in normal penetration depth with steel fibre type.

Fibre Type	Length (mm)	Diameter (mm)	Young's Modulus (kN/mm^2)	Tensile Strength (N/mm^2)	Density (kg/m^3)
ME - Melt Extract Carbon Steel	25	Equiv. to 0.3mm	160	2100	7860
DUO - indented circular drawn brass-coated steel (Duoform)	25	0.25	200	1600	7860
DRA - circular drawn brass-coated steel	25	0.25	200	1600	7860
13K-Kevlar-29 (Type 970)	13	$12x10^{-3}$	58	2760	1440
37K-Kevlar-29 (Type 970)	37	$12x10^{-3}$	58	2760	1440
POL-Forta Fibre latticed bundled poly-propylene	37	N/A	4.8	483	900

Table 4.9 Material properties of fibres used in Quadratic Polynomial Fitting Analysis.

Coded Value			Value of L_i
Water/Cement	Agg/Cement	Fibre Content	
x_1	x_2	x_3	Actual Penetration Path Length
-1	-1	-1	L_1
1	-1	-1	L_2
-1	1	-1	L_3
1	1	-1	L_4
-1	-1	1	L_5
1	-1	1	L_6
-1	1	1	L_7
1	1	1	L_8
$-2^{3/4}$	0	0	L_9
$2^{3/4}$	0	0	L_{10}
0	$-2^{3/4}$	0	L_{11}
0	$2^{3/4}$	0	L_{12}
0	0	$-2^{3/4}$	L_{13}
0	0	$2^{3/4}$	L_{14}
0	0	0	L_{15}
0	0	0	L_{16}
0	0	0	L_{17}
0	0	0	L_{18}
0	0	0	L_{19}
0	0	0	L_{20}

Table 4.10 Relationship between actual penetration path length and coded level values for coefficient calculation

O.P.C.	Water	Zone 2 Limestone Sand	10mm Single Size Aggregate	Fibre Content (% wt)
1.0	0.5	2.67	1.33	0:2.5:5.0:7.5:10.0

Table 4.11 Concrete mix design ratios for limited variable approach (by weight)

Aggregate		Penetration Path Length (mm)	Crater Volume (cm^3)
Limestone	Number of tests	7	9
	Range	69-115	299-737
	Mean	86	357
	Standard Deviation	14	153
Basalt	Number of tests	9	8
	Range	73-108	138-434
	Mean	90	233
	Standard Deviation	13	114
River gravel	Number of tests	7	8
	Range	50-100	180-552
	Mean	78	305
	Standard Deviation	19	105

Table 4.12 Penetration path lengths and crater volumes for specimens containing no fibres.

Coarse Aggregate	Fibre Type	Regression line equation	% fit
Limestone	Melt extract	$\bar{L} = 92.8 - 1.28\ W_f'$	54
	Duoform	$\bar{L} = 90.8 - 1.52\ W_f'$	42
	Drawn	$\bar{L} = 84.4 - 0.48\ W_f'$	14
Basalt	Melt Extract	$\bar{L} = 84.0 + 1.6\ W_f'$	42
	Duoform	$\bar{L} = 85.0 + 0.16\ W_f'$	2
	Drawn	$\bar{L} = 94.4 - 1.08\ W_f'$	24
River gravel	Melt Extract	$\bar{L} = 62.0 + 1.52\ W_f'$	18
	Duoform	$\bar{L} = 76.9 + 0.76\ W_f'$	8
	Drawn	$\bar{L} = 94.8 - 1.52\ W_f'$	36

Table 4.13 Regression line equations and percentage fits for each test series

Degree of Confidence	Predictive Equation	Predicted path length (mm) for any degree of confidence		
		Limestone	Basalt	River Gravel
80%	$L_P = \bar{L} + 0.86\sigma$	95	103	95
90%	$L_P = \bar{L} + 1.32\sigma$	100	110	105
95%	$L_P = \bar{L} + 1.72\sigma$	105	116	113
97.5%	$L_P = \bar{L} + 2.09\sigma$	110	122	121
99%	$L_P = \bar{L} + 2.53\sigma$	115	129	130

Table 4.14 Predicted penetration path lengths for each aggregate type for certain degrees of confidence, irrespective of fibre content.

Test Series	Fibre Content				
	0%	2.5%	5%	7.5%	10%
L/ME	50	36	15	30	56
L/DUO	35	46	15	5	35
L/DRA	7	15	35	33	34
B/ME	50	10	27	9	50
B/DUO	27	31	18	120	2
B/DRA	72	59	22	27	38
RG/ME	16	13	31	37	55
RG/DUO	59	8	34	18	-
RG/DRA	20	30	9	40	47
Average for all series	37	28	23	35	40

Table 4.15 Maximum percentage variation of any crater volume from the mean volume value for a set of three similar tests.

	Fibre Content		
	2.5%	5%	(2.5% + 5%)
All Limestone	122	130	252
All Basalt	136	79	215
All River Gravel	189	176	365
All Melt Extract	157	123	280
All Duoform	145	156	301
All Drawn	145	205	350

Table 4.16 Mean true crater volumes in cm^3 for combined series at different fibre contents.

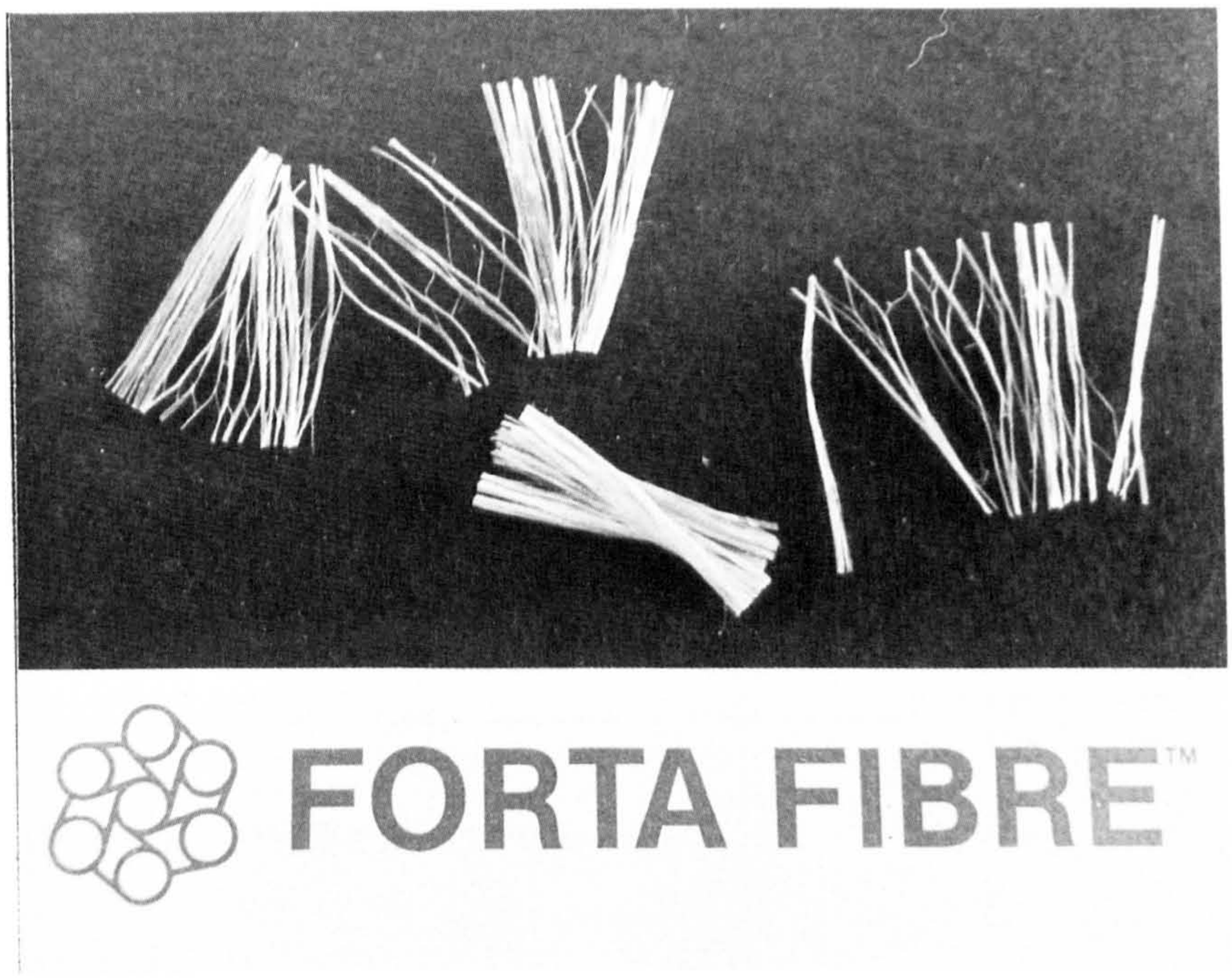

Figure 4.1 Lattice-bundled Polypropylene Fibre

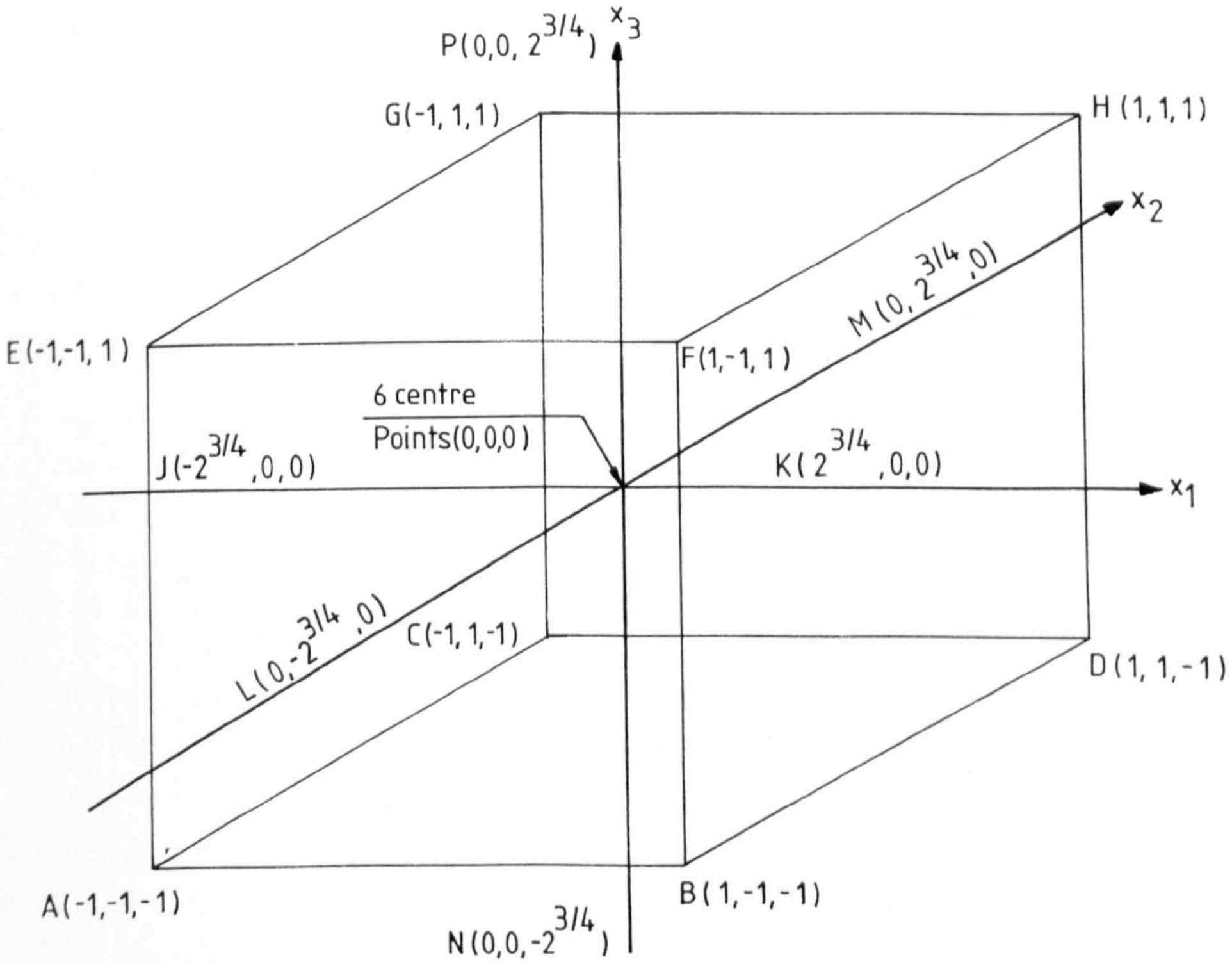

Figure 4.2 Central Composite Rotatable Experimental Design in 3 x-variables

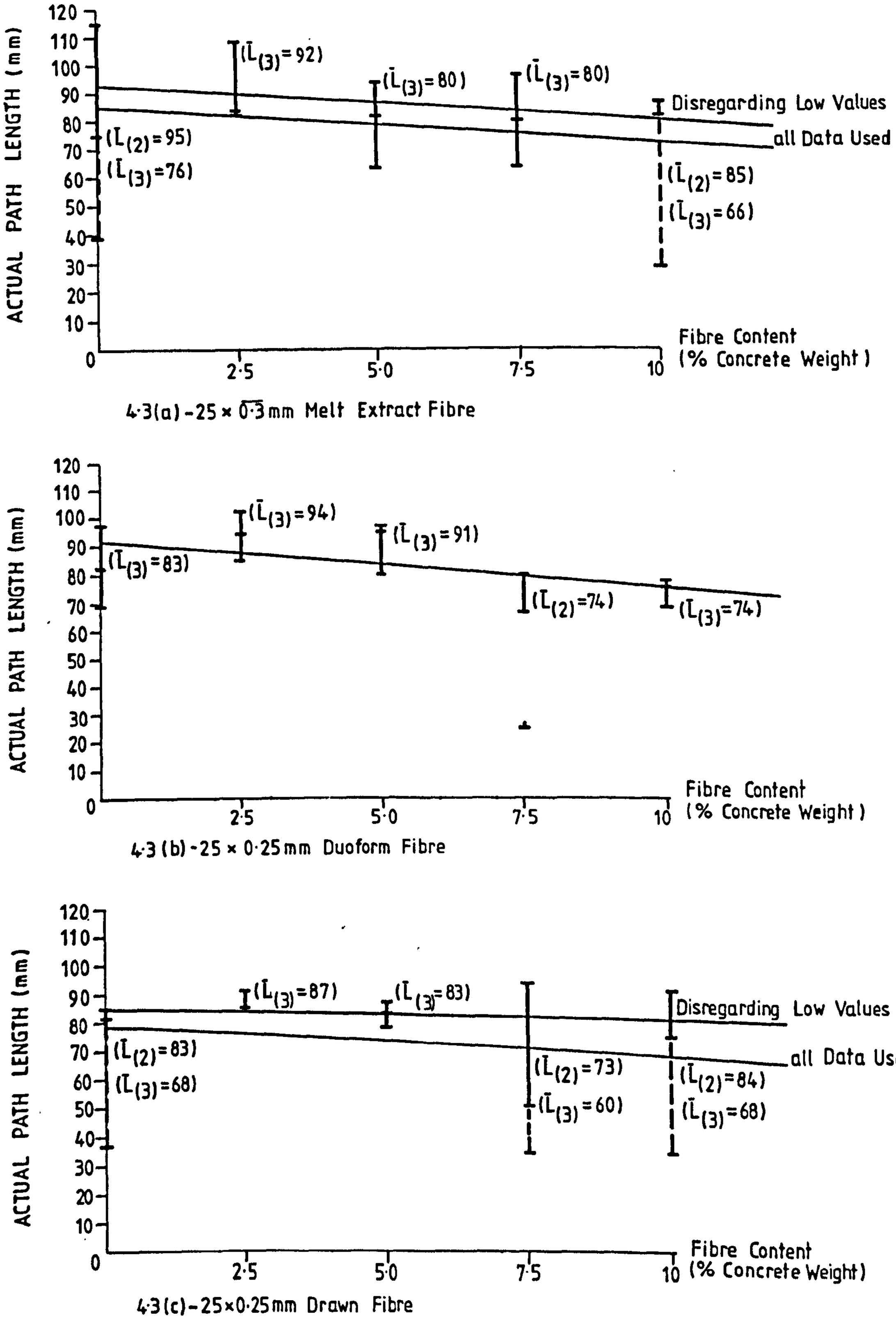

Figure 4.3 Variation of Penetration Path Length With Fibre Content for Limestone Concretes

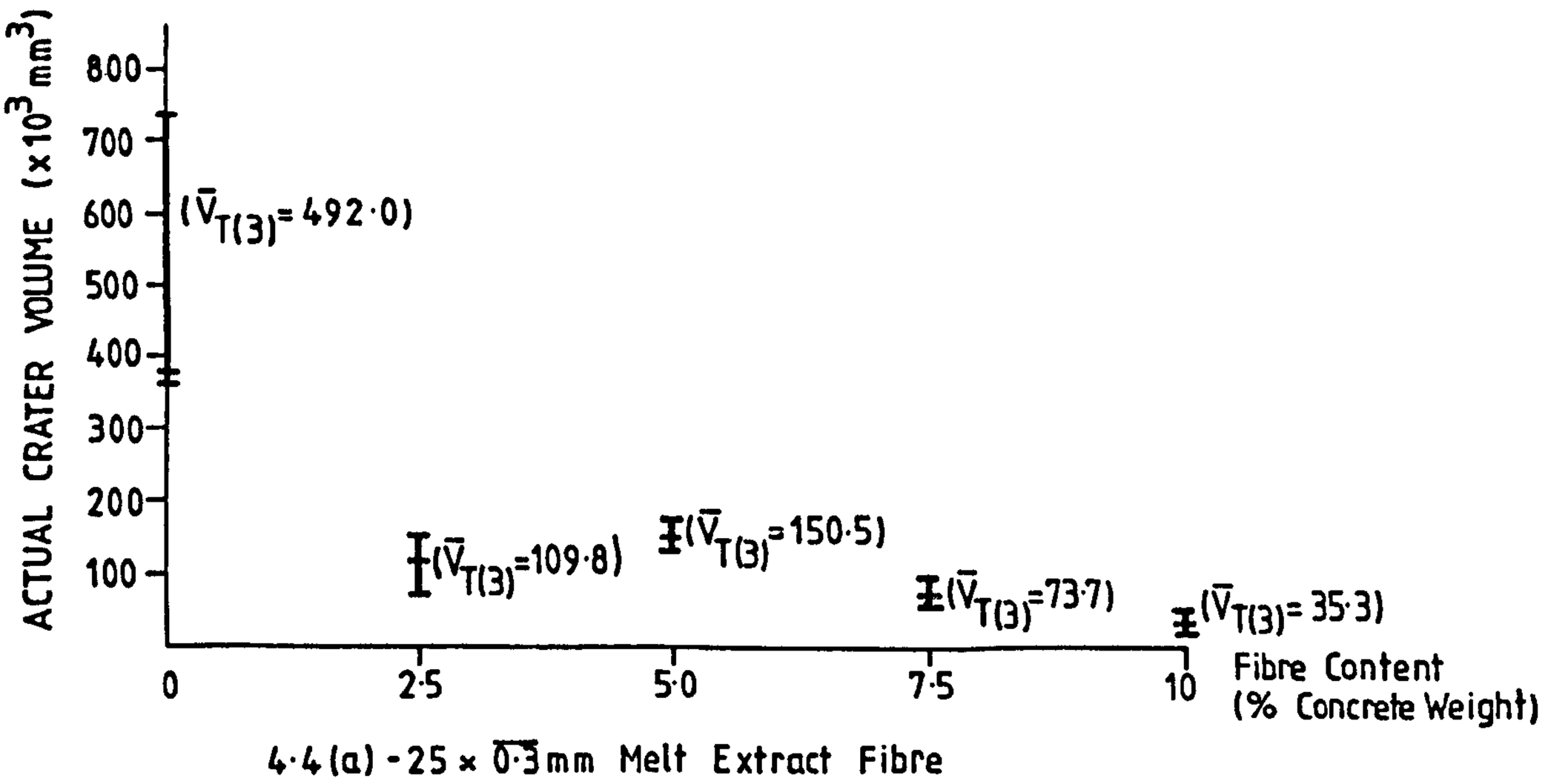

4·4 (a) - 25 × 0·3 mm Melt Extract Fibre

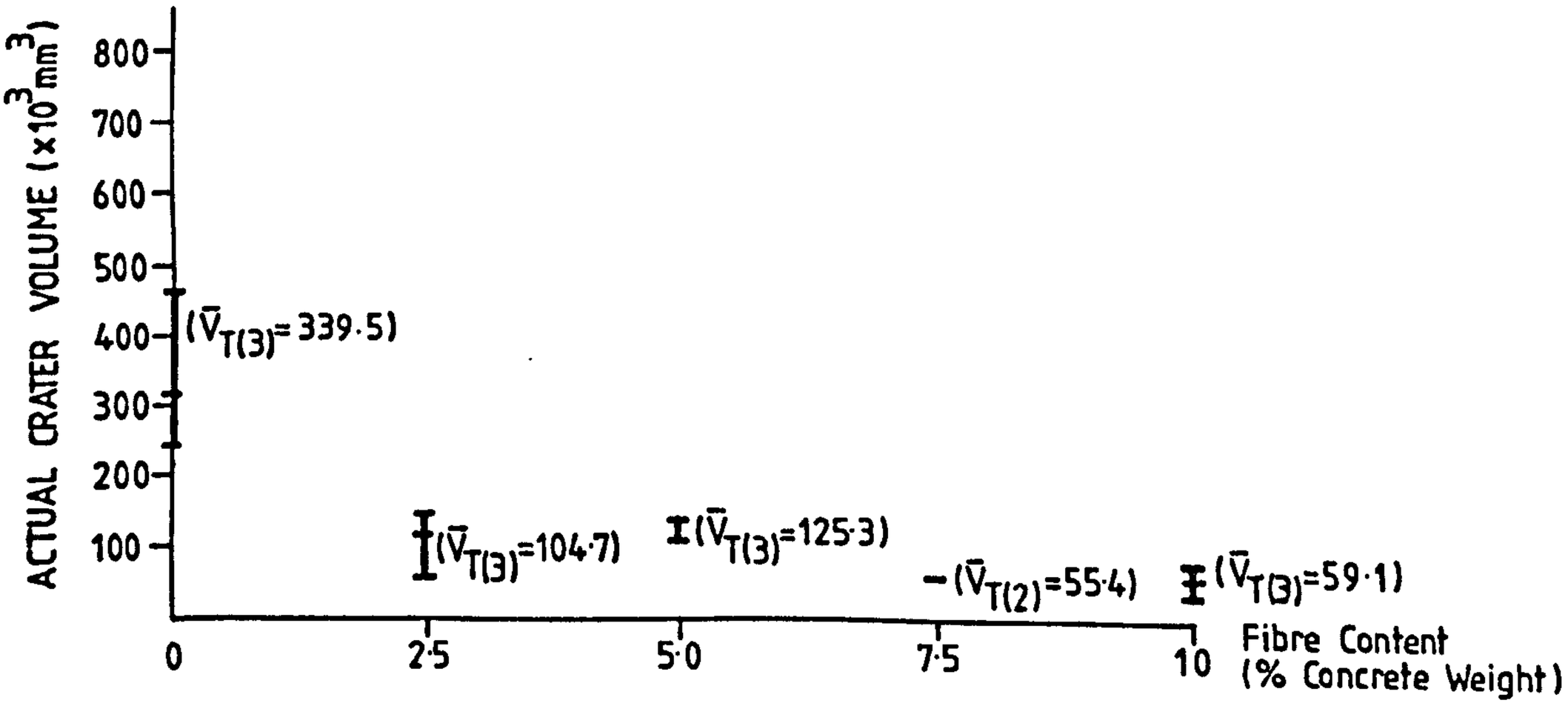

4·4 (b) - 25 × 0·25 mm Duoform Fibre

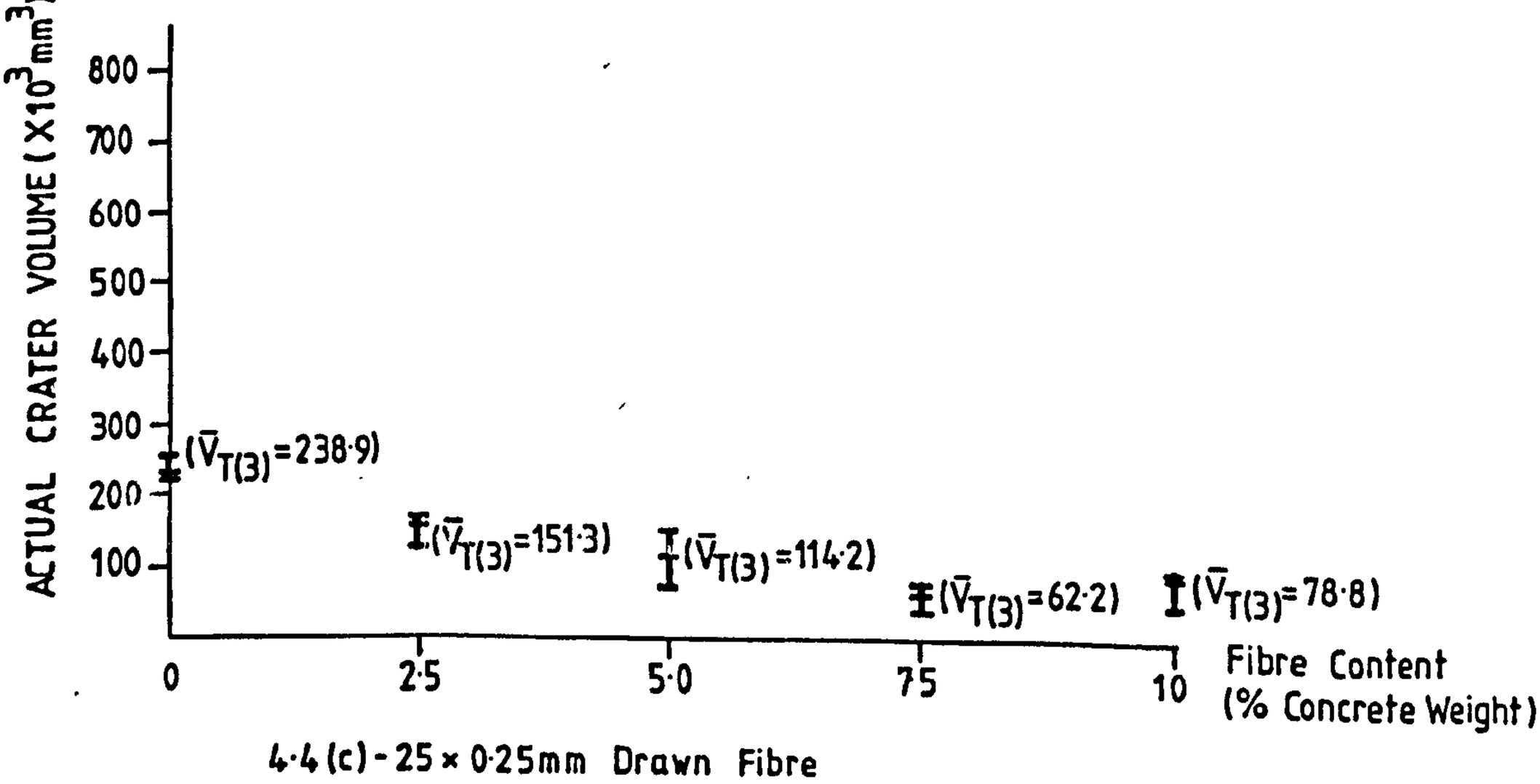

4·4 (c) - 25 × 0·25 mm Drawn Fibre

Figure 4.4 Variation of True Crater Volumes with Fibre Content for Limestone Concretes

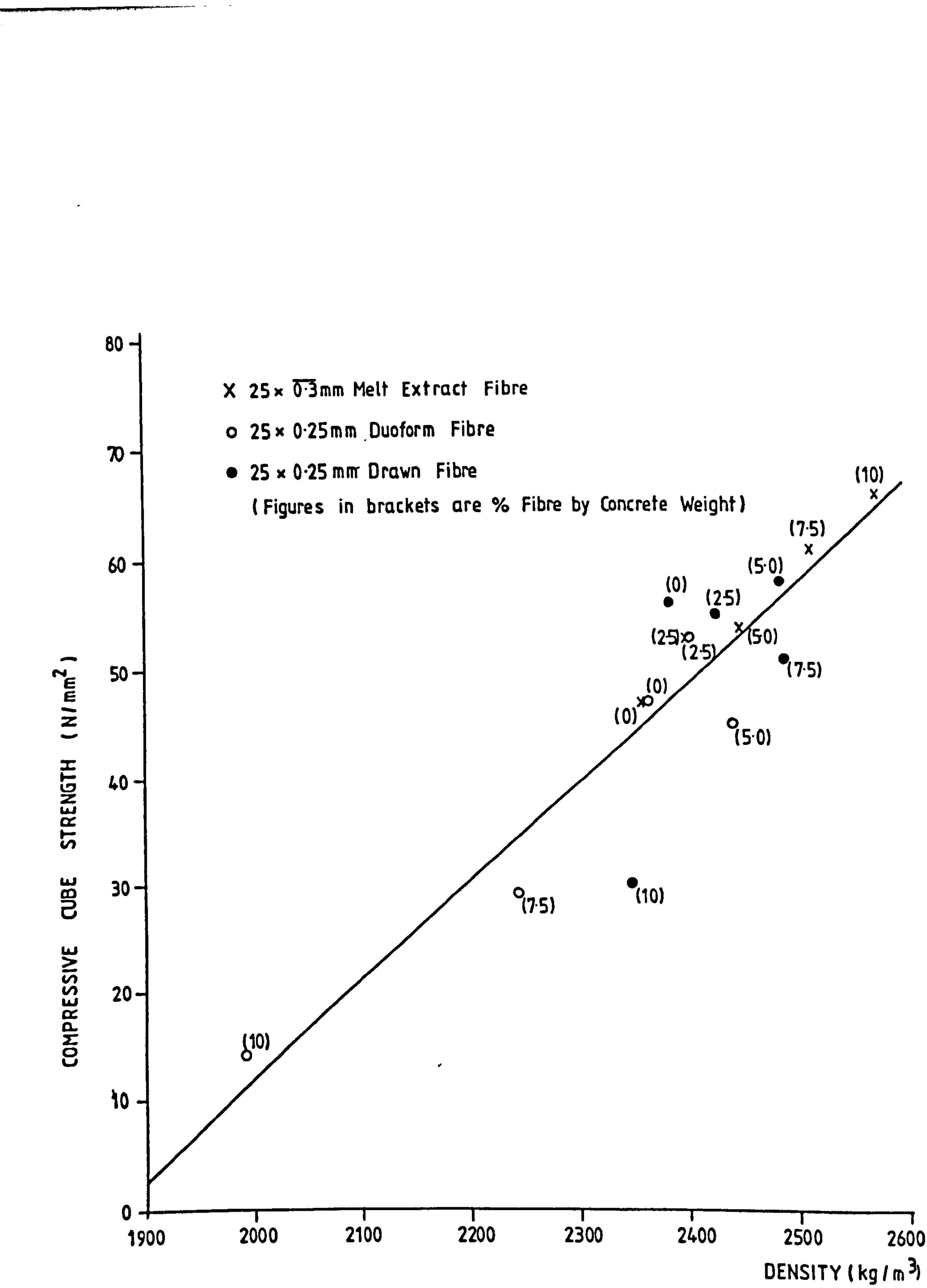

Figure 4.5 7-day Compressive Cube Strength v Density for Limestone Concretes

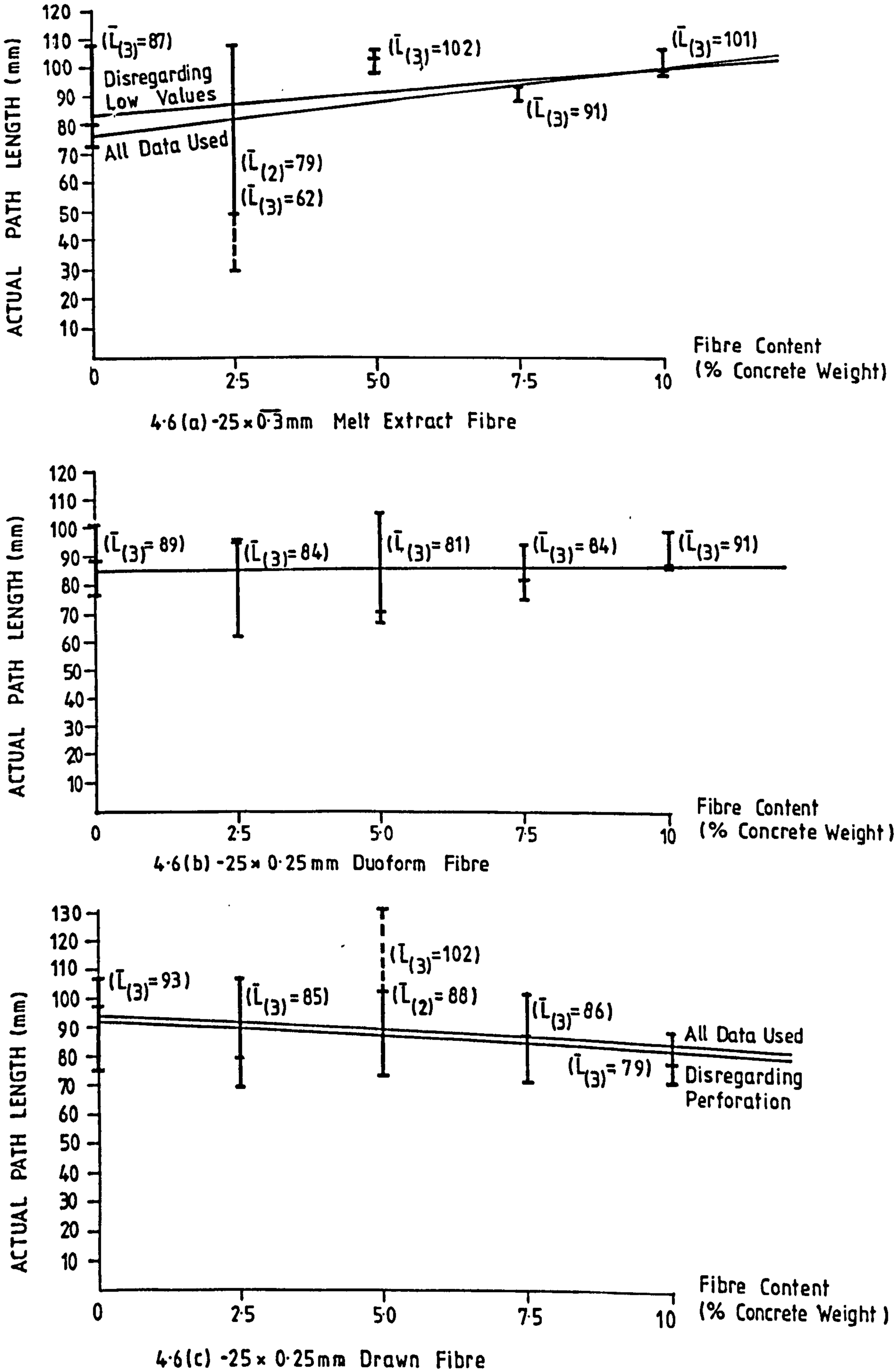

Figure 4.6 Variation of Penetration Path Length with Fibre Content for Basalt Concretes

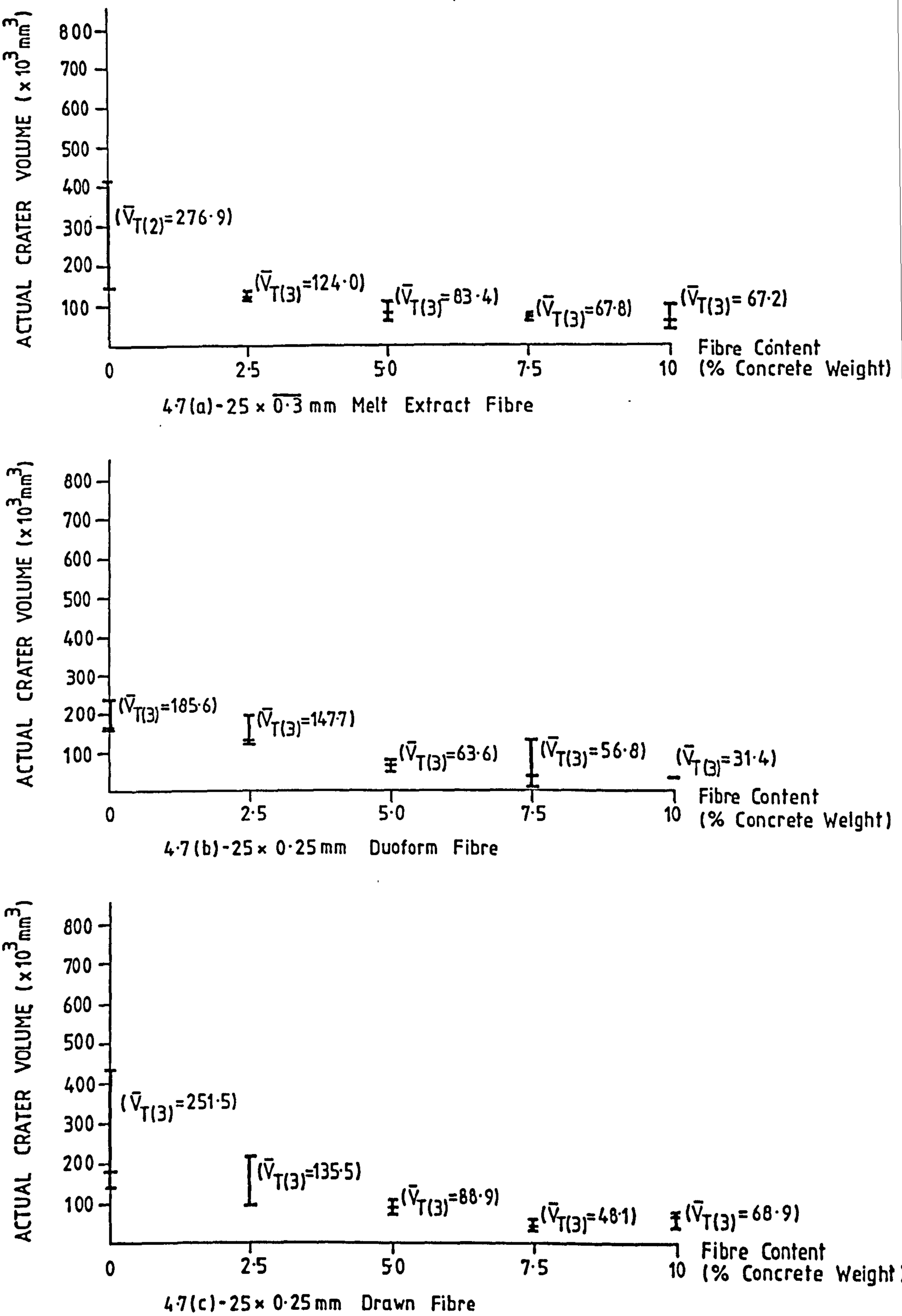

Figure 4.7 Variation of True Crater Volumes with Fibre Content for Basalt Concretes

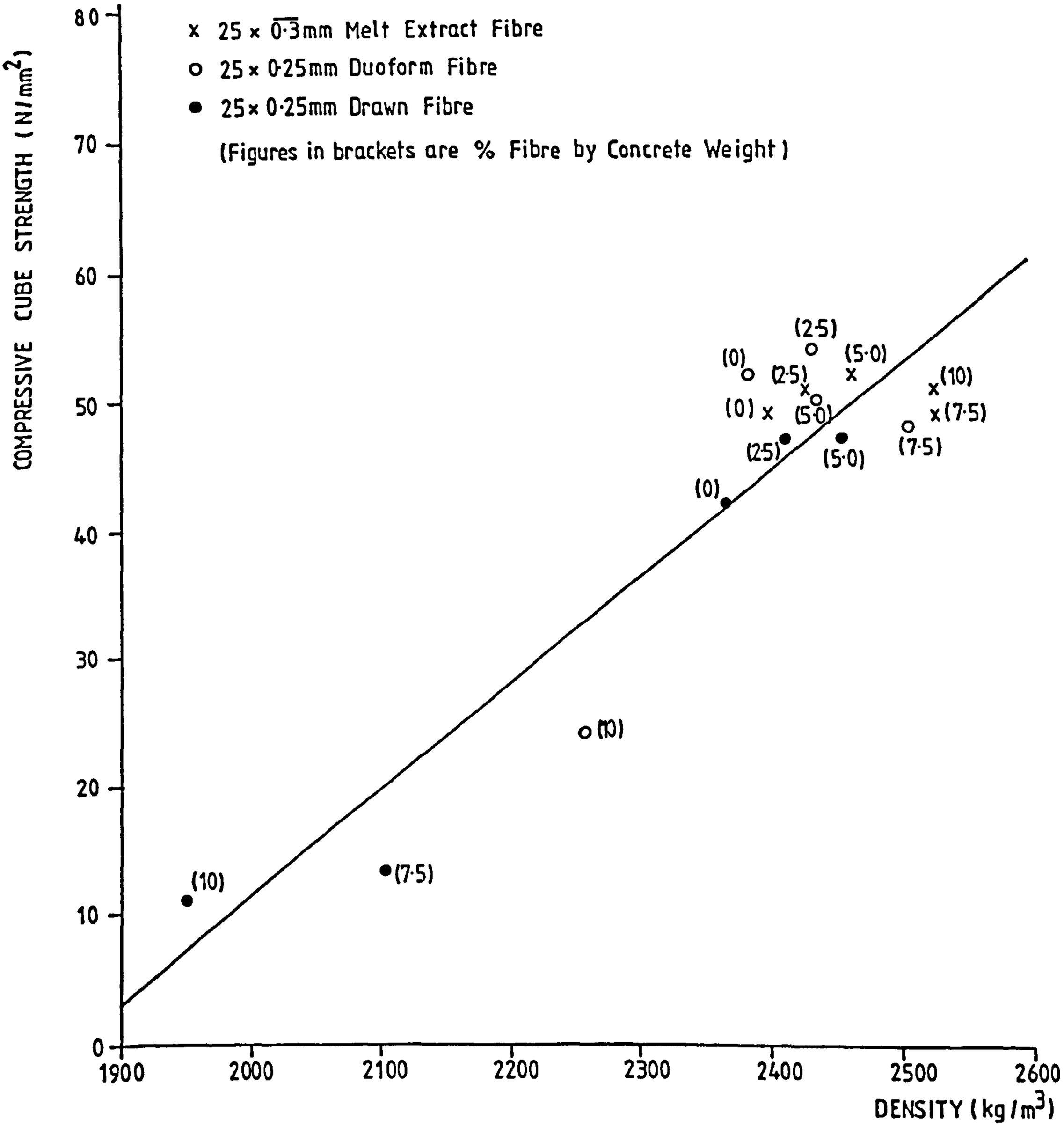

Figure 4.8 7-day Compressive Cube Strength v Density for Basalt Concretes

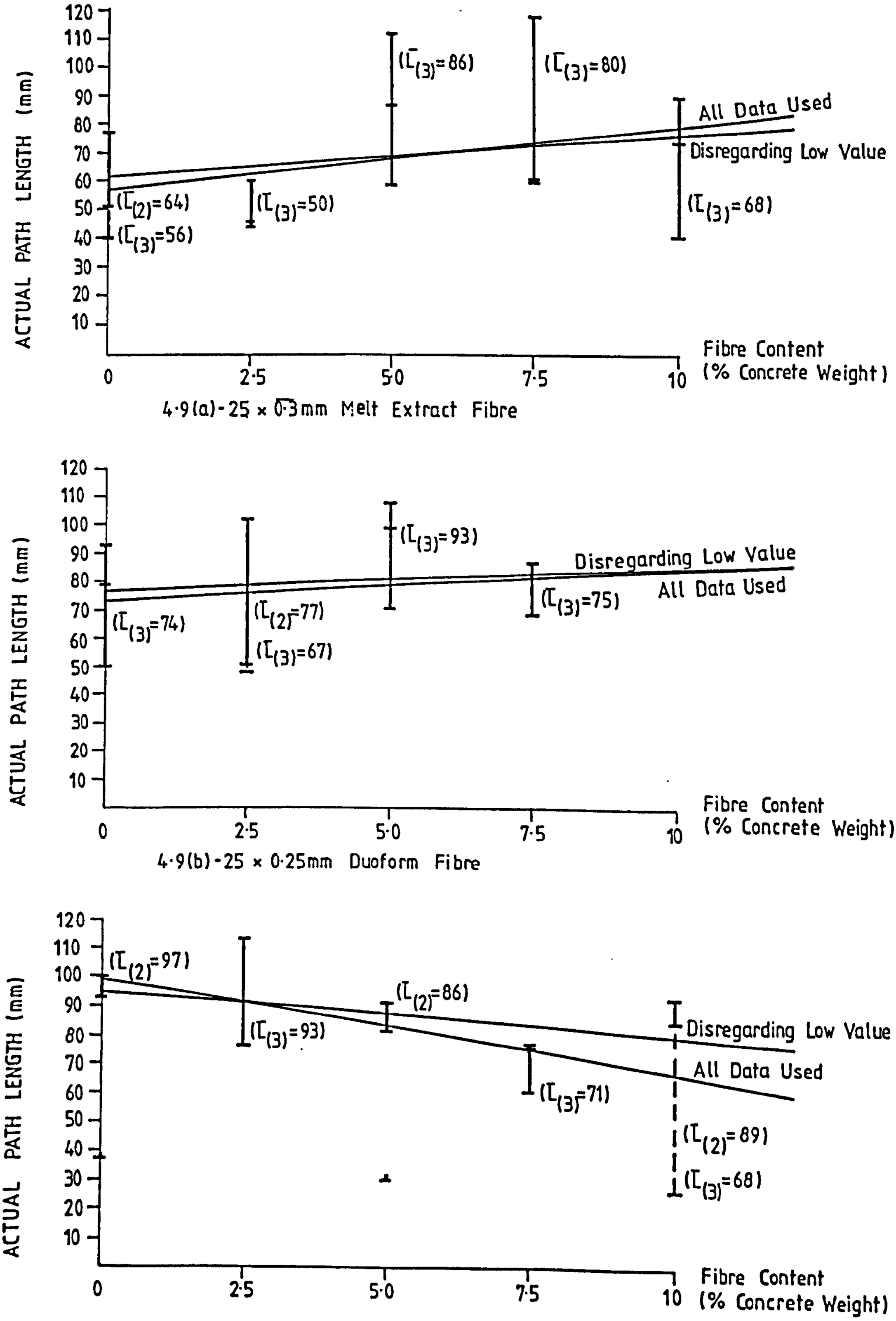

Figure 4.9 Variation of Penetration Path Length with Fibre Content for River Gravel Concretes

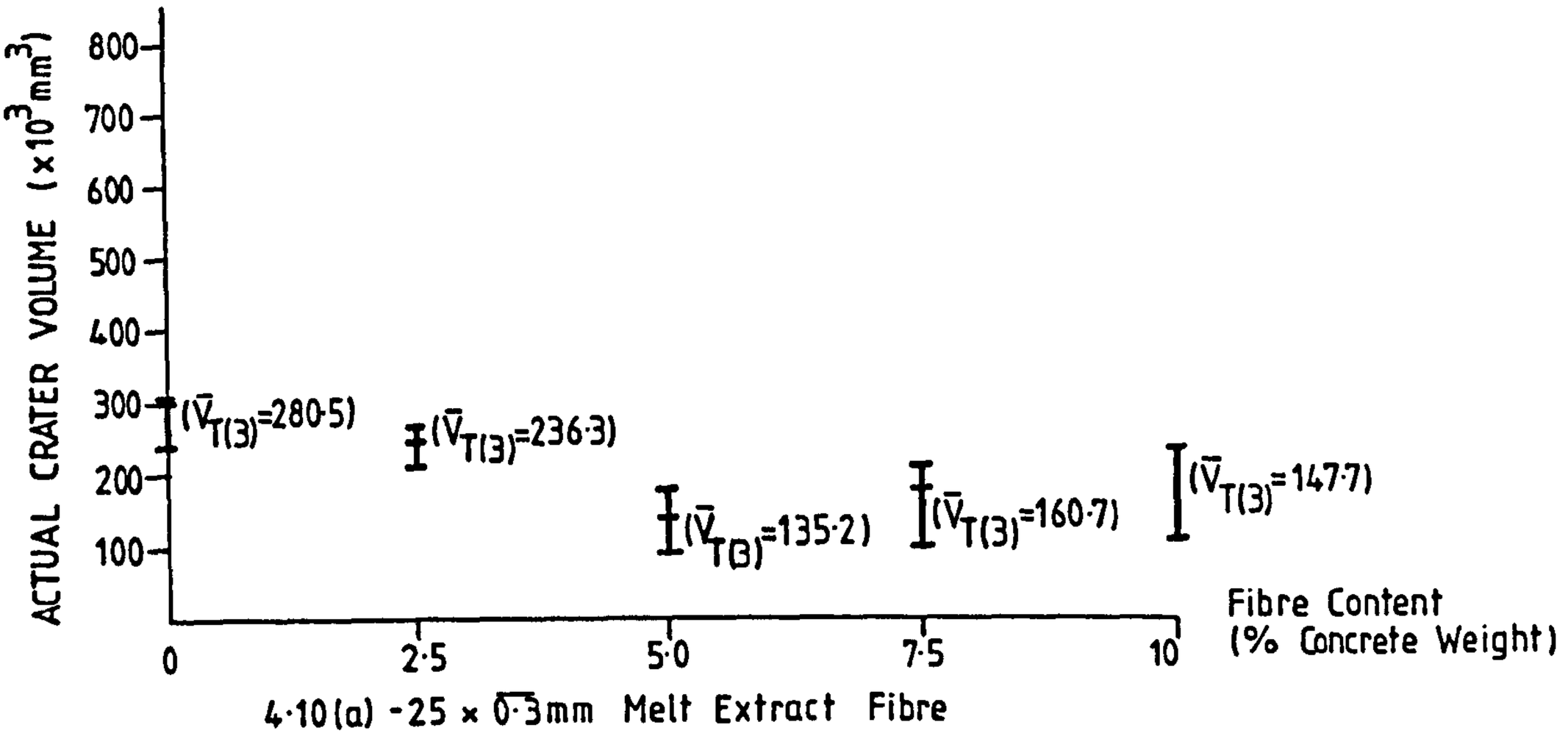

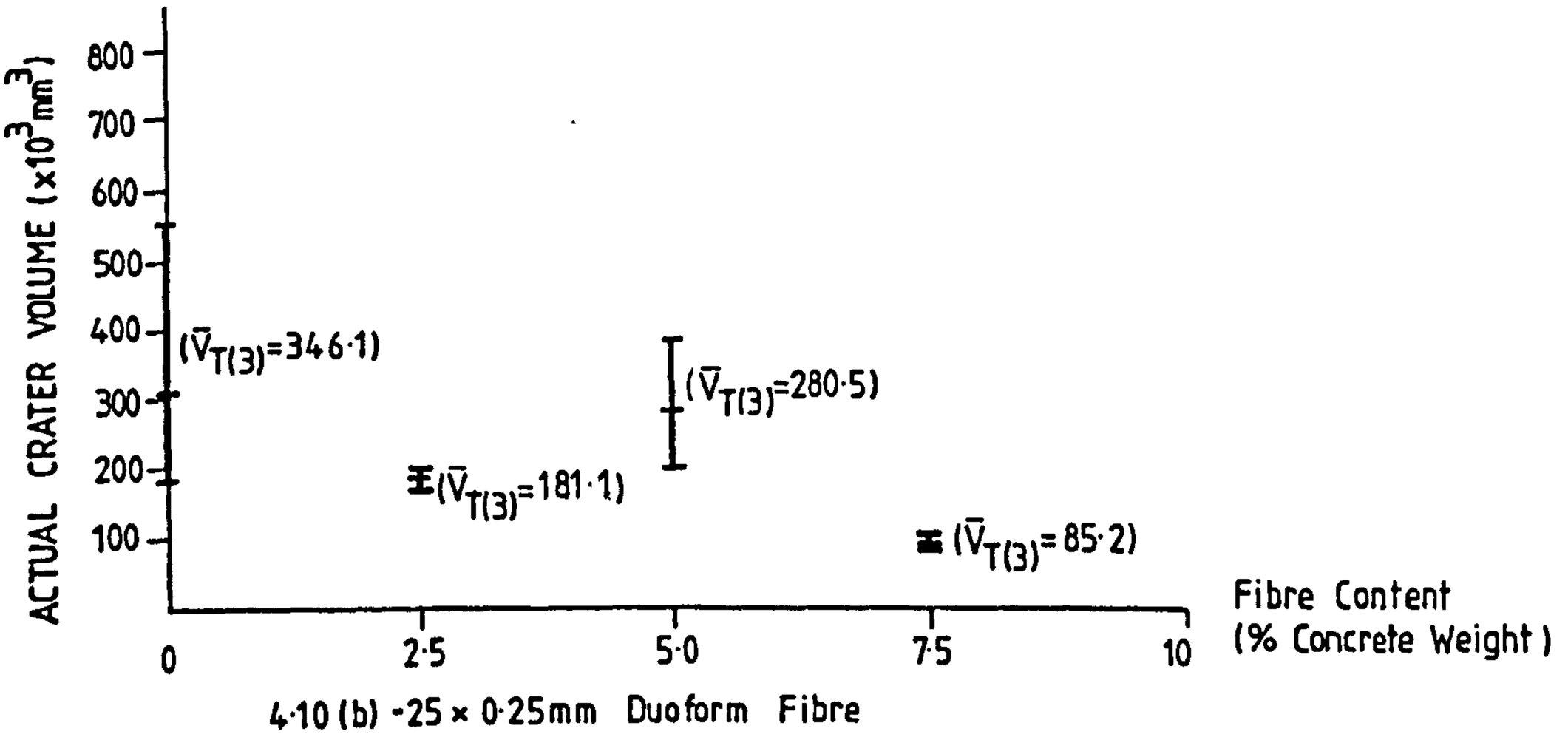

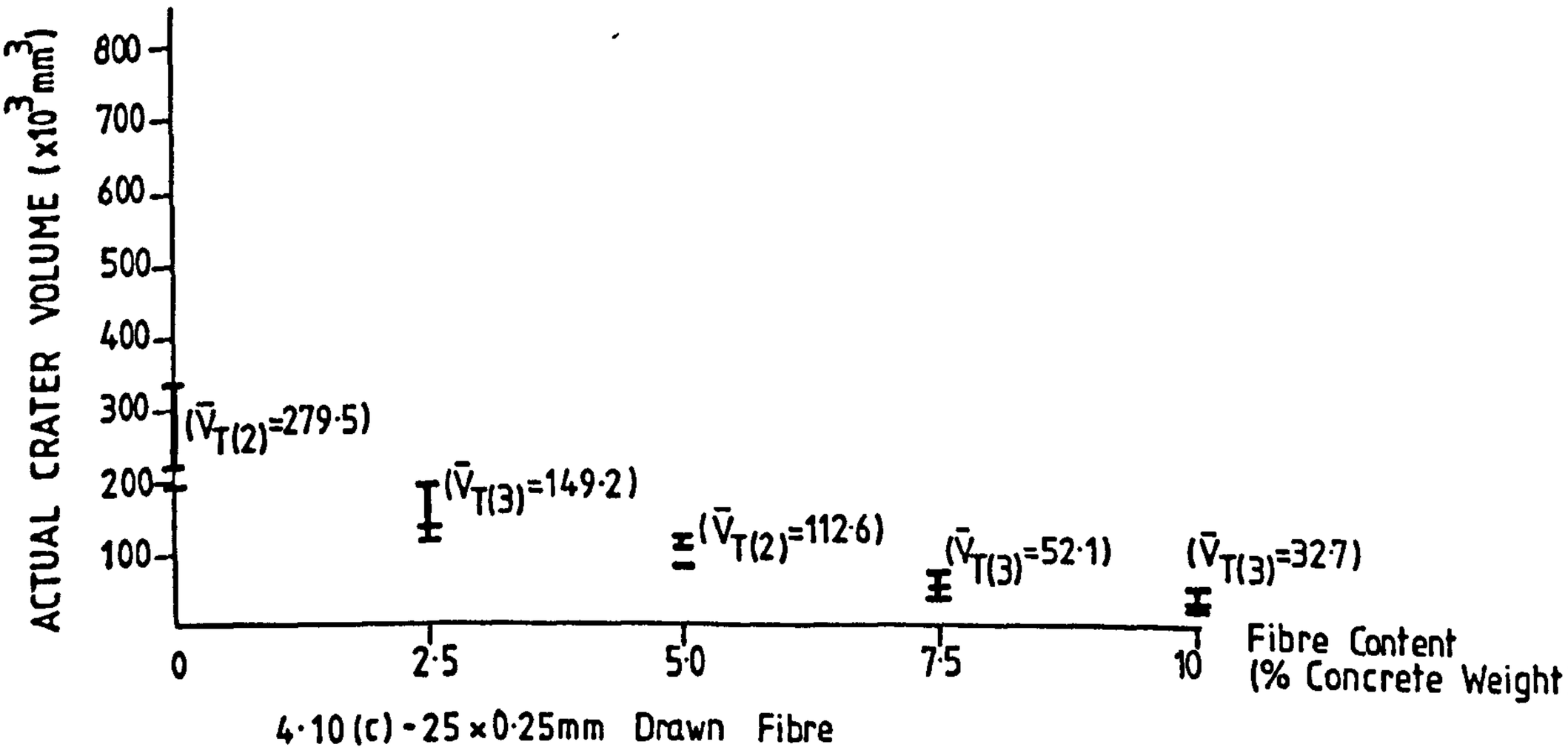

Figure 4.10 Variation of True Crater Volumes with Fibre Content for River Gravel Concretes

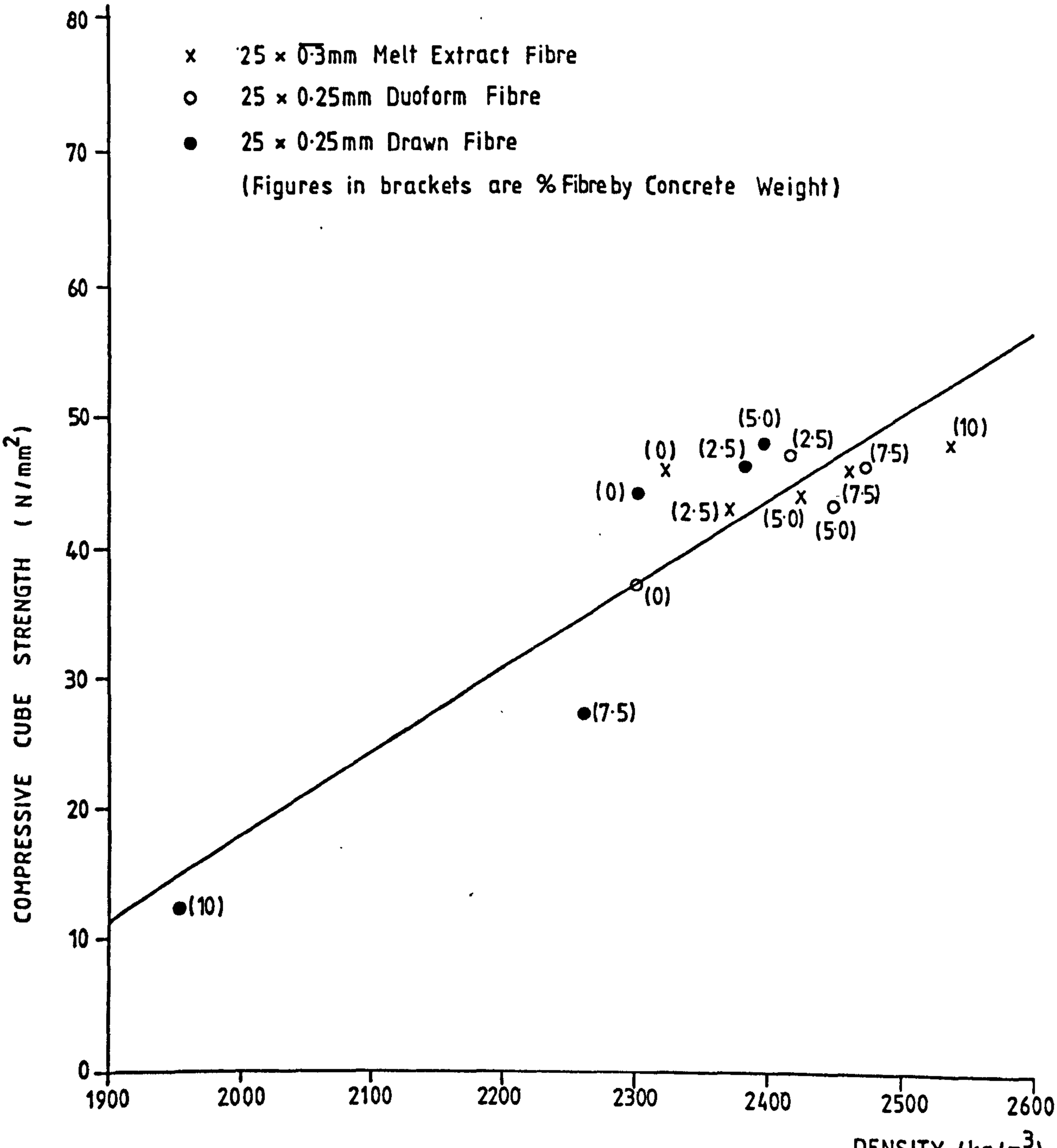

Figure 4.11 7-day Compressive Cube Strength v Density for River Gravel Concretes

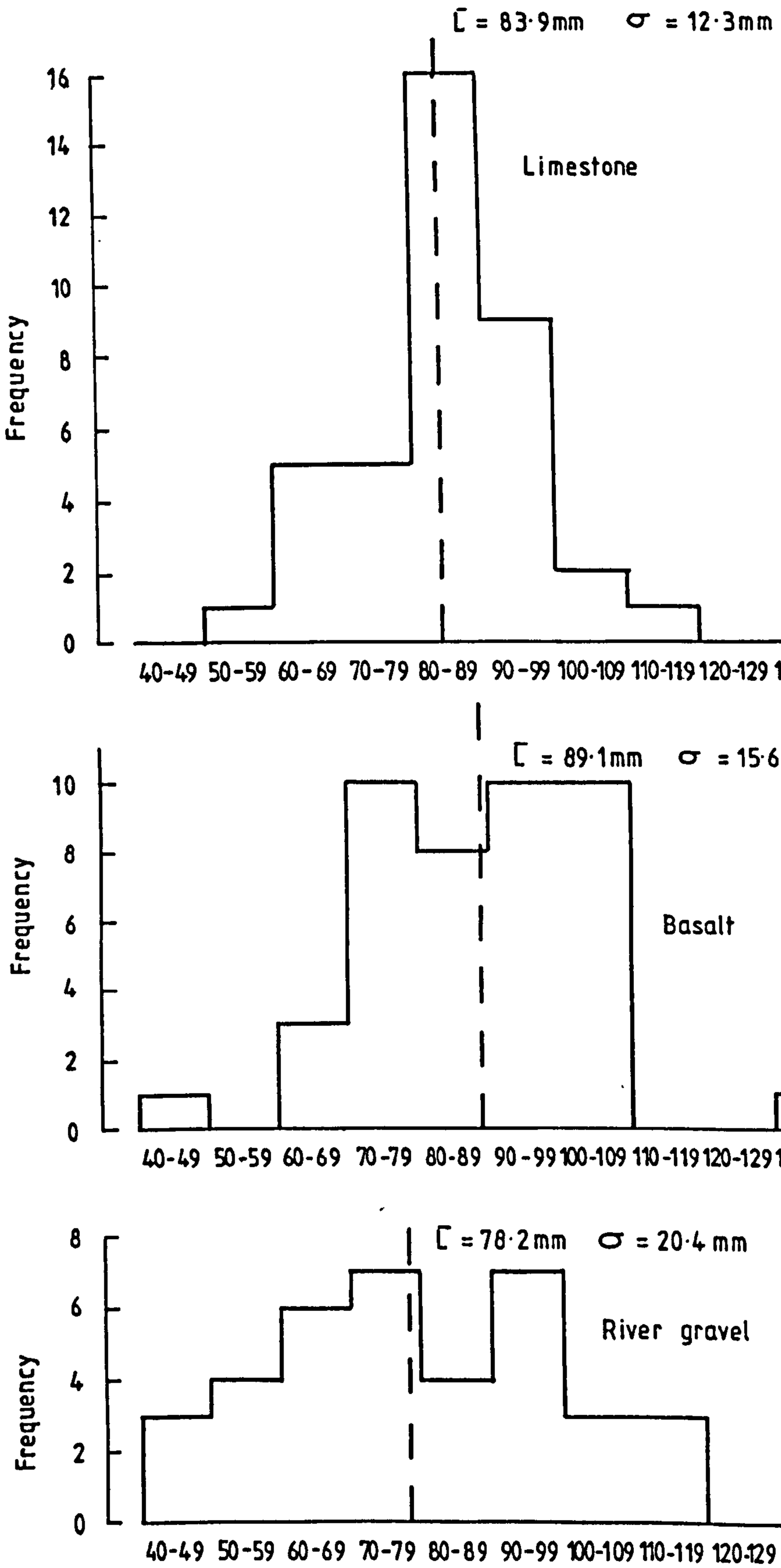

Figure 4.12 Histograms of Penetration Path Length for Each Aggregate Type, Irrespective of Fibre Content

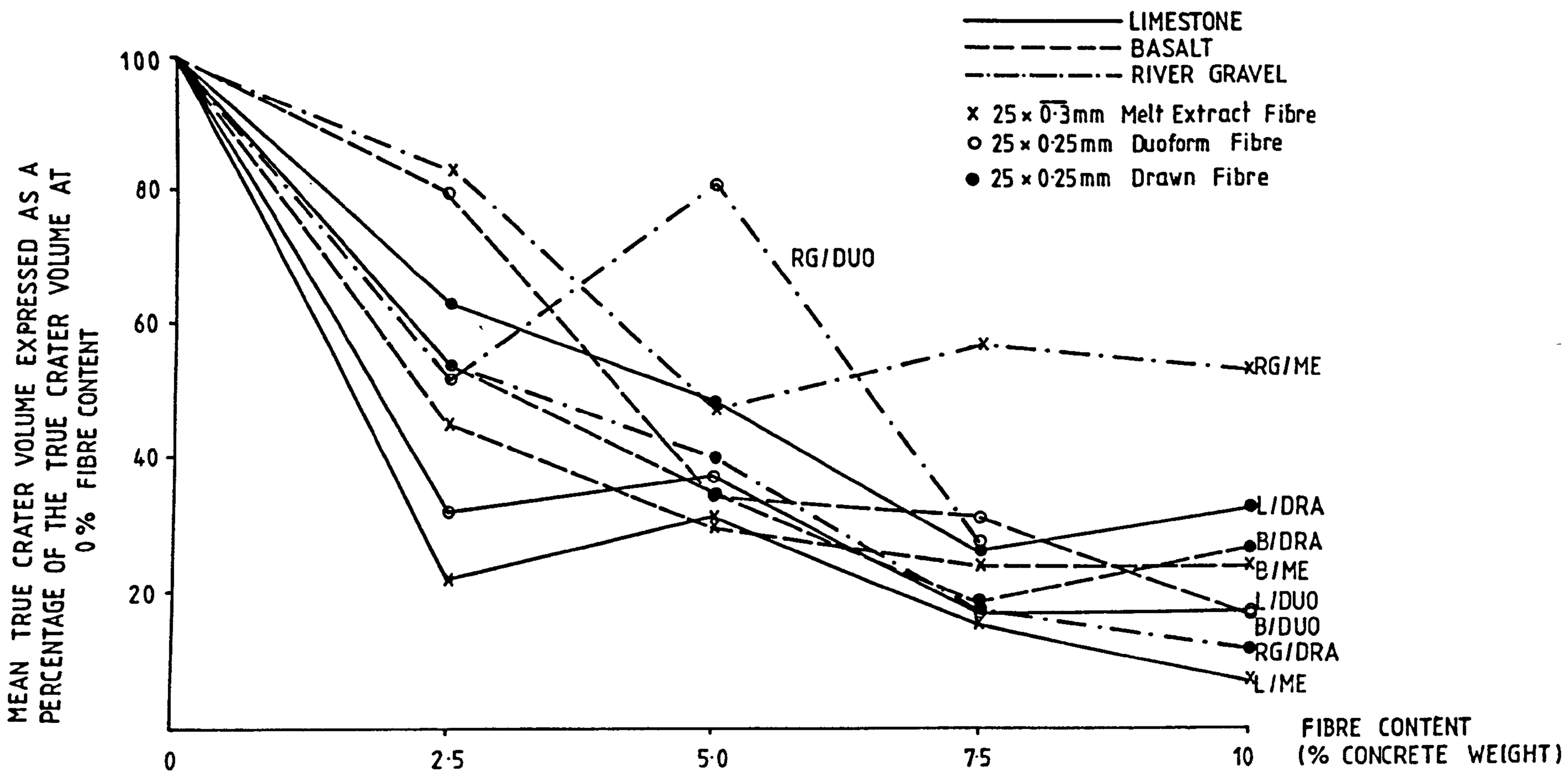

Figure 4.13 Plot of Mean True Crater Volume, Expressed as a Percentage of the Mean True Crater Volume at Zero Percent Fibre Content, Against Fibre Content

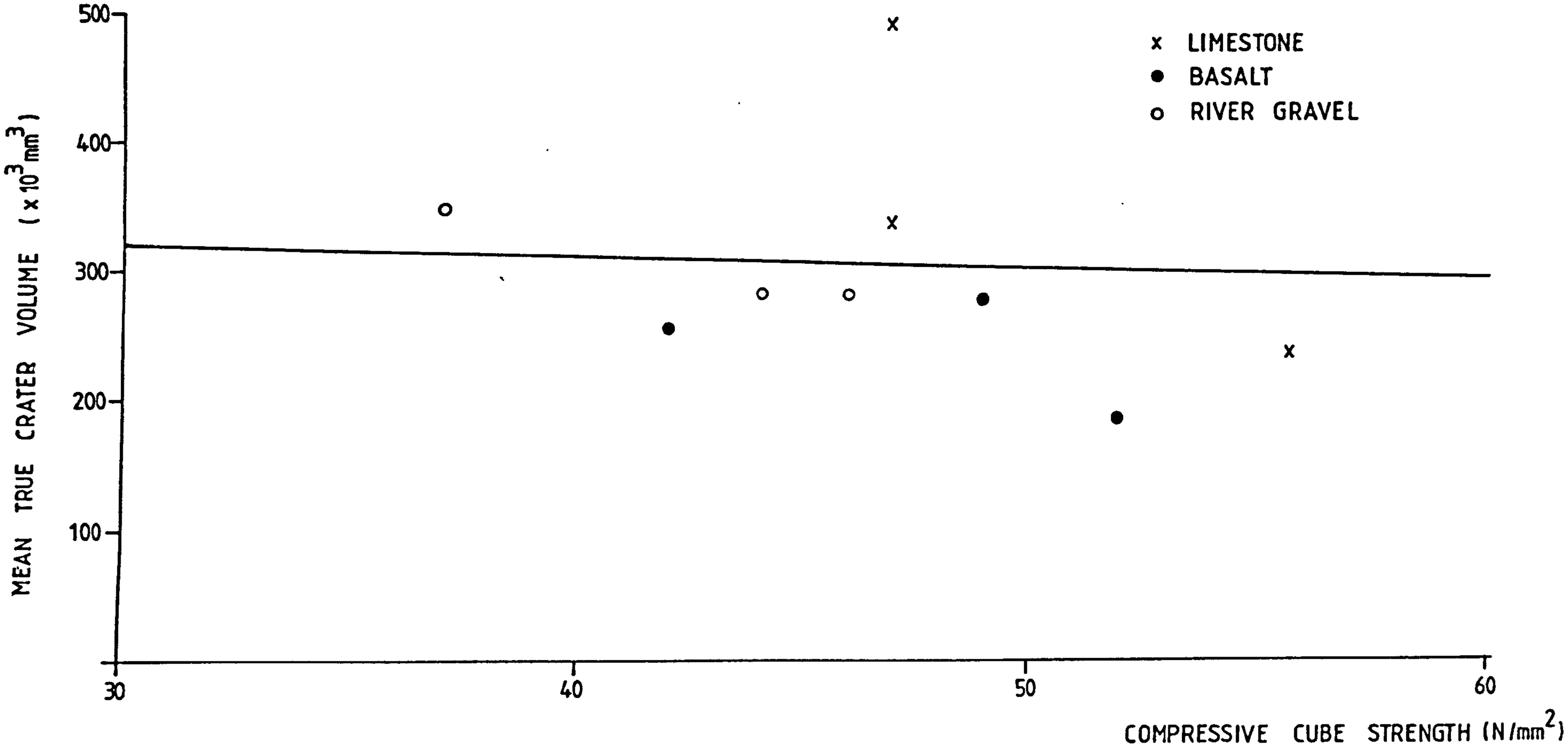

Figure 4.14 Plot of Mean True Crater Volume Against Compressive Cube Strength for Concrete Specimens Without Fibrous Inclusions

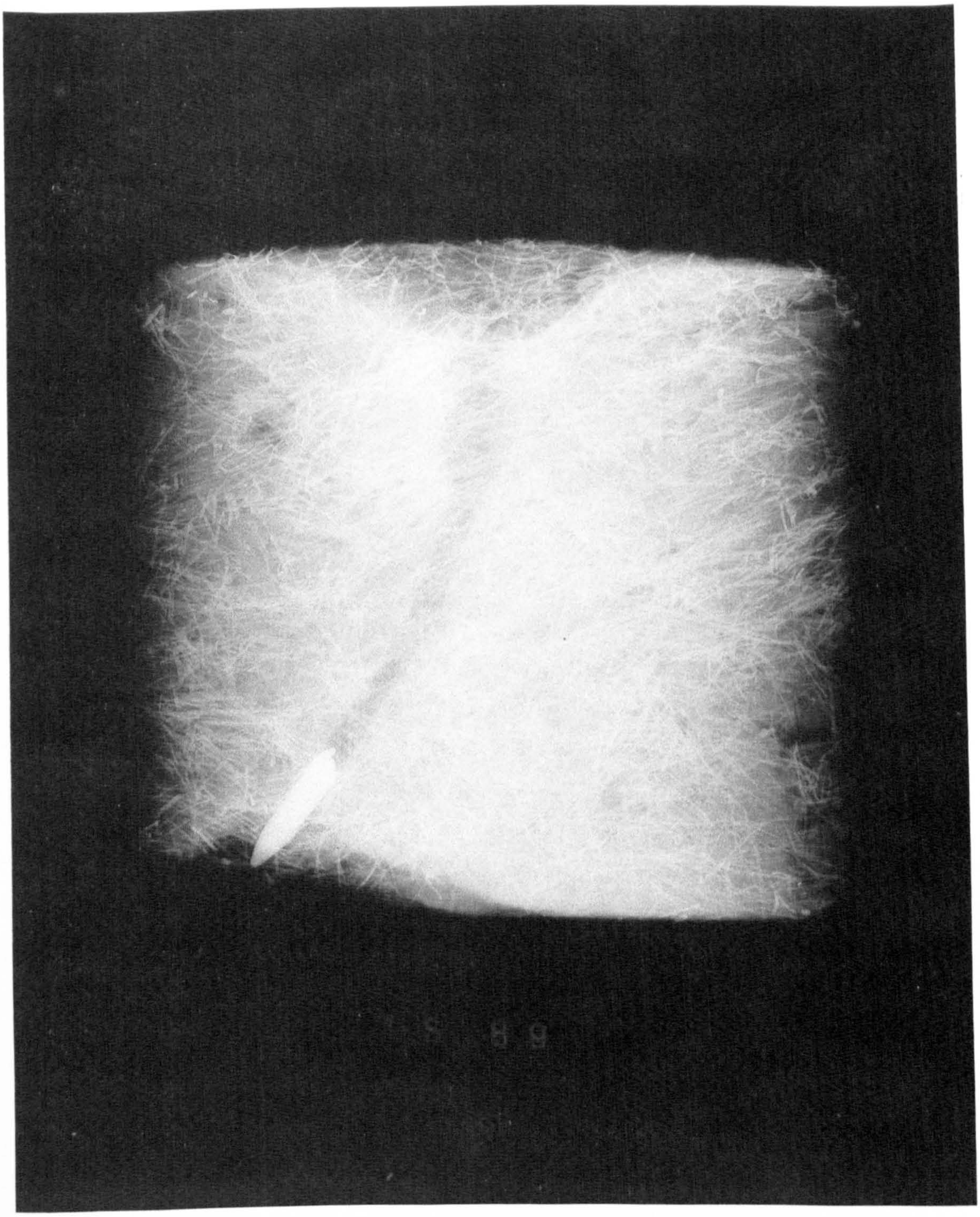

Figure 4.15 X-Ray Photograph through Steel
Fibre Concrete Specimen Number TS89

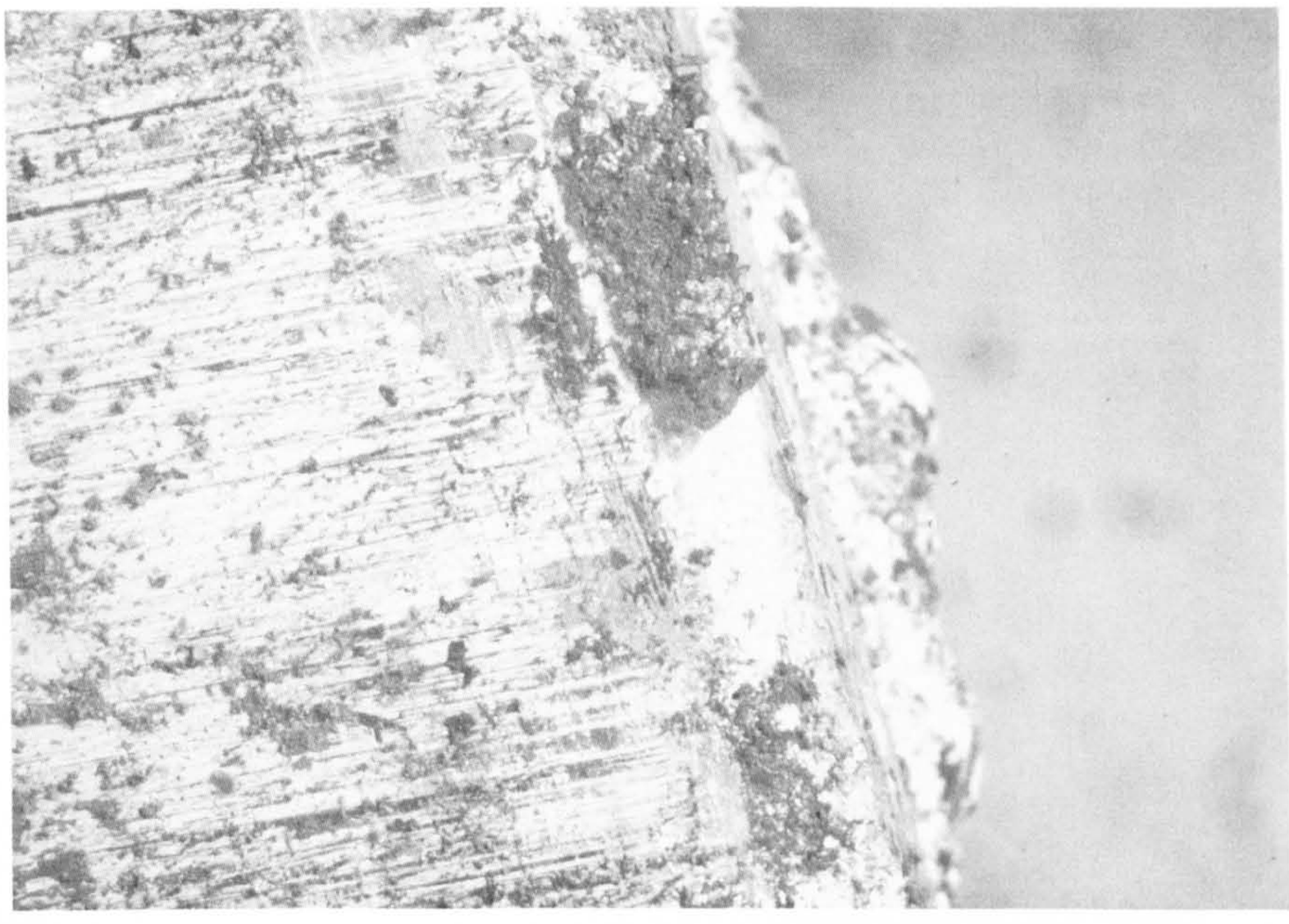

Figure 4.16 Electron Microscope photograph (80 x Magnification) showing hardened steel core surface

Figure 4.17 Hardened steel core after impact into mild steel target

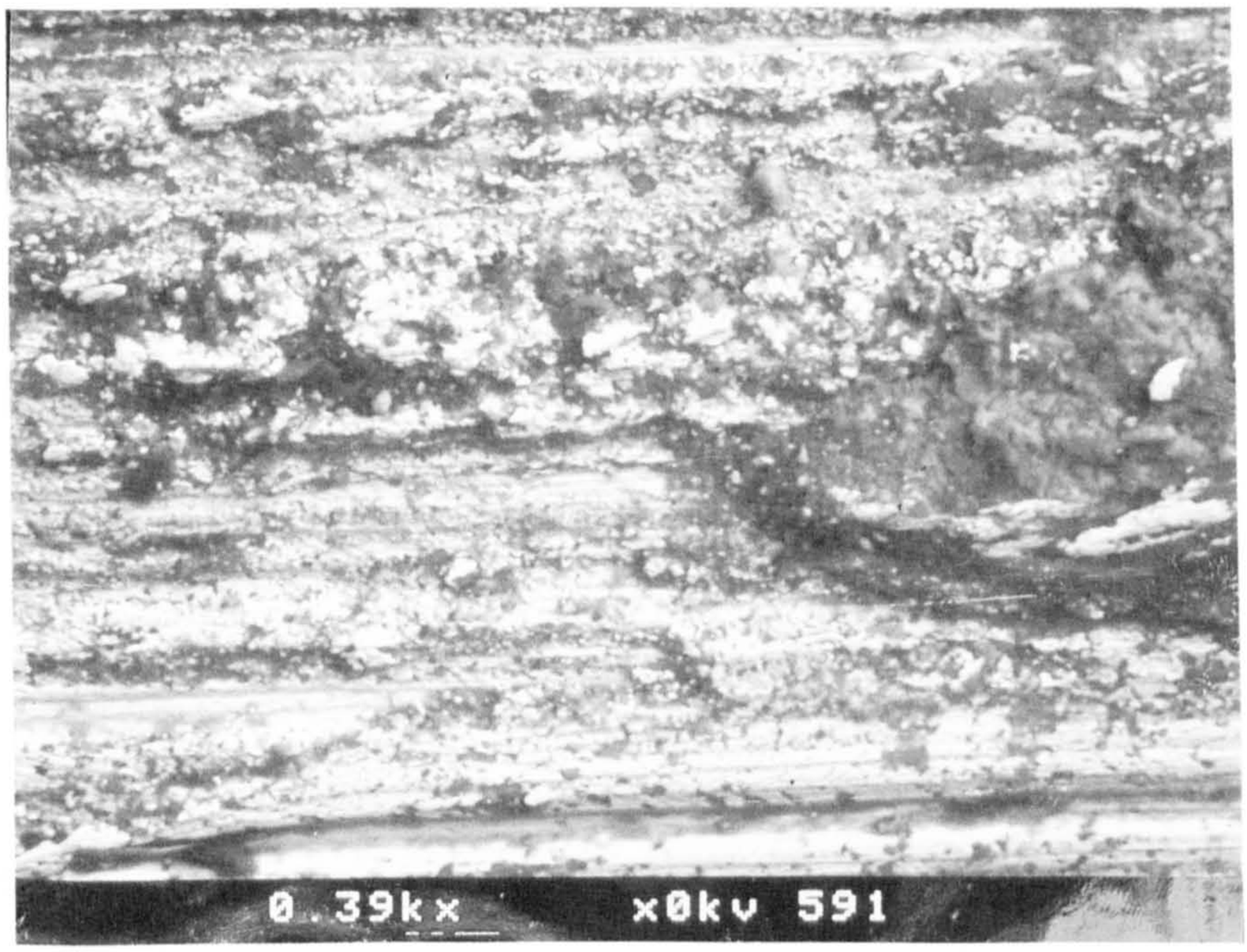

Figure 4.18 Electron Microscope photograph (390 x Magnification) showing hardened steel core surface

CHAPTER 5

EXPERIMENTAL STUDY OF IMPACT AND PENETRATION MECHANISMS

5.1 Background to the Mechanism Tests Carried Out

Following the variability of the results reported in Chapter 4, attempts were made to isolate the various parts of the impact and penetration event. It was hoped to develop an understanding of the processes involved in both the material failure and the projectile motion within the test specimen.

Various categories were postulated to separate the overall event into its component parts. The categories considered were:

Projectile flight,

Projectile impact,

Projectile penetration,

Projectile deceleration,

Target front face damage (cementitious materials)

Existing specimens from the optimisation series described in Chapter 4 were examined to partially provide the data for several of these categories. In conjunction with this, other target materials were used and monitored, in various ways, to provide information on the significant influences for the other categories. Materials used were: fibre reinforced concrete, plain concrete, mortar, mild steel, wax, plasticine, and several mortar/concrete combinations.

Each of the mechanism tests is described in Section 5.2. Individual facets of the overall event, as listed above, are discussed as appropriate in Section 5.3, extracting the relevant data from the tests described. This approach is used as some of the tests carried out provide information in more than a single event category.

The techniques employed included high-speed and ultra-high speed photography and transient recording of various types, as well as simple observations and measurement. Whilst exhaustive testing using each technique was not possible in the time available, it is believed that in many cases the few tests carried out are typical of the likely results and act adequately as both a general guide to expected behaviour and, perhaps more importantly, an indication of potentially successful avenues for further investigation.

5.2 Experimental Techniques Used to Investigate Failure Mechanisms

5.2.1 Use of High Speed Rotating Prism Camera

The flight and impact have been recorded using a Photec IV rotating prism camera. This is a high speed motion picture camera with a capacity of 137m of 16mm cine film. The camera operates by synchronising the motion of a quick-rotating prism with the passage of the film. The framing rate (pictures per second) of the camera may be varied between 100 and 10000 pps, using the standard rotating prism. By incorporating a half-height prism, framing rates of up to 20,000 pps are possible. The rate is controlled by varying the supply voltage to the electric motor. The motor is accelerated from rest to the required framing rate; at this point the event is triggered by the camera. Film is passing through the camera during its acceleration period, so that only a percentage of the total film length is available for recording the event. At a rate of 12,000 pps approximately 11m of a 30m film is used to record the event, the other 19m being sacrificed.

Although the camera is furnished with an f2.8 lens, at such fast framing rates the major difficulty is the provision of a high enough level of illumination. After initial feasibility testing, four 1kW cine lights were placed behind an opaque diffuser and aimed directly at the camera in order to throw the projectile and target motion into silhouette. The arrangement is illustrated in Figure 5.1.

Since the event was triggered by the camera, it was necessary to equip the firing system with safety devices to avoid premature projectile detonation. Figure 5.2 shows the general approach. As the firing solenoid was powered by a rectified mains voltage equivalent to some 450V d.c. it was appropriate to incorporate a system to protect the internal electronics of the camera. A 12V solenoid was connected through a 12V power source in circuit with the footage measurement switch of the camera. When the switch was closed by the camera at the correct framing rate, the solenoid completed the mains firing circuit for the projectile, assuming the safety devices had been unlatched. These devices consisted of the standard arming-key lockout and an isolation lead included to allow the photographic system to be tested without triggering the mains firing system.

The restricted angle of view of the 45mm focal lens, as demonstrated in Figure 5.1, coupled with the relatively high velocity of the projectile, meant that, with a 30m film, a maximum of two frames showing the complete length of the projectile in motion were possible. Another important limitation was the mains electrical supply; the large power surge needed to induce a rapid enough acceleration of the camera motor dictated that light levels much above 6kW could not be used. At higher levels the mains circuit was momentarily overloaded causing the supply to be automatically shut-down. Consequently, a shutter with a 1:2.5 ratio, producing an equivalent shutter speed of 3×10^{-4} second at 12000 pps, was necessary to effect sufficient exposure for each frame. At a projectile velocity of, say, 810m/s the impactor moves approximately 27mm in each frame. Whilst this is acceptable in considering general projectile and spall product trajectory, it is of little use for detailed examination of projectile motion. For this purpose, an ultra-high speed camera (Section 5.2.2) was employed.

Details of two plain concrete specimens, a fibre concrete target and a plasticine model, which were photographed during impact, are given in Appendix VIII.1. Also given are details of the photography.

Figure 5.3 shows a typical sequence of frames obtained. The film was analysed by overlaying, at full scale, each frame on to the preceding one, eventually permitting a time-based "contour" elevation to be drawn. In all cases the blurring effect caused by the necessary exposure duration was considered uniform from frame to frame, not a strictly valid assumption since as each specific point decelerates the blurred length will shorten. Each test gave an individual photographic record, details of which are given below.

Both the velocity of propagation of circumferential material movement on the target surface and also that of the spall product fronts were established by direct measurement. The movement of the upper half of the target was considered independently of the lower section to give two sets of information. The estimated velocities are given in Table 5.1.

RP1

Figure 5.4 shows the material motion as a series of fronts corresponding to known points in time from frame 1 (the first frame showing the projectile in motion) to frame 10, a total interval of 819μs. Figure 5.5 was produced for frames 11 to 16, a further period of 455μs.

RP2

Figure 5.6 and Figure 5.7 show the material motion for frames 1 to 10 and 11 to 19 respectively.

RP3

Adequately referenced data was available only over nine frames. These are represented in Figure 5.8.

Plasticine

Adequately referenced data was available over thirteen frames. These are represented in Figure 5.9. Between frames 12 to 13 it was possible to observe the motion of large discrete spall products; one was taken from each of the upper and lower zones. The velocities measured between the two frames were;

i) Upper spall product velocity = 17.0m/s

ii) Lower spall product velocity = 45.5 m/s

This information is only of limited value since the weight of the particles, and the motion perpendicular to the photographic plane, cannot be accurately assessed.

5.2.2 Use of the Ultra-High Speed Rotating Mirror Camera

To further investigate projectile pre-impact flight, a Barr and Stroud ultra-high speed rotating mirror camera has been utilised. This equipment was fitted with a 35mm focal length lens with a maximum relative aperture of f2.8. The camera was capable of sequentially exposing thirty separate frames on standard 35mm film. This was accomplished through a series of 30 separate internal lens systems located in front of the stationary film, in an arc of approximately 60°.

A projection of the event is delivered to each system in turn via a rapidly rotating two-sided mirror. This turns on a horizontal axis in an evacuated clear glass sphere. It is attached to a small turbine powered by compressed nitrogen. By this means mirror rotations generating framing rates up to two million pictures per second are possible. At such high rates, the major problem is to sufficiently illuminate the event. A high-powered electronic xenon flash unit, capable of a peak energy of 200J for 200μs was employed. This equipment has a 50μs build-up time and a further 50μs delay period, so that light is produced for some 300μs altogether.

Although normally the camera is capable of synchronising mirror rotation speed, event initiation and flash duration, the requirements of

this particular event were outside the range of the electronic control equipment. The camera triggers the event a maximum of 23ms before initiating film exposure. Since the projectile detonation and flight time were relatively uncertain (due to inherent delays in the electrical/mechanical triggering system) - but in any case were greater than 24ms (20m flight at 820m/s) - it was not possible to use the automatic system. As an alternative, all extraneous light in the firing range was extinguished before the projectile was fired and the camera was allowed to run free to approximately 1μs interframe time with the shutter held open. The xenon flash was initiated by the closing of a contact switch, placed ahead of the target and shorted by the projectile passage. The switch consisted of two sheets of conductive material separated by an insulator. Placing the switch 120mm in front of the target and assuming a projectile velocity of 820m/s, allowed the flash unit approximately 150μs to achieve peak illumination before impact. This approach reduced the possibility of multiple exposure caused by repeated rotation of the mirror whilst the shutter remained open (i.e. "over-writing" of the original projectile image).

Two different approaches to the positioning of the flash unit were found to be successful. Figure 5.10 shows an arrangement using a reflective screen to throw the projectile and the target edge into silhouette, whilst a front lit photographic arrangement is illustrated in Figure 5.11. In this case, an illuminated scale was included in the plane of the projectile to aid measurement.

It should be noted that the limited arc of the film resulted in only a small probability of a full photographic record including both projectile flight and impact. At 1μs interframe time the most likely result was a series of photographs of the projectile in flight before impact, with a slight possibility of a second mirror pass causing overwrite.

Appendix VIII.2 gives details of the ultra-high speed rotating mirror camera tests and includes both a typical frontlit and a typical backlit series of photographs showing the projectile in flight.

5.2.3 Impact on a Plasticine Target

A cylindrical target of 100mm diameter and 200mm length was constructed from a plasticine material. Figure 5.12 is an illustration of the model. A series of ten 55mm diameter discs were used to form the core. By alternating different colours a number of boundaries were established between each 20mm thick component. The remainder of the target was produced by placing plasticine circumferentially, again in 10 different coloured layers, around the core.

The unrestrained target was placed 19.89m from the gun barrel end, the axis of the target being in line with the expected trajectory of the projectile. In order to fulfil the photographic requirements discussed in section 5.2.1, remote detonation for the 7.62mm armour-piercing projectile was used.

Although a successful photographic record was obtained (see Appendix VIII.1), Figure 5.13 shows that extensive damage has been caused by a circumferential bursting force propagating from the rear face of the target. The lack of lateral restraint permitted this bursting, and also resulted in the projectile not being located after the event. The extent of the damage destroyed much potential quantitative evidence. However, around the immediate impact zone some valuable information was obtained. Through the thickness of the first disc (20mm) the diameter of the path increased from 12-17mm to 15-20mm (minimum and maximum values respectively). This is consistent with the photographic evidence which clearly showed the target expanding circumferentially from the rear indicating the stress wave travelling toward the front of the cylinder. At the front face impact point significant cratering has occurred to a distance of 5mm outside the entry hole, the material being uplifted by 2-

3mm at the edges. The petalling has manifested itself in a layered manner to a depth of some 2mm. The nature of the internal radial cracking typically shown on the third disc back (i.e. the blue component between 40 and 60mm through the target) is particularly interesting. The disc has been punctured by the projectile and also reshaped by the stress wave effect. As a result the disc was perforated and left as an incomplete annulus. The minimum diameter of the puncture caused by the projectile was some 55mm, whilst the absent portion of the annulus shape had an equivalent diameter of at least 70mm. The radial cracking has occurred from the inside of the annulus in an outward direction. The projectile impact velocity was 820m/s. Assuming that little deceleration has occurred then the projectile will have taken 49μs to reach the front surface of the disc and a further 24μs to pass through it. From the high speed photography, the first material motion indicating tensile reflection of the initial compressive stress wave has occurred definitely by the second frame following impact, between 88μs and 176μs. The inference is thus that projectile passage has occurred well before the consequences of the stress reflection have been experienced. This would explain the noted crack pattern, since the diametric expansion of the target has caused longitudinal tearing to occur, eventually causing the stripping away of complete lengths of the target. In the subsequent local expansion the remainder of the annulus has then been encouraged to invert.

5.2.4 Impact on a Wax Target

To overcome the destructive effect observed in the unrestrained plasticine target, a paraffin wax cylinder was manufactured and placed in a compacted sand-filled box. The target was 350mm long and 135mm in diameter. The central 40mm diameter core was cast as a single unit of uncoloured wax. The remainder of the diameter was then provided by circumferentially laying approximately 15mm thick wax sheets on to the core. Cohesion was encouraged by carrying out this procedure in the

presence of heat. By varying the colours of the wax layers, it was hoped to recognise any lateral movement in the target. That is, sectioning the target would allow the different colours to indicate any differential motion.

The specimen was placed centrally in a 375 x 375 x 375mm timber box, and held in position whilst sharp sand was compacted in 4 layers around it. The front face of the target was carefully squared off and located flush with the visible surface of the sand, the target axis being parallel with the box sides. The open end of the box was then covered with clear polythene sheeting to seal in the sand during impact and the target was placed in position 18.80m from the gun barrel end. The box was carefully located to ensure the wax target axis was coincident with the expected projectile trajectory. See Figure 5.14 for details of the arrangement. A single 7.62 mm A.P. projectile was then remotely fired into the wax target.

The target was carefully sectioned, the stages being shown as Figures 5.15 to 5.17. Whilst this was mainly a qualitative test, it did give some idea of the potential effects in relatively soft targets. In this particular instance the most interesting aspect concerned the very large degree of projectile instability induced during penetration. The impactor almost certainly hit the target face at a normal angle, the symmetry of the initial cratering being taken as adequate evidence. It cratered to a distance of 2mm back from the perimeter of the 10-11mm diameter orifice and had a 0.5-1.0mm elevation at the highest points. Inside the target, the penetration path was uniform for approximately 85mm, at which point the 10-11mm diameter burrow significantly widened into a 50mm diameter chamber as the projectile became progressively less stable. The projectile was located at the bottom of the sand-box oriented at 180° to its original direction of travel. This is in agreement with the path left through the wax, the widening of the penetration burrow being caused by the projectile

tumbling end-over-end whilst also unstably spinning along its major axis, the spin having been imparted by the barrel's rifling.

Whilst no direct chronological evidence was produced by this test, a tentative ordering may be explored by considering the physical evidence in terms of the dynamic material response. This is attempted in Section 5.3.3.

5.2.5 Impact on Mortar Targets

Since concrete may be considered as a composite of coarse aggregate and mortar, it was considered useful to investigate whether the fine aggregate paste acted as anything more than a binder to the coarse material whilst undergoing a severe impact. Earlier work on gravel armour by Finch (1979) has indicated that 150mm of contained loose gravel is adequate to defeat repeated single shots of 0.30" armour-piercing or ball ammunition. This calls into question the role of the mortar, although to permit a sprayed type permanent application a binder is certainly a necessity.

For the first tests, a series of three 450 x 450 x 125mm thickness specimens was cast using a water/cement ratio of 0.6 and an aggregate/cement ratio of 3.0. Ordinary Portland Cement was used in conjunction with Zone 2 limestone sand. A single 7.62mm A.P. projectile was fired at each target when it had attained an age of 7 days. In each case the target was perforated, the penetration path being normal to the target face. Equally important, both front and rear face damage was minimal in all cases. In a single case the projectile was found in the range after the test. The jacket had been stripped from the core only for the initial 1mm of core length as shown in Figure 5.18. This indicates that the 125mm thickness of mortar generated very little resistance to the penetrator.

The information gathered in these basic experiments was supplemented by a further two series of more sophisticated tests described in Sections 5.2.6 and 5.2.7.

5.2.6 Impact on Mortar and Fibre Reinforced Concrete Composite Targets

A series of nine melt extract steel fibre reinforced concrete specimens, each rendered with mortar to achieve a total depth of 125mm, was cast to investigate further the role of the mortar binder and its interaction with the remaining material constituents.

These slabs were cast at each of three fibre concrete thicknesses, 100, 75 and 50mm, the corresponding mortar layers being of 25, ,50 and 75mm thick respectively. After conventionally curing for three days each specimen was subjected to a central impact, on the mortar face, by a 7.62mm A.P. projectile. Target mix details are given in Table 5.2 and impact test results in Table 5.3. In Series A (25mm mortar - 100mm fibre concrete) there is a considerable difference in measured penetration path lengths, specimen 1A having caused the projectile to deviate along a path 52mm greater than the specimen thickness before perforation, whilst in the case of 1B the projectile has halted at 73mm penetration. The corresponding entry crater volumes for these two specimens indicate that the smaller penetration path length has been achieved at a cost of significantly greater disruption of the target. The third specimen in this series was also perforated, a path length of 137mm being generated. The mean path length was thus 129mm within the target.

Series B (50mm mortar - 75mm fibre concrete) adds further weight to an argument that reduced penetration path length may possibly be offset by increased target damage. Targets 2B and 3B have undergone penetrations of approximately equal lengths within the target, generating entry crater volumes of the same order. However, the third specimen (1B) has suffered much greater damage in the area of impact, a crater of some 172 700mm^3 being generated. In this case the penetrator has been deviated to such an extent that it has suffered ejection from the impacted face of the mortar, without ever reaching the fibre reinforced concrete layer. In terms of the

limits for safety, it is probably best to regard this last specimen as untypical. Discounting it then gives a mean value of penetration path length of 122mm.

Series C (75mm mortar - 50mm fibre concrete) generated similar path lengths in two cases (2C and 3C) and a shorter path length in the third, this being the only target which did not suffer perforation. Dissection of the target provided a possible reason for the lesser penetration. The hardened steel core had fractured within the target due to the extent of its angular deviation. Again the greatest amount of front crater damage (though not significantly) was found in this target. For this series the mean penetration path length was 123mm.

Considering all three series, it can be seen that the mean path length values were not significantly different. However, the series with the thickest mortar layer, (75mm (Series C)) certainly suffered the least front face damage. Investigation of the mode of penetration of the projectile through each specimen indicates a probable reason for this.

In all cases where the projectile was subsequently located, the indications were that it had travelled largely undamaged through the mortar layer in a normal attitude. The jacket had stripped only after interaction with the fibre concrete to a depth of up to 35mm. The released core had then undergone an angular change leading to a new straight trajectory before coming to rest. In one case (1C) the core had been fractured by an extreme angular deviation. The inference is thus that the coarse aggregate and/or fibrous inclusion in the composite are sufficiently disrupting to cause the gilding metal sheath of the projectile to strip in a differential manner, thus causing the core to deviate, the deviation possibly being accentuated by direct projectile/aggregate impact.

Having carried out the above tests, the next step was to separate the composite targets into combinations of mortar, plain concrete and fibre reinforced concrete.

5.2.7 Impact on Slabs Consisting of 2 from 3 Combinations of Mortar/Plain Concrete/Fibre Reinforced Concrete

In an attempt to identify the major contributions to the observed projectile behaviour during penetration of fibre concrete containing 10mm coarse aggregate, various composite slabs were cast. Earlier tests suggested it was appropriate to assess possible means of promoting deviation within the target, this appearing to be a valid way of reducing penetration path length, albeit at the cost of increased front face damage should the deviation occur close to the impact surface.

Each specimen was cast so as to have a diagonal interface running from the top of the front face to the bottom of the rear face, effectively giving the projectile a "choice" of material at a depth of 62.5mm below the original impact point, assuming that the penetrator has not commenced deviation before the material interface.

A series of three 450 x 450 x 125mm slabs was cast for each two from three combinations, a total of nine specimens in all. The mix designs used for the component materials are given in Table 5.4. The static properties are also reported in Table 5.4.

Each specimen was positioned with the characteristically weaker material (as defined by compressive strength) being the initially impacted face, this material having zero thickness at the top of the target and 125mm thickness at the bottom edge. Each slab was impacted centrally by a single 7.62mm A.P. projectile. The age of the components at testing varied because each component had to be cast separately, and these ages are indicated in Table 5.5. The results of the tests are given as a series of sketches in Figures 5.19 to 5.27 and are summarised in Table 5.5.

Several of the composite targets suffered de-bonding along the material interface during the impact event, thus reducing the validity of the observations. As expected, the specimens consisting of plain and fibre concrete combinations have the smallest mean penetration path lengths,

followed by the mortar and fibre concrete specimens, the mortar and plain concrete combinations having performed worst. The compressive strengths of the three materials were very similar, implying that strength alone is not the major factor controlling penetration path length. Closer observation of the individual results confirms this. In the case of the PC/FC/1-3 specimens, possible projectile ricochets have been noted within the plain concrete section in two of the three tests, this leading to much reduced path lengths, the projectile not even reaching the fibre concrete component. It would therefore seem that the coarse aggregate has played a significant part in disrupting the penetration.

Studying the targets after the event yielded some interesting information. Each specimen is discussed in turn below;

M/FC/1: (Figure 5.19)

In this case, complete bond failure has not occurred across the specimen interface although the sample has started to separate. Indications are that this separation has commenced very early in the scheme of events since the major cracking has occurred only in the mortar section of the target, this being neither resisted by, nor carried through into, the fibre concrete section.

M/FC/2: (Figure 5.20)

The above comments are also valid for this specimen.

M/FC/3: (Figure 5.21)

This specimen has suffered a complete bond failure. The mortar section was particularly damaged, being separated into three distinct pieces, whilst the impact and penetration zone has experienced major local damage. One item of interest is that the front face spalling in the mortar has occurred, at least in part, before the major cracks have been generated; this view being supported by the existence of a spalled mortar plate which fits directly over a major crack running from the burrow in a

south westerly direction through both mortar and fibre concrete parts of the specimen.

M/PC/1: (Figure 5.22)

Complete separation has occurred between the mortar and plain concrete components. The mortar section has suffered significant cracking, both to the top surface and also, in four cases, running right through the mortar. However, of these four cracks only one may have continued into the plain concrete section of the composite. The mortar has undergone extensive spalling in the impact areas, as the projectile passed through in a normal trajectory. Examination of the plain concrete portion of the target indicates however that the projectile has not been subjected to sufficient resistance to cause it to lose either its external sheath, or perhaps more significantly, the lead sealing, during its passage through the mortar. The projectile was located at the surface of the plain concrete component with 12mm of the complete unit projecting from the concrete. The rear surface of this target has also suffered extensive damage. Four major cracks were discernible carrying through from the back face of the plain concrete to the front face. A small tensile scab has also been generated from the rear face of the specimen.

M/PC/2: Figure 5.23

This specimen provided some very interesting information, though its repeatability is open to conjecture. The mortar section of the target was extensively damaged during the impact and subsequent normal penetration. Four major cracks were noted, as well as a series of smaller surface cracks related to the spall pattern. The specimen has suffered a bond failure very early in the impact event. None of the above cracking has been transferred to the plain concrete part of the target, neither has the projectile continued into this second portion. The penetrator has in fact travelled normally through the mortar section before coming to rest on the surface of the plain concrete, its orientation implying that the projectile

has impacted sideways on to the plain concrete. The most likely explanation for this behaviour would seem to be that the de-bonding of the two materials has occurred sufficiently early, and to such a large degree, that by the time the projectile has passed through the mortar portion of the target the gap between the two constituent materials has been great enough to enhance an existing instability in the projectile, which is specifically designed for penetration only along its major axis. It is especially surprising that the potentially large transference of energy has had no visible effect on the plain concrete target.

M/PC/3: (Figure 5.24)

Again, this target has suffered a bond failure across the constituent material interface. The mortar section has several large cracks running through it, although the spalled area and subsequent crater is significantly smaller than the other two specimens of this series. The three major cracks on the front face of this portion are present, with only slight changes of position, on the rear face also. This face contains the projectile jacket which has stripped at the very edge of the interface, only the hardened steel core then travelling through to the plain concrete section of the target. As a result of what appears to be a completely separate impact, the plain concrete specimen has developed its own crack regime. Two major cracks have occurred, propagating from the outside edge of the target inwards, whilst a third, smaller, crack is also in existence. The projectile core has travelled into this section 43mm, giving a total path of 106mm length.

PC/FC/1:(Figure 5.25)

A single crack has developed on the front face of the plain concrete segment (i.e. the target impact face) coupled with a crater of some 150mm maximum diameter. The penetrator did not travel to the de-bonded second section of this target; instead deviation within the plain concrete caused the core to fracture and come to rest some 75mm after initial impact. The

jacket had by this point been completely stripped from the core. The fibre concrete section of the target did not experience any damage whatsoever.

PC/FC/2: (Figure 5.26)

The main points of the above are also appropriate to this target. That is that the projectile did not reach the fibre concrete segment. The generated crater was 160mm diameter. The most significant difference though is that the missile was not located, there being no penetration path below the base of the crater. The conclusion drawn was that the projectile had undergone an extreme change of direction within the target and had emerged as a ricochet without greatly penetrating the target. The penetration path length was measured to the base of the crater as 37mm.

PC/FC/3: (Figure 5.27)

In this case the target did not de-bond during the impact event. The slab suffered only crater damage of some 170mm diameter. No cracking was discernible on either the front or rear face of the composite target. Again, no projectile was located within the target. A ricochet being indicated, the maximum penetration path length was taken as the crater depth, that is 41mm.

It is interesting to note that in all cases when the observation was possible, the projectile has deviated downwards upon meeting the interface, effectively travelling toward the weaker material.

5.2.8 Impact on Mild Steel Targets

A number of trials were carried out on various types of mild steel specimens to investigate the initial impact and subsequent penetration for a homogeneous material having significant tensile strength. Two different types of target were used, one of a separated nature, the second a single mass.

i) Layered steel plate target

A series of ten 100 x 100 x 12mm thick mild steel plates of Brinell Hardness value 149 were bolted together and embedded in a 450 x 450 x 125mm thick plain concrete specimen, the top surface of the two materials being coincident. The concrete mix ratios by weight were OPC - 1.0, free water - 0.45, 10mm single size limestone (water content 0.48%) - 2.36 and zone 2 limestone sand (water content 5.3%) - 2.36. The concrete was allowed to cure for 14 days at 20± 2°C with a relative humidity of 90°+ before the central steel section of the target was impacted normally by a 7.62mm armour-piercing projectile. Figure 5.28 illustrates the general experimental arrangement; whilst Figure 5.29 shows the target after debonding from the concrete and separation into individual plates. The projectile has penetrated as far as the third plate, the path length being 26mm. The hardened steel core may clearly be seen in the first and second layers. The 24mm length core has remained acceptably perpendicular to the target face. Closer examination of the first section, Figure 5.30, confirms by the symmetry of the petalling that the impact was orthogonal. The gilding metal sheath of the projectile was recovered after the test and this further supports the symmetry of penetrator entry; as shown in Figure 5.30, the stripping has occurred in a uniform manner.

This experiment indicated that a 7.62mm armour-piercing projectile impacting normally at 20m range can be expected to penetrate a restrained mild steel target with a Brinell Hardness value of 149, in an orthogonal manner to a depth approximately equal to the projectile core length.

ii) Solid steel cylinder targets

To assess the importance of orthogonal impact on subsequent penetration two simple tests were carried out.

A 250mm long mild steel cylinder of 75mm diameter and 137 Brinell Hardness, was machined to obtain flat ends at 90° to the major axis. It was placed at 20m range length and orientated carefully so as to be normal

to the envisaged projectile flight path. The target was then impacted by a 7.62mm A.P. projectile. Examination of the sectioned specimen, Figure 5.31, shows that a total penetration depth of 27mm has been attained. The core has remained whole although the only indication of the original copper coloured sheath is a fusing of the mild steel and gilding metal at points within the petalling. It is also clear that the projectile has not penetrated orthogonally, although this has had little effect on the penetration depth. The target was unrestrained; whilst the initial impact was perpendicular, the 8.725kg target has shifted during the impact thereby inducing the projectile deviation.

A superficially similar arrangement was adopted in a second test. However, the target was fully restrained and the projectile was induced to tumble in flight using a 0.25mm thick brass shim placed in the flight path. Figure 5.32 illustrates the effect upon the penetration characteristics. The projectile has impacted sideways causing total disintegration of the projectile and a much reduced penetration path length of some 6-7mm. These simple qualitative tests indicate further that a stable impact may confidently be expected at a 20m range assuming that the projectile is not destabilised by external influences.

5.2.9 Deceleration of the Projectile within Plain Concrete

Several tests were carried out to investigate the rate of velocity reduction for an armour-piercing projectile penetrating a 450 x 450 x 125mm concrete target. Although the results were scattered, a system was developed which at least pointed to the likely orders of magnitude of the rates of velocity change.

Initially, the recording system shown in Figure 5.33 was used, each specimen containing a series of six detectors, 100mm square, placed through the thickness of the concrete at nominally 25mm centres at the centre line. Each detector consisted of a "sandwich" of 0.25mm acetate/0.1mm shim brass/paper/0.1mm shim brass/0.25mm acetate sealed with rubber sealant and

plastic tape to provide a waterproof electrical "make" circuit. The paper ensured that the circuit initially had a infinite resistance across the two brass plates, until shorted by the projectile passage. The detectors were connected to form the resistance breakdown circuit of Figure 5.33 and linked to a Gould OS4000 storage oscilloscope. In these tests, the Barr and Stroud rotating mirror camera was used in an attempt to record projectile impact details. The overall arrangement is thus shown in Figure 5.34. By this means it was hoped to have a full photographic record of the pre-penetration events and a time-based record of the post-impact details.

The resistance breakdown circuit was so designed that as the projectile passed through each detector a sharp step-down of the voltage level would occur as a result of the mechanical bonding of the shim brass plates. Ideally, a series of six square steps would be recorded on the storage oscillscope, if all six detectors were punctured.

Two tests were carried out using this approach. The details of mix design, oscilloscope settings, etc., may be found in Appendix VIII.3. Since the main use of these two tests was to define the types of problem to be overcome, the results are discussed below, before going on to consider the improved techniques developed from them.

TEST V1: The concrete was cured for three days before testing by a single central impact of a 7.62mm A.P. projectile. The event was frontlit using the xenon flash unit and a single 1kW photoflood positioned to highlight the specimen edge, so that it could be photographed using the ultra high speed rotating mirror camera. Details of the photography are given in Appendix VIII.2. The camera was accelerated up to approximately 1μs interframe time, after which the 1kW photoflood was switched on and the projectile was fired, triggering both the flash unit and storage oscilloscope.

Although a trace was captured on the oscillscope, it was of a less well-defined nature than expected, due to the mechanical connection of the

detector plates becoming disrupted as the projectile completed its passage. This caused the oscilloscope trace to "creep" back between each detector perforation, as shown in Figure 5.35, rather than to give the anticipated square steps. This was the trace obtained for the puncturing of three detectors. It was transferred via a Commodore PET 3032 microcomputer to a Computhink mini disk drive before printing on a Hewlett-Packard 7470A plotter.

On coring and sectioning the slab it was found that the detector plates had moved during casting to the positions shown in Figure 5.36. Table 5.6 gives the positions of the detectors and recorded times during the penetration. The third detector possibly caused the projectile to deviate as both the jacket and core had come to rest before passing completely through it.

Correlating the distance between the detectors with the times obtained by assuming perforation at the peak of each oscillation of the trace, the average velocity over the 35mm between detectors 1 and 2 was computed as 36m/s and over the 35mm between detectors 2 and 3 as 35m/s. The photographs did not show the bullet flight or impact. Penetration path length was 57mm.

TEST V2: A second test using a similar technique was carried out. During casting, the detectors were restrained by a small frame to resist gross movement. In this case, the projectile again punctured three detectors, generating two velocity measurements (Table 5.6). The same "creep" phenomenon was noted on the recorded traces, (Figure 5.37) as in test V1. The assessed velocities were 89m/s between detectors 1 and 2 (40mm spacing) and 43m/s over the next 15mm between detector 2 and detector 3. The frontlit photographic technique yielded a very poor quality series of 30 frames (see Appendix VIII.2, Figure VIII.2) showing the projectile in flight, the distance covered over the 30 photographs being 26mm.

Figure 5.38 is a sketch of the cored specimen, it may be seen that the projectile core has stripped its jacket and then fractured within a short distance, the core having deviated quite extensively whilst undergoing break-up to give a total path length of 59mm.

Whilst these tests furnished some valuable information on general technique and, in the case of V2, a series of potentially useful photographs, it was considered that the difficulties inherent in attempting to capture information from six detectors on a single recording channel made it attractive to develop an alternative approach. Little confidence could be attached to velocity measurements which implied that a projectile could penetrate concrete to a depth of over 50mm at a mean velocity of less than 100m/s. Also, the low probability of obtaining photographs using the Barr & Stroud camera, as discussed in Section 5.2.2, prompted a decision to concentrate instead on a more general view of the event, using the Photec IV rotating prism camera which was described in Section 5.2.1 and Appendix VIII.1.

A similar type of "make" detector was used, a series of six again placed centrally at nominally 25mm intervals through each 450 x 450 x 125mm plain concrete specimen. Each detector was connected independently to a capacitance breakdown circuit such as that shown in Figure 5.39. In this case the capacitor was charged immediately before the projectile was detonated. Closing of the two brass plates caused the capacitor to discharge, shown as a voltage change on an oscilloscope trace. Using a two-channel Gould OS4000 storage oscillscope, a two-channel Gould OS4020 storage oscilloscope and two channels of a Biomation four-channel transient recorder, each detector circuit was monitored independently. Details of the system are given in Appendix VIII.3. The event was photographed by the method described in Section 5.2.1, attempting to obtain both projectile flight and target impact information. Two tests, V3 and V4, were carried out, the specimen details being given in Appendix VIII.3.

Test V3: The photographic arrangement worked adequately. providing a series of silhouette type pictures with two frames showing the projectile in flight and many others showing the sequence of target break-up.

Of the recording equipment, the Gould OS4000 and OS4020 oscilloscopes each performed well, generating the data shown in Figure 5.40. Passage through the fifth and sixth detectors, monitored on the Biomation transient recorder was however not apparent. Examining the specimen was unsuccessful, as the 100mm diameter concrete core disintegrated during preparation; it was not possible to ascertain the actual position of the projectile or the detector plates. Using the remainder of the specimen, the positions of the detectors were assessed and spacings are tabulated in Table 5.6. The projectile was assumed to have travelled normally through the concrete (relative to the impact face) and the distances correlated to the times obtained for the first four detectors. As shown in Table 5.6 this implied that the projectile, which had been travelling at 822m/s two metres before impact, had a mean velocity of 665m/s over the first 21mm of penetration, 678m/s between detectors 2 and 3 (24mm spacing) and 311m/s over the next 24mm. It is not feasible that the projectile accelerated through detector 2. The implication is thus that it was not travelling the shortest path between each detector (i.e. an orthogonal one) but was deviating, a more likely circumstance in any case. These values should only be used therefore to represent orders of magnitude, and then with a great deal of caution.

TEST V4: A similar test to V3 was carried out on a second plain concrete specimen. Again the details of mix design, recording equipment settings and photography may be found in Appendix VIII.3.

In this case, a total path length of 120mm was measured in a specimen in which a large amount of vertical detector movement had occurred during casting. There was considerable deviation of the projectile within the specimen.

The Biomation transient recorder failed to record any trace appropriate to passage through detectors 5 and 6. Coring the specimen (Figure 5.41) confirmed that the projectile had punctured only the initial four detectors. Table 5.6 gives the detector positions and timings which were obtained from the information shown in Figure 5.42. The indicated mean velocities were:

702m/s between detectors 1 and 2 (13mm spacing), 630m/s during the next 37mm and 591m/s between detectors 3 and 4 (13mm spacing).

5.2.10 Investigation of Front Face Spalling Using Graphite Detectors

Another technique tentatively examined towards the end of the project was the use of graphite rods to detect front face spalling mechanisms.

To record the point at which spalling commenced it was necessary to produce a detector capable of picking up the initial gross material movement (later to form the crater) around the penetrator. The requirement was thus for a material brittle both in shear and direct tension. After some preliminary testing, it was observed that 0.7mm diameter drawing pencil refills, containing a high proportion of graphite, were particularly suitable. These combined the properties of brittleness and high electrical conductivity, the latter being useful to permit the exact time of breakage to be recorded using electronic sensing equipment.

Having found a suitable detector medium, transducers were produced by directly soldering sheathed wire to each end of the graphite rod. This provided a satisfactory method in terms both of mechanical bond and electrical resistance, the value of the latter being between 1 and 2 Ω for the complete detector including approximately 600mm of copper stranded wire.

A series of six slabs was produced, three of plain concrete and three of fibre reinforced concrete. Mix details are given in Appendix VIII.4.

Four detectors were placed in each specimen orthogonal to the impact face and with one end of each 50mm long rod at the surface,. Great care was necessary to ensure the specimen received adequate compaction by vibration without breaking the detectors. The detectors were initially placed in the positions shown in Figure 5.43, the sets of two lying mutually at right angles. The first pair of each set were 50mm from the centre of the slab and the second pair were nominally a further 25mm away on the same lines.

For the first three tests, carried out on the plain concrete specimens numbered GR/P/1 to GR/P/3, the breaking of the transducer was to be amplified using the system shown in Figure 5.44. That is, at the instant when the graphite rod broke the current would be shunted through the 42kΩ resistance wired in parallel with the now open-circuit detector, causing a voltage change which would be recorded on the transient recorder. Details of the data recorder settings may be found in Appendix VIII.4. The breaking of detectors 1 and 3 were the trigger signals for the OS4000 and OS4020 respectively; the breaking of the second detector (2 and 4) then being recorded, on each respective storage device, relative to the trigger points.

When the first test, GR/P/1, was carried out as described above, neither of the oscilloscopes triggered as only a very small voltage stepdown had been generated when the detector broke. This was surprising since a change of only 0.9v should have been adequate to trigger the devices at the sensitivities used.

For tests GR/P/2 and GR/P/3, the 42kΩ resistors were replaced by 1 MΩ resistors to promote a greater voltage change in the circuit.

In both tests only three detectors were found to be operational after casting. Thus, detector 1 was used to trigger both oscillscopes. In both tests only a very small voltage change, which was incapable of triggering the storage devices, was noted.

At this stage it was realised that the fault was due directly to the detector circuit. The impedance of each oscillscope was approximately 1MΩ, similar to the shunt resistor. Hence when the voltage was shunted as detector 1 broke, the potential drop was balanced either side of the oscilloscope channel input so that no change was registered in the circuit. This situation occurred because neither oscilloscope nor target (and hence detector) was insulated from ground. An alternative amplification and recording circuit was developed which ensured a controlled voltage drop when the detector was broken. This is illustrated as Figure 5.45.

Each of the tests on the fibre reinforced concrete specimens, GR/F/1 to GR/F/3 used this alternative approach. Additionally, by triggering the two storage oscilloscopes simultaneously from a single source it was possible to consider the time of breakage of each detector relative to all others, rather than considering each set of two as a discrete unit. An oscilloscope trigger switch consisting of two sheets of aluminium foil, slightly separated, was placed on the surface of the target over the impact zone. This trigger was insulated from the target using a single sheet of paper. The passage of the projectile then closed the circuit, triggering the storage devices simultaneously.

This revised procedure was used for tests GR/F/1 and GR/F/2. Whilst triggering successfully occurred, only one of the available graphite detectors was broken in each case, giving a single trace but no information on spall material propagation rates.

For test GR/F/3 an alternative oscilloscope triggering unit was tried. Silver-loaded conductive paint was used to paint a grid on the impact zone of slab GR/F/3 and a 'standard' resistance breakdown circuit as shown in Figure 5.44 was employed to trigger the two storage oscilloscopes simultaneously. Figure 5.46 shows the details of the grid used.

In this test the system triggered suitably on projectile impact but again no useful data was recorded on the storage devices.

5.3 General Discussion

5.3.1 Projectile Flight

The projectile used throughout this study has been a standard ordnance 7.62mm armour-piercing bullet, allowed a flight length of generally 20m before impact. Its mean velocity measured at 18m was 808m/s, averaged over all recorded values.

The projectile is energised as follows;

i) the percussion cap is struck by the pin of the firing mechanism;

ii) the propellant ignites, gas pressure then causing the cartridge case to expand and form a gas-tight seal in the rifle breech;

iii) the hardened steel core, surrounded by its ductile gilding metal jacket, is propelled forward to engage in the barrel rifling;

iv) a seal is then formed and the projectile is driven forward with a spiralling motion.

The projectile, upon leaving the barrel, requires a length of flight path to recover from the instability induced by both the imparted spin and the non-symmetry along the longitudinal axis of the jacket seal.

Initial information (Port, (1980)) suggested that at greater than about 12m flight path, the projectile would be stable and expected to impact orthogonally with a target placed perpendicular to the gun barrel axis. Therefore a 20m flight path was selected. However, as a consequence of the inconsistency of the penetration depth results, attempts were made to photograph the projectile flight, at various interframe rates, to confirm the orthogonality of the penetrator at impact.

The photographs acquired using the slower Photec IV rotating prism camera (Section 5.2.1 and Appendix VIII.1) best served this purpose due to the more easily controllable illumination and event synchronisation. A series of images, each with an appropriate reference datum, was produced. Although the projectile was travelling up to 27mm during the exposure of each frame, the overall orientation of the projectile across the camera "window" could generally be observed as perpendicular to the impact face.

The ultra-high speed photographic technique (Section 5.2.2 and Appendix VIII.2) was, of necessity, a rather indiscriminate process. The limitations of the event synchronisation electronics, discussed in Section 5.2.2, meant that a less than 16% probability existed of obtaining a series of 30 photographs. Ultimately only two tests were successful, a frontlit and a backlit one. The information obtained was valuable though tentative.

The results of the frontlit test were disappointing as they showed none of the expected projectile jacket detail, either on the surface or along the trailing edge. However, they did confirm that an orthogonal flight could be expected with the impactor having passed through a trigger switch made up of two 0.001mm thick brass shims.

For the reported backlit test a similar switch, consisting of two 0.1mm thick brass shims, was used to trigger the Xenon flash unit. The resulting photographs indicated that the projectile was destabilised within the last 120mm of its 20m flight path. An end-over-end instability was induced.

A further check on the bullet stability was carried out by impacting a mild steel cylinder (Section 5.2.8). Without any obstruction between the rifle barrel and steel target a stable perpendicular impact was indicated by uniform ductile petalling around the impact point.

However, when a 0.25mm thick brass plate was put in the flight path ahead of the target, it caused the projectile to tumble end over end,

finally impacting the target face sideways and disintegrating. This reduced the penetration depth into the steel from 27mm to 6mm.

From the above evidence it can be concluded that if there is no external interference with the flight path, 20m is sufficient range to ensure normal impact. Brass switching devices placed in the flight path should be no more than 0.002mm total thickness, i.e. 2 x 0.001 shims, otherwise projectile instability may be regenerated with a significant effect on the penetrating power.

5.3.2 Projectile Impact

This aspect was defined as the stage at, and immediately following, the initial projectile-target contact. Its effects have been studied in two distinct manners;

i) during its occurrence, by high-speed photographs, and

ii) by inspection of various impacted materials after the event.

The initial interaction between projectile and target was captured only by the relatively slow Photec IV rotating prism camera. The limitations of this equipment were given in Section 5.2.1, the most significant being the existence of projectile blur at the available exposure rates. However, within the limits of the attained interframe times, trends may be considered.

The method of analysis employed for the successful 16mm films was documented in Section 5.2.1, the obtained data being presented as Table 5.1.

For the impact on plasticine, at an interframe time of 88μs and with a velocity of 820m/s, the projectile has completely disappeared into the target from frame 1 to frame 2. In the same 88μs interval extensive material motion has developed as a semi-transparent conical area, radiating from the impact point. From Table 5.1 it can be seen that a mean circumferential rate of propagation of 20.6m/s was observed for frames f2-

f6 (upper and lower sections). The mean spall velocity was 121.2m/s over frames f2 to f5 (upper) and 198.9m/s between frames f2 to f4 (lower section) giving an overall mean value of 160.1m/s.

Similar considerations were applied to the other three rotating prism camera tests, using concrete-based targets. The analysis of frames as a contour sketch was limited by the point at which a reliable datum could be discerned. Within these constraints the obtained results were acceptably consistent. Average velocities for upper and lower sections of the 'contours' have been given in Table 5.1.

If the data for the 1-2ms interval of the photographs is averaged, the mean rates of propagation of the surface circumferential movement are 32.5, 54.3 and 30.3m/s for targets RP1, RP2 and RP3 respectively, giving an overall average of 39.0m/s.

The mean velocity of the spall products (Table 5.1) showed a considerable reduction with time over the measured frames. In the first 800 or so microseconds (i.e. average value for up to 9 or 10 frames), the mean rate was 109.5m/s. Using frames 11 to 16 (RP1) and 11 to 19 (RP2), the spall velocity was reduced to 38.9m/s.

In order to have confidence in the observed trends it would be necessary to carry out many more trials. This limited set of results does indicate the orders of magnitude of the various material motion velocities. It is particularly interesting that the measured values for spall product velocity show a significant deceleration over the few frames examined.

Examination of non-cementitious targets after impact gave the following dimensions of the craters in the various materials;

Plasticine: 12-17mm diameter, petalling to 3mm height.

Wax: 10-11mm diameter, petalling to 1mm height.

Mild steel: 11-12mm diameter, petalling to 5mm height.

In the cases of the wax and plasticine targets, the jacket did not strip on contact with the target surface and this was reflected in the

measured crater diameters. The upper value for the plasticine target was caused by the extensive stress wave response.

In the mild steel targets, a similar initial crater diameter was observed with a sudden reduction to a 6mm diameter, equivalent to the core diameter, by a depth of 6mm into the target. This indicates the point at which the jacket had been completely stripped from the core.

In all of the ductile materials the extent of target damage was easily defined. Impact damage was more difficult to determine for the brittle cementitious materials, where significant manipulation was necessary to establish the boundaries of affected material (see Section 3.5.2). This was particularly true of the high modulus fibre-reinforced concretes but less significant with the mortar targets.

The photographic records of projectile impact and subsequent target motion gave no evidence that the sub-surface damage was solely a response to the physical presence of the impactor. The conclusion was drawn that this major material movement was probably a result of the stress wave, reflected as tensile from the rear concrete-air interface, acting on a zone of already weakened material. Assuming a stress wave velocity through concrete of 3.5mm/μs (Watson et al.(1985)) and no significant attenuation, the initial compressive stress wave would travel through to, and be reflected back from, the rear surface of a 125mm thick target in (250/3.5=)71μs. In the same time a projectile travelling at 808m/s would, assuming no deceleration at impact, penetrate a distance of 57mm. Allowing for deceleration, using the tentative figures obtained for tests V3 and V4 (Section 5.2.9), the penetration distance would be slightly less, about 50mm.

Hence, the photographs of material motion, with an interframe time of around 88μs (see Section 5.2.1), first show the target movement after the complete reflection of the initial compressive stress wave and following significant penetration of the projectile into the target. It is therefore

not possible to attribute the major material motion solely to the presence of the projectile, without allowing for the other effects of the impact. This also means that, for brittle materials, the examination of the crater zones of the targets following the event is an inappropriate way of assessing the immediate consequences of the projectile presence. That is, the first path of the projectile will almost certainly be completely destroyed during the subsequent spalling and cracking phase of the event.

A potential solution to this difficulty would be to use targets of very great thickness in order to ensure sufficient attenuation of the stress waves before their reflection and influence on the impacted zone. Alternatively, free-standing "trap blocks" with a mechanical impedance similar to the target could be placed in close contact with the rear face to remove the material-air interface; causing the impact wave to pass away from the target, rather than be reflected.

In terms of this study therefore, only the gross effects of the complete event may be considered by the inspection of the post-impacted cementitious targets. This aspect is further explored in Section 5.3.5.

5.3.3 Projectile Penetration

This parameter was one of the major target characteristics reported in Chapter 4. The original intention was to consider the orthogonal distance travelled into the target, so as to minimise the material thickness required to defeat the projectile. The first few series of tests demonstrated that this was not a valid means of assessing the material penetration resistance, as an excessive amount of random deviation, from a straight path, was observed in superficially similar targets. Consequently, actual penetration path length was used to measure the relative capabilities of the various concrete composites.

The tests described in Section 5.2 permitted some of the inconsistencies to be further explored. The effects on various

cementitious and non-cement-based targets were studied by careful post-impact sectioning and the taking of physical measurements.

The target materials have again been classified into ductile and brittle categories. The former included wax and mild steel, the latter the various cement composites. (The unrestrained nature of the single plasticine specimen tested precluded any dissection of the impacted target).

5.3.3.1 Ductile Targets

The mild steel targets included both massive cylinders, large enough that global effects had no influence, and layered 12mm thick plates placed in intimate contact. The penetration response was similar for both. The gilding metal jacket of the impactor was stripped from the hardened steel core during the immediate impact, culminating in a total penetration path of 26mm, the first 5-6mm of which was significantly widened by the material motion as the jacket was stripped.

The exposed burrow was seen to precisely follow the ogive shape of the hardened steel core. As discussed in Section 5.2.8, the path was orthogonal to the target face, so long as the projectile had attained a stable state before striking a restrained target. The significantly thick mild steel was thus capable of containing the hardened steel core, following its stripping, almost within its own length and without either fragmentation or deviation of the projectile. Close examination of the recovered core indicated that the bullet's spinning appeared to continue for approximately 75% of the attained penetration depth, subsequent to the shedding of the enclosing jacket.

In passing through a wax target (see Section 5.2.4) the projectile suffered a total loss of its flight stability. Figure 5.17 illustrates the extensive damage caused by the end over end passage of the jacketed core through the target. The undamaged impactor was located at 180° to its original orientation, at the base of the containing sandbox. As only a

single trial was carried out, it is impossible to confirm the typicality of the observed response. Hypotheses considered for this response included

i) Movement of the whole target, both wax and containing sandbox, as a result of the impact. Such movement was not apparent.

ii) Motion of the wax target within the containing sand, again as a result of the magnitude of the impact. Examination of the target did not support this assessment. The overall shape of the wax target was not significantly changed, nor was the surrounding sand in any way disturbed.

iii) The disruption having occurred as a result of an interaction between the changing target stress field and the penetrating projectile. A tentative value for stress wave velocity through wax, 3.45mm/μs, has been obtained from Morris (1986). An ordering of the events occurring within the target is possible using this value. Initially, an assumption is made that the original impact velocity of 810m/s is not diminished before the projectile becomes unstable (i.e. at 85mm penetration depth). The time for the projectile to travel this 85mm is thus:

$$85\text{mm} \times \frac{1}{810 \times 10^{-3}}\ \mu\text{s/mm} = 105\mu\text{s}$$

In this time, at a velocity of 3.45mm/μs, the stress wave front travels a distance of:

$$3.45\text{mm/}\mu\text{s} \times 105\mu\text{s} = 362\text{mm}$$

through the target. A wax/sand interface occurs at 350mm. Assuming reasonably uniform stress wave transmission, the stress wave front will be continuing in an unchanged form until it reaches the target/air interface and is reflected at a time of 375mm/3.45mm/μs = 109μs from the

impact, as a tensile wave. Alternatively if one assumes that the wax/sand interface promotes a tensile reflection, and taking a worst case, postulates a complete stress reversal at this point, then up to a, 362mm - 350mm =, 12mm thick section of the wax cylinder may, from the rear face forward, be subjected to a tensile stress field at a time of 105μs after impact. In either of these limiting cases, the target, at 85mm from the front face, is still subject to the original compressive stress field when the projectile becomes unstable. The instability was thus categorically not initiated by any significant local change of stress field.

Whilst none of the above adequately explains the observed gross instability, it is however valuable to note the extensive disruption caused to the penetrator by a "soft" target material located in a "hard" restraining medium. This phenomenon was also recorded during several of the trials reported in Chapter 4, particularly when conglomerated Kevlar-29 fibre was incorporated, at high volume concentrations, in plain concrete mixes.

5.3.3.2 Brittle Targets

In Chapter 4 it was concluded that the inclusion of fibres in the types of concrete used in this study had no effect on projectile penetration depth, although a beneficial effect on spall resistance was obtained. The mechanism tests carried out attempted to isolate the various composite constituents to permit the contributory factors to be established.

Several plain mortar targets were fired at (Section 5.2.5) with minimal front face damage and total target perforation, the projectile following a straight path orthogonal to the impacted face. This strongly suggests that the mortar component of the composite acted simply as a binder for the coarser aggregate and fibrous inclusions. Considering the

penetration characteristics of the plain concrete specimens (Chapter 4), some conclusions were drawn on the effect of differing coarse aggregate type. Table 4.12 records that river gravel-based plain concretes gave the lowest mean penetration path lengths, whilst basalt concretes gave the highest values. This ordering of concrete types (i.e. river gravel-based most resistant, followed by limestone-based, with basalt-based concretes least resistant to penetration) is not, as reference to Figures 4.5, 4.8 and 4.11 will confirm, obviously associated purely with the mean compressive strengths of the various concretes. These results are therefore not in agreement with most published penetration equations, such as those reviewed by Sliter (1980) and Haldar and Miller (1982), where, over a wide range of compressive strength values, penetration depth is reduced as concrete compressive strength increases. Most such penetration equations for concrete have been devised on the basis of penetrators which were orders of magnitude greater than the coarse aggregate size. This is not the case in these studies where aggregate and projectile were of similar size. However, Sliter (1980) has reported that the little evidence available on the effect of aggregate size suggests that penetration depth is only weakly influenced by projectile diameter/aggregate size ratio. It is nevertheless recommended that this aspect of resistance to small arms attack should be the subject of a more rigorous study.

One reason for the lower penetration path lengths reported for river gravel concretes is that the mean value is significantly influenced by the relatively larger number of penetrations in river gravel concretes which have been disrupted by either projectile core fracture or ricochets.

In the tests reported in Chapter 4, on targets massive enough to prevent rear face damage, the addition of fibres to the concrete matrix did not reduce actual penetration path length and did not appear to influence the direction of the projectile through the target. Various combinations of mortar, plain concrete and fibre reinforced concrete were tested

(Sections 5.2.6 and 5.2.7) to explore the relative roles of fibre and coarse aggregate in the composite. These confirmed the observations of the main test series. That is, that plain mortar was not effective in resisting penetration, the addition of coarse aggregate being necessary to strip the gilding metal jacket from the hardened steel core. This action was usually observed to be the origin of the projectile deviation. Depending upon the extent and the rate of the direction change, the core could be fractured with a corresponding significant reduction in its efficiency as a penetrator. On several occasions the projectile changed direction by more than 90° resulting in a "ricochet", i.e. the presence of a crater without any sign of the projectile. In these cases it is probable that the projectile has stripped its jacket in contact with coarse aggregate and has then carried out the jacket during the subsequent path change.

In terms of defeating the penetrator the optimum solution would therefore be to disrupt its passage as soon as possible after impact, since a loss of orientation has been seen to produce the most successful path length reduction. The types of concrete used in this study, aiming at homogeneous mixing with various fibres and designed for sprayed application, were not very appropriate materials to induce this disruption. The relatively small proportion of coarse aggregate required to ensure pumpability meant that the projectile had a greater chance of travelling a significant distance into the target before hitting a "hard" material. Further, the limiting of the coarse aggregate to a maximum size of 10mm to try to prevent conglomeration of fibres, meant that the rock particles were possibly less likely to induce instability than had there been larger rock particles in the mortar binder. Indications were that the projectile jacket would be more likely to strip during passage of a "hard" material than the relatively "soft" mortar binder.

Paradoxically, the targets which most severely disrupted the projectile passage were those which were of a mixed construction, with non-resisting voids contained in the surrounding hardened material. As discussed earlier in this section, a wax target caused extreme disorientation of a penetrating projectile. In a similar manner, the sequence of events for specimen M/PC/2 (Section 5.2.7) caused the penetrator to perforate a mortar layer of approximately 60mm thickness before becoming unstable in a void between the mortar and its plain concrete second section. This instability was sufficient to render the projectile incapable of further significant penetration.

An extreme example of this phenomenon is illustrated as Figure 5.47. A specimen containing 2.0% by volume of 13mm length Kevlar-29 polyamide fibre was tested early in the study. At this concentration the fibre tended to conglomerate into soft balls, as the material was similar to cotton wool in nature. As a result, distinct voids were formed in the hardened concrete. On impacting and later sectioning the specimen, the projectile was observed to have stripped its jacket at 78mm depth after an orthogonal impact and initial penetration. The core then exhibited an extreme deviation, turning through 180° in 10-15mm, to come to rest facing in the opposite direction to its original travel. The core was not damaged during this change of trajectory.

5.3.4 Projectile Deceleration

A small number of tests were reported in Section 5.2.9. These attempted to assess the rate of velocity reduction of a penetrator passing through a plain concrete matrix. A potentially successful technique was developed (tests V3 and V4) which indicated the likely order of deceleration values. Figure 5.48 shows the penetration depth - time plot for these specimens assuming orthogonal penetration.

The figures obtained appear to indicate that the initial impact and penetration (to a depth of approximately 20mm) results in a velocity

reduction of 15-20% of the impact velocity. In the case of V4, it is possible to suggest that the physical action of stripping the projectile jacket (at 43mm path length) did not greatly affect the rate of velocity reduction, occurring as it did between detectors 2 and 3, for which a mean velocity of 630m/s was obtained. According to the figures recorded, the projectile was travelling at a significant rate (591m/s) at a distance of 55mm before its final resting position. Thus, the conclusion appears that the penetrator on becoming unstable (after jacket shedding) has progressively decelerated, at an increasing rate, as the angular deviation increased through the target. What cannot be defined was which of these phenomena was cause and which was effect. As already suggested, these tests should be mainly considered as development exercises. It is possible also that the very presence of the detectors in the specimens may have altered the recorded penetration characteristics. Under ideal circumstances, time-related X-ray photography would be a more appropriate way of assessing this aspect of the impact event.

5.3.5 Target Front Face Damage (Cementitious Materials)

This facet of the event was useful mainly as an assessment of the near impact surface damage to the specimen and as an indication of the continuing structural integrity of the specimen against further attack. It was established by the measurement of a "true" crater volume. A consistent method of appraisal was developed and the results were reported in Chapter 4 for all main series specimens.

In Sections 5.2.5 and 5.2.6 the influences of the various concrete constituent materials on this damage parameter were further investigated. The information was used to initiate the process of separating this complex aspect of the material response into component parts, assessing both the sequence of the failure processes and also the contributions of each of the constituent materials of the fibre concretes.

The plain mortar targets of Section 5.2.5 suffered insignificant front face damage, a burrow being formed from very close to the front surface of the impacted specimen. Little resistance to penetration was generated, the projectile cores not being stripped of their surrounding jackets.

The specimens comprising increasing thicknesses of mortar on a steel fibre concrete backing (Section 5.2.6) showed similar minor damage at the greatest thicknesses of mortar (75mm) but exhibited increasing front spall damage with decreasing mortar depth. In those cases where the stripped jacket of the projectile was found, it was removed only during contact with the fibrous concrete part of the target, the penetrator passing orthogonally through the mortar section. In a single case, the projectile was rendered sufficiently unstable to ricochet within the 50mm mortar facing of the target before reaching the concrete backing. A very large front crater was formed, with no burrow formation or sub-surface cracking. The intimation is that two very different front damage mechanisms were operating in these tests on mortar-faced fibre-reinforced concrete. In the first, a near reversal of the projectile occurs close to the surface of the target, that is a "ricochet" causing the already penetrated material to suffer further local disruption before being ejected, possibly both ahead of and around the projectile. Such a response generates a large, non-symmetrical front-face crater with no evidence of burrow formation.

The second mechanism, a consequence of deeper projectile penetration into the composite target, has a greater number of facets. It is apparent from earlier trials that the mortar presented little resistance to the projectile, hence the front face damage sustained was most likely generated by the impact on the underlying fibre concrete layer. This would explain the increasing damage occurring to targets having mortar layers of decreasing thickness; that is the first significant effects of the impact were closer to the mortar-air interface with targets having thin facings of

mortar than with the targets having thicker mortar components. As a corollary to this, the front face damage is not solely a response to the approach of the tensile wave front caused by the reflection of the initial compressive wave from the rear face of the target. If it was, then it would be reasonable to expect the greatest degree of attenuation for the targets with a mortar/concrete interface close to the impact face (ie the thinnest mortar layers), with possibly a corresponding reduction in damage; this was not the observed damage response. For specifically layered mortar/fibre concrete targets therefore, the immediate front face damage mechanism would appear to be a consequence of the impact into the more resistant underlying fibre concrete; a general hypothesis for the front face damage to concrete targets is given below.

In Chapter 4 a comparison of "actual crater volume", representing the quantity of target impact face damage, was carried out for plain and various fibre concretes. This indicated a reduction of up to 70% in front face spall volume, in a consistent manner, at percentages of up to 5.0% fibre content by concrete weight. At greater percentage fibre contents, the crater volume continued to reduce, but significantly greater variability of results was noted as a consequence of the increasing heterogeneity. The role of the fibres in decreasing the target front face damage will be discussed here.

In both plain and fibre-reinforced concretes the immediate post-impact "apparent" crater was typically of up to 50mm depth, with the angle formed by the side faces tending towards the obtuse, relative to the target front face, with depth. As shown in Figure 3.13, on the surface of this cratering, below the impact face of the target, though higher than the burrow initiation point, there normally existed a region of obvious cracking, developing from the central impact position and propagating outward and upward. The "true" crater assessed in this study was defined by positively removing the loose material down to these cracks, to locate

the limits of the local damage. This action tended to produce a crater of a characteristic type, with a steep sided inner section and a less steeply raked outer. The plan shape of this crater was not very predictable, rarely being symmetrical, as illustrated by Figures 5.25 to 5.27, for concrete targets. In general terms it was found that the less the percentage fibre content, the greater the overall plan area of the target front face damage; to the point were significant target heterogeneity was generated, when crater diameter was likely to reduce.

The steep sided "apparent" crater cross-section is thought to be formed by the immediate effects of the penetrator presence. Upon first penetrating, comminution will occur ahead of the projectile, whilst a radial pressure is exerted also. On any particular particle, this applied pressure will be resisted by the material directly behind it, thus setting up a tensile Poisson stress. Hence, a particle crack is initiated, and at the surface of the target this crack will tend to be parallel to the front face. However, as the penetration increases, some particles at the outer edges of the developing "apparent" crater will, as a consequence of higher adjacent particles not having been fully removed, have some small shear resistance. This is an accelerating effect, causing increased shear resistance with depth. Thus the angle of cracking will tend to steepen as the projectile penetrates, until the shearing resistance of the concrete is sufficient to permit the projectile to generate, by very localised comminution, a parallel burrow through the specimen. The stripping of the projectile jacket logically occurs at a point where the shear resistance of the immediate crater zone becomes more significant than the bond strength of the projectile components.

The often reported crack-resisting capabilities of high modulus fibres is thought to have an influence on the higher part of the crater zone, controlling the progress of the sub-surface cracking. Considering a

sub-surface crack position propagating from a depth of 35mm into the crater zone;

Time for initial stress wave to reflect with the rear target/air interface and reach the sub-surface cracking propagation point. = $\frac{125mm + (125-35)mm}{3.5mm/\mu s}$ = 61μs

From the deceleration tests (Section 5.2.9), a mean velocity of 670m/s has been assumed over the first 50mm of penetration. In 61μs, the projectile would travel some 41mm into the concrete by the time of the return of the initial compressive stress wave as a tensile front. As a result of the projectile passage, material would already have been accelerated locally into motion by the "shearing" action discussed earlier. This means that an effective concrete-air interface, within the depth of the target, would exist. Assuming the ultimate dynamic tensile strength of the concrete to be locally exceeded, the correct conditions were present to cause cracking to develop. Such cracking manifests as an uplifting action, the angle of the cracking being shallow relative to the target impact face. The width of the outward and upward fracturing reducing with increasing radius from the crater centre. That is, the cracking is a consequence of an uplifting action, hinged at the extreme edge of the "true" crater.

At levels of fibre concentration sufficiently high to produce a vastly heterogeneous voided target, front face damage continued to decrease with increasing fibre content. It is feasible that such greatly voided composites had little integrity and thus provided very significant damping of the internal stress wave transmission, greatly reducing its damage capability, whilst providing less than usual resistance to penetration.

It is of interest to note that rendering the projectile unstable within the target has, for various materials, been shown to be the most effective means of reducing penetration. Hence, the removal of loosened material to locate the "true" crater boundaries could be considered detrimental to the continued success of the target against further attack.

That is, the very presence of areas of varying density and stability may possibly cause a significant, though unpredictable, level of projectile instability to occur in any subsequent attack. Whilst this may be true in practice; in the interests of consistency, and to provide the limits for safety, it was considered prudent to remove the loosened material to assess the consequences of single shot tests.

5.3.6 Summary of Failure Mechanisms in Concrete Targets

The various facets of the event may be tentatively ordered on the basis of the results obtained in the tests reported earlier in this chapter.

On energising the electrical firing system, the 7.62mm A.P. projectile will be propelled from the barrel with a concentric spin induced by the rifling. Some 25ms or so later, having travelled a distance of 20m, the projectile will impact the target. The missile velocity at 18m flight length measured an average 808m/s.

A compressive wave front will be established at the impact, radiating into a 125mm thick target at a velocity of 3.5mm/μs. Some 36μs later this front will reach the rear concrete-air interface and be reflected as a tensile stress wave. This stress reversal will then continue to occur, at a diminishing rate, throughout the event. Notwithstanding this, the wave front interface will locally change position during the overall event, coming ever closer to the rear face as the crater develops.

Within approximately 20mm of target penetration, in a period of some 30μs or so, the projectile will have decelerated to around 670 m/s.

Some 45μs or so later, certainly within 90μs of the first impact, a fine powder debris will be ejected as a hollow cone around the edge of the projectile burrow. This is likely to be loosened and comminuted material accelerated into motion by the tensile wave front passing toward the impacted face of the target. By the time that the reflected wave has reached the target front surface the missile will have penetrated a further

30mm or so, to a total depth of say 50mm. During this period, it is probable that the "uplifting" of larger pieces of the target, within the eventual "true" crater area, will also have begun as a consequence of the same tensile front acting in the area of the developing (and subsequently destroyed) burrow being formed by penetrator passage. This phenomenon will manifest itself as diagonal cracking radiating from slightly above the eventually exposed burrow.

The quantity of fine debris leaving the target will increase with time as a result of the propagation of a circumferential surface movement at a velocity of about 39m/s, starting between 90μs and 180μs after first impact.

Within the first 90μs of impact, corresponding to approximately 50mm depth of projectile penetration, changes will have occurred to the missile. Assuming it has impinged upon a coarse aggregate inclusion it will have shed its gilding metal jacket, with little consequent loss of velocity. Following this it is most likely that the hardened steel core will begin to deviate, in three dimensions, at an increasing rate from the orthogonal path it has held until this point. The increasing rate of angular deviation may or may not be associated with a corresponding increase in the rate of projectile deceleration; however, the projectile is likely to come to rest within the target, in most cases.

The spall product motion will be continuing throughout the above-described projectile deceleration and subsequent halt. However, its velocity will be reducing with elapsed time. Measured values were 100m/s over the initial 800μs or so of motion, reducing to 39m/s over the next 700μs. By this point, some 1600-1700μs after impact, all of the reported experimental methods had either failed or become unacceptably inconsistent. It is, however, probable that spall product motion will continue until the attenuating stress field can no longer overcome the material inertia.

It should be recognised that the above is no more than an approximate scenario of events. Until significantly more trials are performed this assessment should be considered as nothing more than a very tentative hypothesis. It should be used only to define the most useful potential areas for further experimentation and perhaps the appropriate time intervals for these areas.

Specimen	Estimated Average Velocity (m/s)			
	Circumferential Propagation		Spall Product	
	Upper Section	Lower Section	Upper Section	Lower Section
RP1	25.3(f4-f9*) 27.5(f11-f16)	42.9(f4- f9) 34.1(f11-f16)	95.2(f4-f10) 46.2(f11-f16)	130 (f4-f10) --
RP2	56.2(f4-f10) 33.7(f11-f19)	73.0(f4-f10) --	102.1(f4-f10) 31.6(f11-f19)	101.2(f4-f10) --
RP3	27.5(f3- f8)	33.0(f3- f5)	--	119 (f3- f9)
Plasticine	18.5(f2- f6)	22.7(f2- f6)	121.2(f2- f5)	198.9(f2- f4)

* Figures in brackets indicate frame numbers over which velocities were assessed.

Table 5.1 Estimated average velocities for circumferential material movement on the target surface and spall product front.

		Component	
		Mortar	Fibre Content
Mix Design (ratio by weight)	OPC	1.0	1.0
	Free Water	0.55	0.55
	10mm single size limestone	-	3.0
	Zone 2 limestone sand	3.0	3.0
% melt extract fibre by concrete wt.		-	6.7
Aggregate	limestone	-	1.1
m/c (% dry mass)	sand	5.5	5.2

Table 5.2 Details of mixes for mortar/fibre concrete composite targets.

Specimen Number	Entry Crater True Volume ($mm^3 \times 10^3$)	Penetration Path Length (mm)	Remarks
1A	86.7	177	Perforation
2A	122.6	73	
3A	64.6	137	Perforation
1B	172.7	33	Ricochet
2B	38.9	131	Perforation
3B	92.8	114	
1C	34.0	106	Fractured core
2C	14.3	132	Perforation
3C	33.8	131	Perforation

a) Individual test results

Specimen Type	Mortar Thickness (mm)	Fibre Concrete Thickness (mm)	Mean True Crater Volume ($mm^3 \times 10^3$)	Mean Penetration Path Length (mm)
A	25	100	91.3	129
B	50	75	101.4	122*
C	75	50	27.4	123

* Specimen 1B ignored

b) Summary of results

Table 5.3 Results of impact tests on mortar/fibre concrete composite targets.

		Component		
		Mortar	Plain Concrete	Fibre Concrete
Mix Design (ratio by weight)	OPC	1.0	1.0	1.0
	Free Water	0.5	0.5	0.5
	10mm single size river gravel	-	1.33	1.33
	Zone 2 limestone sand	3.0	2.67	2.67
% melt extract fibre (25mm x $\overline{0.3}$mmø) by concrete weight		-	-	2.5
Aggregate m/c (% dry mass)	river gravel	1.79	1.79	1.79
	sand	1.80	1.80	1.80
Compressive Strength (N/mm²)		41.5	41.9	43.3
Density (kg/m³)		2226	2307	2345

Table 5.4 Details of mixes and material properties for mortar/plain concrete/fibre concrete composite targets.

Specimen Number	Age at testing (days)	Penetration Path Length (mm)	Mean Penetration Path Length (mm)	Depth into Second Material (mm)
PC/FC/1	9/7	110	)	47
PC/FC/2	9/7	37	) 63	0
PC/FC/3	9/7	41	)	0
M/FC/1	8/7	75	)	13
M/FC/2	8/7	108	) 87	45
M/FC/3	8/7	83	)	20
M/PC/1	7/8	75	)	13
M/PC/2	7/8	102	) 94	0
M/PC/3	7/8	106	)	42

Table 5.5 Summary of results of impact test on mortar (M)/plain concrete (PC)/fibre concrete (FC) composite targets.

Detector Step	Specimen number											
	V1			V2			V3			V4		
	Detector Spacing (mm)	Time Step (μs)	Mean Velocity (m/s)	Detector Spacing (mm)	Time Step (μs)	Mean Velocity (m/s)	Detector Spacing (mm)	Time Step (μs)	Mean Velocity (m/s)	Detector Spacing (mm)	Time Step (μs)	Mean Velocity (m/s)
1*- 2	20	550	36	40	450	89	21	31.6	665	13	18.5	702
2 - 3	35	1000	35	15	350	43	24	35.4	678	37	58.7	630
3 - 4	12	Detector 4 not punctured		20	Detector 4 not punctured		24	77.2	311	13	22.0	591
4 - 5	27			22			23	results not available		40	Detector 5 not punctured	
5 - 6	30			29			23			15		

* Detector 1 is the impact face for V1 and V2 and 13mm and 9mm below the surface for V3 and V4 respectively.

Table 5.6 Spacing of detectors and computed velocities in projectile deceleration tests.

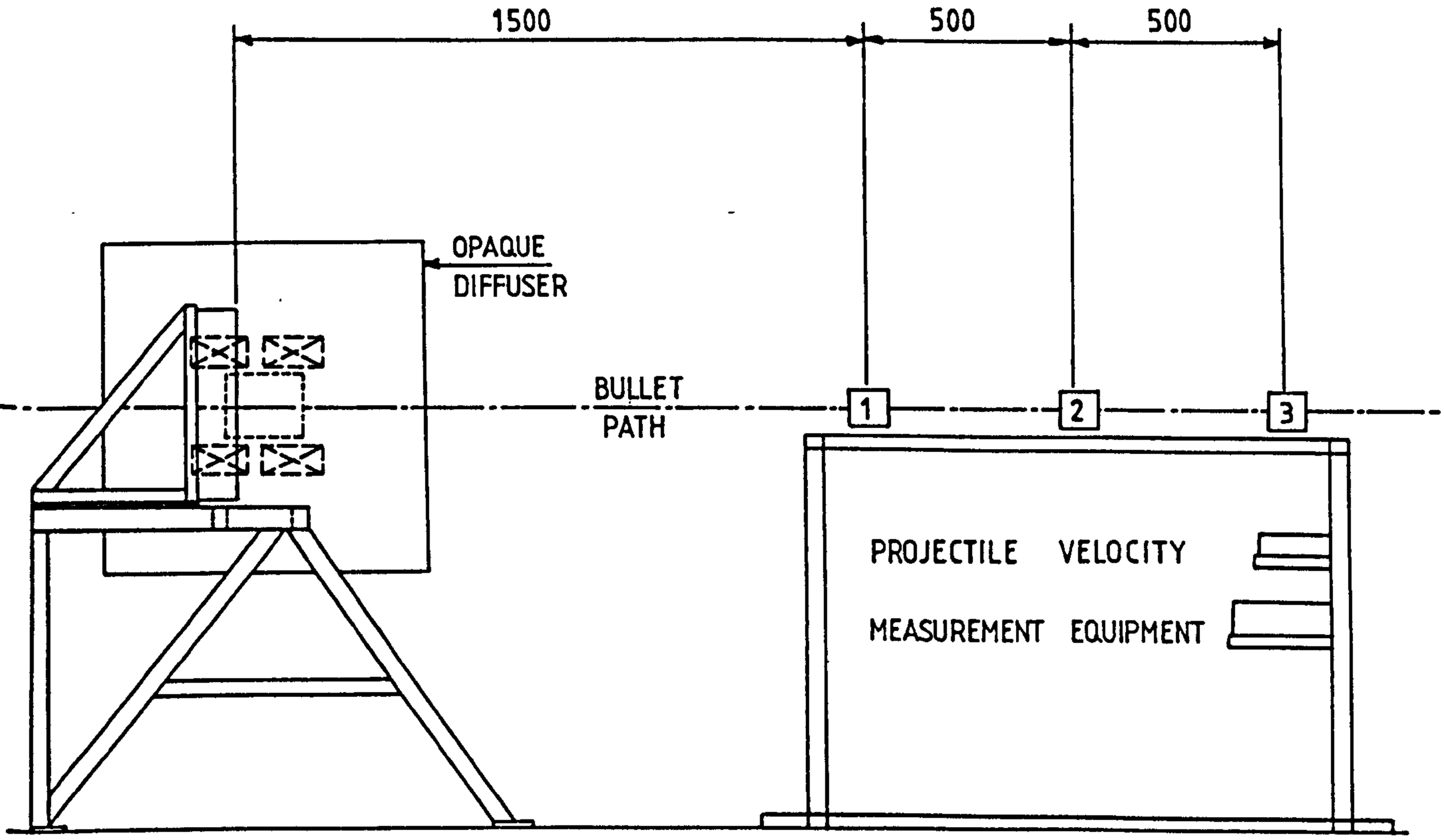

Figure 5.1 General Arrangement of Illumination for High Speed Rotating Prism Camera Tests. View From Camera. (Camera "window" shown dotted)

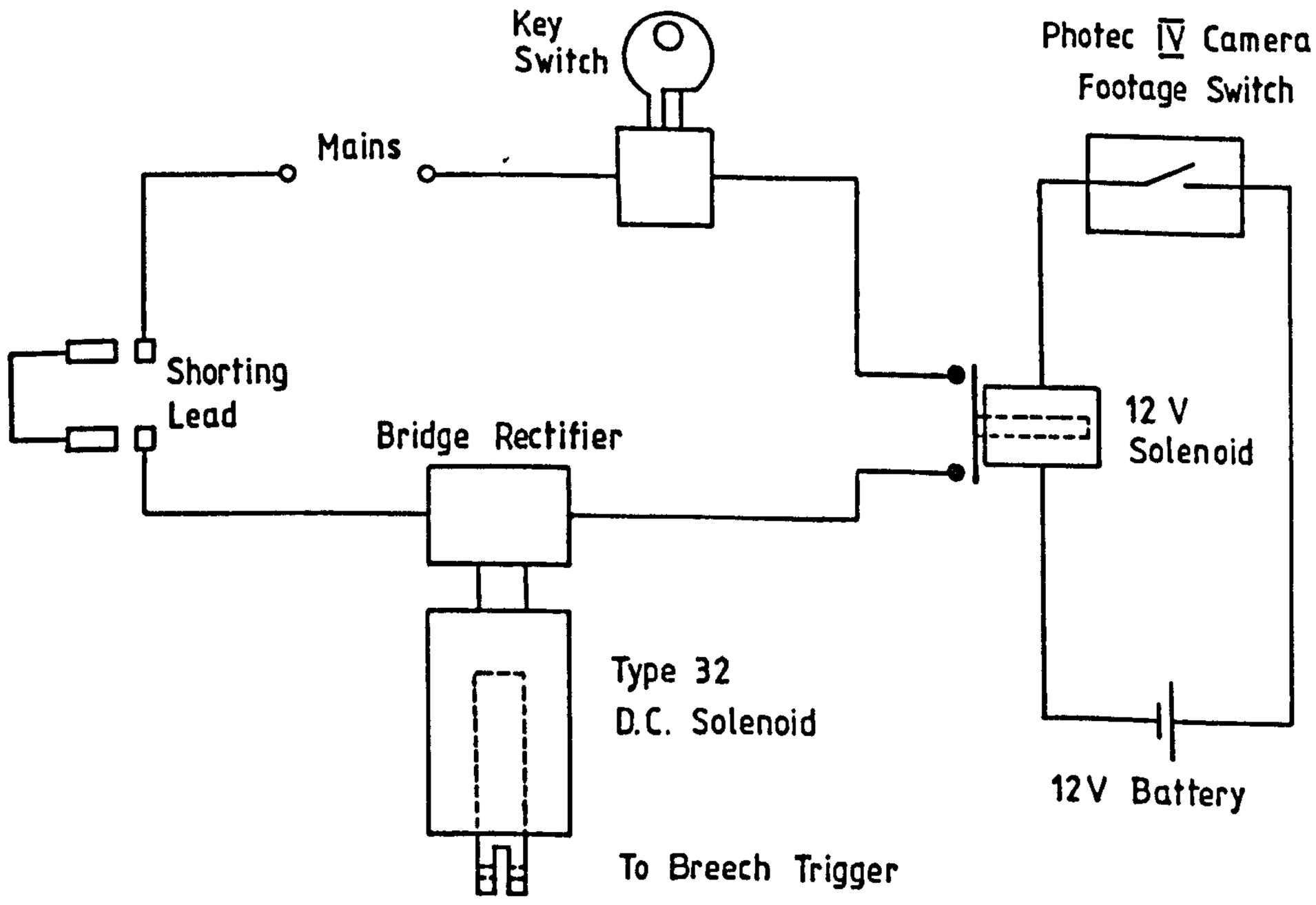

Figure 5.2 Firing Initiation System Used for High Speed Rotating Prism Camera Tests

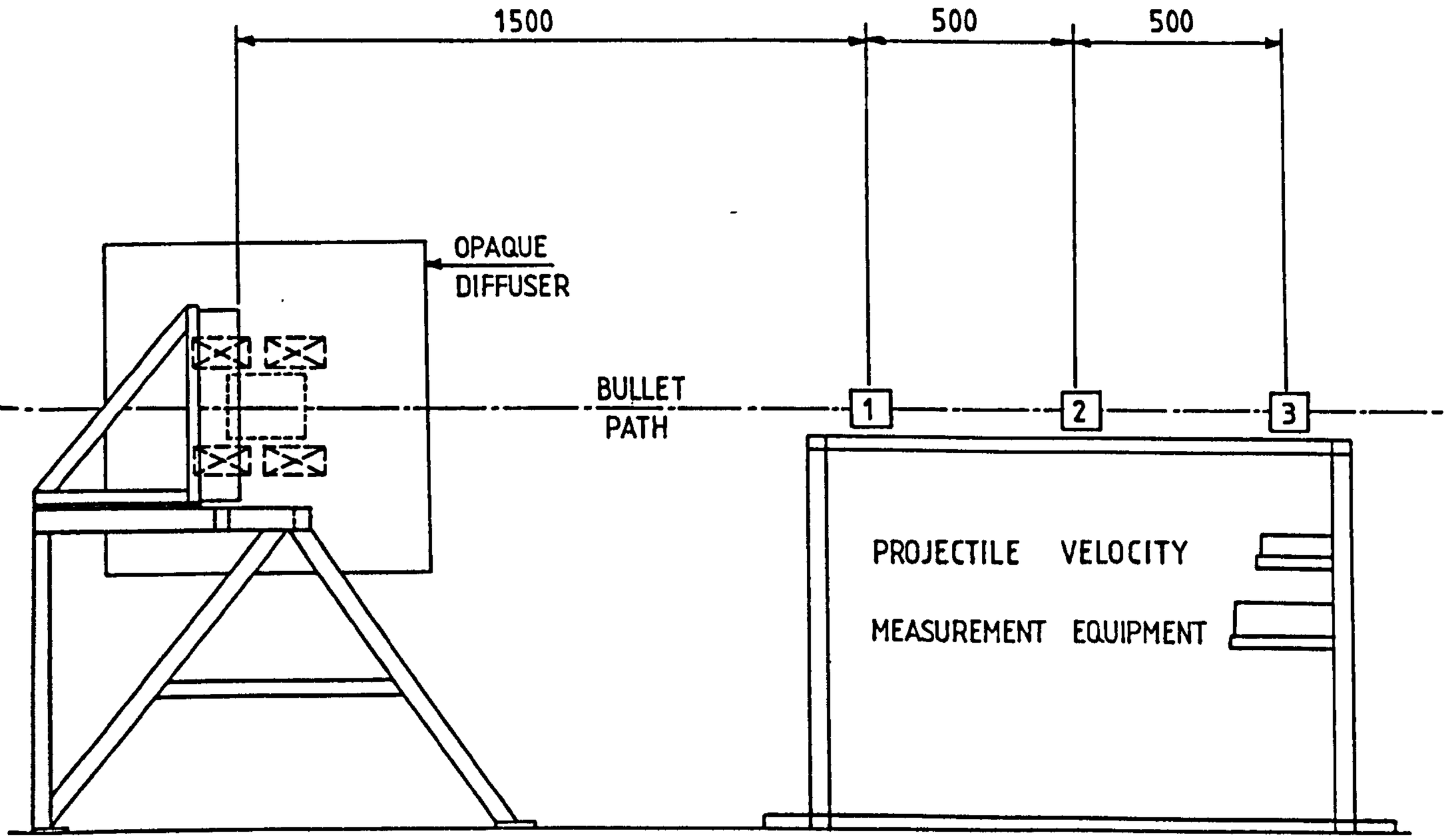

Figure 5.1 General Arrangement of Illumination for High Speed Rotating Prism Camera Tests. View From Camera. (Camera "window" shown dotted)

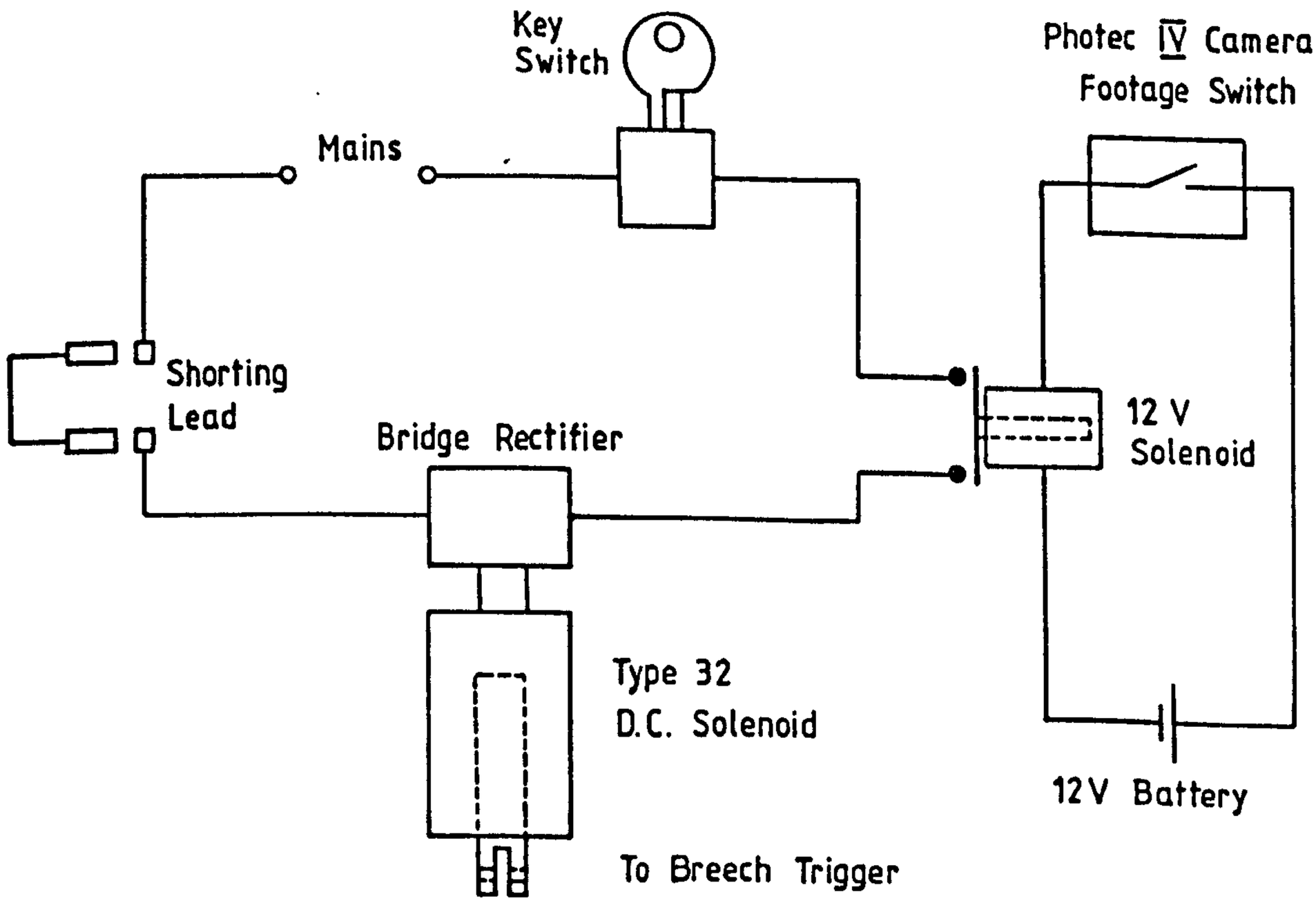

Figure 5.2 Firing Initiation System Used for High Speed Rotating Prism Camera Tests

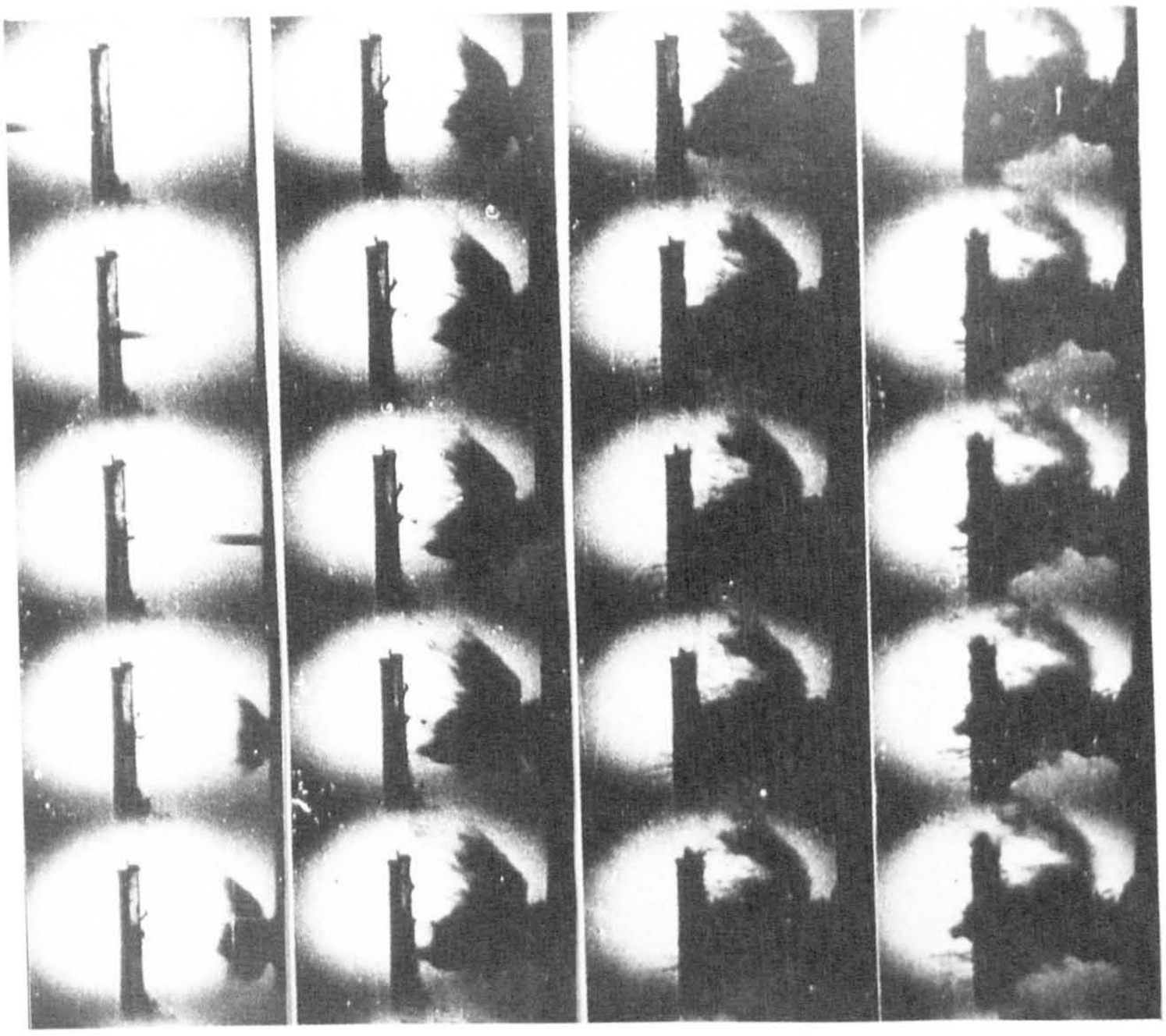

Figure 5.3 Typical photographic sequence obtained from High Speed Rotating Prism Camera tests (Interframe time = 91μs - Test RP1)

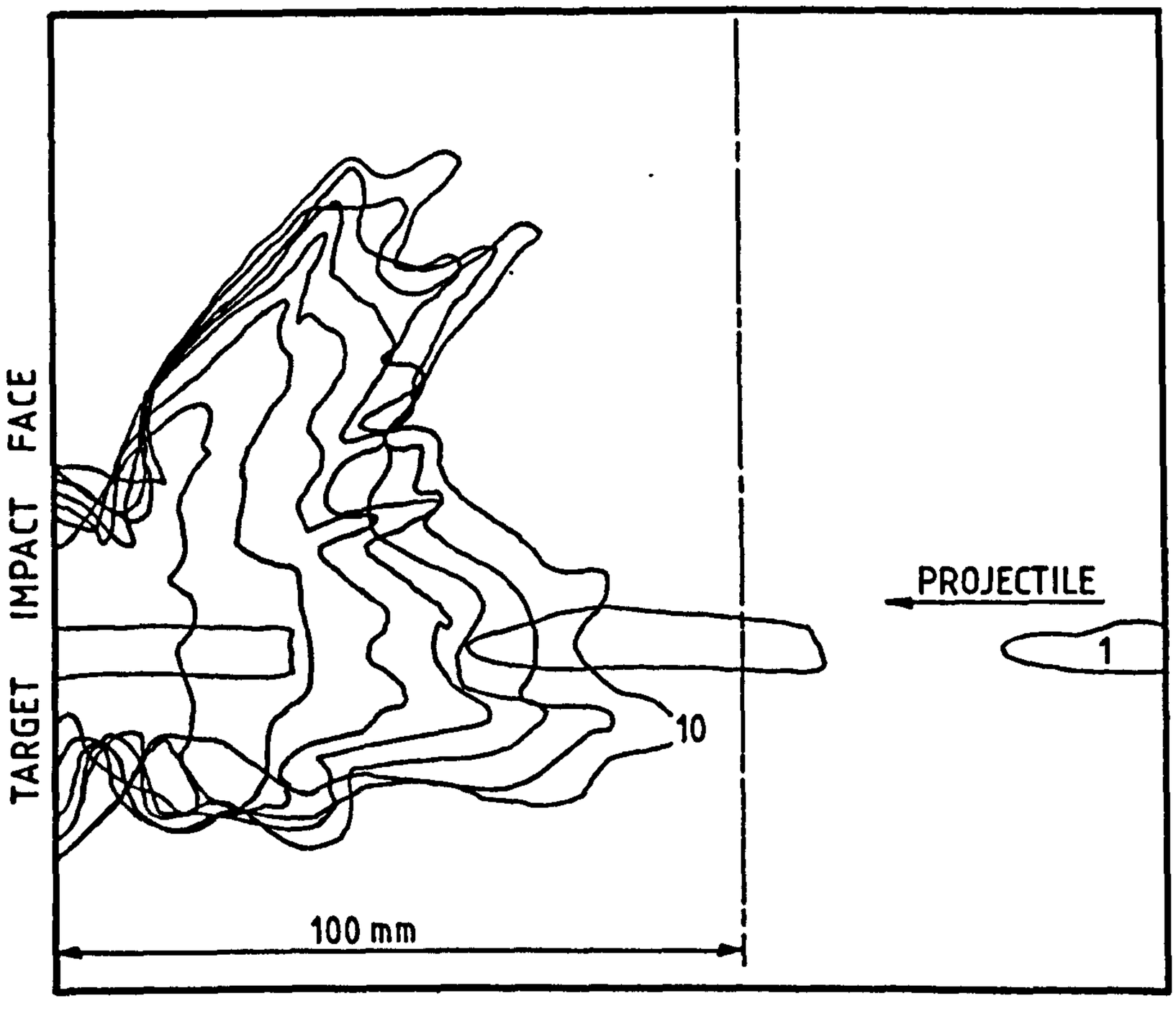

Figure 5.4 "Contours" Produced for Specimen RP1 showing Material Motion - Frames 1 to 10 (Interframe time 91μs)

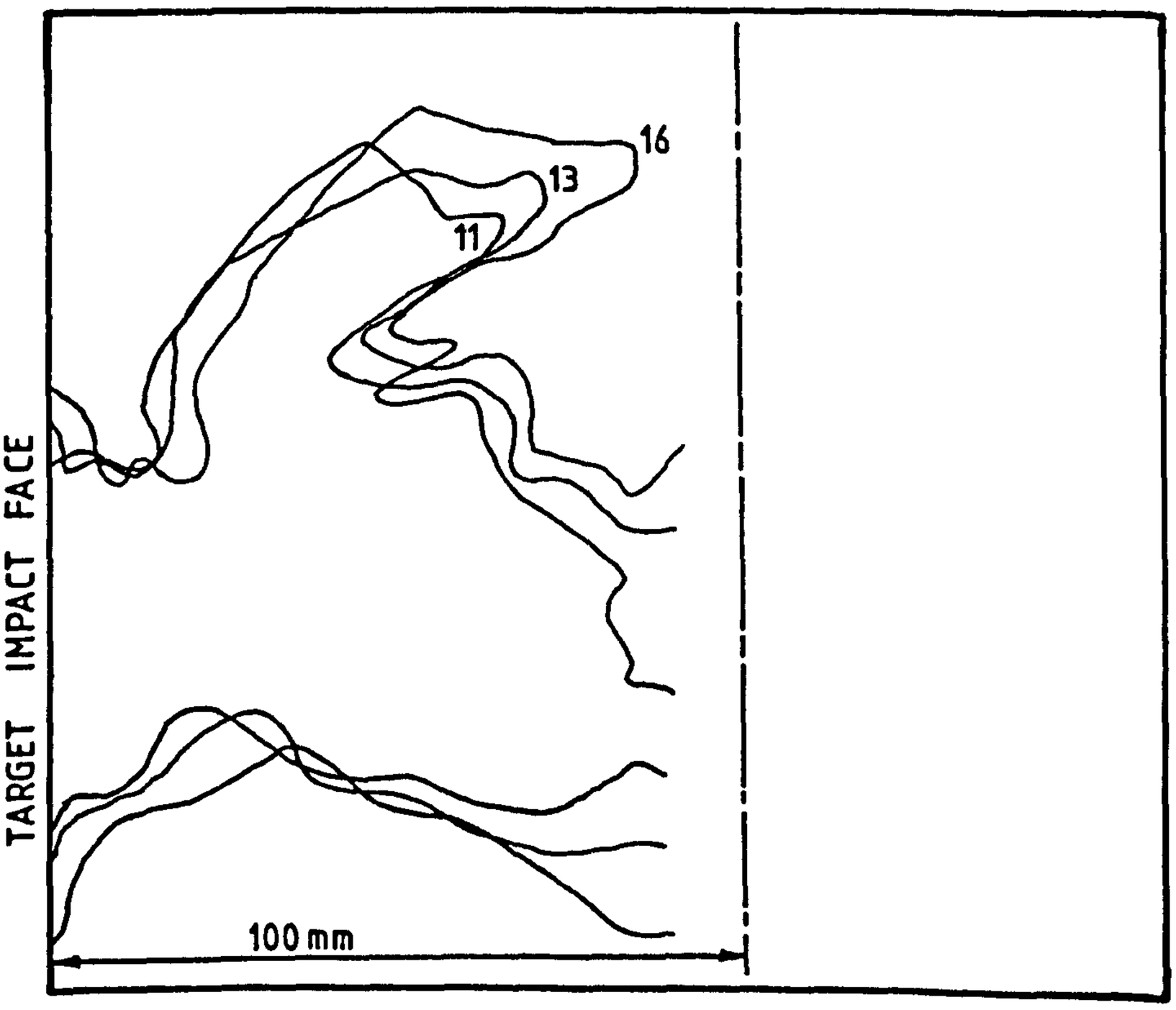

Figure 5.5 "Contours" Produced for Specimen RP1 Showing Material Motion - Frames 11 to 16 (Interframe time 91μs)

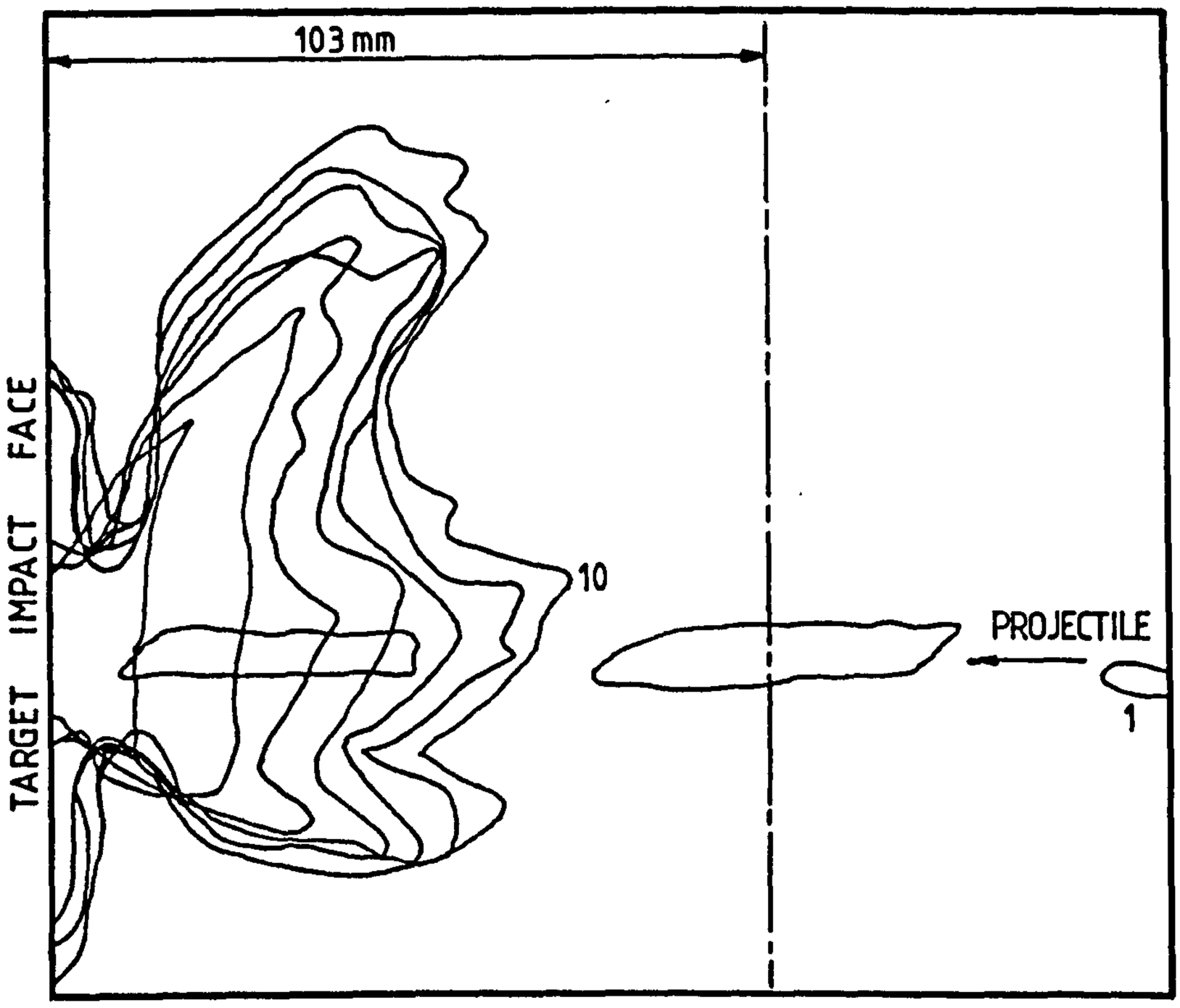

Figure 5.6 "Contours" Produced for Specimen RP2 Showing Material Motion - Frames 1 to 10 (Interframe time 78μs)

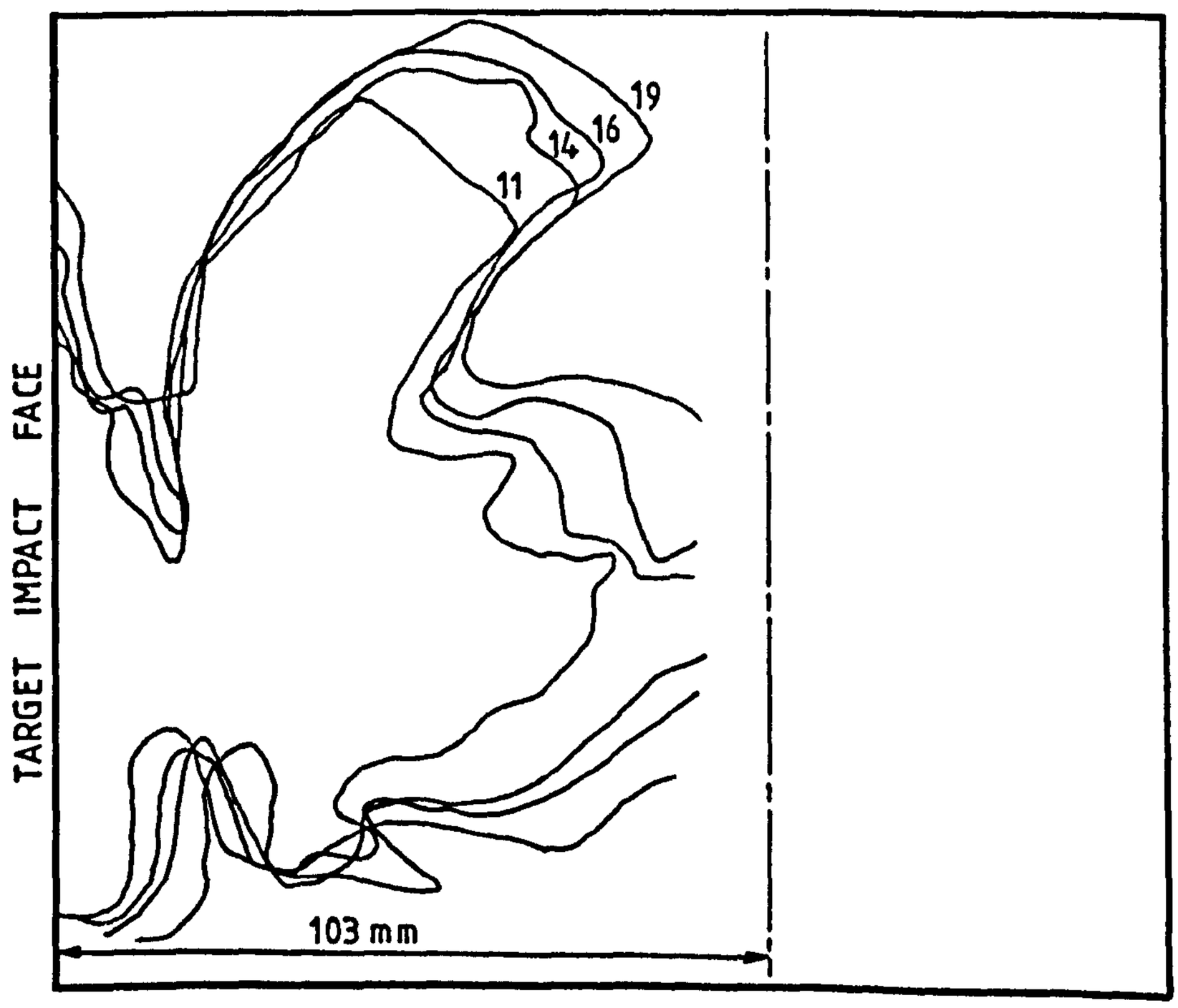

Figure 5.7 "Contours" Produced for Specimen RP2 showing Material Motion - Frames 11 to 19 (Interframe time 78μs)

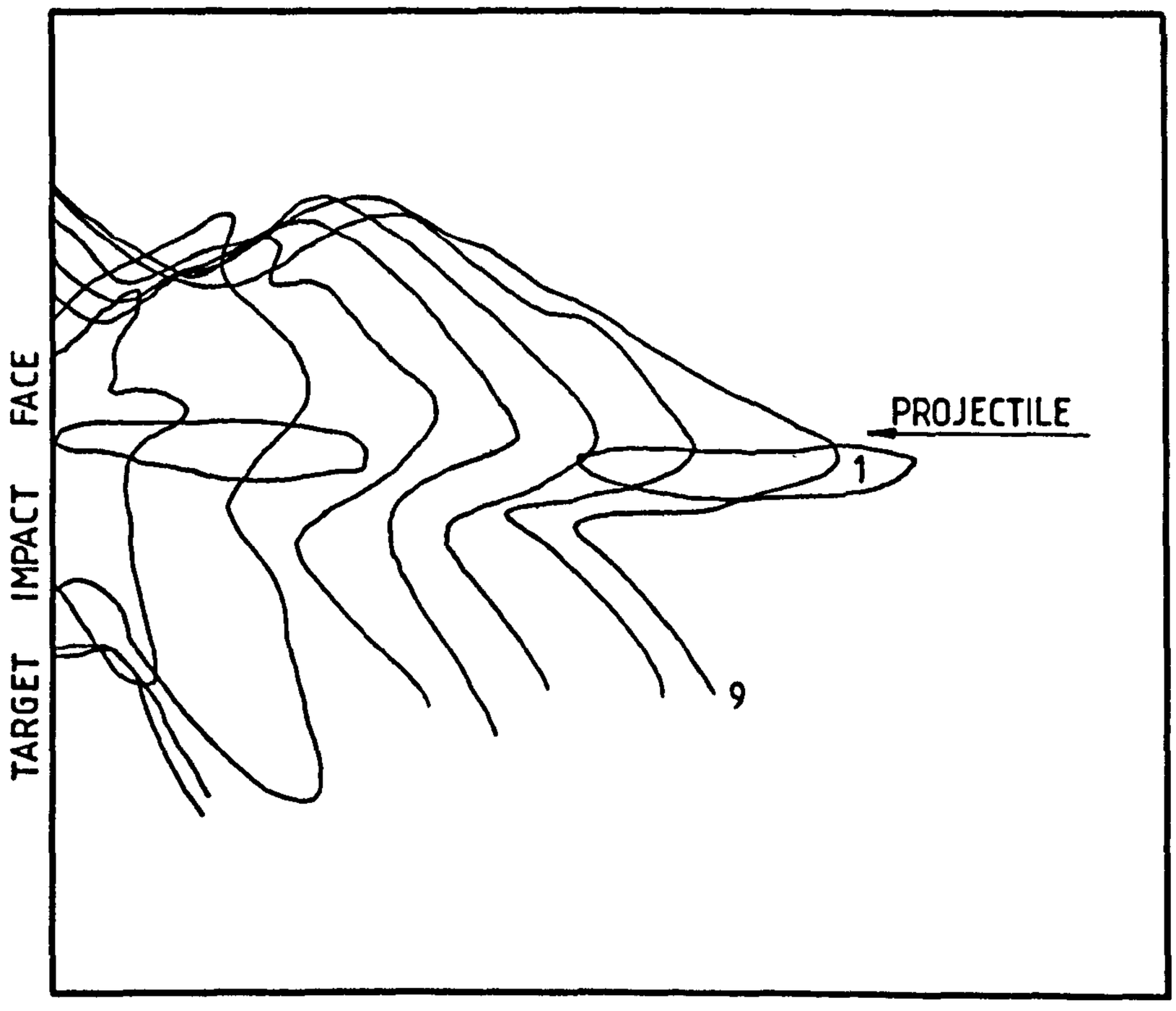

Figure 5.8 "Contours" Produced for Specimen RP3 Showing Material Motion - Frames 1 to 9 (Interframe time 92μs)

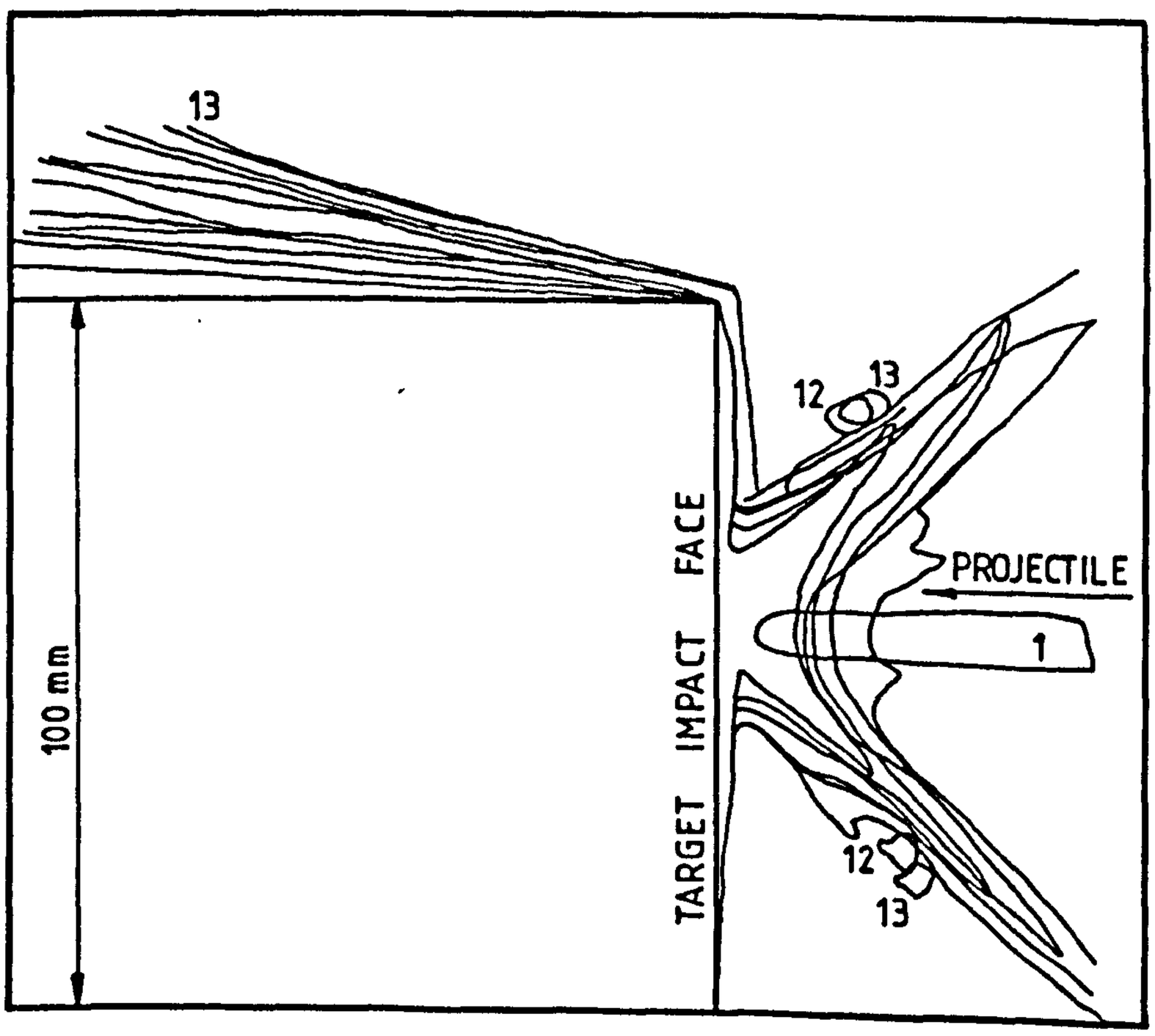

Figure 5.9 "Contours" Produced for Plasticine Specimen Showing Material Motion - Frames 1 to 13 (Interframe time 88μs)

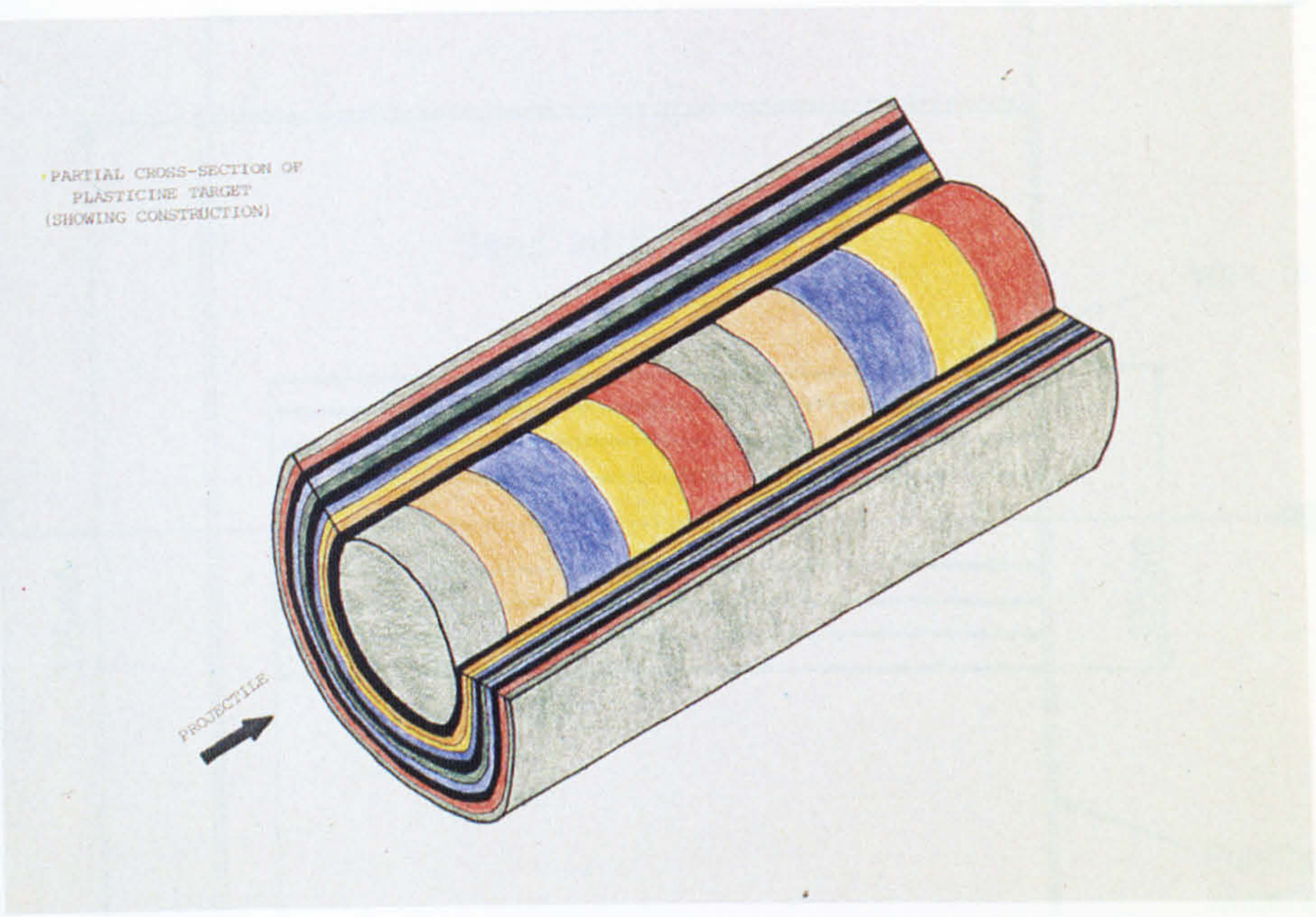

Figure 5.12 Cut-away section of Plasticine Target

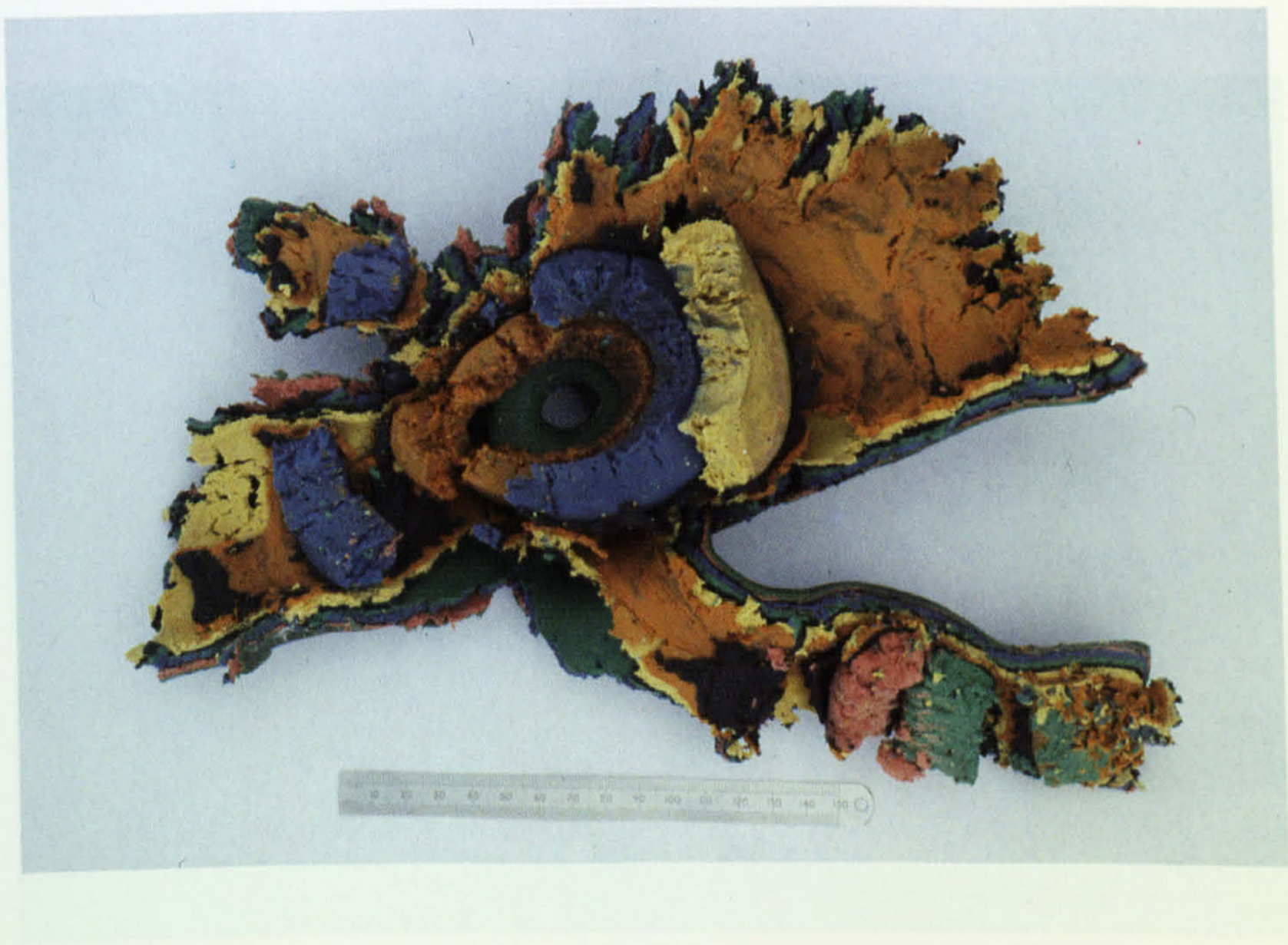

Figure 5.13 Plasticine Target after impact

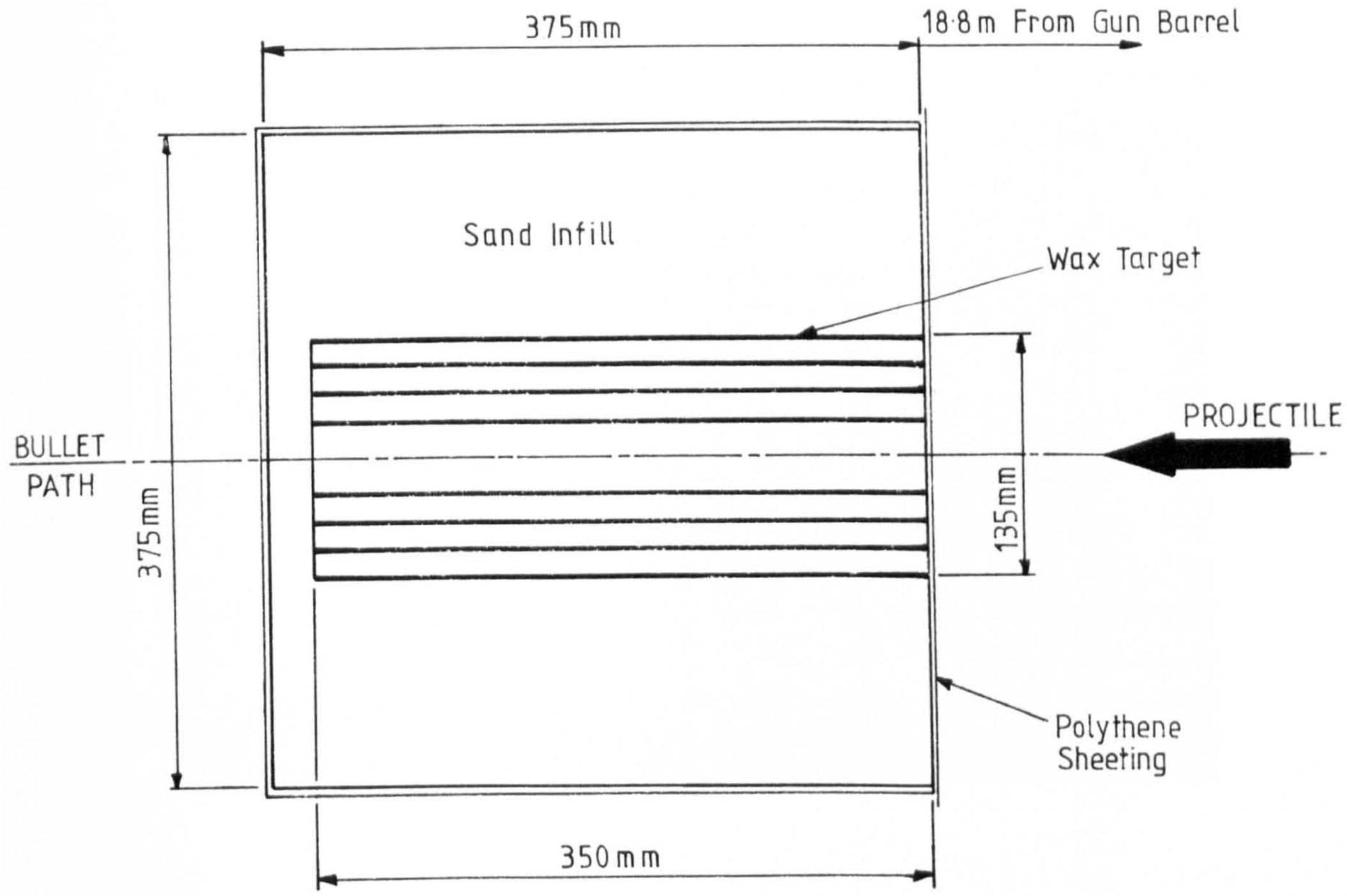

Figure 5.14 Section through Wax Specimen within Timber Target Holder

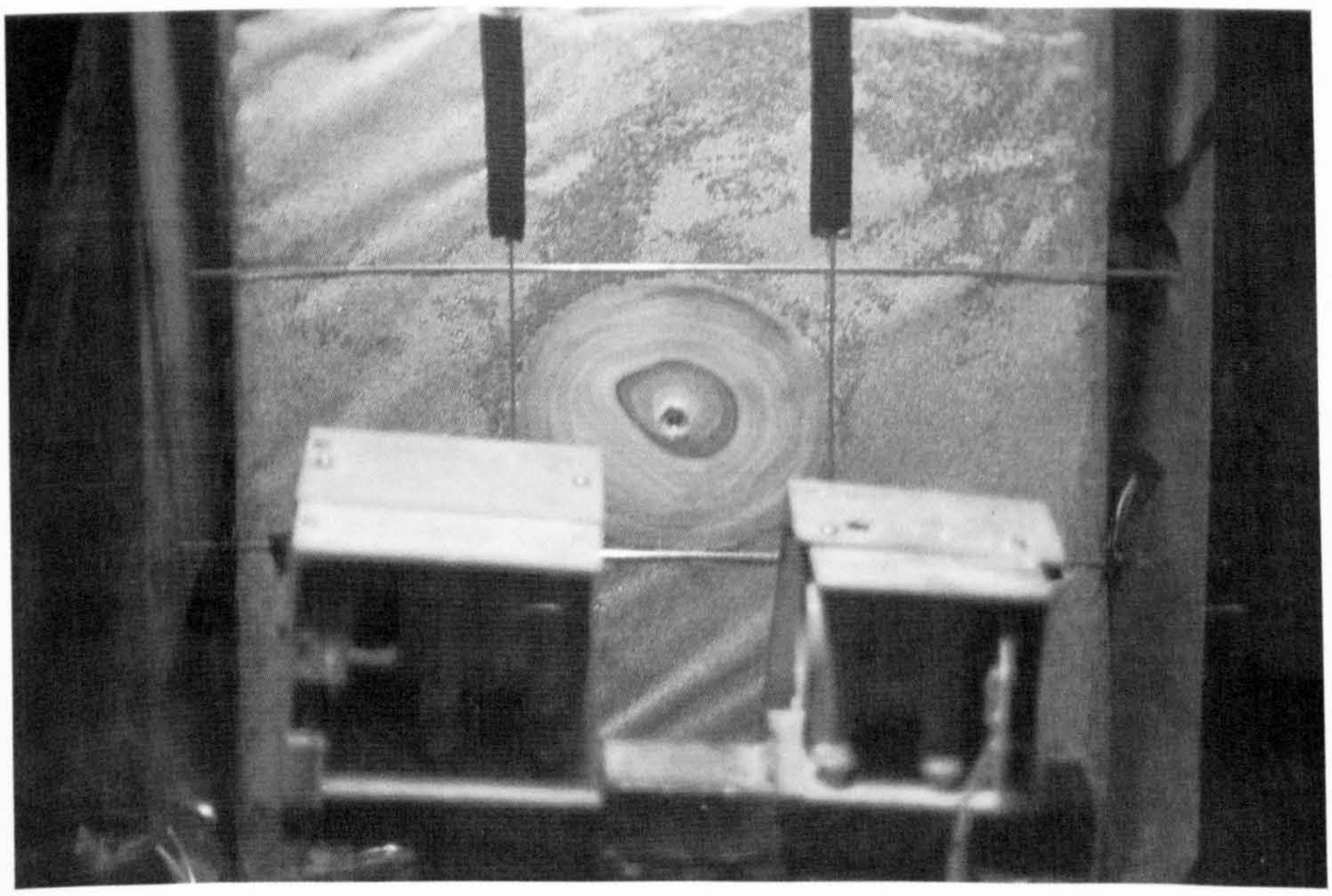

Figure 5.15 Wax Specimen Sectioning - Initial Stage

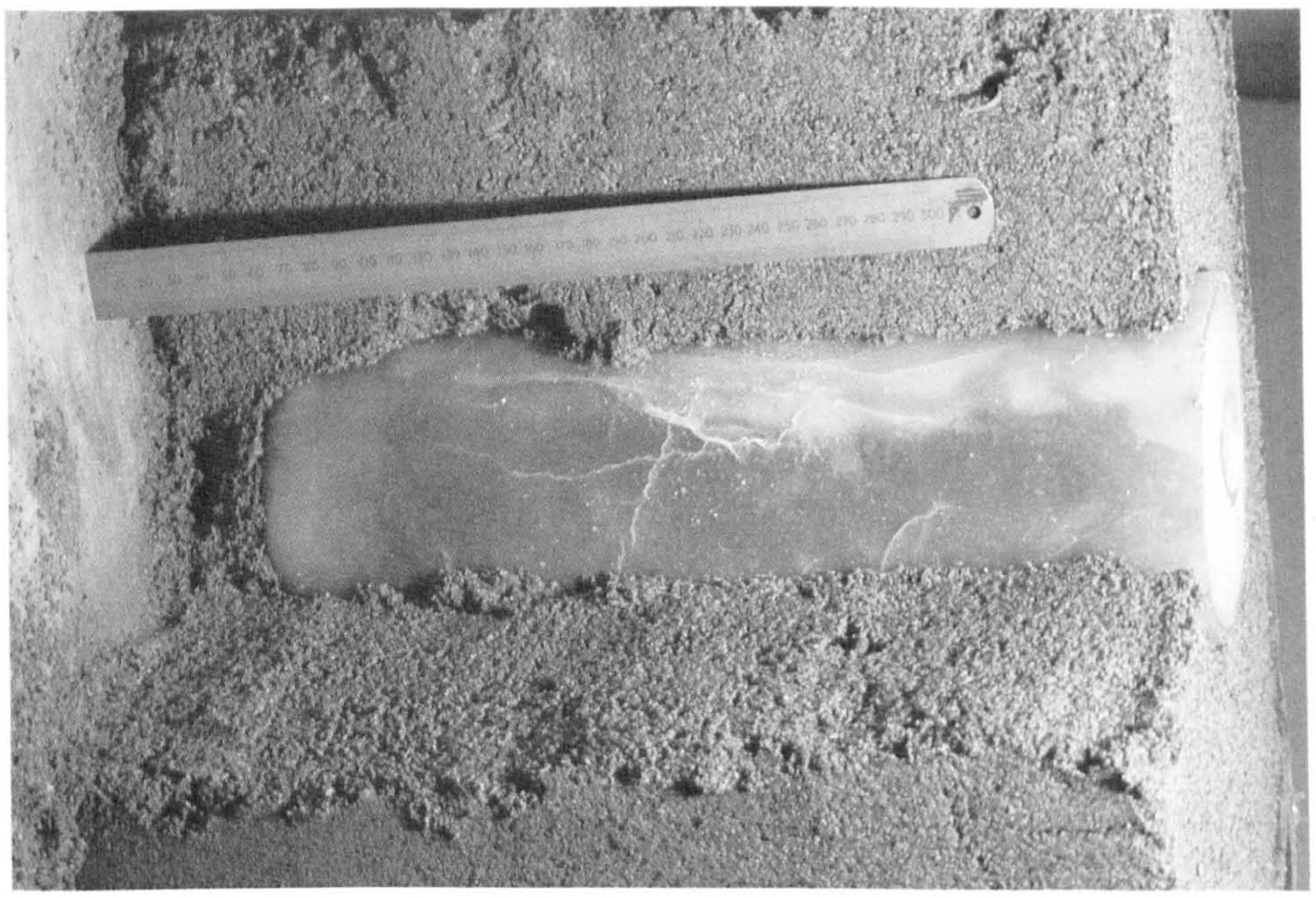

Figure 5.16 Wax specimen sectioning - second stage

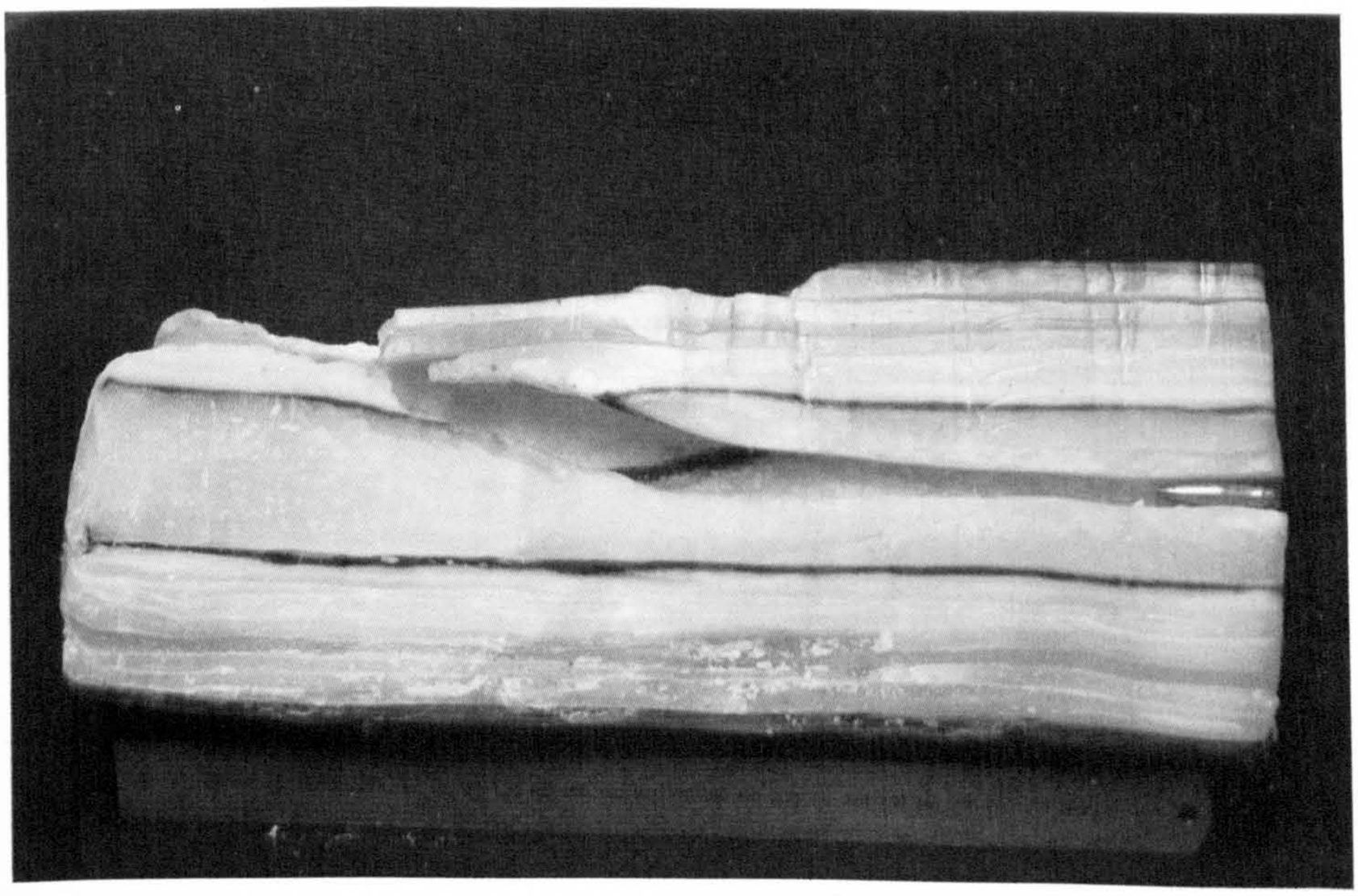

Figure 5.17 Wax specimen sectioning - final stage

Figure 5.18 Projectile after penetration of mortar target

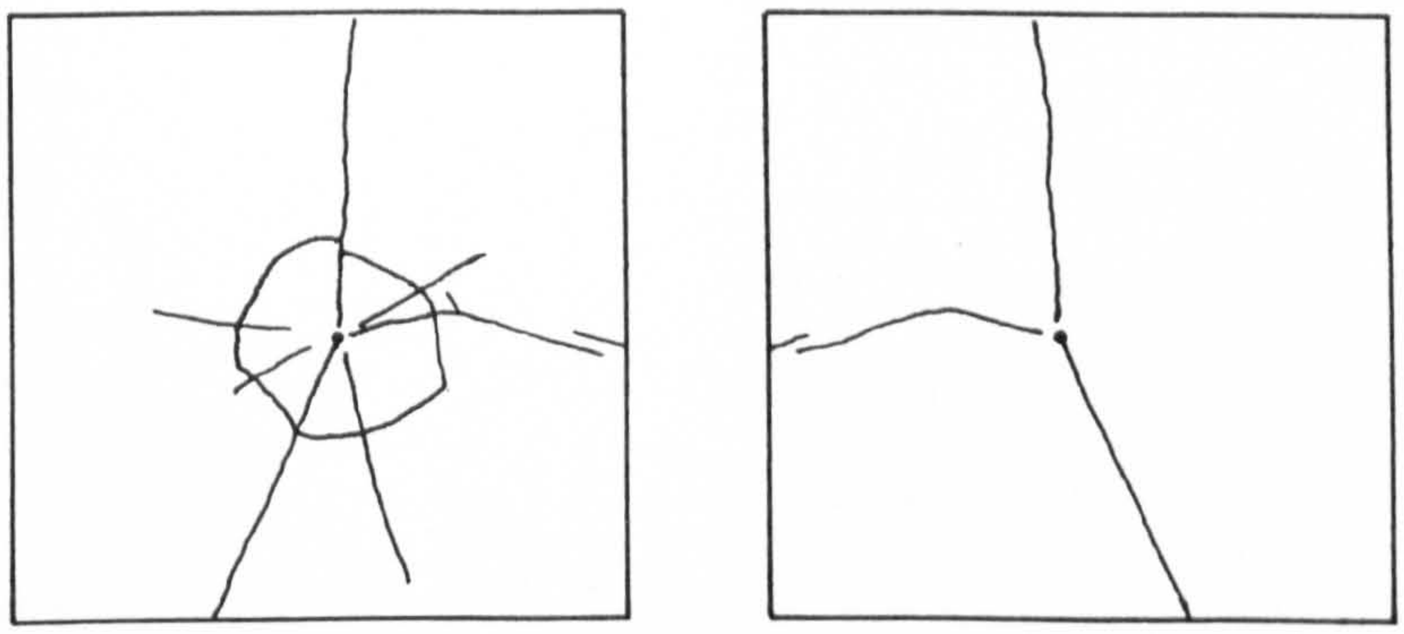

Figure 5.19 Sketches showing post-impact damage M/FC/1

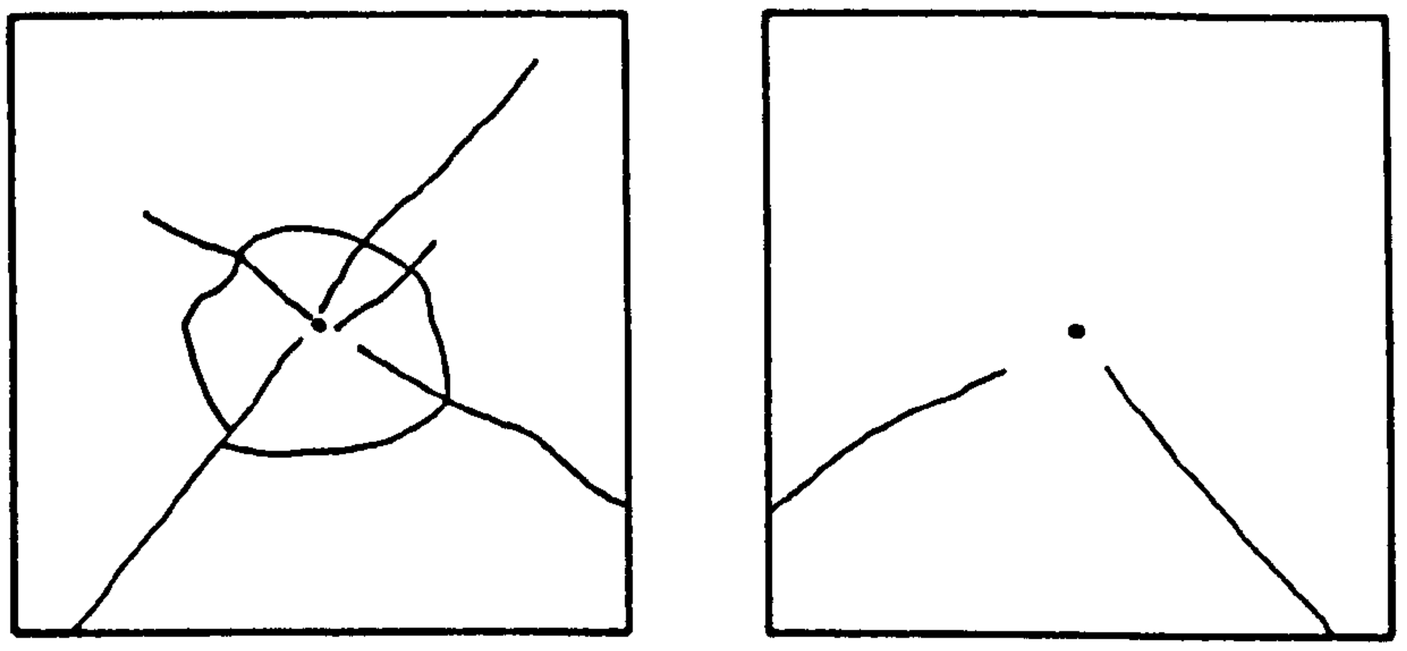

Figure 5.20 Sketches Showing Post-Impact Damage M/FC/2

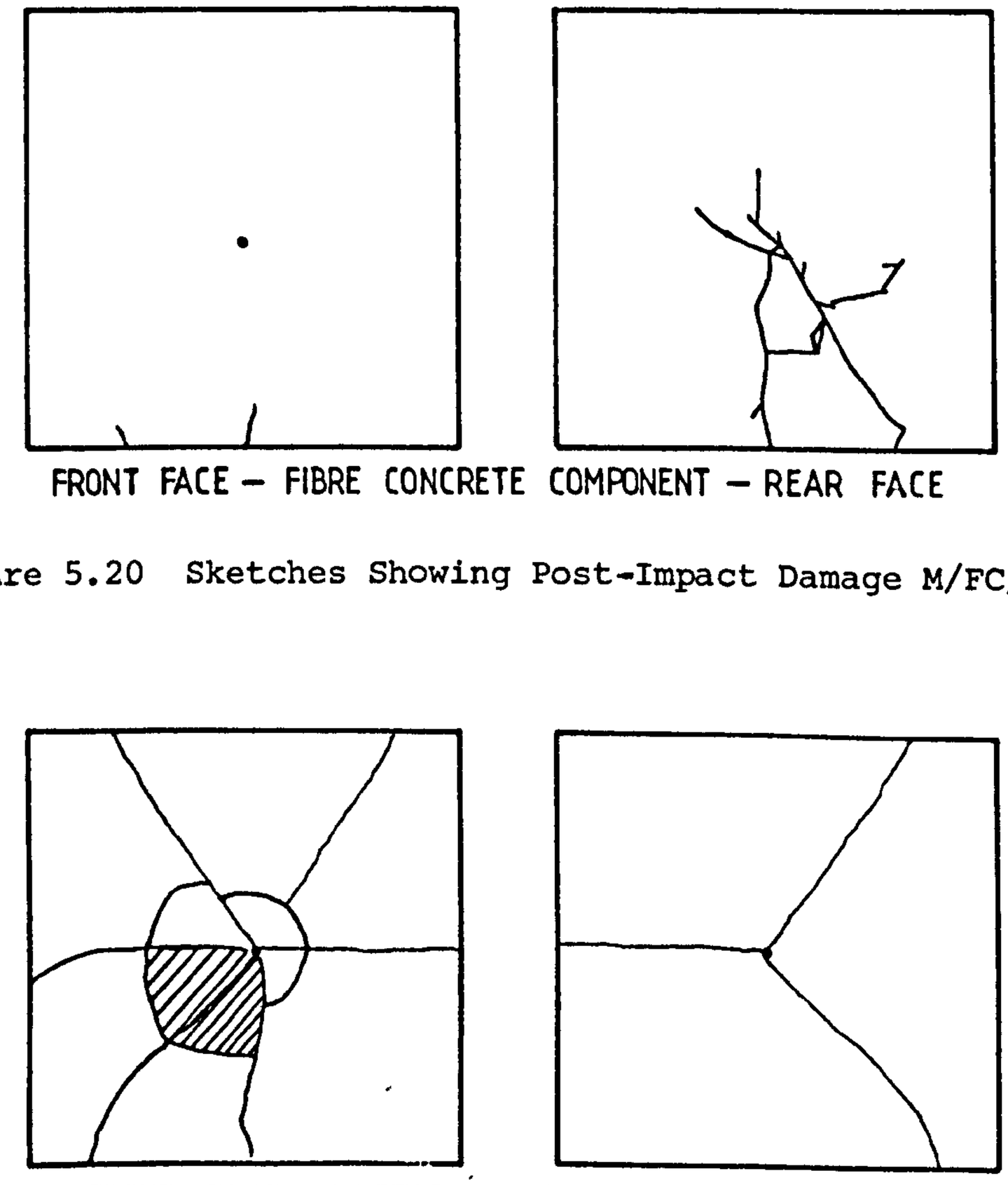

Figure 5.21 Sketches Showing Post-Impact Damage M/FC/3

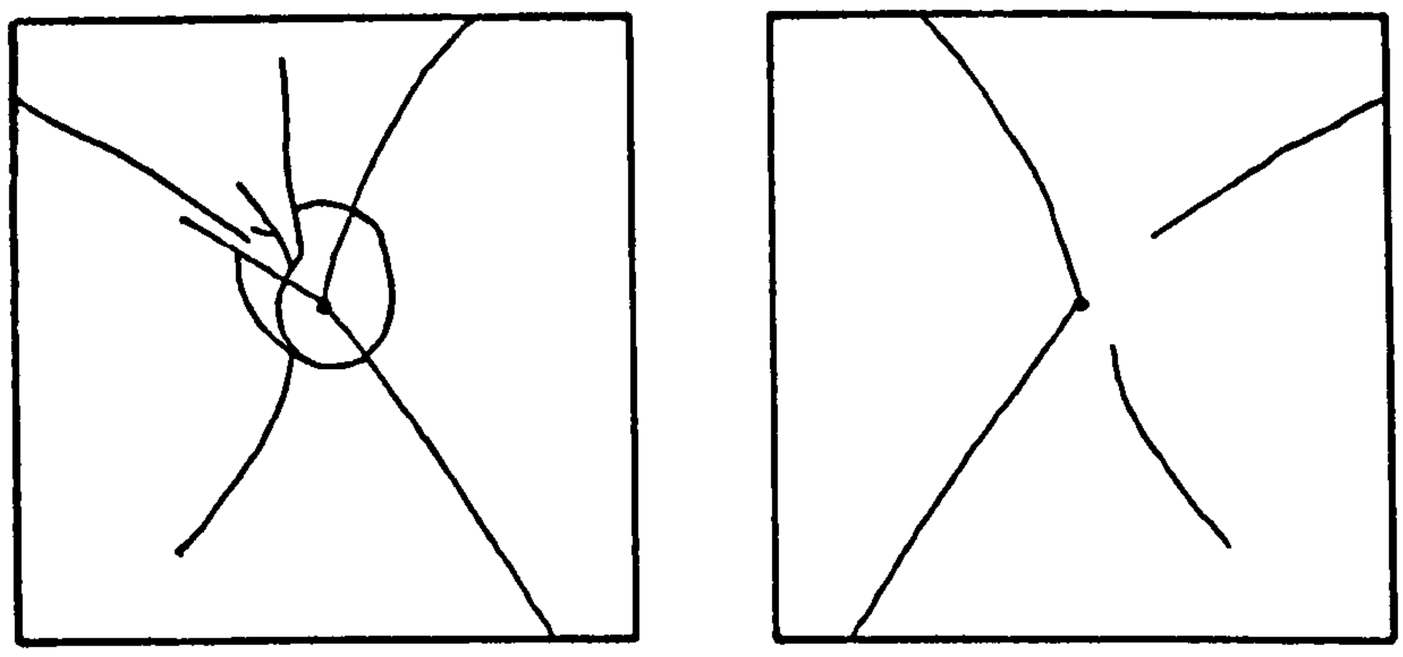

FRONT FACE – MORTAR COMPONENT – REAR FACE

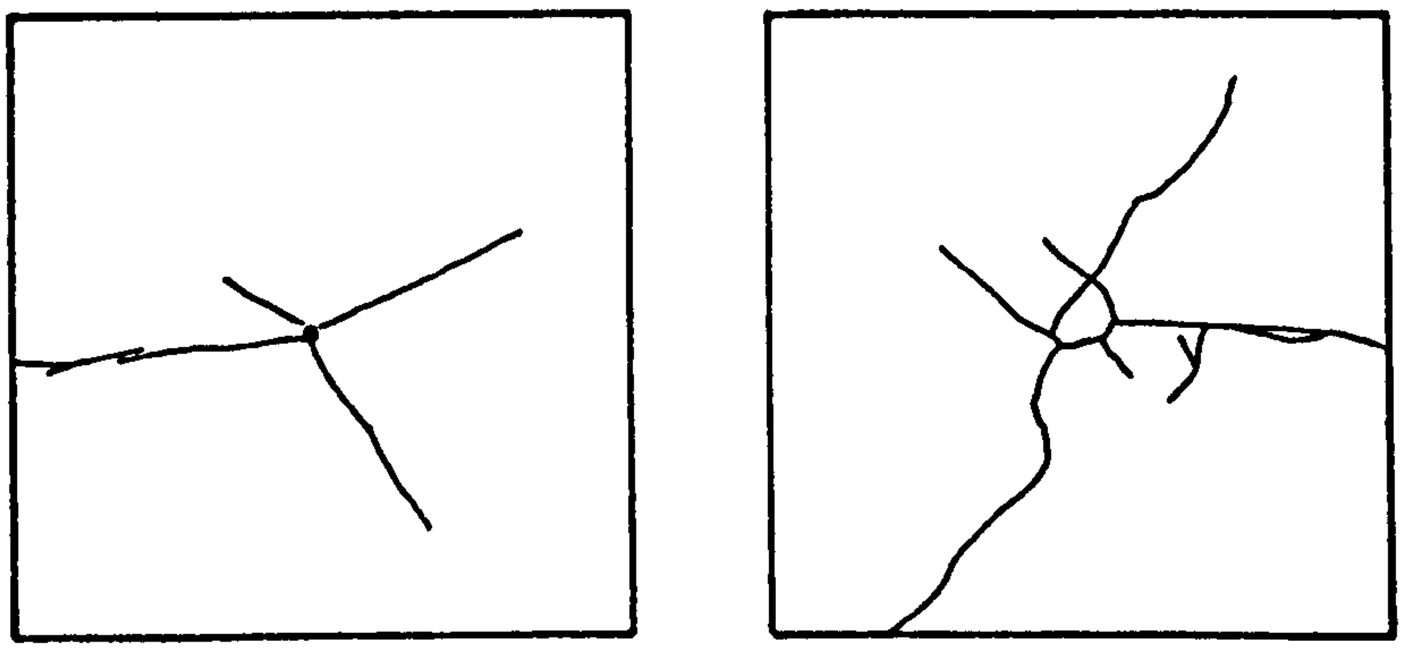

FRONT FACE – PLAIN CONCRETE COMPONENT – REAR FACE

Figure 5.22 Sketches Showing Post-Impact Damage M/PC/1

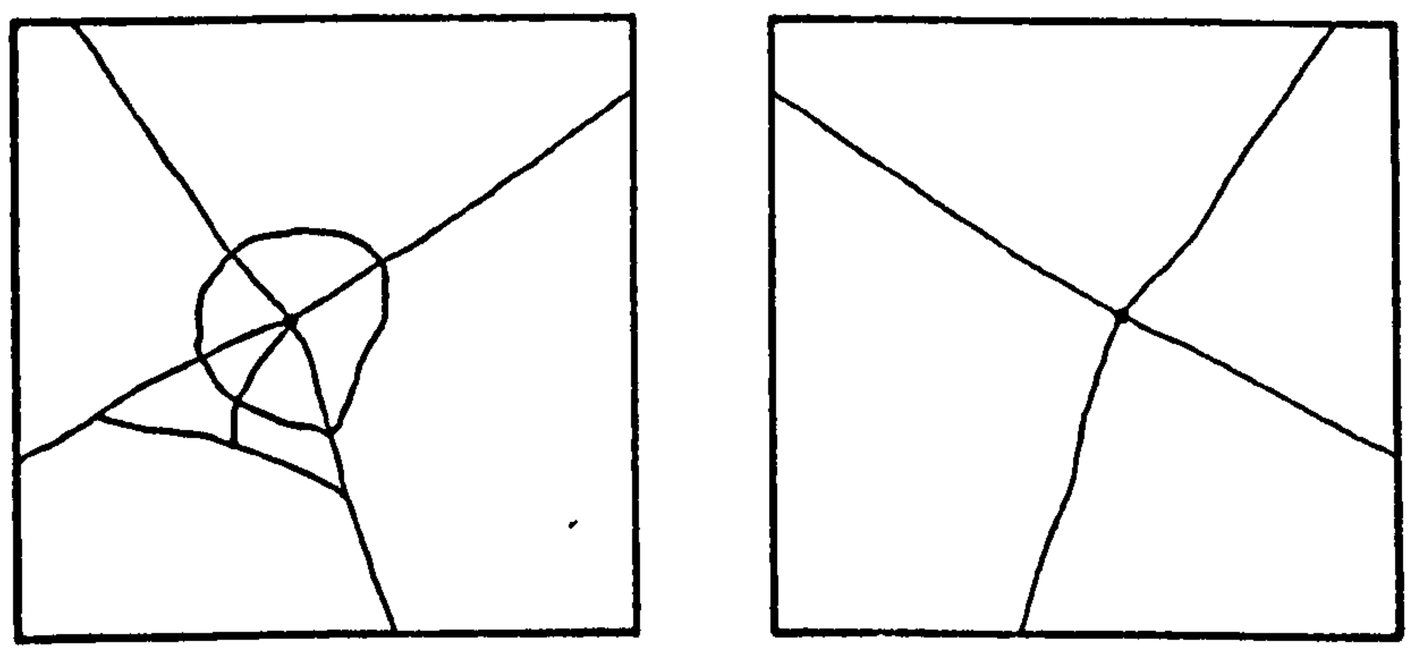

FRONT FACE – MORTAR COMPONENT – REAR FACE

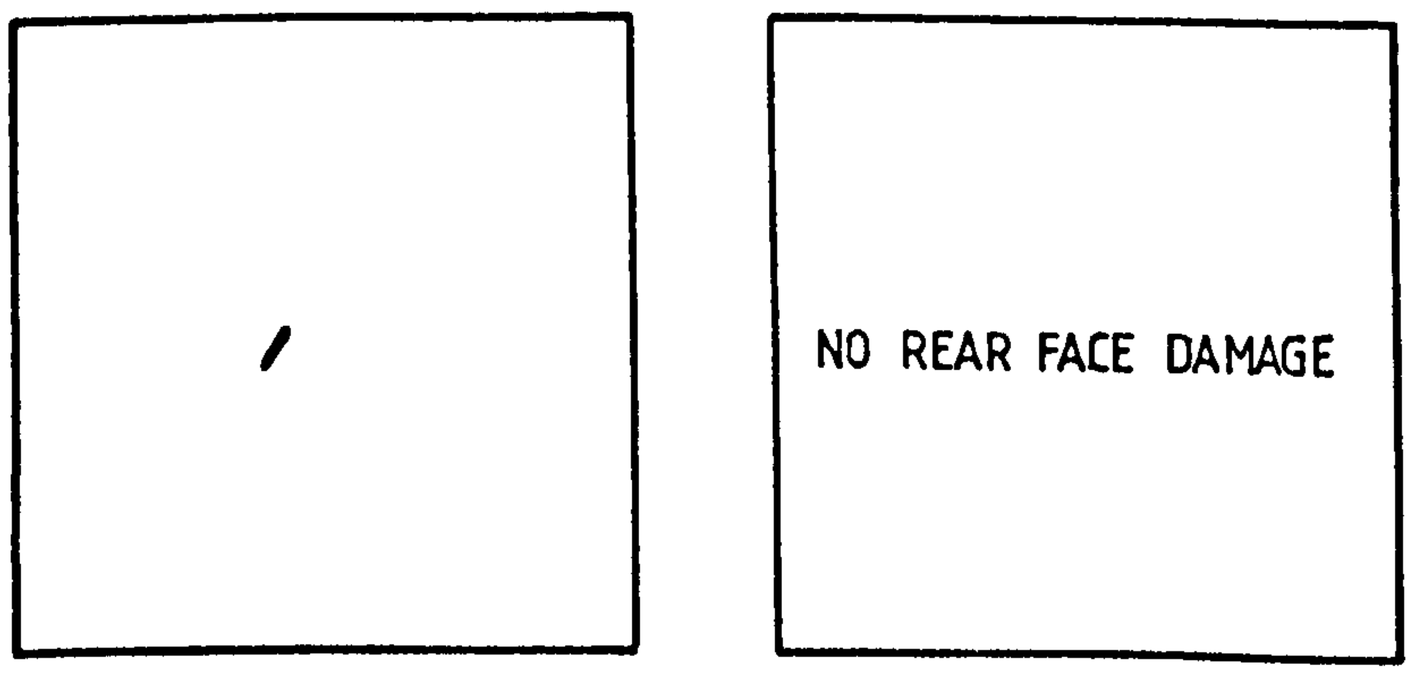

FRONT FACE – PLAIN CONCRETE COMPONENT – REAR FACE

Figure 5.23 Sketches Showing Post-Impact Damage M/PC/2

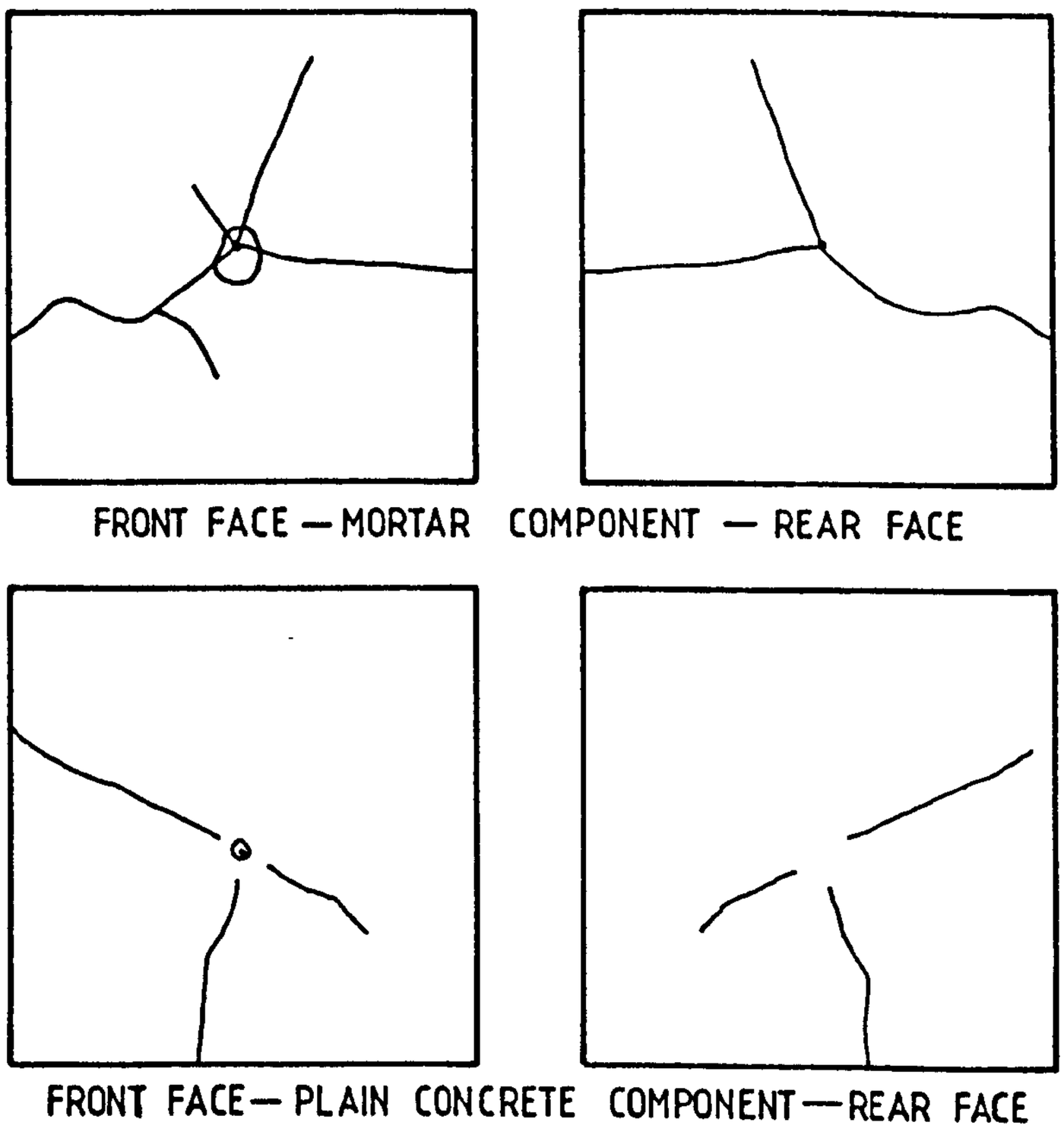

Figure 5.24 Sketches Showing Post-Impact Damage
M/PC/3

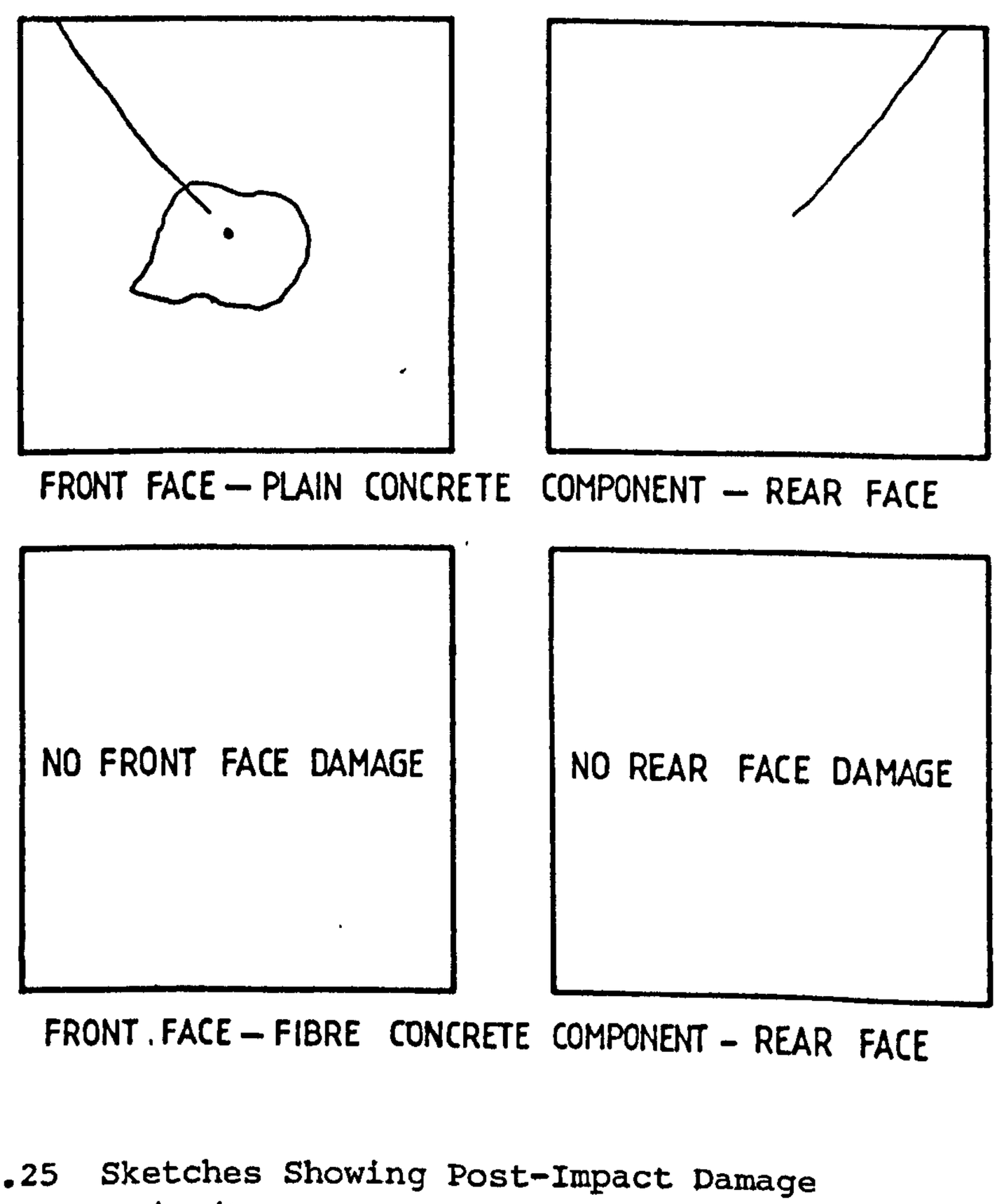

Figure 5.25 Sketches Showing Post-Impact Damage
PC/FC/1

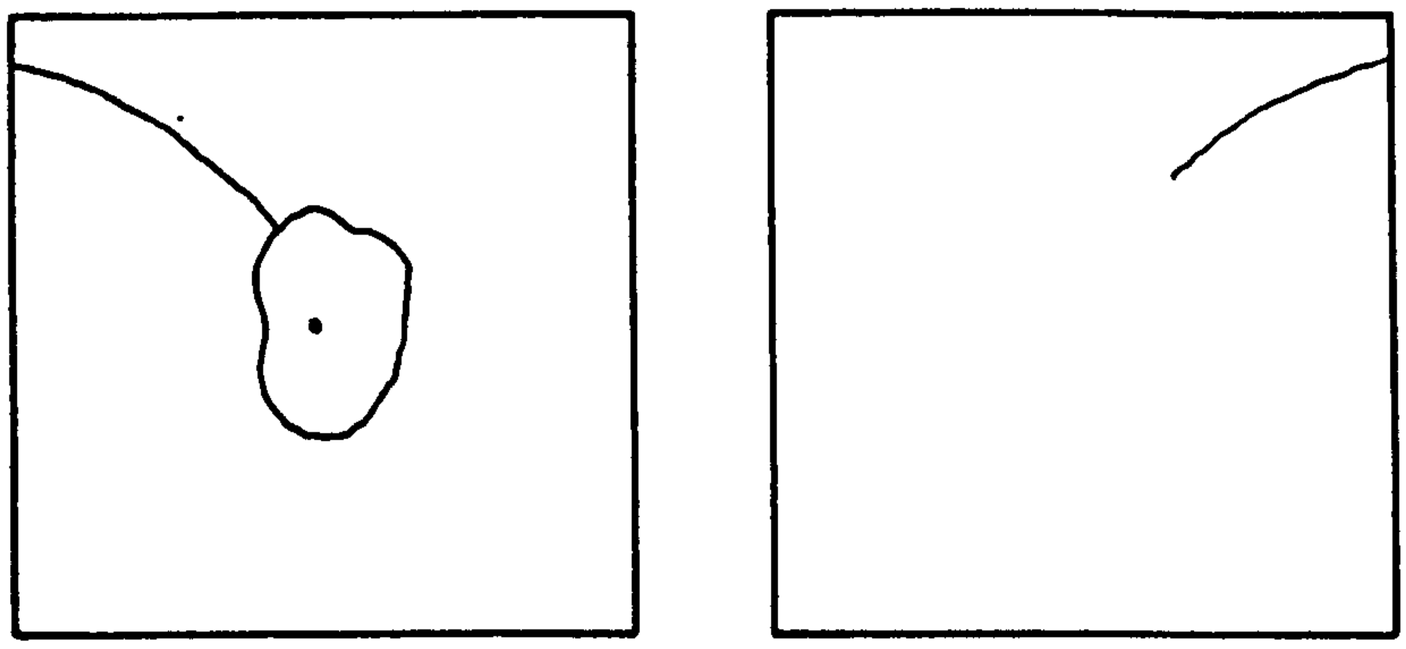

Figure 5.26 Sketches Showing Post-Impact Damage PC/FC/2

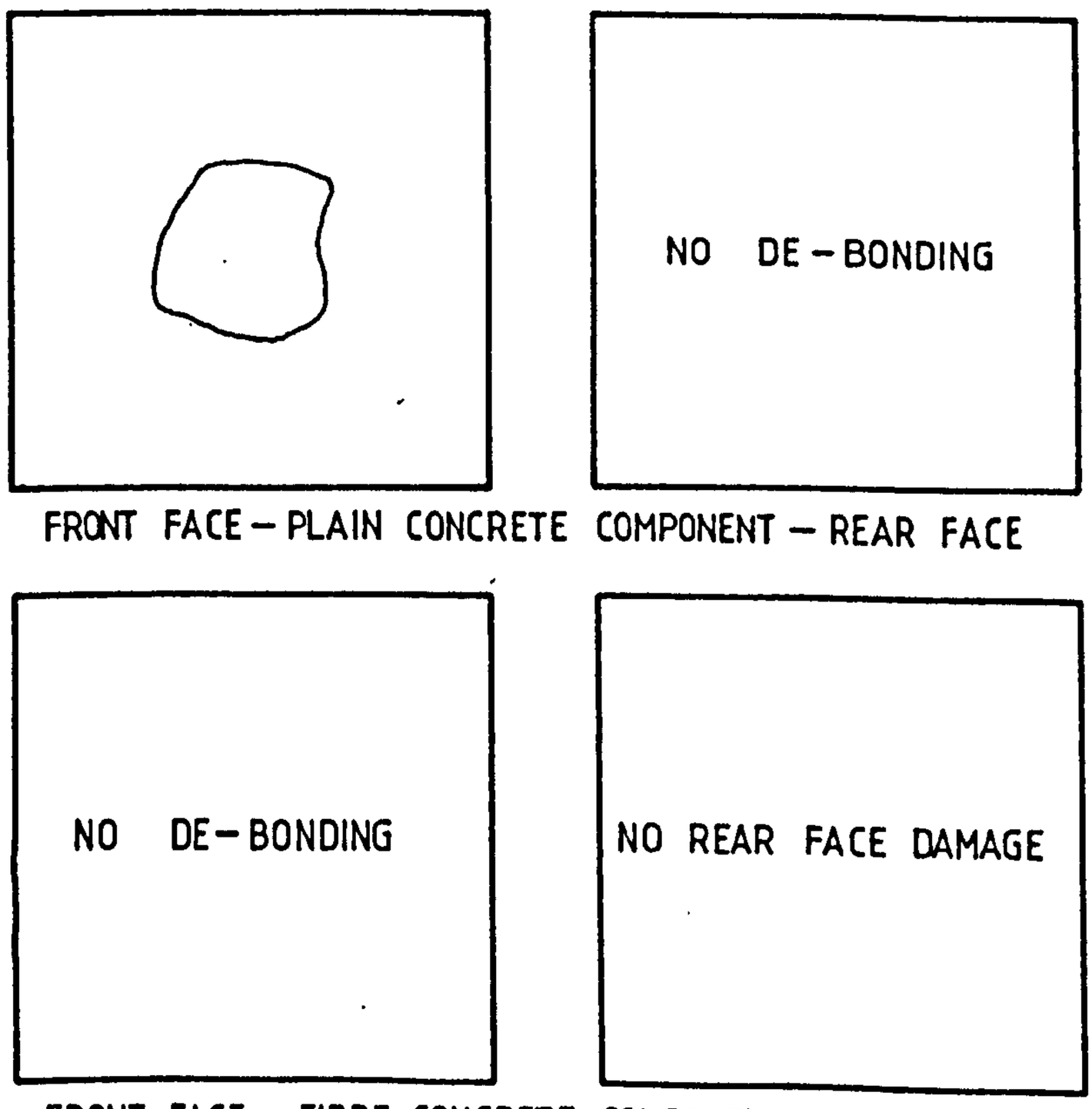

Figure 5.27 Sketches Showing Post-Impact Damage PC/FC/3

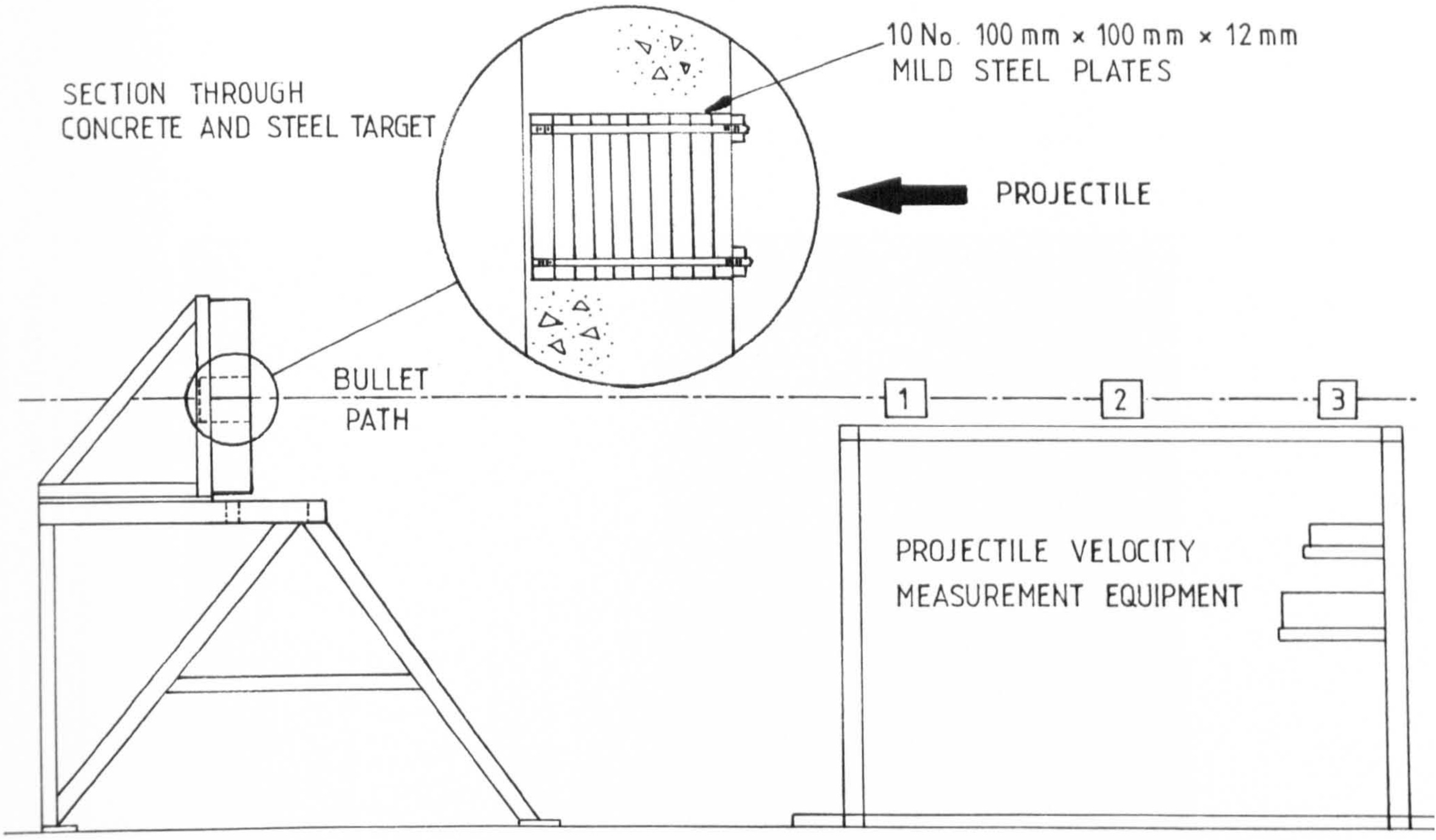

Figure 5.28 General arrangement of Layered Steel Plates in Concrete Target

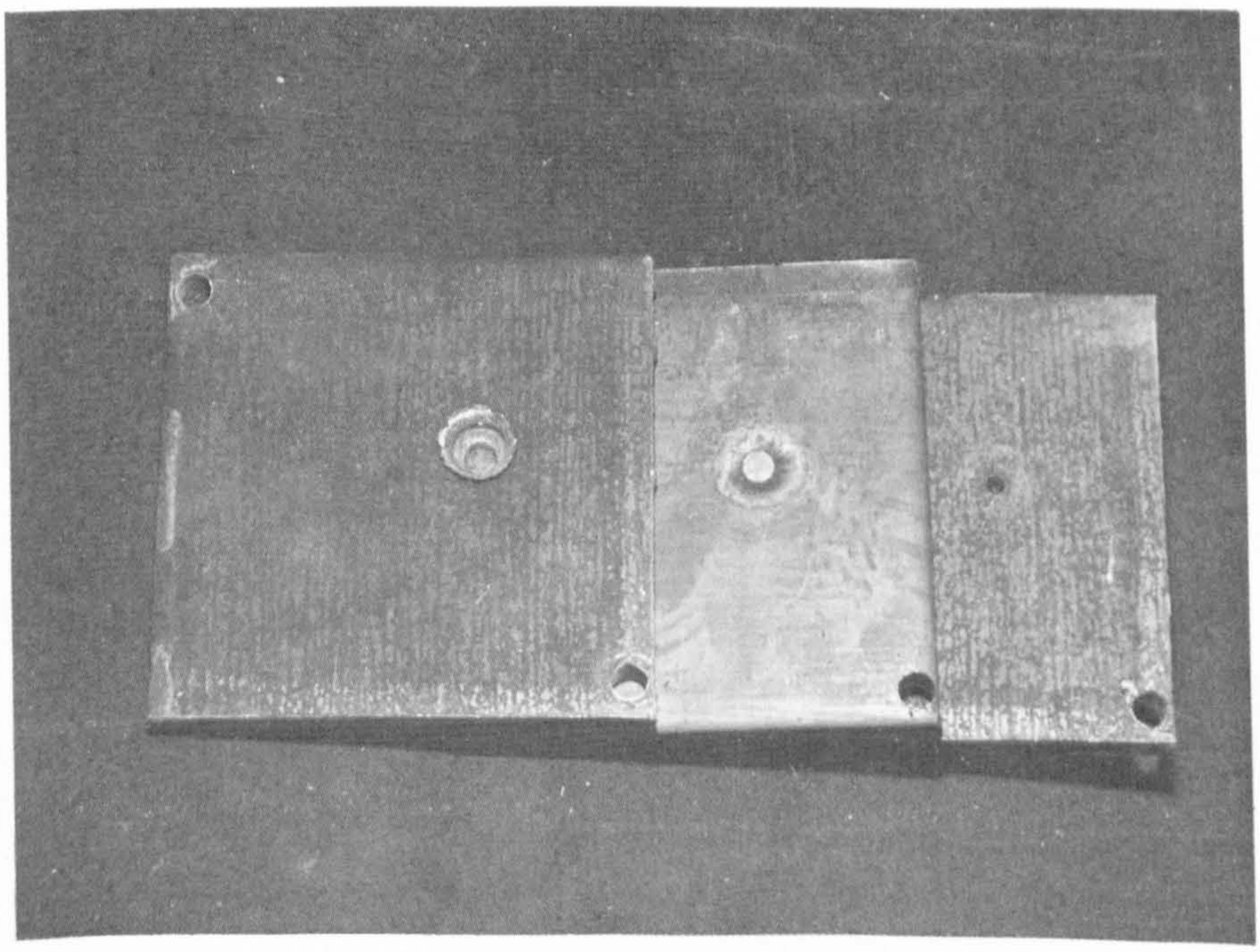

Figure 5.29 Initial three 12mm mild steel plates after impact

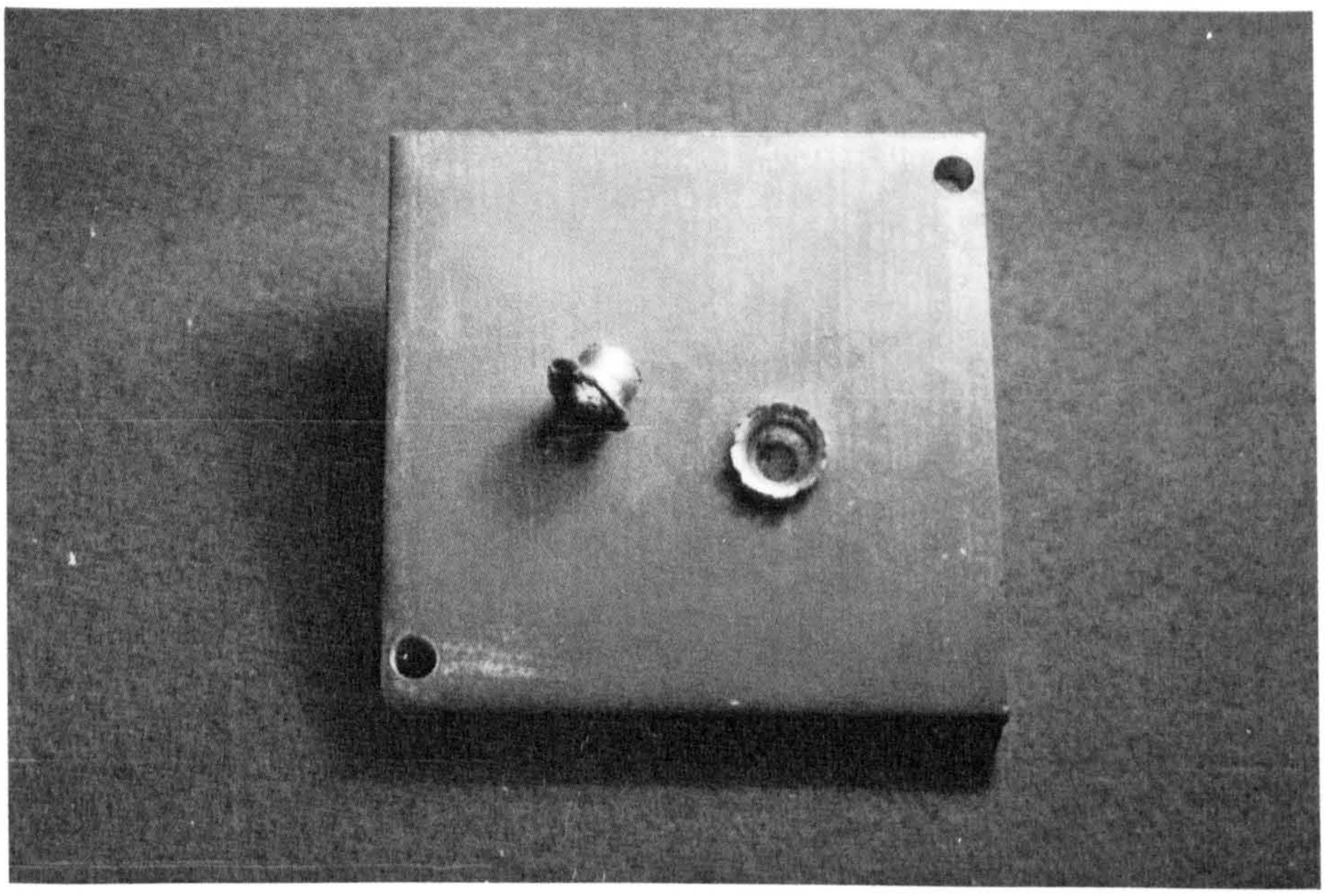

Figure 5.30 Detail of uppermost 12mm mild steel plate and recovered guilding metal jacket

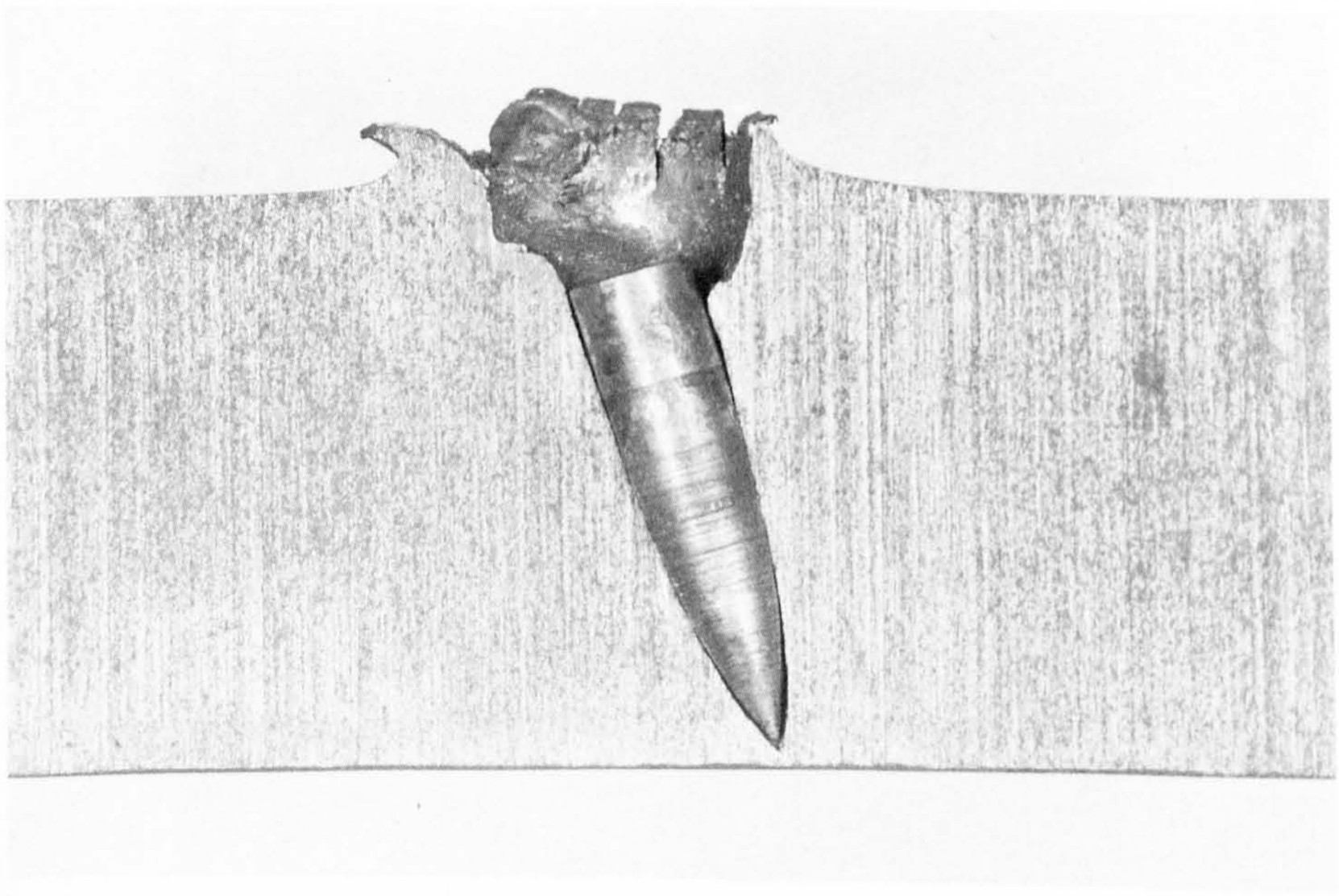

Figure 5.31 Sectioned cylindrical mild steel target

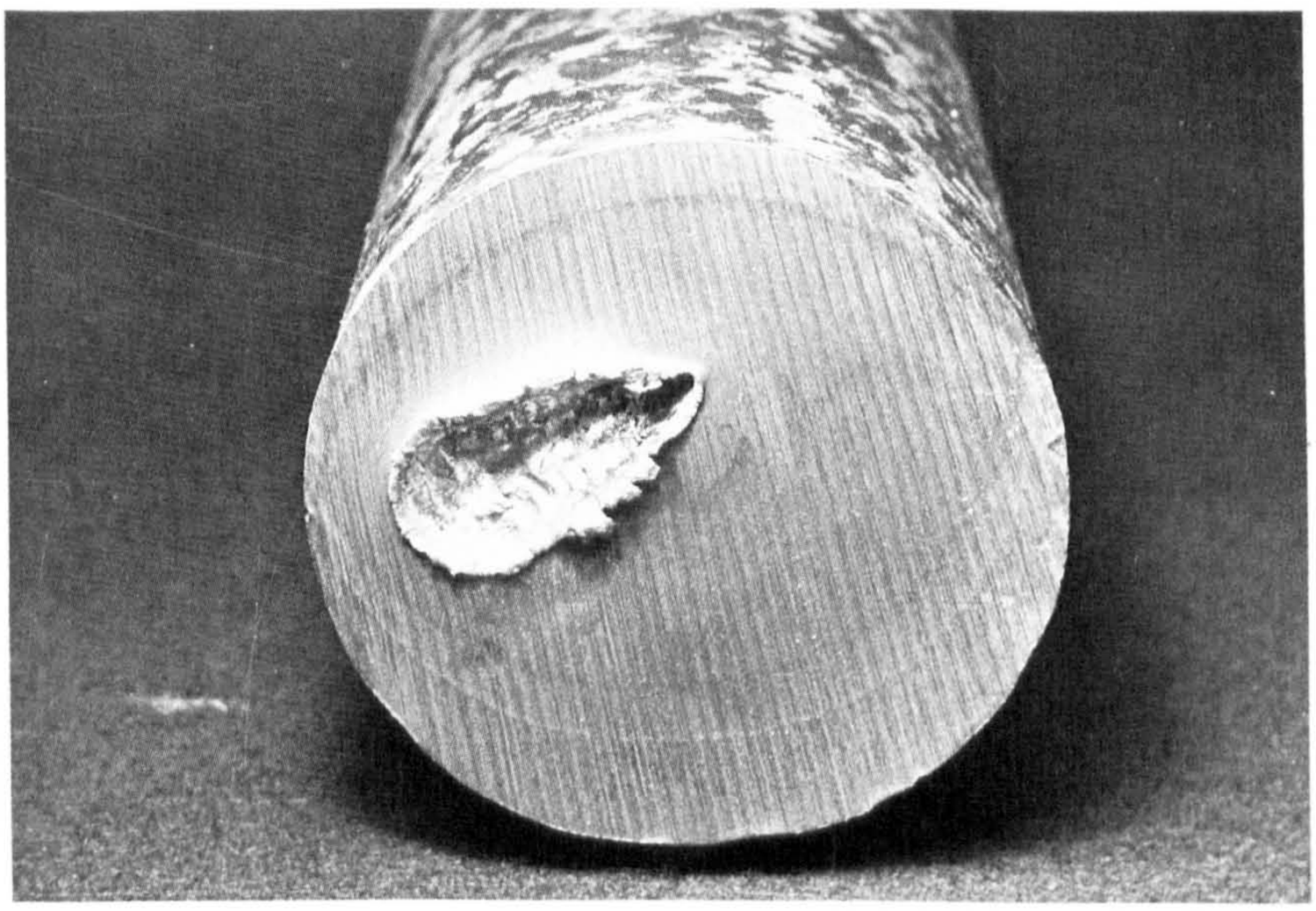

Figure 5.32 Cylindrical mild steel target after oblique impact

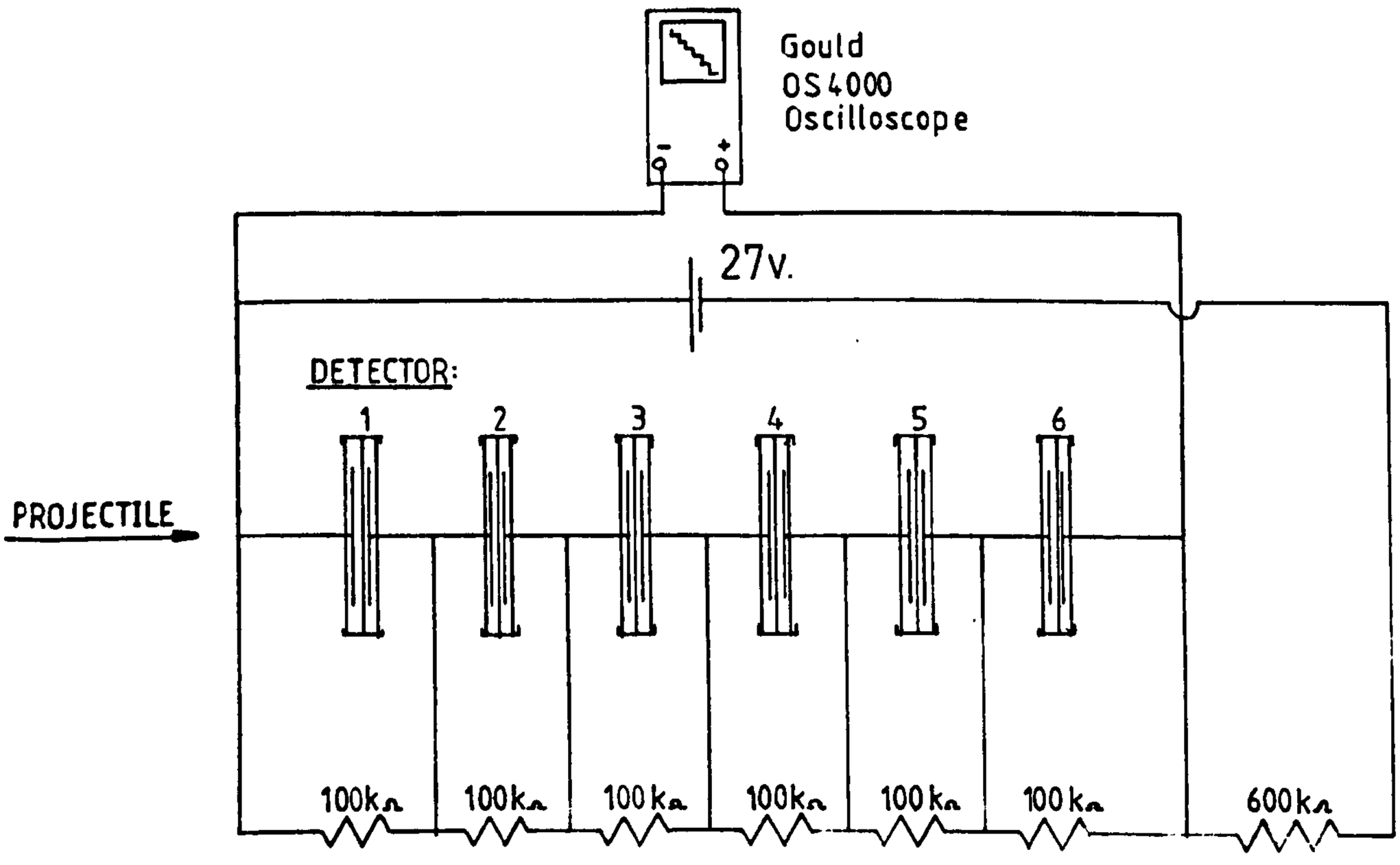

Figure 5.33 Velocity Through Concrete - Detector Circuit
Progressive Resistance Breakdown

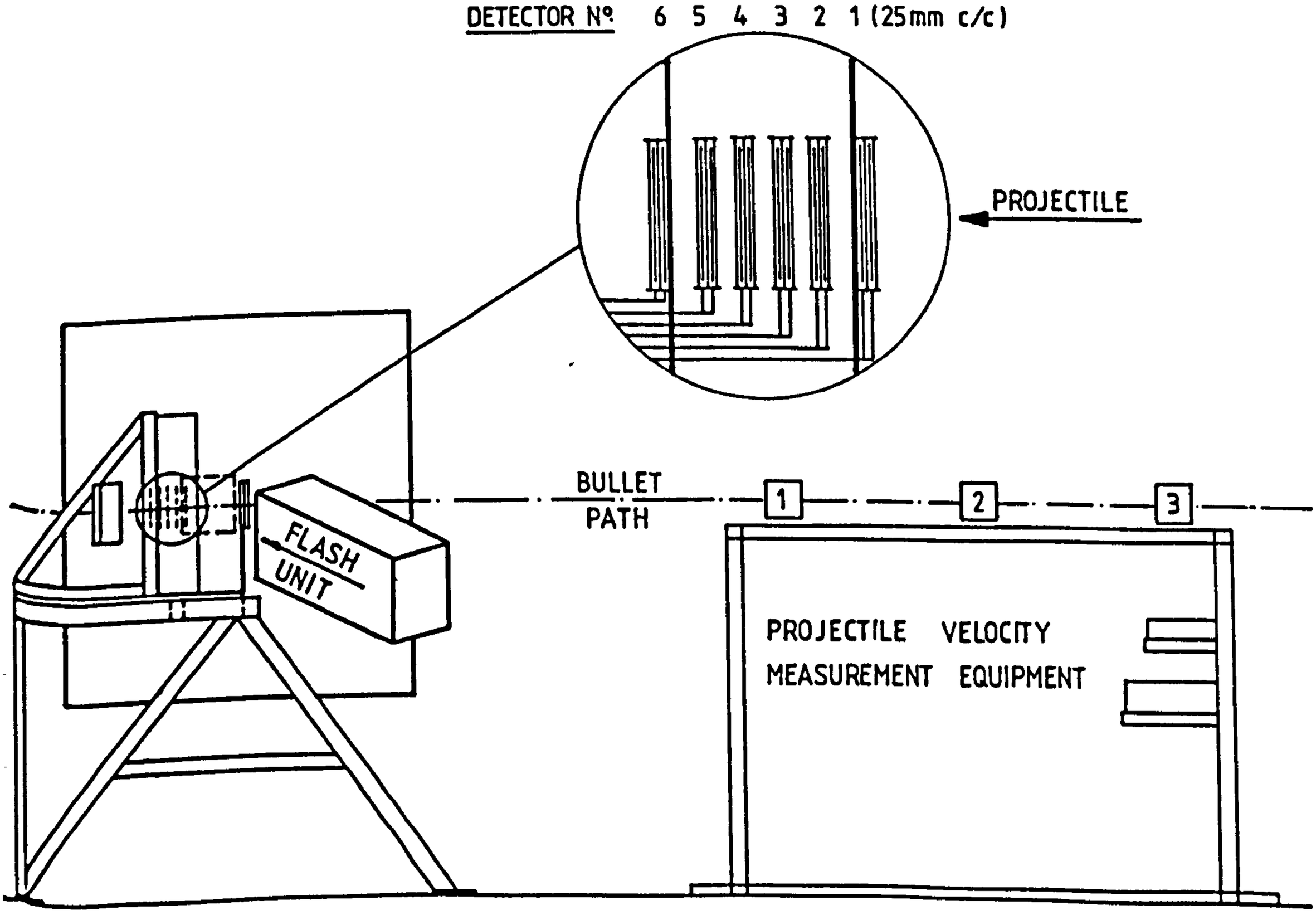

Figure 5.34 General Arrangement for Measurement of Projectile
Deceleration Within Plain Concrete Targets

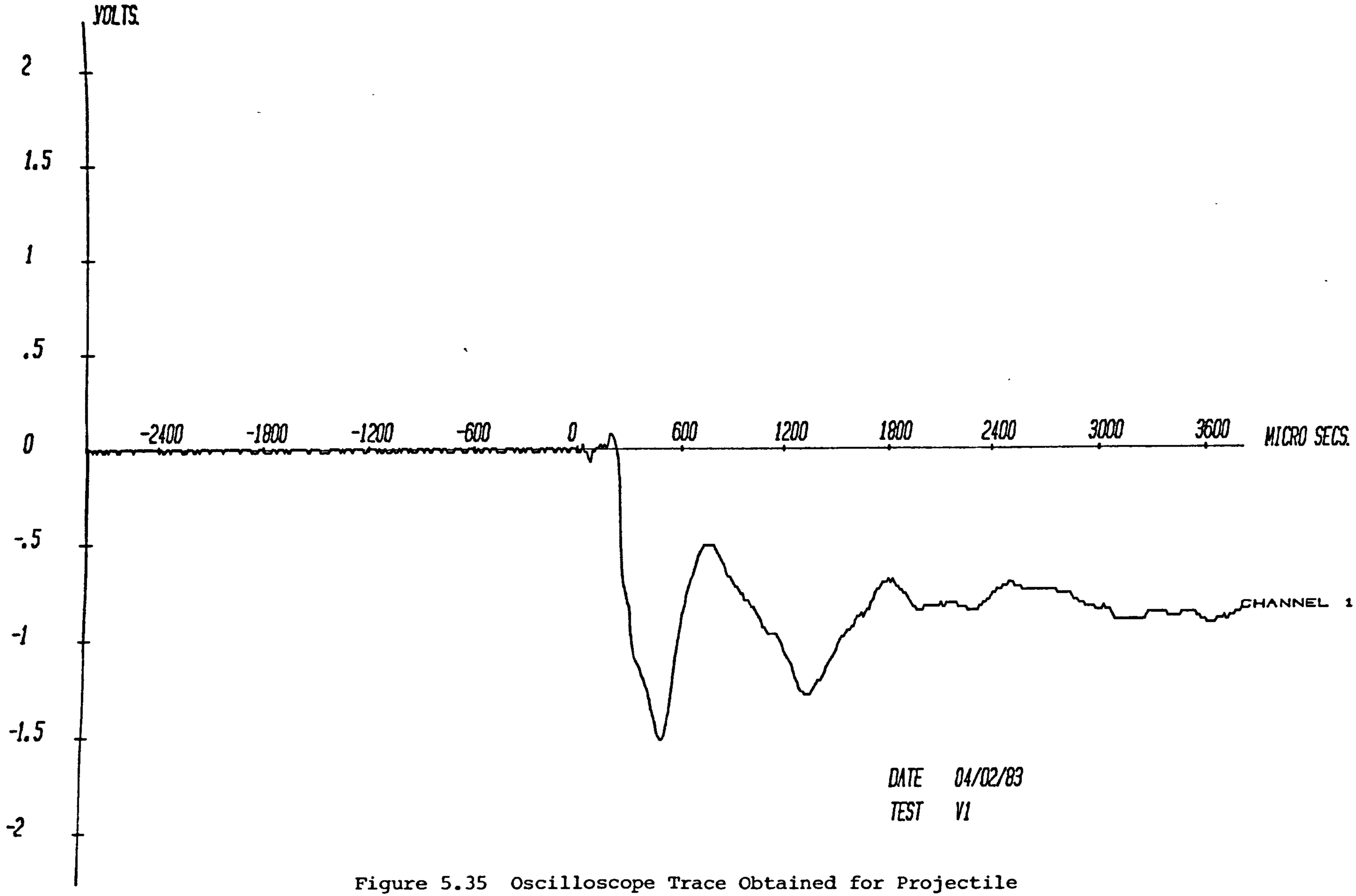

Figure 5.35 Oscilloscope Trace Obtained for Projectile Retardation Test V1

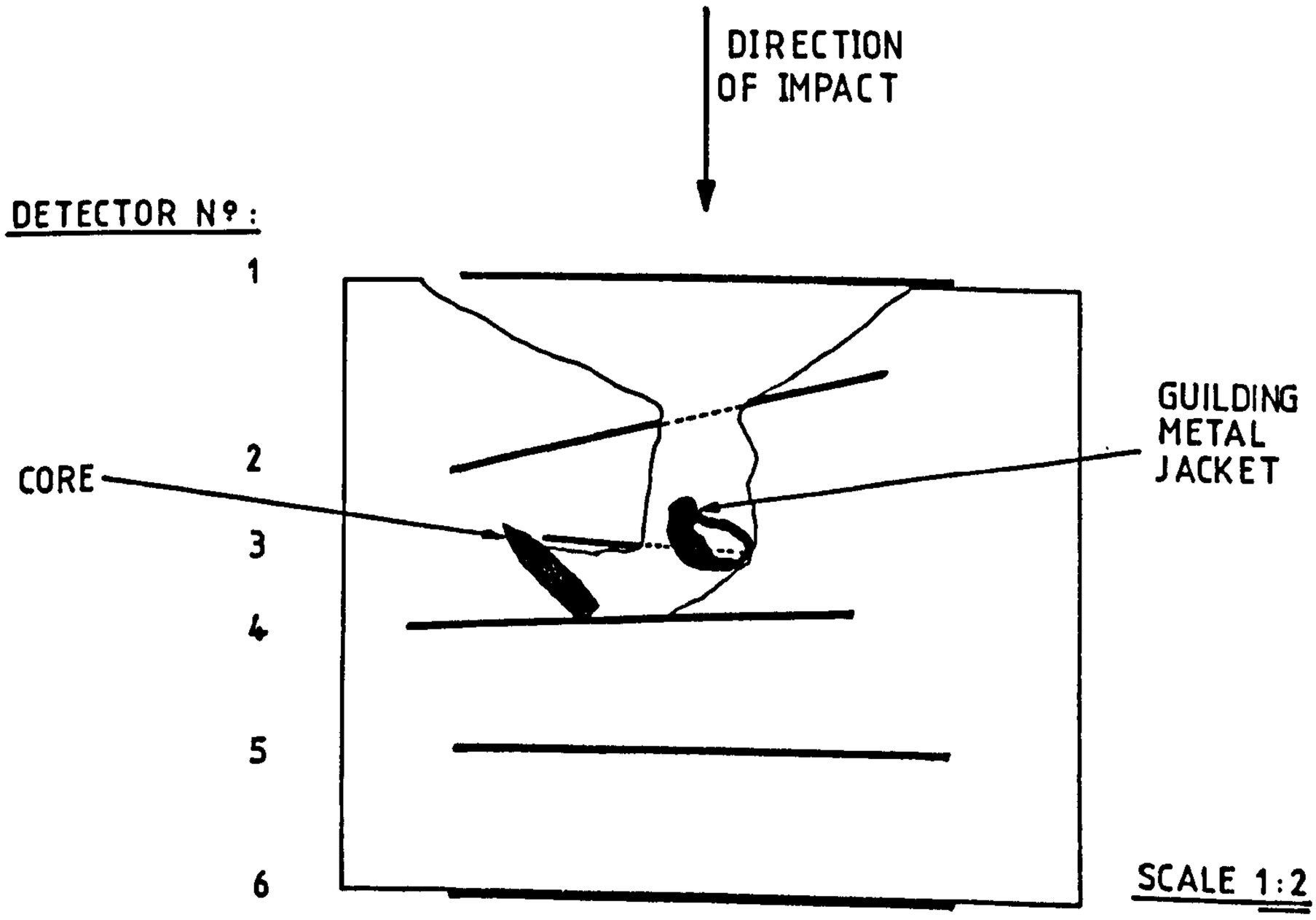

Figure 5.36 Cross-Section of Core taken after Velocity Retardation Test V1

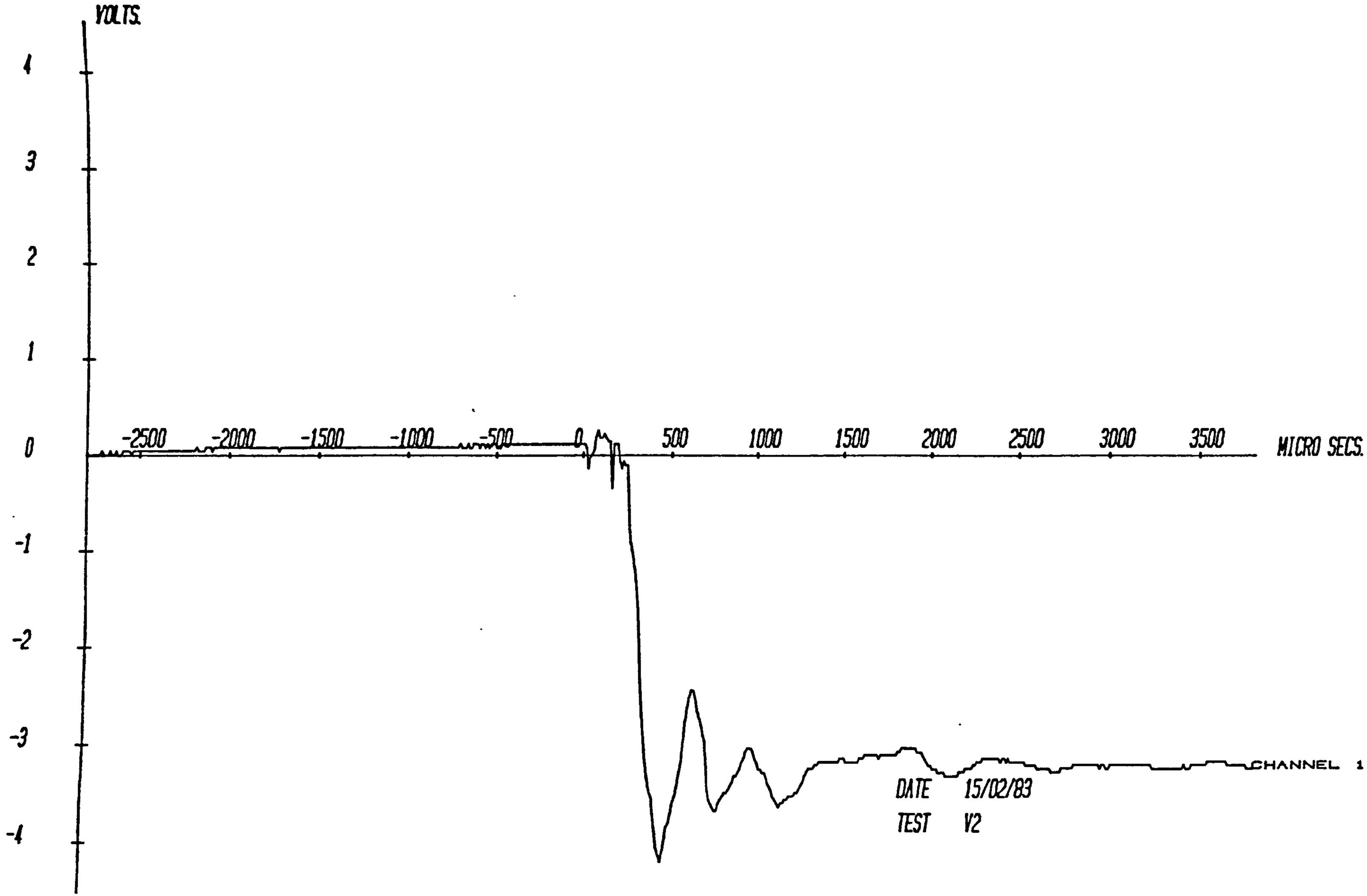

Figure 5.37 Oscilloscope Trace Obtained for Projectile Retardation Test V2

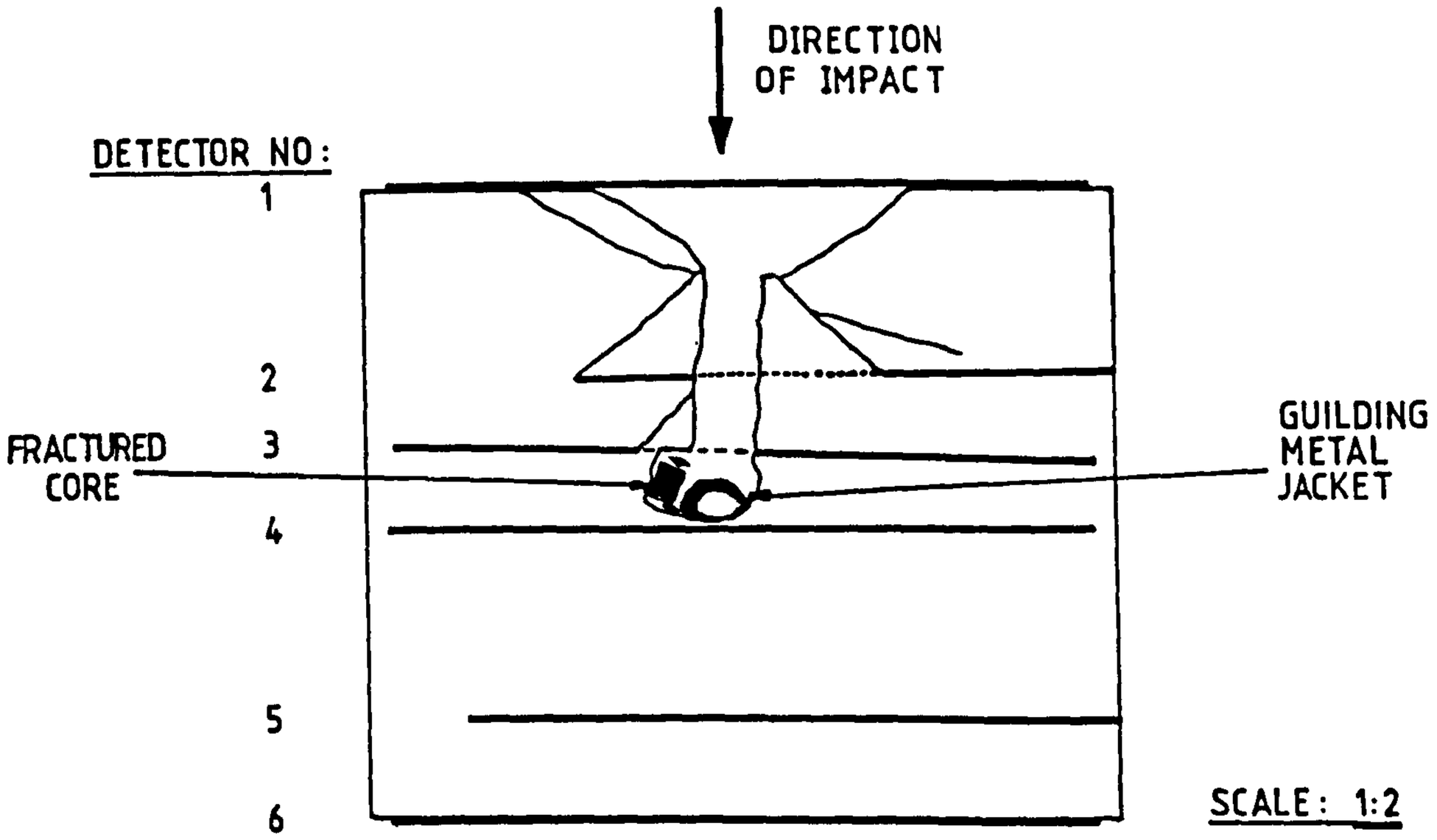

Figure 5.38 Cross-Section of Core taken after Velocity Retardation Test V2

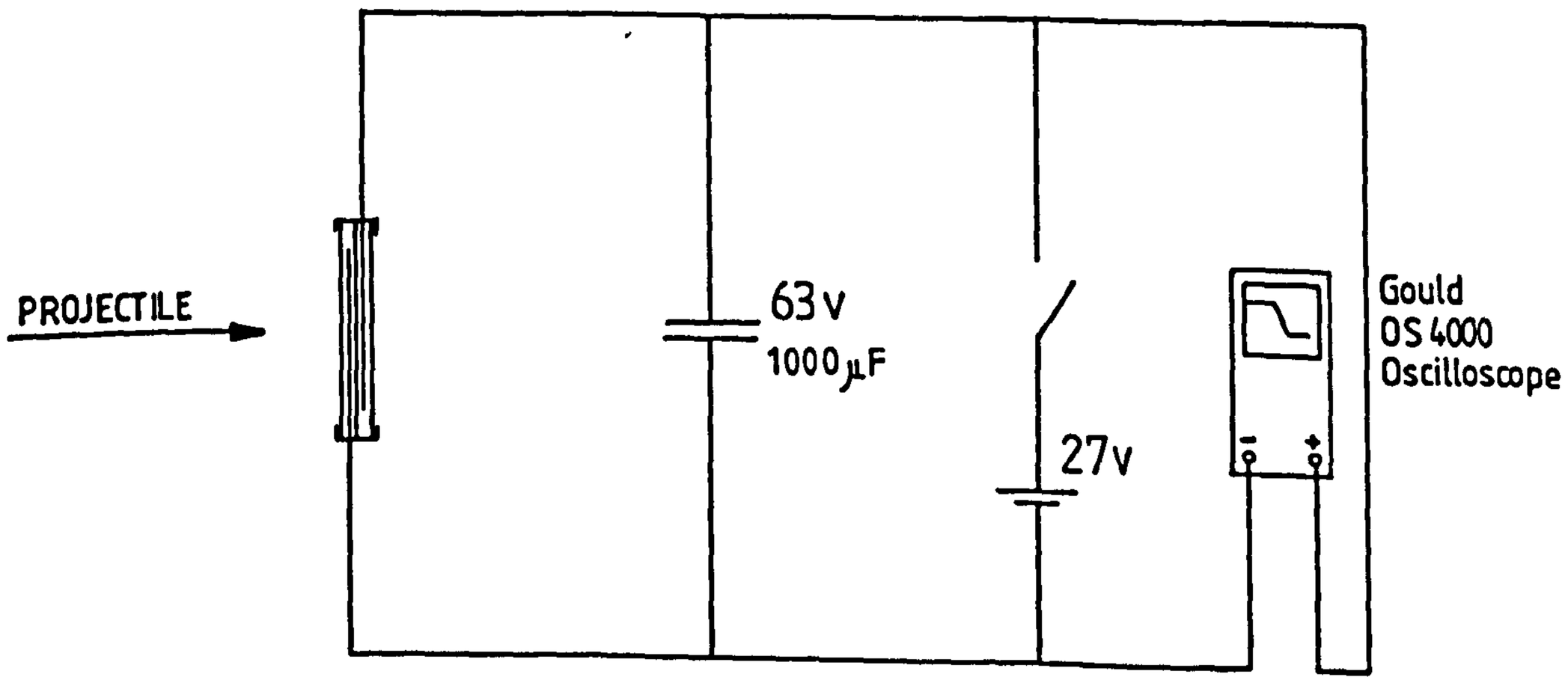

Figure 5.39 Single Detector Capacitance Breakdown Circuit

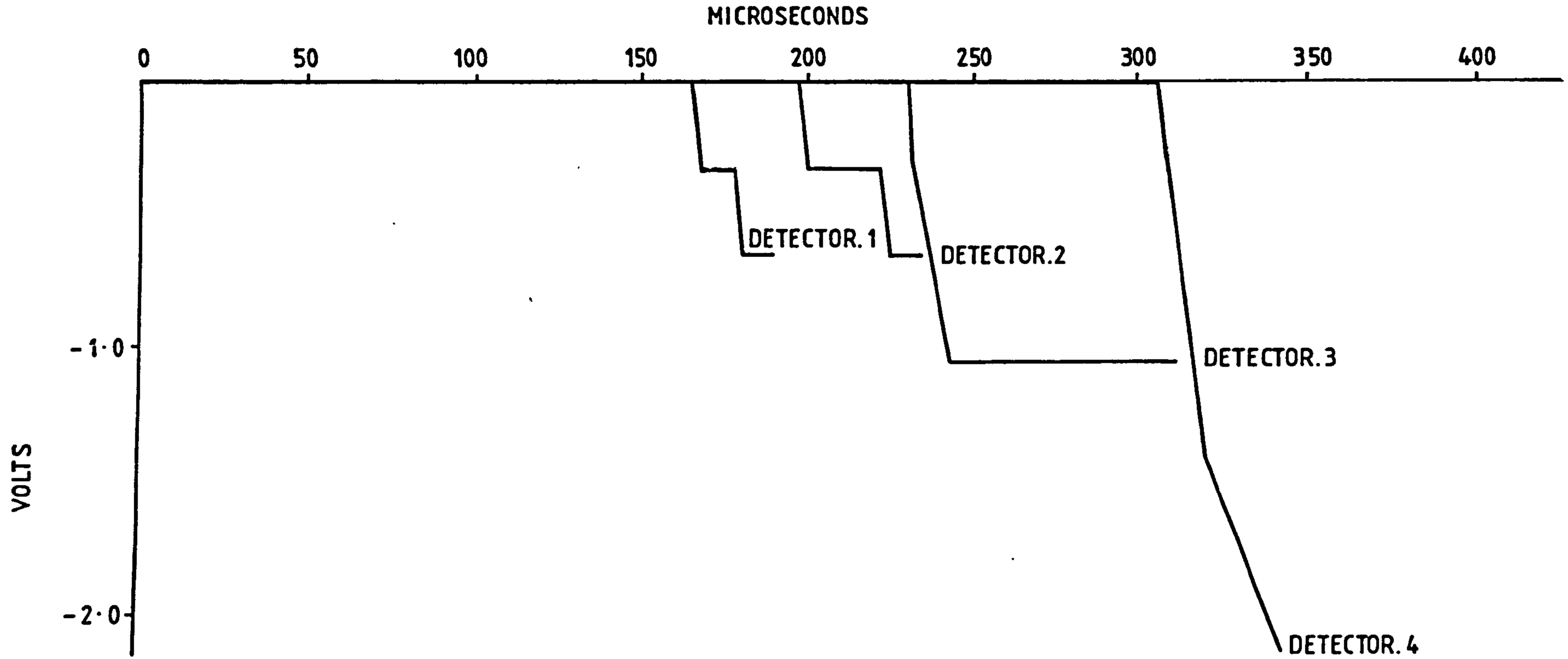

Figure 5.40 Plot of Oscilloscope Data Obtained for Projectile Retardation Test V3

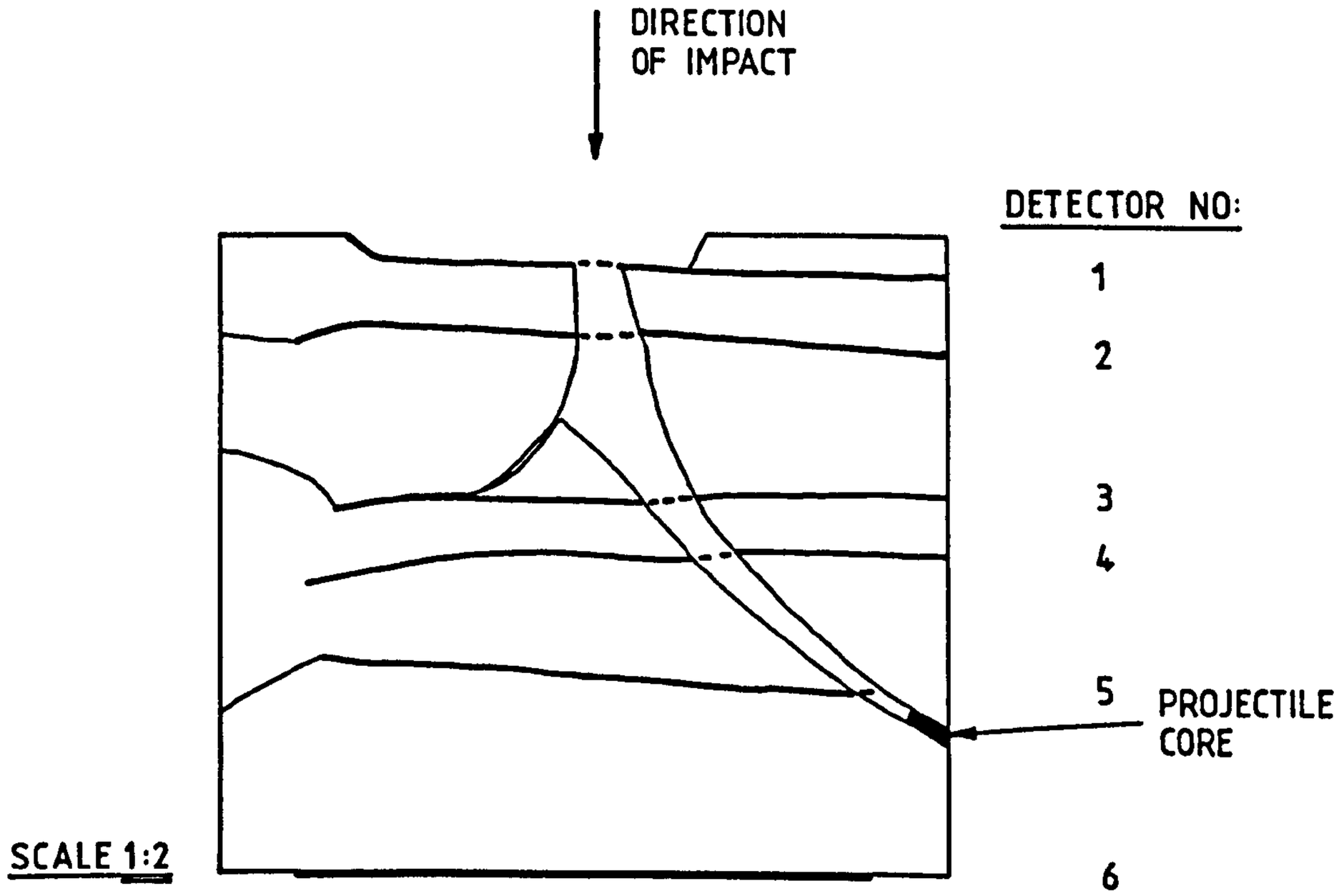

Figure 5.41 Cross-Section of Core taken after Velocity Retardation Test V4

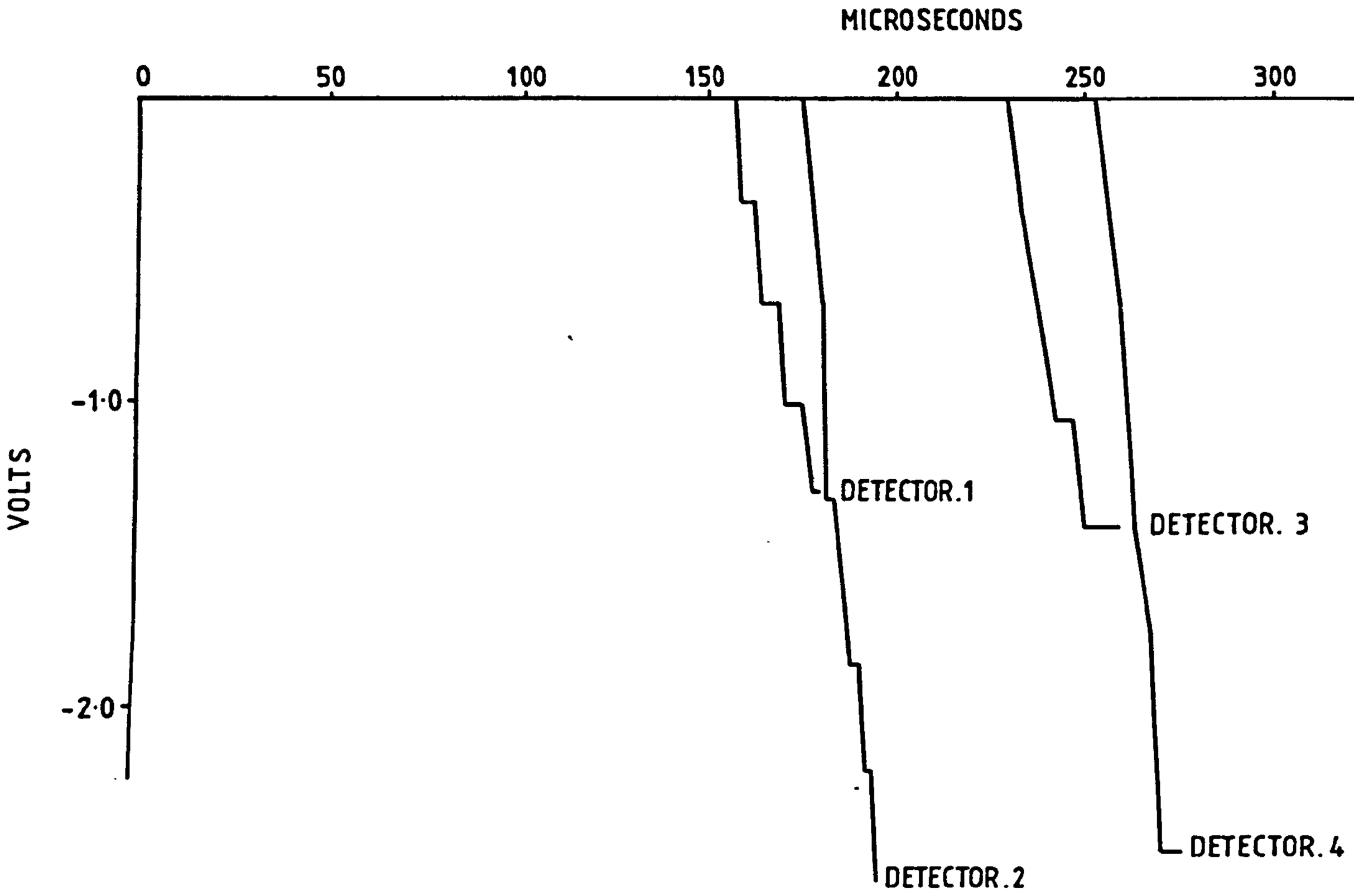

Figure 5.42 Plot of Oscilloscope Data Obtained for Projectile Retardation Test V4

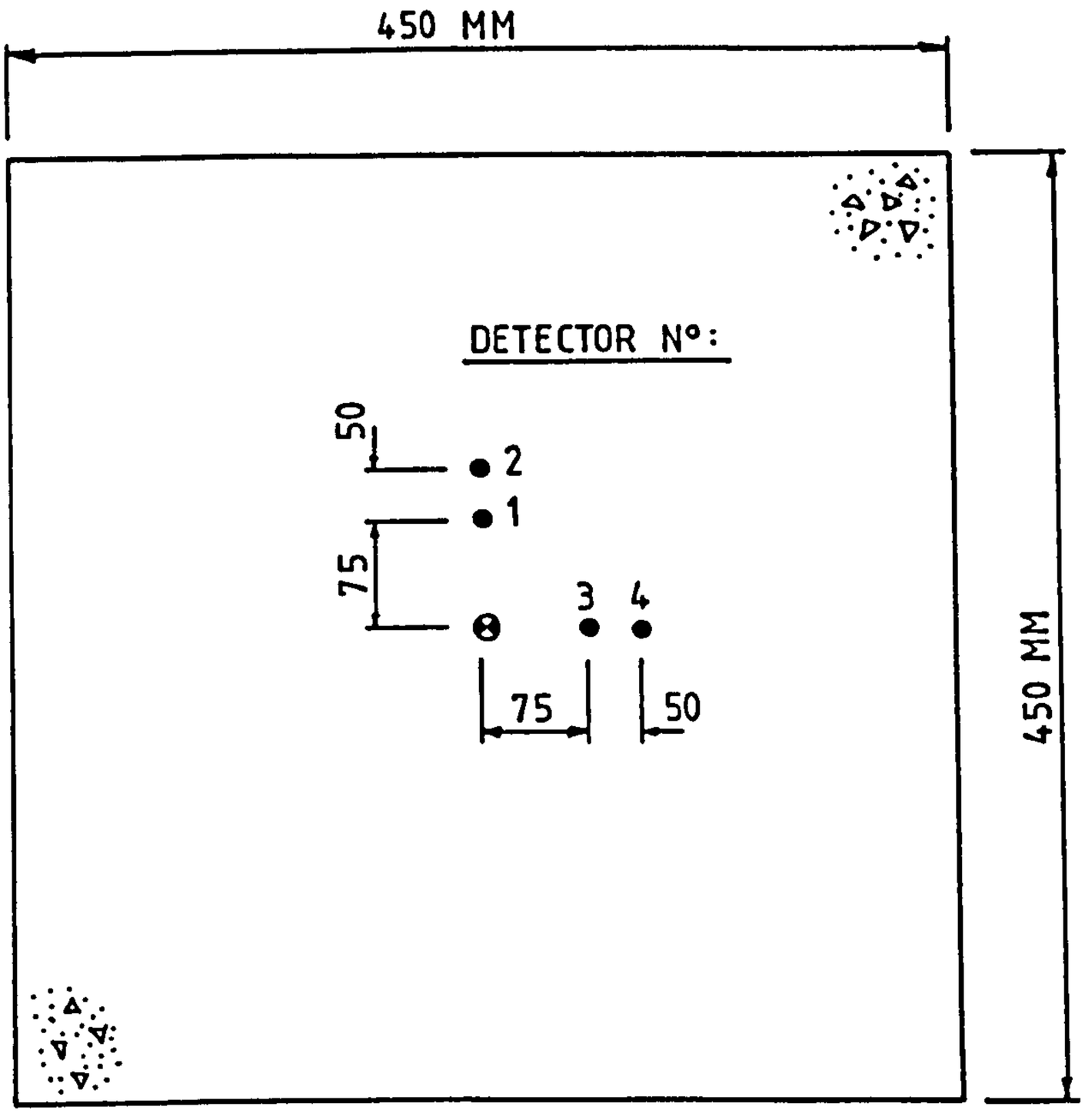

Figure 5.43 Positions of Graphite Spall Detectors on Specimen Impact Face

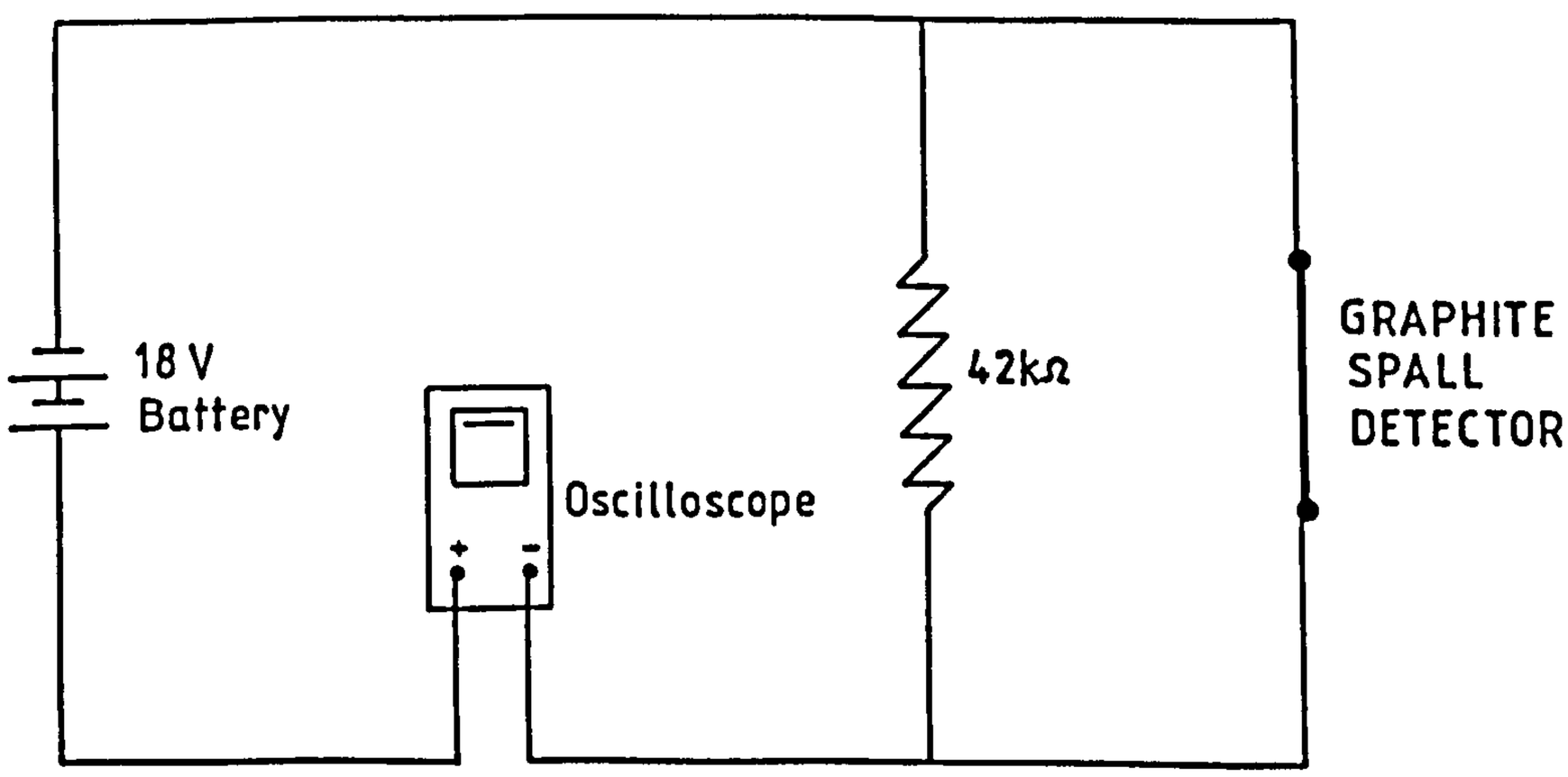

Figure 5.44 Spall Detector Amplification Circuit

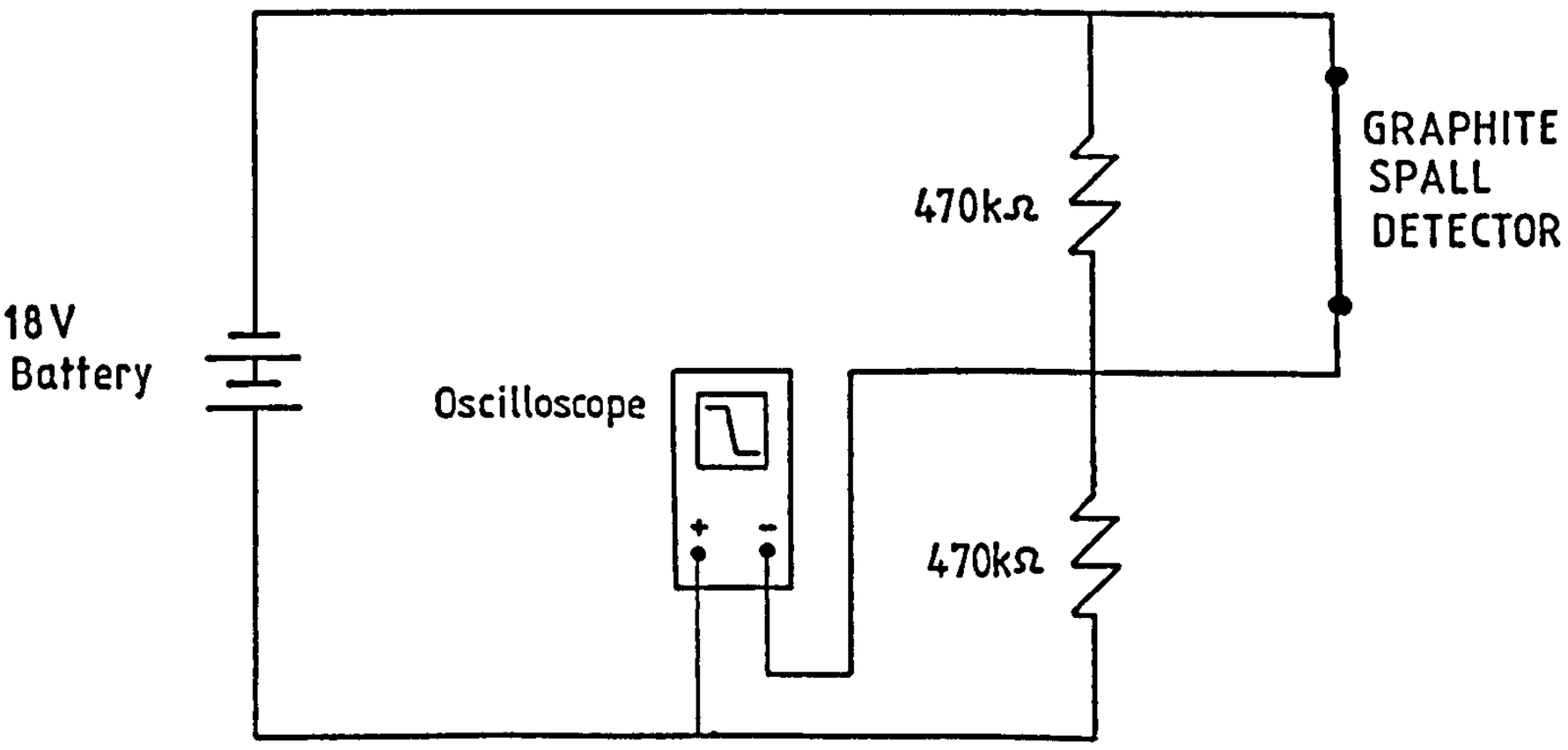

Figure 5.45 Alternative Spall Detector Amplification Circuit

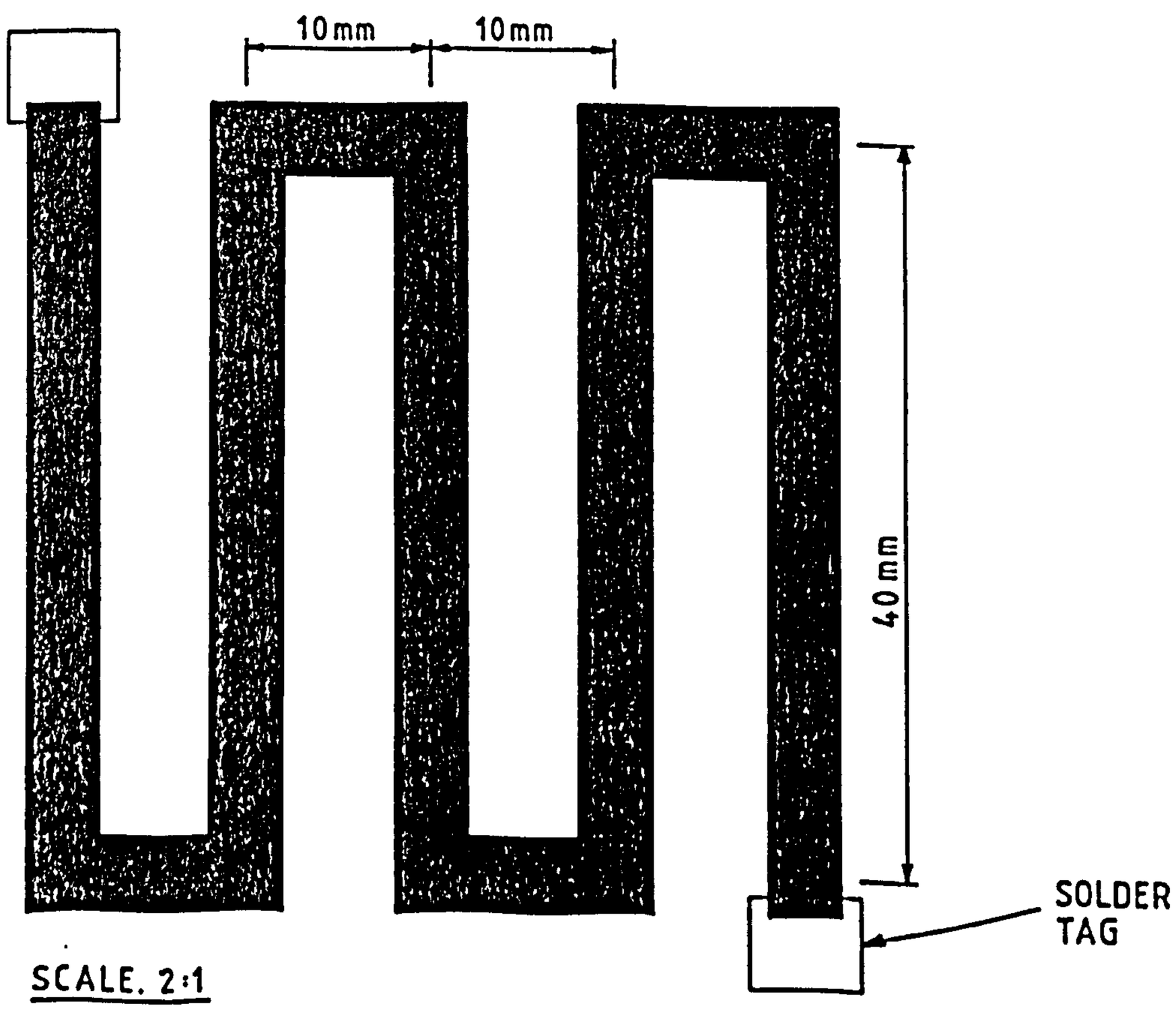

Figure 5.46 Silver-loaded Conductive Paint Grid

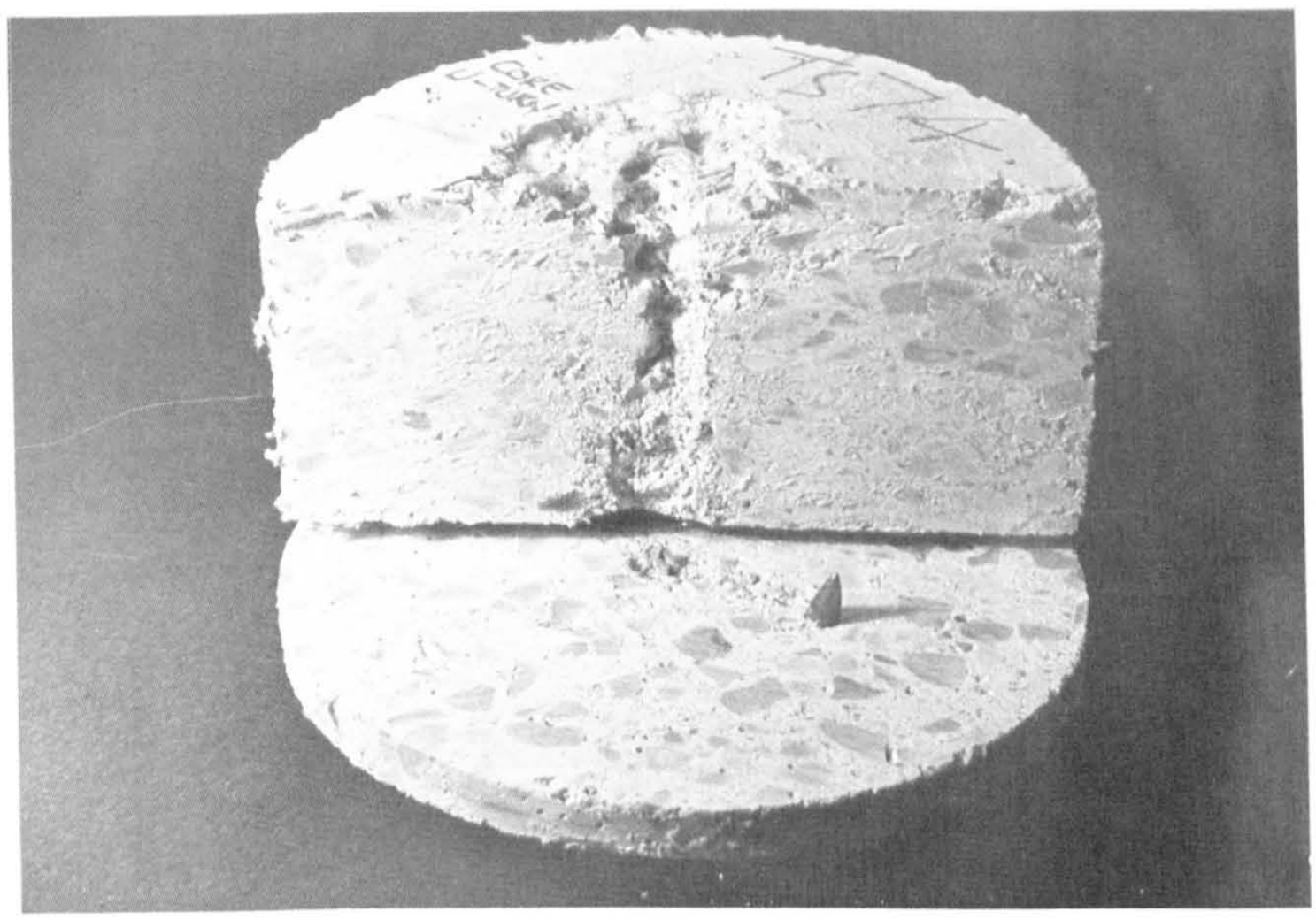

Figure 5.47 Cross-section of Kevlar-29 reinforced concrete specimen showing gross projectile deviation

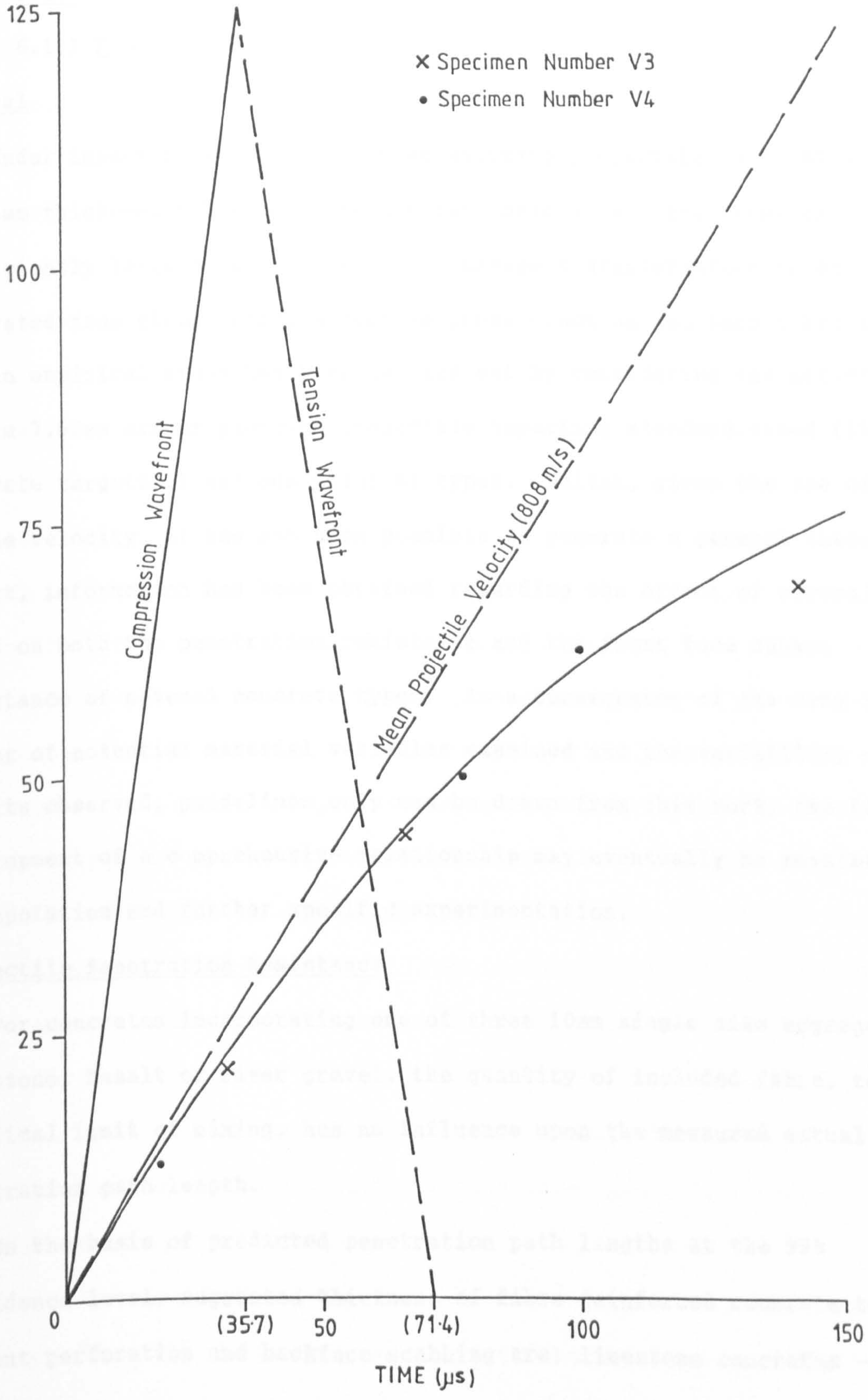

Figure 5.48 Penetration Path Length against Elapsed Time for Deceleration Test Specimens V3 and V4

CHAPTER 6

CONCLUSIONS AND RECOMMENDATIONS FOR FUTURE WORK

6.1 Conclusions

6.1.1 Fibre Reinforced Concrete

General

1. Under impact from a 7.62mm armour piercing projectile, a 450mm x 450mm x 125mm thickness fibre concrete specimen held in a rigid frame is sufficiently large to enable the local damage characteristics to be separated from global effects such as gross cracking and target break-up.
2. An empirical study has been carried out by considering the effects of a single 7.62mm armour piercing projectile impacting standard sized fibre concrete targets of various material types. Whilst, given the use of a single velocity, it has not been possible to generate a general theorem for impact, information has been obtained regarding the effect of several fibre types on both the penetration resistance and the front face damage resistance of several concrete types. As a consequence of the very large number of potential material variables examined and the variability of results observed, guidelines only can be drawn from this work; the future development of a comprehensive relationship may eventually be possible by extrapolation and further specific experimentation.

Projectile Penetration Resistance

3. For concretes incorporating one of three 10mm single size aggregates; limestone, basalt or river gravel, the quantity of included fibre, to the practical limit of mixing, has no influence upon the measured actual penetration path length.
4. On the basis of predicted penetration path lengths at the 99% confidence level, suggested thickness of fibre reinforced concrete to prevent perforation and backface scabbing are; limestone concretes - 115mm,

basalt and river gravel concretes - 130mm. The former value is less because of the greater consistency of results noted for limestone based concretes.

Front Spall Resistance

5. Addition of between 2.5% and 5.0% steel fibre by concrete weight significantly reduces spall crater volume. At the higher concentration concretes containing melt extract or Duoform steel fibres may perform slightly better than those containing drawn steel (smooth circular) fibres of an equal aspect ratio. Further, such concretes cast with limestone or basalt coarse aggregate experience slightly less spalling than those incorporating river gravel aggregate.

6.1.2 Impact and Penetration Mechanisms

6. Initial impact damage of concrete targets is generally masked by the subsequent cracking and spalling induced by the changing stress field. That is, post-event observation is not a valid way to assess the immediate first impact damage. One of two different mechanisms appears normally responsible for the observable target damage. In the first, the projectile enters the target and begins to move the surrounding material locally by comminution and lateral shear displacement. At this stage, the penetrator is turned and a "ricochet" with no subsequent burrow formation occurs. The second, more usual and more complex situation, is a combination of an identical local shearing ("bursting") and comminution phase, but with burrow formation as the penetrator travels deep enough for sufficient target shear resistance to be generated, with consequential stripping of projectile coverings. In both cases, the earliest shear indications are destroyed by the subsequent specimen motion (caused by reflected tensile stress waves from the rear target-air interface) generating uplift from the internal crater-air interfaces.

7. Tentative results indicate that a 15-20% velocity reduction may be expected within the first 20mm of penetration of a concrete target by a

7.62mm armour-piercing projectile. The subsequent stripping of the gilding metal jacket of the projectile occurs with only little corresponding reduction in velocity. However, the induced deviation causes (or possibly is generated by) increased deceleration. The extent of this deviation is likely to be significant in a concrete target; as a consequence, actual projectile path length, rather than orthogonal depth of penetration, should be used as a damage parameter.

8. Concrete targets impacted by a 7.62mm armour-piercing projectile generated a mean rate of propagation of the surface circumferential motion of 39m/s. The mean spall product velocity showed a significant reduction with time after impact, from 110m/s over the initial 800μs to 39m/s for the next 700μs period.

9. The most efficient way to defeat a penetrating 7.62mm AP projectile is to induce instability to as great a degree as soon as possible after impact. Concrete targets, containing coarse aggregate and in particular "hard" river gravel, generated this result with the greatest frequency. Mortar targets presented little resistance to penetration at 125mm thickness; the penetration path was most likely to be a straight line continuation of the flight path. High proportions of fibres in a concrete mix, causing a voided composite with inadequate structural performance, were also capable of causing gross projectile deviation and instability, though such a response was not predictable. Reduced front face spalling was a further advantage as a consequence of stress wave damping and disruption.

6.2 Recommendations for Future Work

6.2.1 Fibre Reinforced Concrete

1. Since fibre content has little effect on penetration resistance, any further assessment of fibre reinforced concretes should concentrate on reduction of front face spall damage and, possibly, rear face scabbing. The effects of repeated impact should be examined.
2. A controlled study of the influence of concrete water content on impact damage should be undertaken to assess the acceptability of using the "dry mix" spraying process.
3. Since stress wave transmission and projectile stability are influenced by non-homogeneities, the performance of fibre reinforced concretes which contain microcracks, air voids or some other "soft" inclusions should be studied.
4. The performance of targets produced by a spraying process should be examined to see if stratification promoted by spraying affects performance under impact and penetration.
5. Means of applying fibre reinforced concretes with aggregate particles larger than 10mm should be examined, since large particles appear to have a beneficial effect on penetration resistance.
6. The resistance of fibre reinforced concretes to small explosive charges should be examined.
7. The data produced in this study should be assessed with regard to existing predictive equations for projectile penetration.

6.2.2 Impact and Penetration Mechanisms

8. The techniques initiated in this study to examine the impact and penetration events should be further developed.
9. Ultra high speed and high speed photography should be used to assess the energy transferred to spall products.

10. The graphite detector technique which was developed during this study should be used for a more detailed examination of front face spalling, including an examination of the target parameters which influence spalling.

11. The deceleration of the projectile within the material should be studied in more detail.

12. Stress wave propagation and attenuation within an impacted material should be further investigated.

13. Methods of inducing projectile instability, both before and during penetration, should be further explored.

REFERENCES

ADELI, H., AMIN, A.M., SIERAKOWSKI, R.L. (1985) : "Damage Prediction for Impacted Concrete Structures", Proceedings of the Second Symposium on Interaction of Non-Nuclear Munitions with Structures, Florida, April 1985, pp. 326-332.

ALLEN, R.T. (1974) : "Prediction of the Deceleration of an Earth Penetrating Vehicle", Informal Report SSS-IR-74-2192, April 1974, Systems Science and Software, La Jolla, California.

AMERICAN CONCRETE INSTITUTE COMMITTEE 544(1973) : "State-of-the-Art Report on Fiber Reinforced Concrete", Proceedings of the ACI (American Concrete Institute Journal), Volume 70, Part 2, No. 11, pp. 729-744, November 1973.

AMERICAN CONCRETE INSTITUTE COMMITTEE 54 (1978): "Measurement of Properties of Fiber Reinforced Concrete", Proceedings of the ACI (American Concrete Institute Journal), Volume 75, No. 7, pp. 284-289, July 1978.

AMERICAN CONCRETE INSTITUTE (1966) : "Shotcreting", Special Publication No. 14, ACI Committee 506, Detroit, 1966.

ANDERSON, W.F., WATSON, A.J., JOHNSON, M.R. (1980) : "The Properties of an Elastomeric and Rock Composite", Final Report, MOD Agreement AT/2031/082MV, June 1980.

AUSTIN, C.F., PRINGLE, J.K. (1971) : "Variables of Concrete and Their Effect on Penetration by Projectiles (U)", Naval Weapons Center, November 1971, R73/471.

BACKMAN, M.E., GOLDSMITH, W. (1978) : "The Mechanics of Penetration of Projectiles into Targets", International Journal of Engineering Science, Volume 16, No. 1, pp. 1-99, 1978.

BARR, B.I.G., LIU, K., DOWERS, R.C. (1982) : "A Toughness Index to Measure the Energy Absorption of Fibre Reinforced Concrete", The International Journal of Cement Composites and Lightweight Concrete, Volume 4, No. 4, pp. 221-227, November 1982.

BERNARD,R.S. (1976) : "Development of a Projectile Penetration Theory, Report 2. Deep Penetration Theory for Homogeneous and Layered Targets", Army Engineer Waterways Experiment Station, Vicksburg, Mississippi, February 1976.

BERNARD, R.S. (1980) : "Earth Penetration Research", Structures Laboratory, US Army Corps of Engineers Information Exchange Bulletin, Volume 0-80-4, October 1980.

BERNARD, R.S., HANAGUD, S.V. (1975) : "Development of a Projectile Penetration Theory, Report 1. Penetration Theory for Shallow to Moderate Depths", Army Engineer Waterways Experiment Station, Vicksburg, Mississippi, June 1975.

BERRIAUD, C., VERPEAUX, P., JAMET, R. (1982) : "Concrete Wall Perforation by Rigid Missile", Proceedings of the Symposium on Concrete Structures Under Impact and Impulsive Loading, Berlin, June 1982, pp. 358-367.

BIENIAWSKI, Z.T. (1968) : "An Application of High Speed Photography to the Determination of Fracture Velocity in Rock", Proceedings of the 8th International Congress on High speed Photography, 1968, pp. 440-443.

BIJEN, J. (1983) : "Durability of Some Glass Fiber Reinforced Cement Composites", American Concrete Institute Journal, July-August, 1983, pp. 305-311.

BRITISH STANDARDS INSTITUTION (1972) : The Structural Use of Concrete, Part 1 : Design, Materials and Workmanship, CP 110 : Pt 1 : 1972.

BRITISH STANDARDS INSTITUTION (1975) : BS 812 : Methods for Sampling and Testing of Mineral Aggregates, Sands and Fillers, Part 2 : Physical Properties, Part 3 : Mechanical Properties.

BRITISH STANDARDS INSTITUTION (1978) : BS 12 : Specification for Ordinary and Rapid-hardening Portland Cement. Composition, Manufacture and Chemical and Physical Properties.

BRITISH STANDARDS INSTITUTION (1973) : BS 882, 1201 : Specifications for Aggregates for Natural Sources for Concrete (Including Granolithic), Part 2; Metric Units.

BRITISH STANDARDS INSTITUTION (1970) : BS 1881 : Methods of Testing Concrete, Part 3 : Methods of Making and Curing Test Specimens, Part 4 : Methods of Testing Concrete for Strength.

BRITISH STANDARDS INSTITUTION (1971) : BS 4408, Part 4 : Recommendations for Non-destructive Methods of Test for Concrete; Surface Hardness Methods.

BRITISH STANDARDS INSTITUTION (1974) : BS 4408, Part 5 : Recommendations for Non-destructive Methods of Test for Concrete; Measurement of the Velocity of Ultrasonic Pulses in Concrete.

BUTLER, D.K. (1975) : "An Analytical Study of Projectile Penetration into Rock", Army Engineer Waterways Experiment Station, Vicksburg, Mississippi, AEWES-TR-5-75-7.

CHABOWSKI, A.J., BRYDEN-SMITH, D.W. (1980) : "Internal Fracture Testing of In-Situ Concrete : A Method of Assessing Compressive Strength", Building Research Establishment Information Paper IP 22/80, October 1980.

CHAVEZ, D.J., CASSINO, V. (1975) : "Effect of Pavement Design on Cratering Damage from Penetrating Weapons", Eric H. Wang Civil Engineering Research Facility, University of New Mexico, October 1975.

CLIFTON, J.R. (1982) : "Penetration Resistance of Concrete : A Review", U.S. National Bureau of Standards, Washington, D.C., January 1982.

CLIFTON, J.R., KNAB, L.I. (1983) : "Impact Testing of Concrete", Cement and Concrete Research, Volume 13, No. 4, pp. 541-548, 1983.

COCHRAN, W.G., COX, G.M. (1957) : "Experimental Designs", Published Wiley Publications, New York, 1957

CONCRETE INTERNATIONAL (1981) : State-of-the-Art Assessment of Sprayed Concrete Production - Complete Issue, Volume 3, No. 1, January 1981.

CONCRETE SOCIETY (1980) : "The Concrete Society Code of Practice for Sprayed Concrete", Publications Sales Unit, Cement and Concrete Association, Wexham Springs, Slough, SL3 6PL. Reference Number 53.030.

DEERE, D.U. (1964) : "Technical Description of Rock Cores for Engineering Purposes", Rock Mechanic and Engineering Geology, Volume 1, No. 1, pp. 17-22.

DEERE, D.U., MILLER, R.P. (1966) : "Engineering Classification and Index Properties for Intact Rock"; Technical Report No AFWL-TR-65-116, Air Force Weapons Laboratory, Alberquerque, New Mexico, December 1966.

DEGEN, P.P. (1980) : "Perforation of Reinforced Concrete by Rigid Missiles", Journal of the Structural Division, Proceedings of the American Society of Civil Engineers, Volume 106, ST. 7, July 1980.

DENSON, R., MONAHAN, A. (1980) : "SACON - A Candidate for MOUT Ranges", Structures Laboratory, US Army Corps of Engineers. Information Exchange Bulletin, Volume 0-80-4, October 1980.

EDINGTON, J., HANNANT, D.J. (1972) : "Steel Fibre Reinforced Concrete, The Effect of Fibre Orientation of Compaction by Vibration", Materials and Structures, Volume 5,No. 25, pp. 41-44. January/February 1972.

EULER, L. (c. 1750) : "Neue Grundsvatze der Artillerie"; Berlin, 1745, reprinted as "Euler's Opera Omnia; Volume 14, Series II, Tenbner, Berlin, 1922.

FINCH, R.F. (1977) : "Acceptance Report on Christchurch Blocks"; Procurement Executive, Ministry of Defence, MVEE (Christchurch), Report No. 77508, April 1977.

FINCH, R.F. (1979) : "Ballistic Testing of Gravel Armour"; Procurement Executive, Ministry of Defence, MVEE (Christchurch), Report No. 78520, August 1979.

FORRESTAL, M.J., LONGCOPE, D.B. (1982) : "Closed-form Solutions for Forces on Conical-nosed Penetrators into Geological Targets with Constant Shear Strength", Mechanics of Materials, No. 1, 1982, pp. 285-295.

GIBBS, F.W., PRESCOTT, P.F. (1974) : "A Preliminary Investigation into Gravel Armour"; Technical Memo. 78450, Ministry of Defence, MVEE (Christchurch).

HADALA, P.F. (1975) : "Evaluation of Empirical and Analytical Procedures Used for Predicting the Rigid Body Motion of an Earth Penetrator", Army Engineer Waterways Experiment Station, Vicksburg, Mississippi, AEWES-MISC-PAPER-5-75-15.

HALDAR, A., MILLER, F.J. (1982) : "Local Effects Evaluation of Concrete Structures", Proceedings of RILEM-CEB-IABSE-Interassociation Symposium on Concrete Structures under Impact and Impulsive Loading, West Berlin, June 1982, pp. 345-357.

HANNANT, D.J. (1978) : "Fibre Cements and Fibre Concretes", Published John Wiley & Sons, Chichester, 1978.

HENAGER, C.H. (1981) : "Steel Fibrous Shotcrete : A Summary of the State-of-the-Art", Concrete International, January 1981, pp. 50-58.

HENAGER, C.H. (1983) : "The Use of Steel-Fibre Reinforced Concrete in Containment and Explosive-resistant Structures", Proceedings of the Symposium on "The Interaction of Non-Nuclear Munitions with Structures", US Air Force Academy, Colorado, May 1983.

HIBBERT, A.P., HANNANT, D.J. (1978): "The Design of an Instrumented Impact Test Machine for Fibre Concretes", Proceedings of the International Symposium on "Testing and Test Methods of Fibre Cement Composites", Sheffield, April 1978, pp. 107-120.

HUMMEL (1959) : "Das Beton", ABC, (Berlin, W.Ernst 1959).

HULSEWIG, M., STILP, A., PAHL, H. (1982) : "Behaviour of Fibre Reinforced Concrete Slabs under Impact Loading", Proceedings of RILEM-CEB-IABSE-IASS-Interassociation Symposium on "Concrete Structures under Impact and Impulsive Loading", West Berlin 1982, pp. 322-328.

JOHNSON, W. (1972) : "Impact Strength of Materials", Published by Edward Arnold Ltd., London 1972.

JONAS, G.H., ZUKAS, J.A. (1978) : "Mechanics of Penetration : Analysis and Experiment", International Journal of Engineering Science, Volume 16, No. 11, pp. 879-903, 1978.

LITTLEJOHN, G.S. (1980) : "Wet Process Shotcrete", Proceedings of the Symposium on Sprayed Concrete, The Concrete Society, April 1980.

LONGCOPE, D.B., FORRESTAL, M.J. (1983) : "Penetration of Targets Described by a Mohr-Coulomb Failure Criterion with a Tension Cut-off", Journal of Applied Mechanics, Volume 50, No. 2, June 1983, pp. 327-333.

MANGAT, P.S. (1976) : "Tensile Strength of Steel Fibre Reinforced Concrete", Cement and Concrete Research, Volume 6, pp. 245-252, 1976.

McCURRICH, L.H., ADAMS, M.A.J. (1973) : "Fibres in Cement and Concrete", Concrete, Volume 7, No. 4, Current Practice Sheet No. 5, pp. 51-53, April 1973.

MORGAN, D.R. (1981) : "Steel Fibre Shotcrete - A Laboratory Study", Concrete International, January 1981, pp. 70-74.

MORRIS, D.R. (1986) : Private Communication.

MURFF, J.D., COYLE, H.M. (1973) : "Prediction Method for Projectile Penetration", Journal of the Soil Mechanics and Foundations Division, American Society of Civil Engineers, Volume 99, No. SM11, pp. 1033-1037, November 1973.

NARAYANAN, R., KAREM-PALANJIAN, A.S. (1982) : "Factors Influencing the Workability of Steel-Fibre Reinforced Concrete - Part 1", Concrete, October 1982, pp. 45-48.

NAUS, D.J., WILLIAMSON, G.R. (1976) : "Ballistics Tests of Fibrous Concrete Dome and Plate Specimens", Construction Engineering Research Laboratory, Technical Report M-179, PO Box 4005, Champaign, IL 61820, April 1976.

NEVILLE, A.M. (1981) : "Properties of Concrete", Pitman Books Ltd., London, 1981.

PAKOTIPRAPHA, B., PAMA, R.P., LEES, L. (1974) : "Mechanical Properties of Cement Mortar with Randomly Oriented Short Steel Wires", Magazine of Concrete Research, Volume 26, No. 86, pp. 3-15, March 1974.

PETRY, L. (1910) : "Monographies de Systems d'Artillerie", Brussels, 1910.

PONCELOT, J.V.(1829) : "Cours de Mechanique Industrielle", 1829, First Edition.

PORT, W.J. (1980) : "Concrete Rendering as a Means of Increasing the Ballistic Resistance of Masonry-Type Buildings, and Evaluation of Slabcon", 1980.

PORT, W.J. (1980) : Private Communication.

RAMAKRISHNAN, V., COYLE, W.V., DAHL, F.L., SCHRADER, E.K. (1981) : "A Comparative Evaluation of Fiber Shotcretes", Concrete International, January 1981, pp. 59-69.

RAOUF, Z.A., AL-HASSINI, S.T.S., SIMPSON, J.W. (1976) : "Explosive Testing of Fibre-Reinforced Cement Composites", Concrete, Volume 10, No. 4, pp. 28-30, April 1976.

RAOUF, Z.A., HUSSAIN, S. (1984) : "Technical Notes : Some Properties of Steel Fibre Concrete at Early Ages", International Journal of Cement Composites and Lightweight concrete, Volume 6, No. 2, May 1984, pp. 117-121.

RESAL, H. (1895) : "Sur la Penetration d'un Projectile dans les Semifluides et les Solides, Cr.20, pp. 397-401, On file at Princeton University, USA.

RILEM TECHNICAL COMMITTEE 19-FRC (1977) : "Fibre Concrete Materials", Materials and Structures, Volume 10, No. 56, pp. 103-120, 1977.

ROBINS, B. (1742) : "New Principles of Gunnery", London 1742.

ROHANI, B. (1975) : "Analysis of Projectile Penetration Into Concrete and Rock Targets", Army Engineer Waterways Experimental Station, Vicksburg, Mississippi, AEWES-MISC-PAPER-S-75-25, September 1975.

ROMUALDI, J.P., MANDEL, J.A. (1964) : "Tensile Strength of Concrete Affected by Uniformly Distributed and Closely Spaced Short Lengths of Wire Reinforcement", Journal of the American Concrete Institute, Proceedings, Volume 61, No. 6, pp. 657-672, June 1964.

ROSS, B., HANAGUD, S.V. (1971) : "Penetration Studies of Ice with Application to Arctic and Subarctic Warfare; Final Report, Phase IV", Submarine Arctic Warfare and Scientific Program, Contract No. 00014-68-A-0243, Stanford Research Institute, Menlo Park, California, April 1971.

ROYAL ULSTER CONSTABULARY (1976) : "Tests on Bullet Resistant Qualities of "Steelcrete" and "Polycrete"", Internal Communication, January 1976.

RYAN, T. (1975) : "Steel Fibres in Gunite-An Appraisal", Tunnels and Tunnelling, July 1975, pp. 74-76.

SEDGEWICK, R.T., HAGEMAN, L.J., HERRMANN, R.E., WADELL, J.L. (1978) : "Numerical Investigations in Penetration Mechanics", International Journal of Engineering Science, Volume 16, No. 11, pp. 859-869, 1978.

SHAH, S.P., RANGAN, B.V. (1971) : "Fibre Reinforced Concrete Properties" Journal of the American Concrete Institute, Title No. 68-14, pp. 126-135, February 1971.

SLITER, G.E. (1980) : "Assessment of Empirical Concrete Impact Formulas", Journal of the Structural Division, American Society of Civil Engineers, Volume 106, No. ST. 5, pp. 1023-1045, May 1980.

SPRAYED CONCRETE SYMPOSIUM (C180) (1980) : Proceedings of the Symposium on Sprayed Concrete, London, April 1980.

SWAMY, R.N. (1974) : "The Technology of Steel-Fibre Reinforced Concrete for Practical Applications", Proceedings of the Institution of Civil Engineers, Part 1, August 1974, pp. 143-159.

SWAMY, R.N., JOJAGHA, A.H. (1982) : "Impact Resistance of Steel Fibre Reinforced Lightweight Concrete", The International Journal of Cement Composites and Lightweight Concrete, Volume 4, No. 4, November 1982, pp. 209-220.

SWAMY, R.N., RIGBY, G. (1971) : "Dynamic Properties of Hardened Paste, Mortar, and Concrete", Materiaux et Constructions, Volume 4, No. 19, 1971, pp. 13-40.

SWAMY, R.N., STAVRIDES, H. (1976) : "Some Statistical Considerations of Steel Fibre Composites", Cement and Concrete Research, Volume 6, pp. 201-216, 1976.

TATTERSALL, G.H., URBANOWICZ, C.R. (1974) : "Bond Strength in Steel-Fibre-Reinforced Concrete", Magazine of Concrete Research, Volume 26, No. 87, pp. 105-113, June 1974.

VANZANT, B.W. (1963) : "Dynamic Rock Penetration Tests at Atmospheric Pressure", Proceedings of the Fifth Symposium on Rock Mechanics, University of Minnesota, May 1962, pp. 61-91.

VERHAGEN, A.H. (1978) : "Testing of Fibre Reinforced Concrete on Impact", Proceedings of the International Symposium "Testing and Test Methods of Fibre Cement Composites", Sheffield, April 1978, pp. 99-105.

VISALVANICH, K., NAAMAN, A.E. (1983) : "Fracture Model for Fiber Reinforced Concrete", ACI Journal, Title No. 80-14, March-April 1983, pp. 128-138.

WATSON, A.J., ANDERSON, W.F., ARCHER, B. (1979) : "Properties of Concrete when Subjected to High Rates of Strain", MOD Agreement AT/2031/087/RAR, Report No. 4195/00/06, December 1979.

WATSON, A.J., ANDERSON, W.F., ARCHER, B. (1985): "Properties of Concrete when Subjected to High Rates of Stress", Final Report, MOD Agreement AT/2031/087/RAR, July 1985.

WALTON, P.L., MAJUMDAR, A.J. (1978) : "Properties of Cement Composites Reinforced with Kevlar Fibres", Building Research Establishment Current Paper No. CP 57/78, July 1978.

WECHARATANA, M., SHAH, S.P (1983) : "A Model for Predicting Fracture Resistance of Fiber Reinforced Concrete", Cement and Concrete Research, Volume 13, pp. 819-829, 1983.

WILKINS, M.L. (1978) : "Mechanics of Penetration and Perforation", International Journal of Engineering Science, Volume 16, No. 11, pp. 793-807, 1978.

WOLFE, W.E., COLTHARP, D.R. (1985) : "Predicting Concrete Spall Resulting from Dynamic Loading", Proceedings of the Second Symposium on "The Interaction of Non-nuclear Munitions with Structures", Florida, USA, April 1985.

WOLFERSBERGER, J.R. (1985) : "Concrete Breaching Data Base Search and Concrete Penetration Analysis", Proceedings of the Second Symposium on "The Interaction of Non-nuclear Munitions with Structures", Florida, USA, April 1985.

YOUNG, C.W. (1969) : "Depth Penetration for Earth-penetrating Projectiles", Journal of the Soil Mechanics and Foundations Division, American Society of Civil Engineers, Volume 95, No. SM 3, pp. 803-817, May 1969.

YOUNG, C.W. (1972) : "Empirical Equations for Predicting Penetration Performance in Layered Earth Materials for Complex Penetrator Configurations", Sandia Laboratories, Alberquerque, New Mexico, SC-DR-720523, December 1972.

ZAID, A.I.O., EL-KALAY, A., TRAVIS, F.W., (1973) : "An Examination of the Perforation of a Mild Steel Plate by a Flat-Ended Cylindrical Projectile", International Journal of Mechanical Science, Vol. 15, Part 1, pp. 129-143, 1973.

APPENDICES

APPENDIX I

PROGRESS REPORTS AND PUBLICATIONS

PROGRESS REPORTS:

ANDERSON, W.F., WATSON, A.J. and ARMSTRONG, P.J., 'Projectile penetration into composite materials'.

Report No	4167/09/01	March 1981	122pp
	4167/09/02	September 1981	69pp
	4167/09/03	March 1982	51pp
	4167/09/04	September 1982	57pp
	4167/09/05	March 1983	97pp

PUBLICATIONS:

ANDERSON, W.F., WATSON, A.J. and ARMSTRONG, P.J. 'High velocity projectile impact on fibre reinforced concrete'. Proc. Interassociation Symposium on Concrete Structures Under Impact and Impulsive Loading, Berlin, pp.368-378 (1982).

ANDERSON, W.F., WATSON, A.J. and ARMSTRONG, P.J. 'High velocity penetration into fibre reinforced concrete materials - protection of buildings'. Proc. Symposium on the Interaction of Non-Nuclear Munitions with Structures, Colorado Springs, Vol.1, pp.17-22 (1983).

ANDERSON, W.F., WATSON, A.J. and ARMSTRONG, P.J. 'Fibre reinforced concretes for the protection of structures against high velocity impact'. Proc. Int.Conf. on Structural Impact and Crashworthiness, London, Vol.2, pp.687-695 (1984).

APPENDIX II

MANUFACTURERS AND SUPPLIERS OF MATERIALS AND EQUIPMENT

II.1 Materials

II.1.1 Concrete Materials

Ordinary Portland Cement	Blue Circle Ltd Hope Cement Works Hope Derbyshire
Zone 2 limestone sand	Tarmac Roadstone Ltd Dale Road Matlock Derbyshire DE4 3PL
10mm single size limestone	Tarmac Roadstone Ltd Dale Road Matlock Derbyshire DE4 3PL
10mm single size basalt	Tarmac Roadstone Ltd Dale Road Matlock Derbyshire DE4 3PL
10mm single size river gravel	ARC Eastern (Hemington Quarry) Ashby Road Shepshed Nr Loughborough Leicestershire LE12 9BU

II.1.2 Fibres

All of the following were received from MVEE (Christchurch);

38 x 0.3mm diameter mild steel circular section
27 x 1.0mm diameter mild steel circular section
35 x 0.3mm diameter melt extract carbon steel
30 x 0.3mm diameter cold-drawn steel circular section

Melt extract carbon steel (ME) 25 x 0.3mm diameter	Fibre Technology Winsey Way Somercotes Derbyshire D55 4LS

Circular drawn brass-coated indented carbon steel-Duoform -25 x 0.25mm diameter (DUO)	National Standard Co Ltd P O Box 23 Stourport Road Kidderminster DY11 7QX
Circular drawn brass-coated carbon steel - 25 x 0.25mm diameter (DRA)	National Standard Co Ltd P O Box 23 Stourport Road Kidderminster DY11 7QX
13mm and 37mm length Kevlar-29 (Type 970) polyamide (13K and 37K)	Du Pont de Nemours International S.A. 50-52, Route des Acacias Ch-1211 Geneva 24 Switzerland
37mm length FORTA FIBRE lattice-bundled Type W polypropylene (POL)	Forta Fibre Inc. World Agents 147 Broad Street Grove City Penna 16127 USA

II.2 Equipment

II.2.1 Specimen Production

Creteangle type ME pan mixer (capacity 0.113m³)	Edward Benton & Co Ltd Creteangle Works Brook Lane Ferring Worthing West Sussex BN12 5LP
100mm concrete cube moulds and siphon can equipment	KAYEX-CAPCO P O Box 19 Elton Park Works Hadleigh Road Ipswich Suffolk IP2 OHY
Kango 950 electric percussion hammer	Robson Power Tools 409 Petre Street Sheffield S4 8LL
Concrete coring drill and 100mm diameter diamond-tipped bit	ELE International Ltd Eastman Way Hemel Hempstead Herts HP2 7HB
Concrete saw and fibre blades	Clipper Manufacturing Co Barkby Road Leicester

125mm stroke length Linear Variable Displacement Transducer (LVDT)	Novatech Measurements Ltd 83 Castleham Road St Leonards on Sea East Sussex TN38 9NT

II.2.2 Ballistics Equipment

7.62mm A.P. and ball ammunition	Conjay Arms Co Ltd 118 Craven Park Road London NW1D 8QD
No 3 pressure housing and 7.62mm proof barrel	Woolwich Arsenal via MVEE Barrack Road Christchurch
Replacement 7.62mm proof barrel	QAD (Ordnance) SA & SAA Q.T.C Cold Meece Nr Stone Staffordshire ST15 OQR
Firing Solenoid	Phillips Control (Sales) Ltd Church Path Lynchford Road Farnborough Hants
Type E30-2 Constant Power Supply	Farnell Instruments Ltd Sandbeck Way Wetherby LS22 4DH
50mm focal length biconvex lenses	Griffin & George Bishop Meadow Road Loughborough Leicestershire LE11 ORG
Photodiode Circuitry	R S components Ltd P O Box 99 Corby Northants NN17 9RS
Racal-Dana 9903 and 9904 Electronic timers	Racal-Dana Instruments Ltd Duke Street Windsor Berkshire SL4 1SB

II.2.3 Computing and Data Acquisition

8-bit Petset 1 Analogue-Digital Converter	Connecticut Microcomputer Inc 34 Del Mar Drive Brookfield CT 06804 USA

Commodore 3032-32K Microcomputer Commodore 3022 Printer Computhink 400K dual disk drive Hewlett Packard 7470A Plotter	Datron Micro Centre 2 Abbeydale Road Sheffield 7
Photec IV 16mm high speed rotating prism camera	Hadland Photonics Ltd Newhouse Laboratories Newhouse Road Bovingdon Hemel Hempstead Hertfordshire HP3 OEL
Barr and Stroud ultra-high speed rotating mirror camera	Hadland Photonics Ltd (as above)
Xenon electronic flash unit	Hadland Photonics Ltd (as above)
1kW Cine Lights	Ron Harrison Photographic 77-79 London Road Sheffield 2
Gould OS4000 storage oscilloscope Gould OS4020 storage oscilloscope	Gould Advance Ltd Roebuck Road Hainault Essex 1G6 3UE
Biomation four channel transient recorder	Gould Advance Ltd (as above)
PLMS-10 electrical resistance strain gauges	Techni Measure Ltd Alexandra Buildings 59 Alcester Road Studley Warwickshire B80 7NJ

II.3 Sundries

Shell mould release oil	Shell Lubricants UK Manchester Lubricants Marketing Centr 7 Oxford Road Manchester
Capacitors, Resistors, Switches, Connectors, Silver-loaded conductive paint	R S Components Ltd P O Box 99 Corby Northants NN17 9RS
10mm perspex sheet 12mm perspex sheet 0.25mm acetate sheet	V T Plastics Ltd Shoreham Street Sheffield S1 4SR
Compressed Nitrogen	British Oxygen Co Ltd Bawtry Road Brinsworth Rotherham S60 5NT

Shim brass (0.001mm, 0.1mm, 0.25mm)	I M I Righton Ltd Tyler Street Sheffield S9 1GG
Paraffin Wax	J Preston Ltd Netherthorpe Road Sheffield S3 7EY
Plasticine	Peter Pan Playthings (1983) Ltd Bretton Way Bretton Peterborough PE3 8YA
12mm mild steel plate 75mm diameter mild steel section	Gardner Steel Ltd Clubmill Road Sheffield S6 2FH

APPENDIX III

RELATIONSHIP BETWEEN FIBRE VOLUME, THEORETICAL FIBRE WEIGHT AND PRACTICAL FIBRE WEIGHT

In theoretical treatments of fibre-reinforced composites, the included fibre is generally defined in terms of V_f, the volume of fibre present in the composite. This is not an appropriate quantity to allow the batching and manufacture of the material, for which a weight of fibre per weight of composite is more useful. However, two alternative treatments exist to relate fibre weight to a particular fibre volume;

i) In theoretical analysis;

$$W_f = \frac{\text{Weight of fibre}}{\text{Weight of matrix + weight of fibre}} \times 100 \text{ percent}$$

$$W_f = \frac{V_f\rho_f}{V_m\rho_m + V_f\rho_f} \times 100\% \qquad \text{...Eq.AIII.1}$$

Where W_f = 'theoretical' fibre weight

V = Volume

ρ = Density

f = Fibre

m = matrix

ii) In practical work

$$W'_f = \frac{\text{Weight of fibre}}{\text{Weight of matrix}} \times 100\%$$

$$W'_f = \frac{V_f\rho_f}{V_m\rho_m} \times 100\% \qquad \text{...Eq.AIII.2}$$

Where W'_f = 'practical' fibre weight

All other symbols are as above

In this study, the weight of fibre has, in all cases, been calculated as a percentage using equation AIII.2.

APPENDIX IV

COMPUTER PROGRAME FOR CRATER VOLUME ANALYSIS

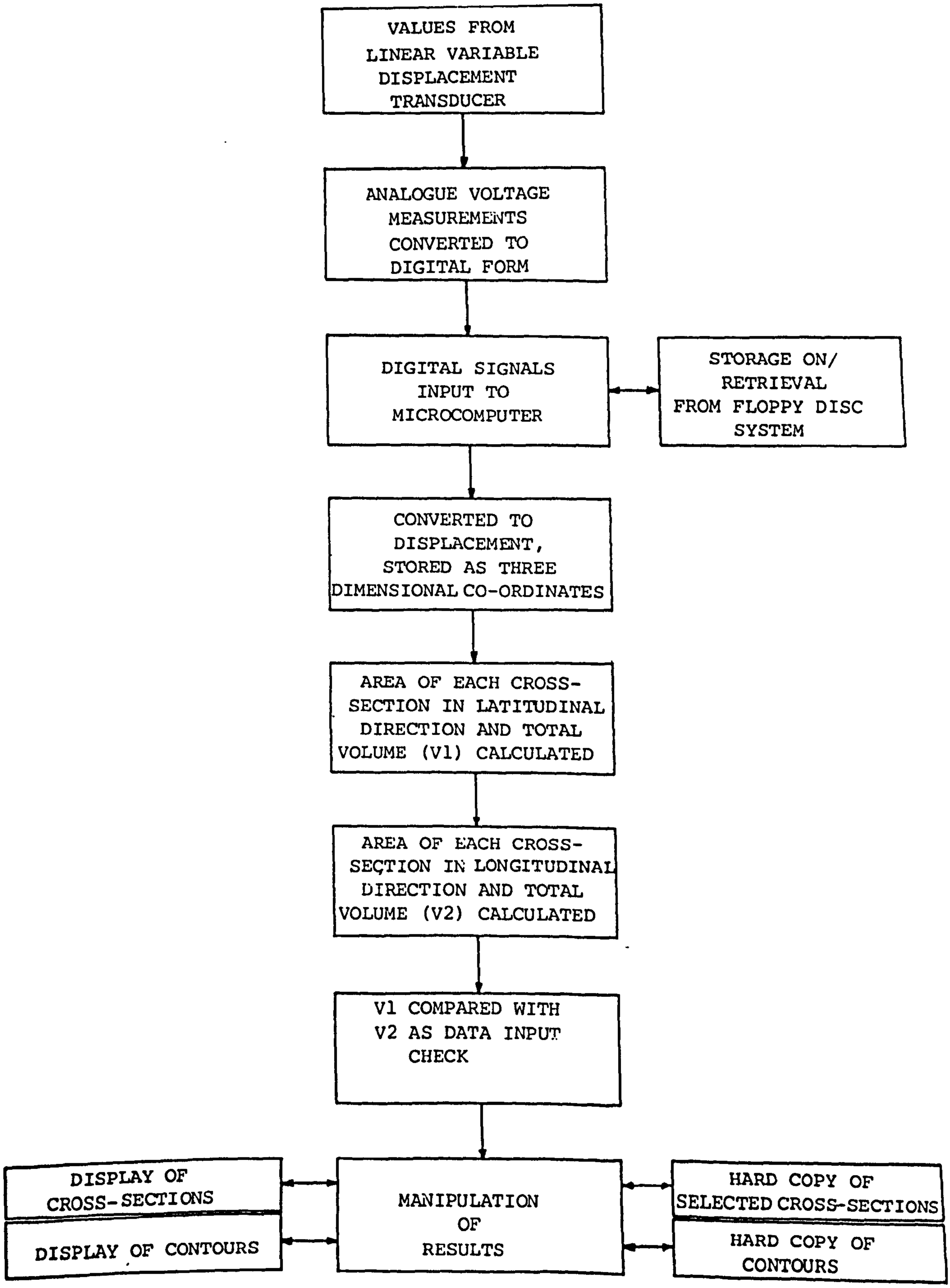

Flow Chart for Manipulation of Crater Data

```
 10 REM   CRATER VOLUME ANALYSIS II
 20 PRINT"■■                          MENU                              "
 30 PRINT"■CONNECTION AND MEASUREMENT DETAILS.....C"
 40 PRINT"■DATA STORAGE/DATA RETRIEVAL.............D"
 50 PRINT"■TO CALCULATE CRATER AREAS AND VOLUME...V"
 60 PRINT"■TO DISPLAY SELECTED CRATER PROFILES....T"
 70 PRINT"■TO PRINT SELECTED CRATER PROFILES......P"
 80 PRINT"■TO FINISH FOR NOW.....................F"
 90 GETC$:IFC$=""THEN90
100 IFC$="C"THEN GOSUB1000:GOTO20
110 IFC$="D"THEN GOSUB3000:GOTO20
120 IFC$="V"THEN GOSUB4000:GOTO20
130 IFC$="T"THEN GOSUB5000:GOTO20
140 IFC$="P"THEN GOSUB6000:GOTO20
150 IFC$<>"F"THEN20
160 END
1000 REM CONNECTION &MEASUREMENT DETAILS
1010 PRINT"■■TO INPUT THE DATA VIA THE KEYBOARD.....K"
1020 PRINT"■TO INPUT DATA VIA THE A/D CONVERTER....C"
1030 GETB$:IF B$=""THEN1030
1040 IFB$="K"THEN1060
1050 IFB$<>"C"THEN1010
1055 GOTO1915
1060 PRINT"■■TRANSDUCER STROKE LENGTH 125MM ? (Y/N)  "
1070 GETA$:IF A$=""THEN1070
1080 IFA$="Y"THEN1110
1090 IFA$<>"N"THEN1060
1100 GOTO1120
1110 SL%=125:GOTO1150
1120 PRINT"■■TYPE IN THE STROKE LENGTH IN MM"
1130 INPUTSL%
1140 PRINT"■                                                  "
1150 PRINT"■■STROKE LENGTH=■";SL%"MM"
1160 REM NEXT SEGMENT DEFINES THE GRID     SPACING AND SIZE
1170 PRINT"■                                                  "
1180 PRINT"■■SELECT REQUIRED PROFILE SPACING"
1190 PRINT"■■5MM      10MM      25MM     50MM "
1200 INPUTA%
1210 PRINT"■■■SELECT THE RELEVANT GRID SIZE AND PRESS "
1220 PRINT"■     THE APPROPRIATE KEY BELOW                    "
1230 PRINT"■                                                  "
1240 PRINT"■RED GRID.....................................R"
1250 PRINT"■BLACK GRID...................................B"
1260 PRINT"■WHITE GRID...................................W"
1270 GETD$:IFD$=""THEN 1270
1280 IFD$="R"THEN1320
1290 IFD$="B"THEN1370
1300 IFD$<>"W"THEN1210
1310 GOTO1420
1320 X%=100/A%:IFA%>5THENX%=X%+1
1330 PRINT"■ARE THE PARAMETERS CORRECT ? (Y/N)"
1340 GETE$:IFE$=""THEN1340
1350 IFE$="N"THEN1060
1360 DIMC(X%,X%):DIMD(X%,X%):GOTO1470
1370 X%=150/A%:IFA%>5THENX%=X%+1
1380 PRINT"■ARE THE PARAMETERS CORRECT ? (Y/N)"
1390 GETE$:IFE$=""THEN1390
```

```
1400 IFE$="N"THEN1060
1410 DIMC(X%,X%):DIMD(X%,X%):GOTO1470
1420 X%=200/A%:IFA%>5THENX%=X%+1
1430 PRINT"ARE THE PARAMETERS CORRECT ? (Y/N)"
1440 GETE$:IFE$=""THEN1440
1450 IFE$="N"THEN1060
1460 DIMC(X%,X%):DIMD(X%,X%)
1470 REM NEXT SEGMENT DEFINES GRADIENT          AND INTERCEPT OF THE LINEARI
1480 PRINT"PLACE THE PROBE ON THE GRID SURFACE    "
1490 PRINT" TO GIVE ZERO DISPLACEMENT OF THE PROBE "
1500 PRINT"                                       "
1510 PRINT"    INPUT THE CORRESPONDING VOLTAGE    "
1520 REM THIS VOLTAGE IS THE INTERCEPT AT              DISPLACEMENT = 0
1530 INPUTC:C=(INT(C*50+0.5))/50
1540 PRINT"       EXTEND THE PROBE TO GIVE"SL%"MM(MAXIMUM) DISPLACEMENT
1550 PRINT"                                       "
1560 PRINT"    INPUT THE CORRESPONDING VOLTAGE    "
1570 INPUT VE
1580 M=(VE-C)/SL%
1590 PRINT" ARE THE PROBE PARAMETERS CORRECT? (Y/N)"
1600 GETF$:IF F$=""THEN1600
1610 IFF$="N"THEN1480
1620 PRINTTHE PROBE SHOULD NOW BE PLACED IN THE   "
1630 PRINT"TOP LEFT-HAND CORNER OF THE GRID        ":PRINT
1640 PRINT"WORK FROM LEFT TO RIGHT ONLY, ONE ROW    "
1650 PRINT"     AT A TIME,INPUTTING THE VOLTAGE    "
1660 PRINT"NO MATTER WHAT SPACING IS USED, ALWAYS, "
1670 PRINT"     BEGIN AND END ON THE GRID EDGE     "
1680 X=X%*X%
1690 POKE53,120
1700 FOR K=1TOX
1710 INPUTP:IF P=0THENP=C
1720 POKE(30976+K),INT(P*50+0.5):H=PEEK(30976+K)/50:PRINTH
1730 T1=INT(K/1000)
1740 T2=INT(K/100)-T1*10
1750 T3=INT(K/10)-T1*100-T2*10
1760 T4=INT(K)-T1*1000-T2*100-T3*10
1770 POKE33270,T1+176:POKE33271,T2+176:POKE33272,T3+176:POKE33273,T4+176
1780 NEXTK
1790 PRINT"       I        J       DISPLACEMENT(MM)   "
1800 FORI=1TOX%
1810 FORJ=1TOX%
1820 D(I,J)=((PEEK(30976+J+(I-1)*X%)/50)-C)/M
1830 PRINT"        "I"      "J"              "D(I,J)"      "
1840 NEXTJ
1850 NEXTI
1860 PRINT"IS THE DATA TO BE STORED ON DISC?(Y/N)   "
1870 GETG$:IFG$=""THEN1870
1880 IFG$="N"THEN GOTO1910
1890 IFG$<>"Y"THEN1860
1900 GOSUB3000
1910 RETURN
1915 REM NEXT SEGMENT ALLOWS DIRECT INPUT                    FROM AN A/D CONVERTER
1920 PRINTTRANSDUCER STROKE LENGTH 125MM ? (Y/N)   "
1930 GETA$:IF A$=""THEN1930
1940 IFA$="Y"THEN1970
1950 IFA$<>"N"THEN1920
1960 GOTO1980
1970 SL%=125:GOTO2010
1980 PRINTTYPE IN THE STROKE LENGTH IN MM"
```

```
1990 INPUTSL%
2000 PRINT"■                                    "
2010 PRINT"■STROKE LENGTH=■";SL%"MM"
2020 REM NEXT SEGMENT DEFINES THE GRID      SPACING AND SIZE
2030 PRINT"■                                    "
2040 PRINT"■SELECT REQUIRED PROFILE SPACING"
2050 PRINT"■5MM      10MM       25MM     50MM "
2060 INPUTA%
2070 PRINT"□■SELECT THE RELEVANT GRID SIZE AND PRESS "
2080 PRINT"■     THE APPROPRIATE KEY BELOW          "
2090 PRINT"■                                        "
2100 PRINT"■RED GRID.....................................R"
2110 PRINT"■BLACK GRID...................................B"
2120 PRINT"■WHITE GRID...................................W"
2130 GETD$:IFD$=""THEN 2130
2140 IFD$="R"THEN2180
2150 IFD$="B"THEN2230
2160 IFD$<>"W"THEN2070
2170 GOTO2280
2180 X%=100/A%:IFA%>5THENX%=X%+1
2190 PRINT"■ARE THE PARAMETERS CORRECT ? (Y/N)"
2200 GETE$:IFE$=""THEN2200
2210 IFE$="N"THEN1920
2220 DIMC(X%,X%):DIMD(X%,X%):GOTO2330
2230 X%=150/A%:IFA%>5THENX%=X%+1
2240 PRINT"■ARE THE PARAMETERS CORRECT ? (Y/N)"
2250 GETE$:IFE$=""THEN2250
2260 IFE$="N"THEN1920
2270 DIMC(X%,X%):DIMD(X%,X%):GOTO2330
2280 X%=200/A%:IFA%>5THENX%=X%+1
2290 PRINT"■ARE THE PARAMETERS CORRECT ? (Y/N)"
2300 GETE$:IFE$=""THEN2300
2310 IFE$="N"THEN1920
2320 DIMC(X%,X%):DIMD(X%,X%)
2330 POKE59459,0
2340 POKE59468,PEEK(59468)AND254
2350 Q=PEEK(59457):Q=0
2360 PRINT"□■PLACE THE PROBE ON GRID SURFACE TO GIVE "
2370 PRINT"■    ZERO DISPLACEMENT OF THE PROBE       "
2380 PRINT
2390 PRINT"■ PRESS THE BLUE BUTTON ON THE PROBE BOX "
2400 REM THIS IS THE DIGITAL VALUE AT                    DISPLACEMENT=0
2410 IF(PEEK(59469)AND2)=0THEN2410
2420 C=PEEK(59457):PRINT"■C="C
2430 T=TI
2440 IFTI<T+30THEN2440
2450 Q=PEEK(59457):Q=0
2460 PRINT"■EXTEND THE PROBE TO GIVE "SL%"MM
2470 PRINT"■      (MAXIMUM) DISPLACEMENT             "
2480 PRINT"■ PRESS THE BLUE BUTTON ON THE PROBE BOX "
2490 IF(PEEK(59469)AND2)=0THEN2490
2500 VE=PEEK(59457):PRINT"■VE="VE
2510 T=TI
2520 IFTI<T+30THEN2520
2530 Q=PEEK(59457):Q=0
2540 M=(VE-C)/SL%
2550 PRINT"■ ARE THE PROBE PARAMETERS CORRECT? (Y/N)"
2560 GETF$:IF F$=""THEN2560
2570 IFF$="N"THEN2330
2580 PRINT"□■THE PROBE SHOULD NOW BE PLACED IN THE   "
```

```
2590 PRINT"■TOP LEFT-HAND CORNER OF THE GRID          ":PRINT
2600 PRINT"■WORK FROM LEFT TO RIGHT ■ONLY,■ONE ROW    "
2610 PRINT"■ AT A TIME,PRESSING THE BUTTON EACH TIME"
2620 PRINT: PRINT"■■NO MATTER WHAT SPACING IS USED,■ALWAYS,■ "
2630 PRINT"■     BEGIN AND END ON THE GRID EDGE     ■"
2640 POKE53,120
2650 FORI=1TOX%
2660 FORJ=1TOX%
2670 IF(PEEK(59469)AND2)=0THEN2670
2680 C(I,J)=PEEK(59457):PRINTC(I,J)
2690 T=TI
2700 IFTI<T+30THEN2700
2710 Q=PEEK(59457):Q=0
2720 T=J+(I-1)*X%
2730 T1=INT(T/1000)
2740 T2=INT(T/100)-T1*10
2750 T3=INT(T/10)-T1*100-T2*10
2760 T4=INT(T)-T1*1000-T2*100-T3*10
2770 POKE33390,T1+176:POKE33391,T2+176:POKE33392,T3+176:POKE33393,T4+176
2780 NEXTJ
2790 NEXTI
2800 PRINT"■■     I          J          DISPLACEMENT(MM)    "
2810 FORI=1TOX%
2820 FORJ=1TOX%
2830 D(I,J)=INT((C(I,J)-C)/M+0.5)
2840 PRINT"     "I"        "J"                    "D(I,J)"   "
2850 NEXTJ
2860 NEXTI
2870 PRINT"■IS THE DATA TO BE STORED ON DISC?(Y/N)   "
2880 GETH$:IFH$=""THEN2880
2890 IFH$="N"THENGOTO2920
2900 IFH$<>"Y"THEN2870
2910 GOSUB3000
2920 RETURN
3000 REM DATA INPUT/DATA RETRIEVAL
3010 PRINT"■■ IS DATA TO BE STORED OR RETRIEVED?(S/R)"
3020 GETJ$:IFJ$=""THEN3020
3030 IFJ$="S"THEN3050
3040 IFJ$="R"THEN3250
3050 D$="":I$=""
3060 PRINT"■■          GIVE THE DATA A NAME          "
3070 INPUTD$
3080 PRINT"■DISC DRIVE NUMBER?"
3090 INPUTD:PRINT:PRINT"■DATE?":INPUTI$:PRINT
3100 #0DISK,D,"W",D$,I$
3110 R$=""
3120 #WDISK,R$
3130 R$=STR$(A%):#WDISK,R$
3140 R$=STR$(X%):#WDISK,R$
3150 FORI=1TOX%
3160 FORJ=1TOX%
3170 R$=STR$(D(I,J)):#WDISK,R$
3180 NEXTJ
3190 NEXTI
3200 PRINT"■          DATA NOW STORED ON DISC          "
3210 #CDISK
3220 PRINT"■   PRESS C TO CONTINUE     "
3230 GETK$:IFK$=""THEN3230
3240 RETURN
3250 REM DATA RETRIEVAL SEGMENT
```

```
3260 PRINT"■■TYPE IN DATAFILE NAME"
3270 INPUTD$:PRINT
3280 PRINT"■DISC DRIVE NUMBER?"
3290 INPUTD:PRINT
3300 I$="":R$=""
3310 $ODISK,D,"R",D$,I$
3320 PRINTD$;"BEING RECOVERED","DATE RECORDED";I$:PRINT
3330 $RDISK,R$:PRINTR$
3340 IFR$<>""THENA%=VAL(R$):GOTO3360
3350 GOTO3330
3360 $RDISK,R$:X%=VAL(R$)
3370 PRINT"■■      I        J       DISPLACEMENT(MM)"
3380 FORI=1TOX%
3390 FORJ=1TOX%
3400 $RDISK,R$:D(I,J)=VAL(R$)
3410 PRINT"      "I"      "J"           "D(I,J)"
3420 NEXTJ
3430 NEXTI
3440 PRINT"■GRID SPACING=";A%"MM":PRINT
3450 PRINT"■ARRAY SIZE=";X%"BY";X%"
3460 PRINT:PRINT:PRINT"■          DATA NOW RECOVERED          "
3470 $CDISK
3480 PRINT"      ■  PRESS C TO CONTINUE  ■          "
3490 GETL$:IFL$=""THEN3490
3500 RETURN
4000 REM NEXT SEGMENT CALCULATES AREA OF          EACH PROFILE AND TOTAL VOL
4010 IFA%=5THEN GOSUB10000:RETURN
4020 GOSUB11000:RETURN
5000 REM   NEXT SEGMENT DISPLAYS PROFILES                    AS REQUIRED
5010 PRINT"■■    EVERY NTH PROFILE MAY BE DISPLAYED  "
5020 PRINT"■   IN EITHER ROW OR COLUMN DIRECTION    "
5030 PRINT:PRINT:PRINT"  ■ DO YOU WISH TO RETURN TO MENU? Y/N ■ "
5040 GETW$:IF W$=""THEN5040
5050 IFW$="Y"THEN RETURN
5060 IFW$<>"N"THEN5030
5070 PRINT"■■    IF N=          NUMBER OF PROFILES=   "
5080 FORI=1TO10
5090 G%=INT(X%/I+.5)
5100 PRINT"      "(I)"              "G%"          "
5110 NEXTI
5120 PRINT:PRINT"■    INPUT THE VALUE OF N REQUIRED    "
5130 INPUTN%
5140 G%=INT(X%/N%+.5)
5150 PRINT"■■ EVERY "N%"TH PROFILE IS TO BE DISPLAYED"
5160 PRINT"■  THIS GIVES A TOTAL OF "G%" EACH WAY   "
5170 PRINT:PRINT:PRINT"■  ARE THE PROFILES TO BE DISPLAYED IN   "
5180 PRINT"■          ROWS OR COLUMNS? R/C          "
5190 GETX$:IFX$=""THEN5190
5200 IFX$="R"THEN5230
5210 IFX$<>"C"THEN5170
5220 GOTO5470
5230 REM   VDU PLOT, ROW DIRECTION
5240 FORI=1TOX%STEPN%
5250 PRINT"■■   PROFILE NUMBER "I", AREA="E(I)"MM2    "
5260 D1=0:PRINT:PRINT"■ MAGNIFICATION FACTOR? "
5270 INPUTM:PRINT"■"
5280 FORL=0TO24STEPM:FORJ=0TO39
5290 POKE32728+40*L+J,99:NEXTJ:NEXTL
5300 PRINTINT(5/M+.5)"MM":PRINT:PRINT:PRINT:
5310 PRINTINT(25/M+.5):PRINT:PRINT:PRINT:PRINT
```

```
5320 PRINTINT(50/M+.5):PRINT:PRINT:PRINT:PRINT
5330 PRINTINT(75/M+.5):PRINT:PRINT:PRINT:PRINT
5340 PRINTINT(100/M+.5):PRINT:PRINT"      ■ PRESS C TO CONTINUE ■"
5350 FORJ=1TOX%
5360 Y0=INT(M*D(I,J)/5+.5)
5370 X8=INT(32728+(Y0+2)*40-(X%-D1)*40/X%)
5380 IFX8>33728ORX8<32728THEN5420
5390 IFINT(Y0/2)=Y0/2THENY2=123:GOTO5410
5400 Y2=126
5410 POKEX8,Y2
5420 D1=D1+1
5430 NEXTJ
5440 GETY$:IFY$=""THEN5440
5450 NEXTI
5460 GOTO5000
5470 REM  NEXT SECTION DISPLAYS VARIOUS                PROFILES IN COLUMNS
5480 FORJ=1TOX%STEPN%
5490 PRINT"■■  PROFILE NUMBER "J",AREA="F(J)"MM2"
5500 D1=0:PRINT:PRINT"■  MAGNIFICATION FACTOR?":INPUTM:PRINT"■"
5510 FORI=0TO24STEPM:FORL=0TO39
5520 POKE32728+40*I+L,99:NEXTL:NEXTI
5530 PRINTINT(5/M+.5)"MM":PRINT:PRINT:PRINT
5540 PRINTINT(25/M+.5):PRINT:PRINT:PRINT:PRINT
5550 PRINTINT(50/M+.5):PRINT:PRINT:PRINT:PRINT
5560 PRINTINT(75/M+.5):PRINT:PRINT:PRINT:PRINT
5570 PRINTINT(100/M+.5):PRINT:PRINT"    ■    PRESS C TO CONTINUE   ■   "
5580 FORI=1TOX%
5590 Y0=INT(M*D(I,J)/5+.5)
5600 X0=INT(32728+(Y0+2)*40-(X%-D1)*40/X%)
5610 IFX0>33728ORX0<32728THEN5650
5620 IFINT(Y0/2)=Y0/2THENY1=123:GOTO5640
5630 Y1=126
5640 POKEX0,Y1
5650 D1=D1+1
5660 NEXTI
5670 GETZ$:IFZ$=""THEN5670
5680 NEXTJ
5690 GOTO5000
10000 REM AREA OF PROFILES AT 5MM SPACING

10010 REM        # ROWS TAKEN FIRST #
10020 S=0:VR=0:DIME(X%)
10030 FORI=1TOX%
10035 FORJ=1TOX%
10040 S=(D(I,1)+D(I,X%))/2
10050 S=S+D(I,J)
10060 NEXTJ
10070 REM   AREA OF ITH PROFILE=E(I)
10080 E(I)=A%*S
10090 NEXTI
10100 PRINT"■ARE PROFILE AREAS REQUIRED?(Y/N)
10110 GETM$:IFM$=""THEN10110
10120 IFM$="Y"THEN10150
10130 IFM$<>"N"THEN10100
10140 GOTO
10150 PRINT"■          ■          IN ROWS          ■          ":PRINT
10160 PRINT"■        PROFILE          AREA(MM2)          "
10170 FORI=1TOX%
10180 PRINT"          "(I)"              "E(I)"    "
10190 NEXTI
```

```
10200 PRINT"■              PRESS C TO CONTINUE              "
10210 GETH$:IFH$=""THEN10210
10220 REM   VOLUME SYMBOL IN ROW                    DIRECTION IS VR
10230 VR=(E(1)+E(X%))/2
10240 FORI=2TO(X%-1)
10250 VR=VR+E(I)
10260 NEXTI
10270 VR=VR*A%
10280 REM  AREA IS NOW CALCULATED IN                  COLUMN DIRECTION
10290 S=0:VC=0:DIMF(X%)
10300 FORJ=1TOX%
10310 S=(D(1,J)+D(X%,J))/2
10320 FORI=2TO(X%-1)
10330 S=S+D(I,J)
10340 NEXTI
10350 F(J)=A%*S
10360 NEXTJ
10370 PRINT"■■ARE AREAS REQUIRED(COLUMN)PROFILES?(Y/N)"
10380 GETP$:IFP$=""THEN10380
10390 IFP$="Y"THEN10420
10400 IFP$<>"N"THEN10370
10410 GOTO10490
10420 PRINT"■                ■ IN COLUMNS ■                "
10430 PRINT"■        PROFILE              AREA(MM2)          "
10440 FORJ=1TOX%
10450 PRINT"            "(J)"                  "F(J)"        "
10460 NEXTJ
10470 PRINT"          ■ PRESS C TO CONTINUE ■                "
10480 GETQ$:IFQ$=""THEN10480
10490 REM  VOLUME SYMBOL IN COLUMNS IS VC
10500 VC=(F(1)+F(X%))/2
10510 FORJ=2TO(X%-1)
10520 VC=VC+F(J)
10530 NEXTJ
10540 VC=VC*A%
10550 PRINT"■■ CRATER VOLUME (BY ROWS)="VR"MM3 "
10560 PRINT:PRINT"■ CRATER VOLUME (BY COLUMNS)="VC"MM3 "
10570 N=ABS(VR-VC)
10580 PRINT:PRINT"■ NUMERICAL DIFFERENCE="N
10590 MV=(VR+VC)/2
10600 PRINT:PRINT"■ MEAN VALUE FOR CRATER VOLUME="MV"MM3 "
10610 PRINT:PRINT"                ■ PRESS C TO CONTINUE ■          "
10620 GETR$:IFR$=""THEN10620
10630 RETURN
11000 REM PROFILE AREAS AT A% SPACING
11010 REM  -TRP.RULE WITH END CRN
11020 REM      #INITIALLY IN ROWS#
11030 DIME(X%):S=0:VR=0
11040 FORI=1TOX%
11050 IFX%<4THEN11120
11060 S=(D(I,1)+D(I,X%-1))/2
11070 FORJ=2TO(X%-2)
11080 S=S+D(I,J)
11090 NEXTJ
11100 GOTO11130
11110 REM      AREA SYMBOL IS E(I)
11120 E(I)=A%*(D(I,1)+D(I,X%-1))/2+(A%-5)*(D(I,X%-1)+D(I,X%))/2:GOTO11140
11130 E(I)=(A%*S)+(A%-5)*(D(I,X%-1)+D(I,X%))/2
11140 NEXTI
11150 PRINT"■■ ARE PROFILE AREAS IN ROWS REQUIRED(Y/N)"
```

```
11160 GETR$:IFR$=""THEN11160
11170 IFR$="Y"THEN11200
11180 IFR$<>"N"THEN11150
11190 GOTO11270
11200 PRINT"■                    ■  IN ROWS   ■              "
11210 PRINT"■        PROFILE          AREA(MM2)          "
11220 FORI=1TOX%
11230 PRINT"          "(I)"              "E(I)"          "
11240 NEXTI
11250 PRINT:PRINT"■  PRESS C TO CONTINUE   "
11260 GETS$:IFS$=""THEN11260
11270 REM  VOLUME SYMBOL IN ROWS IS VR
11280 VR=(E(1)+E(X%-1))/2
11290 IFX%<4THEN11330
11300 FORI=2TO(X%-2)
11310 VR=VR+E(I)
11320 NEXTI
11330 VR=A%*VR+((A%-5)*(E(X%-1)+E(X%))/2)
11340 REM  PROFILE AREAS IN COLUMNS IS                    NOW CALCULATED
11350 DIMF(X%):S=0:VC=0
11360 FORJ=1TOX%
11370 IFX%<4THEN11430
11380 S=(D(1,J)+D(X%-1,J))/2
11390 FORI=2TO(X%-2)
11400 S=S+D(I,J)
11410 NEXTI
11420 GOTO11450
11430 F(J)=A%*(D(1,J)+D(X%-1,J))/2+(A%-5)*(D(X%-1,J)+D(X%,J))/2
11440 GOTO11460
11450 F(J)=(A%*S)+(A%-5)*(D(X%-1,J)+D(X%,J))/2
11460 NEXTJ
11470 PRINT"■■ ARE PROFILE AREAS(COLUMNS)REQUIRED(Y/N)"
11480 GETT$:IFT$=""THEN11480
11490 IFT$="Y"THEN11520
11500 IFT$<>"N"THEN11470
11510 GOTO11600
11520 PRINT"                  ■ IN COLUMNS ■              "
11530 PRINT:PRINT"          PROFILE          AREA(MM2)          "
11540 FORJ=1TOX%
11550 PRINT"              "(J)"              "F(J)"          "
11560 NEXTJ
11570 PRINT:PRINT"■  PRESS C TO CONTINUE   "
11580 GETU$:IFU$=""THEN11580
11590 REM  VOLUME SYMBOL IN COLUMNS IS VC
11600 VC=(F(1)+F(X%-1))/2
11610 IFX%<4THEN11650
11620 FORJ=2TO(X%-2)
11630 VC=VC+F(J)
11640 NEXTJ
11650 VC=VC*A%+((A%-5)*(F(X%-1)+F(X%))/2)
11660 PRINT"■■ CRATER VOLUME(BY ROWS)="VR"MM3 "
11670 PRINT:PRINT"■ CRATER VOLUME(BY COLUMNS)="VC"MM3 "
11680 N=ABS(VR-VC)
11690 PRINT:PRINT"■ NUMERICAL DIFFERENCE="N
11700 MV=(VR+VC)/2
11710 PRINT:PRINT"■ MEAN CRATER VOLUME="MV"MM3 "
11720 PRINT:PRINT:PRINT"■  PRESS C TO CONTINUE   "
11730 GETV$:IFV$=""THEN11730
11740 RETURN
READY.
```

DERIVATION OF RESPONSE SURFACE COEFFICIENT EQUATIONS AND MICROCOMPUTER PROGRAM LISTING

V.1 Derivation of Response Surface Coefficient Equations

The following is based upon an approach documented by Cochran and Cox (1957).

CENTRAL COMPOSITE ROTATABLE DESIGN FOR THREE PRIMARY QUANTITATIVE INDEPENDENT VARIABLES

Coded Values			Arithmetical products of x_1, x_2, x_3						Actual Pen.Path Length (mm)
Water: Cement	Agg: Cement	Fibre Content							
x_1	x_2	x_3	x_1^2	x_2^2	x_3^2	x_1x_2	x_1x_3	x_2x_3	L_i
-1	-1	-1	1	1	1	1	1	1	L_1
1	-1	-1	1	1	1	-1	-1	1	L_2
-1	1	-1	1	1	1	-1	1	-1	L_3
1	1	-1	1	1	1	1	-1	-1	L_4
-1	-1	1	1	1	1	1	-1	-1	L_5
1	-1	1	1	1	1	-1	1	-1	L_6
-1	1	1	1	1	1	-1	-1	1	L_7
1	1	1	1	1	1	1	1	1	L_8
$-2^{\frac{3}{4}}$	0	0	$2^{\frac{3}{2}}$	0	0	0	0	0	L_9
$+2^{\frac{3}{4}}$	0	0	$2^{\frac{3}{2}}$	0	0	0	0	0	L_{10}
0	$-2^{\frac{3}{4}}$	0	0	$2^{\frac{3}{2}}$	0	0	0	0	L_{11}
0	$2^{\frac{3}{4}}$	0	0	$2^{\frac{3}{2}}$	0	0	0	0	L_{12}
0	0	$-2^{\frac{3}{4}}$	0	0	$2^{\frac{3}{2}}$	0	0	0	L_{13}
0	0	$2^{\frac{3}{4}}$	0	0	$2^{\frac{3}{2}}$	0	0	0	L_{14}
0	0	0	0	0	0	0	0	0	L_{15}
0	0	0	0	0	0	0	0	0	L_{16}
0	0	0	0	0	0	0	0	0	L_{17}
0	0	0	0	0	0	0	0	0	L_{18}
0	0	0	0	0	0	0	0	0	L_{19}
0	0	0	0	0	0	0	0	0	L_{20}

Then the coefficients are derived using the following development of the published solutions;

$$b_o = 0.166338 \sum_{i=1}^{20} L_i - 0.056791 \sum_{j=1}^{3} \sum_{i=1}^{20} (x_j^2 \, L_i)$$

$$b_j = 0.073224 \sum_{i=1}^{20} (x_j \, L_i)$$

$$b_{jk} = 0.125000 \sum_{i=1}^{20} (x_j x_k L_i)$$

$$b_{jj} = 0.062500 \sum_{i=1}^{20} (x_j^2 \, L_i) + 0.006889 \sum_{j=1}^{3} \sum_{i=1}^{20} (x_j^2 . L_i) - 0.056791 \sum_{i=1}^{20} L_i$$

[Cochran and Cox (1957)]

That is:

$$b_o = 0.166338 \sum_{i=1}^{20} L_i - 0.056791 \{[1.L_1 + 1.L_2 + 1.L_3 + 1.L_4 + 1.L_5 + 1.L_6 + 1.L_7 + 1.L_8 + 2^{\frac{3}{2}}.L_9 + 2^{\frac{3}{2}}.L_{10}] + [1.L_1 + 1.L_2 + 1.L_3 + 1.L_4 + 1.L_5 + 1.L_6 + 1.L_7 + 1.L_8 + 2^{\frac{3}{2}}.L_{11} + 2^{\frac{3}{2}}.L_{12}] + [L_1 + L_2 + L_3 + L_4 + L_5 + L_6 + L_7 + L_8 + 2^{\frac{3}{2}}.L_{13} + 2^{\frac{3}{2}}.L_{14}]\}$$

$$\therefore b_o = 0.166338 \sum_{i=1}^{20} L_i - 0.056791 \left[3 \sum_{i=1}^{8} L_i + 2^{\frac{3}{2}} \sum_{i=9}^{14} L_i\right] \quad \text{...Eq.4.2}$$

$$b_1 = 0.073224 \, [-1.L_1 + 1.L_2 - 1.L_3 + 1.L_4 - 1.L_5 + 1.L_6 - 1.L_7 + 1.L_8 - 2^{\frac{3}{4}}.L_9 + 2^{\frac{3}{4}} L_{10}]$$

$$\therefore b_1 = 0.073224 \left[\sum_{i=1}^{8} (-1)^i L_i + 2^{\frac{3}{4}} \sum_{i=9}^{10} (-1)^i L_i\right] \quad \text{...Eq.4.3}$$

$$b_2 = 0.073224 \, [-1.L_1 - 1.L_2 + 1.L_3 + 1.L_4 - 1.L_5 - 1.L_6 + 1.L_7 + 1.L_8 - 2^{\frac{3}{4}}.L_{11} + 2^{\frac{3}{4}}.L_{12}]$$

$$\therefore b_2 = -0.073224 \, [(L_1 + L_2 + L_5 + L_6) - (L_3 + L_4 + L_7 + L_8) + 2^{\frac{3}{4}}(L_{11} - L_{12})] \quad \text{...Eq.4.4}$$

$$b_3 = 0.073224 \, [-1.L_1 - 1.L_2 - 1.L_3 - 1.L_4 + 1.L_5 + 1.L_6 + 1.L_7 + 1.L_8 - 2^{\frac{3}{4}}.L_{13} + 2^{\frac{3}{4}}.L_{14}]$$

$$\therefore b_3 = -0.073224 \left[\sum_{i=1}^{4} .L_i - \sum_{i=5}^{8} .L_i + 2^{\frac{3}{4}}(L_{13} - L_{14})\right] \quad \text{...Eq.4.5}$$

$$b_{12} = 0.125000\ [1.L_1 - 1.L_2 - 1.L_3 + 1.L_4 + 1.L_5 - 1.L_6 - 1.L_7 + 1.L_8]$$

$$\therefore b_{12} = 0.125000\ [(L_1 + L_4 + L_5 + L_8) - (L_2 + L_3 + L_6 + L_7)] \quad \ldots \text{Eq.4.6}$$

$$b_{13} = 0.125000\ [1.L_1 - 1.L_2 + 1.L_3 - 1.L_4 - 1.L_5 + 1.L_6 - 1.L_7 + 1.L_8]$$

$$\therefore b_{13} = 0.125000\ [(L_1 + L_3 + L_6 + L_8) - (L_2 + L_4 + L_5 + L_7)] \quad \ldots \text{Eq.4.7}$$

$$b_{23} = 0.125000\ [1.L_1 + 1.L_2 - 1.L_3 - 1.L_4 - 1.L_5 - 1.L_6 + 1.L_7 + 1.L_8]$$

$$\therefore b_{23} = 0.125000\ [(L_1 + L_2 + L_7 + L_8) - (L_3 + L_4 + L_5 + L_6)] \quad \ldots \text{Eq.4.8}$$

$$b_{11} = 0.062500\ [1.L_1 + 1.L_2 + 1.L_3 + 1.L_4 + 1.L_5 + 1.L_6 + 1.L_7 + 1.L_8 + 2^{\frac{3}{2}}.L_9 + 2^{\frac{3}{2}}.L10] + 0.006889\ \{[1.L_1 + 1.L_2 + 1.L_3 + 1.L_4 + 1.L_5 + 1.L_6 + 1.L_7 + 1.L_8 + 2^{\frac{3}{2}}.L_9 + 2^{\frac{3}{2}}L_{10}] + [1.L_1 + 1.L_2 + 1.L_3 + 1.L_4 + 1.L_5 + 1.L_6 + 1.L_7 + 1.L_8 + 2^{\frac{3}{2}}.L_{11} + 2^{\frac{3}{2}}L._{12}] + [1.L_1 + 1.L_2 + 1.L_3 + 1.L_4 + 1.L_5 + 1.L_6 + 1.L_7 + 1.L_8 + 2^{\frac{3}{2}}.L_{13} + 2^{\frac{3}{2}}.L_{14}]\} - 0.056791 \sum_{i=i}^{20}.L_i$$

$$\therefore b_{11} = \frac{0.062500 \sum_{i=1}^{8} L_i + 2^{\frac{3}{2}} \sum_{i=9}^{10} L_i] + 0.006889\ [3 \sum_{i=1}^{8}.L_i + 2^{\frac{3}{2}} \sum_{i=9}^{14} L_i] - 0.056791 \sum_{i=1}^{20} L_i}{} \quad \ldots \text{Eq.4.9}$$

$$b_{22} = 0.062500\ [1.L_1 + 1.L_2 + 1.L_3 + 1.L_4 + 1.L_5 + 1.L_6 + 1.L_7 + 1.L_8 + 2^{\frac{3}{2}}.L_{11} + 2^{\frac{3}{2}}L_{12}] + 0.006889\ \{[1.L_1 + 1.L_2 + 1.L_3 + 1.L_4 + 1.L_5 + 1.L_6 + 1.L_7 + 1.L_8 + 2^{\frac{3}{2}}.L_9 + 2^{\frac{3}{2}}.L_{10}] + [1.L_1 + 1.L_2 + 1.L_3 + 1.L_4 + 1.L_5 + 1.L_6 + 1.L_7 + 1.L_8 + 2^{\frac{3}{2}}.L_{11} + 2^{\frac{3}{2}}.L_{12}] + [1.L_1 + 1.L_2 + 1.L_3 + 1.L_4 + 1.L_5 + 1.L_6 + 1.L_7 + 1.L_8 + 2^{\frac{3}{2}}.L_{13} + 2^{\frac{3}{2}}.L_{14}]\} - 0.056791 \sum_{i=1}^{20}.L_i$$

$$\therefore b_{22} = \frac{0.0625000\ [\sum_{i=1}^{8}.L_i + 2^{\frac{3}{2}} \sum_{i=1}^{12}.L_i] + 0.006889\ [3 \sum_{i=1}^{8}.L_i + 2^{\frac{3}{2}} \sum_{i=9}^{14}.L_i] - 0.056791 \sum_{i=1}^{20}.L_i}{} \quad \ldots \text{Eq.4.10}$$

$$b_{33} = 0.062500\ [1.L_1 + 1.L_2 + 1.L_3 + 1.L_4 + 1.L_5 + 1.L_6 + 1.L_7 + 1.L_8 + 2^{\frac{3}{2}}.L_{13} + 2^{\frac{3}{2}}.L_{14}] + 0.006889\ \{[1.L_1 + 1.L_2 + 1.L_3 + 1.L_4 + 1.L_5 + 1.L_6 + 1.L_7 + 1.L_8 + 2^{\frac{3}{2}}.L_9 + 2^{\frac{3}{2}}.L_{10}] + [1.L_1 + 1.L_2 + 1.L_3 + 1.L_4 + 1.L_5 + 1.L_6 + 1.L_7 + 1.L_8 + 2^{\frac{3}{2}}.L_{11} + 2^{\frac{3}{2}}.L_{12}] + [1.L_1 + 1.L_2 + 1.L_3 + 1.L_4 + 1.L_5 + 1.L_6 + 1.L_7 + 1.L_8 + 2^{\frac{3}{2}}.L_{13} + 2^{\frac{3}{2}}.L_{14}]\} - 0.056791 \sum_{i=1}^{20} L_i$$

$$\therefore b_{33} = \frac{0.062500\ [\sum_{i=1}^{8} L_i + 2^{\frac{3}{2}} \sum_{i=13}^{14} L_i] + 0.006889\ [3 \sum_{i=1}^{8} L_i + 2^{\frac{3}{2}} \sum_{i=9}^{14} L_i] - 0.056791 \sum_{i=1}^{20} L_i}{\text{...Eq.4.11}}$$

V.2 Computer listings for relevant programs

A program was written in BASIC for the Commodore PET 3032 micro-computer. This carried out the following:

i) Calculated values of b_o-b_{33} using the measured actual penetration path length values (L_i).

ii) Calculated the predicted path lengths for the twenty actual path length combinations and carried out a statistical λ^2 - test, indicating the lack of fit of the prediction equation relative to the measured results.

iii) Fitted all of the 5^3=125 combinations of the 3 x-variables to the prediction equation to locate the combination yielding the minimum penetration depth.

A listing of the program is given overleaf.

COMPUTER PROGRAM FOR

APPLICATION OF RESPONSE SURFACE THEORY

```
10 REM   CO-EFFICIENT CALCULATION
20 DIML(20):DIMP(20)
30 PRINT"TYPE IN PEN. DEPTHS IN ORDER"
40 FORI=1TO20
50 INPUTL(I):PRINT"L("I")="L(I)"MM"
60 NEXT
70 Q=0
80 FORI=1TO8
90 Q=Q+L(I)
100 NEXT
110 M=0
120 FORI=9TO20
130 M=M+L(I)
140 NEXT
150 R=Q+M
160 M=0
170 FORI=9TO14
180 M=M+L(I)
190 NEXT
200 S=M*(2^1.5)
210 B0=0.166338*R-0.056791*(3*Q+S)
220 M=0
230 M=-L(1)+L(2)-L(3)+L(4)-L(5)+L(6)-L(7)+L(8)
240 N=0
250 N=-(2^.75)*(L(9)-L(10))
260 B1=0.073224*(M+N)
270 T=L(11)-L(12)
280 B2=-0.073224*((L(1)+L(2)+L(5)+L(6))-(L(3)+L(4)+L(7)+L(8))+(2^.75)*T)
290 M=0
300 M=-L(1)-L(2)-L(3)-L(4)+L(5)+L(6)+L(7)+L(8)
310 N=0
320 N=-(2^.75)*(L(13)-L(14))
330 B3=0.073224*(M+N)
340 B4=0.125000*((L(1)+L(4)+L(5)+L(8))-(L(2)+L(3)+L(6)+L(7)))
350 B5=0.125000*((L(1)+L(3)+L(6)+L(8))-(L(2)+L(4)+L(5)+L(7)))
360 B6=0.125000*((L(1)+L(2)+L(7)+L(8))-(L(3)+L(4)+L(5)+L(6)))
370 M=0:N=0:P=0
380 K=2^1.5
390 B4=0.125000*((L(1)+L(4)+L(5)+L(8))-(L(2)+L(3)+L(6)+L(7)))
400 B5=0.125000*((L(1)+L(3)+L(6)+L(8))-(L(2)+L(4)+L(5)+L(7)))
410 B6=0.125000*((L(1)+L(2)+L(7)+L(8))-(L(3)+L(4)+L(5)+L(6)))
420 M=0:N=0:P=0
430 K=2^1.5
440 M=K*(L(9)+L(10))
450 N=K*(L(11)+L(12))
460 P=K*(L(13)+L(14))
470 B7=0.062500*(Q+M)+0.006889*(3*Q+S)-0.056791*R
480 B8=0.062500*(Q+N)+0.006889*(3*Q+S)-0.056791*R
490 B9=0.062500*(Q+P)+0.006889*(3*Q+S)-0.056791*R
```

```
500 PRINT" THE CO-EFFICIENTS ARE:
510 PRINT:PRINT"B0="B0
520 PRINT:PRINT"B1="B1
530 PRINT:PRINT"B2="B2
540 PRINT:PRINT"B3="B3
550 PRINT:PRINT"B12="B4
560 PRINT:PRINT"B13="B5
570 PRINT:PRINT"B23="B6
580 PRINT:PRINT"B11="B7
590 PRINT:PRINT"B22="B8
600 PRINT:PRINT"B33="B9
700 PRINT:PRINT" PRESS C TO CONTINUE "
710 GETA$:IFA$=""THEN710
720 IFA$<>"C"THEN710
730 P(1)=B0-B1-B2-B3+B4+B5+B6+B7+B8+B9
740 P(2)=B0+B1-B2-B3-B4-B5+B6+B7+B8+B9
750 P(3)=B0-B1+B2-B3-B4+B5-B6+B7+B8+B9
760 P(4)=B0+B1+B2-B3+B4-B5-B6+B7+B8+B9
770 P(5)=B0-B1-B2+B3+B4-B5-B6+B7+B8+B9
780 P(6)=B0+B1-B2+B3-B4+B5-B6+B7+B8+B9
790 P(7)=B0-B1+B2+B3-B4-B5+B6+B7+B8+B9
800 P(8)=B0+B1+B2+B3+B4+B5+B6+B7+B8+B9
810 P(9)=B0-2^.75*B1+(2^.75)^2*B7
820 P(10)=B0+2^.75*B1+(2^.75)^2*B7
830 P(11)=B0-2^.75*B2+(2^.75)^2*B8
840 P(12)=B0+2^.75*B2+(2^.75)^2*B8
850 P(13)=B0-2^.75*B3+(2^.75)^2*B9
860 P(14)=B0+2^.75*B3+(2^.75)^2*B9
870 P(15)=B0
880 P(16)=B0
890 P(17)=B0
900 P(18)=B0
910 P(19)=B0
920 P(20)=B0
930 PRINT"                  PATH LENGTHS                    "
940 PRINT:PRINT"   SLAB        PREDICTED  (MM)  ACTUAL    "
950 FORI=1TO10
960 PRINT:PRINT"     "I"          "P(I)"     "L(I)"
970 NEXTI
980 PRINT"PRESS C TO CONTINUE"
990 GETA$:IFA$=""THEN990
1000 IFA$<>"C"THEN990
1010 PRINT"                  PATH LENGTHS                    "
1020 PRINT:PRINT"   SLAB        PREDICTED  (MM)  ACTUAL    "
1030 FORI=11TO20
1040 PRINT:PRINT"     "I"          "P(I)"     "L(I)"
1050 NEXTI
1060 PRINT"PRESS C TO CONTINUE"
1070 GETC$:IFC$=""THEN1070
1080 IFC$<>"C"THEN1070
```

```
1090 REM TO CALCULATE SIGNIFICANCE
1100 S=0
1110 FORI=1TO20
1120 S=S+((L(I)-P(I))^2)/P(I)
1130 NEXTI
1140 IFS>38.9THENGOTO1290
1150 IFS<38.9THENT=99.5
1160 IFS<36.2THENT=99
1170 IFS<32.9THENT=97.5
1180 IFS<30.1THENT=95
1190 IFS<27.2THENT=90
1200 IFS<22.7THENT=75
1210 IFS<18.3THENT=50
1220 IFS<14.6THENT=25
1230 IFS<11.7THENT=10
1240 IFS<10.1THENT=5
1250 IFS<8.91THENT=2.5
1260 IFS<7.63THENT=1.0
1270 IFS<6.84THENT=0.5
1280 PRINT"THE SURFACE IS VALID WITH "T"%CHANCE OF ERROR ("100-T"% S.L.)":GOTO
                                                                          1300
1290 PRINT" SURFACE IS NOT VALID AT A C.L. OF <0.5%"
1300 PRINT:PRINT"KEY S TO RE-START,OR C TO CONTINUE"
1310 GETC$:IF C$=""THEN1310
1320 IFC$="S"THENGOTO30
1330 IFC$<>"C"THEN1310
1340 REM TO FIND OPTIMUM COMBINATION
1350 Q=200:A=0:B=0:C=0
1360 FORI=1TO5
1370 FORJ=1TO5
1373 PRINT" PRESS C TO CONTINUE "
1375 PRINT"   X1    X2    X3    PREDICTION (MM)"
1380 FORK=1TO5
1390 IFI=1THENX1=-2^.75
1400 IFI=2THENX1=-1
1410 IFI=3THENX1=0
1420 IFI=4THENX1=1
1430 IFI=5THENX1=2^.75
1440 IFJ=1THENX2=-2^.75
1450 IFJ=2THENX2=-1
1460 IFJ=3THENX2=0
1470 IFJ=4THENX2=1
1480 IFJ=5THENX2=2^.75
1490 IFK=1THENX3=-2^.75
1500 IFK=2THENX3=-1
1510 IFK=3THENX3=0
1520 IFK=4THENX3=1
1530 IFK=5THENX3=2^.75
1540 R=B0+B1*X1+B2*X2+B3*X3+B4*X1*X2+B5*X1*X3+B6*X2*X3+B7*X1*X1+B8*X2*X2+B9*X3*
                                                                          *X3
1545 PRINT"    "X1"        "X2"        "X3"      "R"
1550 IFR>QTHENGOTO1570
1560 Q=R:A=X1:B=X2:C=X3
1570 NEXTK
1575 GETC$:IFC$=""THEN1575
1577 IFC$<>"C"THEN1575
1580 NEXTJ
1590 NEXTI
1600 PRINT" THE MINIMUM PREDICTED FAIL. DEPTH ="Q"MM"
1610 PRINT:PRINT" FOR THIS :"
1620 PRINT:PRINT"      X1="A
1630 PRINT:PRINT"      X2="B
1640 PRINT:PRINT"      X3="C
READY.
```

APPENDIX VI

RESULTS OF RESPONSE SURFACE THEORY PENETRATION TESTS

(i) SERIES ME/B/1-ME/B/20

Concrete Cast

Quantitative Independent Variable Ranges

Variable	Coded Levels				
	$-2^{3/4}$	-1	0	1	$2^{3/4}$
X_1: Water : Cement Ratio	0.35	0.39	0.45	0.51	0.55
X_2: Agg : Cement Ratio (Fine : Coarse 1:1)	1:3.0	1:3.8	1:5.0	1:6.2	1:7.0
X_3: Fibre Content (% weight by concrete weight)	0	1.4	3.5	5.6	7.0

Aggregate Moisture Contents

Zone 2 Limestone Sand

Standard Siphon Can Test

V_w = 279ml, V_b = 249ml, V = 500ml

Percentage moisture content by dry mass = $\frac{V_w - V_b}{2000 - V - V_w} \times 100\%$

= 2.5%

10mm Single Size Basalt

Standard Siphon Can Test

V_w = 224ml, V_b = 164ml, V = 500ml

Percentage moisture content by dry mass = 4.7%

All aggregate moisture taken as free.

Actual Mix Designs

(Using Coded Level Values and taking aggregate moisture content into account)

450x450x 125mm Slab No.	Ordinary Portland Cement (kg)	Free Water (kg)	10mm Single Size Basalt (kg)	Zone 2 Limestone Sand (kg)	Fibre* (kg)
ME/B/ 1	14.3	3.6	28.5	27.9	1.04
2	14.0	5.2	27.9	27.3	1.04
3	9.8	1.6	31.8	31.2	1.04
4	9.7	3.3	31.3	30.1	1.04
5	14.3	3.4	28.5	27.9	4.17
6	14.0	5.2	27.9	27.3	4.17
7	9.8	1.6	31.8	31.2	4.17
8	9.7	3.3	31.3	30.1	4.17
9	11.7	2.0	30.7	30.0	2.60
10	11.4	4.3	29.7	29.1	2.60
11	16.7	5.7	26.3	25.7	2.60
12	8.8	1.8	32.2	31.6	2.60
13	11.5	3.1	30.2	29.5	0
14	11.5	3.1	30.2	29.5	5.21
15, 16, 17	All as one mix	36.7	9.9	96.1	94.1	8.29
	Three 100x100x100mm cubes cast also (C1,C2,C3)				
18, 19, 20	All as one mix	36.7	9.9	96.1	94.1	8.29
	Three 100x100x100mm cubes cast also (C4,C5,C6)				

* 25mm x 0.3mm Melt Extract steel fibre

Cured in a controlled facility @ 20±2°C. R.H. > 90%

Firing Tests (3-Day)

Single Central impact 7.62mm A.P. bullet.

Slab No.	Penetration Path Length (mm)		
ME/B/ 1		81	
2		91	
3		108	
4		90	
5		86	
6		114	
7		135(P)	
8		137	
9		145(P)	
10		117	
11		145(P)	
12		132	
13		131	
14		99	
15	Mean = 93mm	(88)	Mean path length = 92mm
16	s.d. = 5.7mm	(99)	Standard deviation = 5.8mm
17		(91)	
18	Mean = 90mm	(83)	
19	s.d. = 7.0mm	(91)	
20		(97)	

P = Perforation

3-Day Compressive Strength Tests

Cube No.	Density (kg/m³)	Compressive Strength (N/mm²)
SLABS (ME/B/C1	2560	53
15/16/ (ME/B/C2	2520	45
17 (ME/B/C3	2530	46
	Mean = 2540	Mean = 48
SLABS (ME/B/C4	2620	52
18/19/ (ME/B/C5	2510	40
20 (ME/B/C6	2590	49
	Mean = 2570	Mean = 47

Statistical Analysis

Slab No. ME/B/	Actual Penetration Depth (mm)	Predicted Penetration Depths (mm) for incremental steps of 5mm to Perforated Values						
		0	5	10	15	20	25	30
1	81	111	113	114	115	117	118	119
2	91	112	114	116	117	119	121	123
3	108	125	126	127	127	128	129	129
4	90	98	97	96	94	93	92	91
5	86	98	100	102	103	106	108	110
6	114	117	117	117	117	117	117	117
7	135(P)	134	133	132	131	130	129	128
8	137	126	125	125	124	124	124	123
9	145(P)	120	118	117	115	113	112	110
10	117	114	114	114	114	114	114	114
11	145(P)	115	112	109	106	104	91	88
12	132	134	135	137	137	139	140	142
13	131	95	94	92	91	89	88	87
14	99	107	107	107	106	106	106	106
15	88	92	92	92	92	92	92	92
16	99	92	92	92	92	92	92	92
17	91	92	92	92	92	92	92	92
18	83	92	92	92	92	92	92	92
19	91	92	92	92	92	92	92	92
20	97	92	92	92	92	92	92	92

λ^2-Test: Confidence Level		<0.5%	<0.5%	<0.5%	<0.5%	<0.5%	<0.5%	<0.5%
Independent quantitative variable combination yielding minimum path length	x_1	0	0	1	1	1	1	1
	x_2	0	0	1	1	1	1	1
	x_3	-1	-1	$-2^{3/4}$	$-2^{3/4}$	$-2^{3/4}$	$-2^{3/4}$	$-2^{3/4}$
Minimum Predicted Path Length (mm)		91.7	91.2	90.5	88.6	86.3	85.0	83.2

Table VI.I- Statistical Analysis for ME/B/1-20

(ii) SERIES DUO/B/1 - DUO/B/20

Due to a delay in receiving the necessary fibres for this series, it was carried out in two parts. The initial casting was carried out on 01:11:82, whilst the remainder was produced on 21:2:83. For this reason, the mix design weights have different allowances for aggregate moisture content.

Quantitative Independent Variables Ranges

Variable	Coded Levels				
	$-2^{3/4}$	-1	0	1	$2^{3/4}$
X_1: Water - Cement ratio	0.35	0.41	0.50	0.59	0.65
X_2: Agg : Cement ratio (Fine : Coarse 2.1)	1:3.0	1:3.4	1:4.0	1:4.6	1:5.0
X_3: Fibre Content (% wt. by concrete wt.)	0	1.8	4.5	7.2	9.0

Aggregate Moisture Content

Concrete Cast 01/11/82

Zone 2 Limestone Sand

Standard Syphon Can Test

V_w = 305ml, V_b = 249ml, V = 500ml.

% Moisture content by dry mass = 4.7%

10mm Single Size Basalt

V_w = 225ml, V_b = 175ml, V = 500ml.

% Moisture content by dry mass = 3.9%

Slabs 1-9 cast on this date.

Concrete Cast 21/02/83

Zone 2 Limestone Sand

Standard Siphon Can Test

V_w = 285ml, V_b = 249ml, V = 500ml.

% Moisture Content by dry mass = 3.0%

10mm Single Size Basalt

V_w = 226ml, V_b = 175ml, V = 500ml.

% Moisture content by dry mass = 4.0%

Slab 10-20 cast on this date.

All aggregate moisture taken as free.

Actual Mix Designs

(Using Coded Level Values and taking aggregate moisture into account.)

450x450x 125mm Slab No.	Ordinary Portland Cement (kg)	Free Water (kg)	10mm Single Size Basalt (kg)	Zone 2 Limestone Sand (kg)	Fibre* (kg)
DUO/B/ 1	16.0	4.2	18.7	37.7	1.38
2	15.4	6.8	18.1	36.4	1.38
3	12.8	2.6	20.4	40.9	1.38
4	12.4	4.8	19.7	39.8	1.38
5	16.0	4.2	18.7	37.8	5.53
6	15.4	6.8	18.1	36.4	5.53
7	12.8	2.6	20.4	40.9	5.53
8	12.4	4.8	19.7	39.8	5.53
9	14.4	2.5	19.8	40.0	3.46
10	13.6	7.0	18.8	37.3	3.46
11	17.1	6.9	17.8	35.2	3.46
12	11.8	3.9	20.5	40.6	3.46
13	17.1	6.3	23.6	46.9	0
14	17.1	6.3	23.6	46.9	6.91
15) All 16) as 17) one mix	50.5	18.4	69.9	138.9	10.23
	Three 100 x 100 x 100 cubes cast also (C1,C2,C3)				
18) All 19) as 20) one mix	50.5	18.4	69.9	138.9	10.23
	Three 100 x 100 x 100 cubes cast also (C4,C5,C6)				

* 25 x 0.25mm Duoform indented brass-coated steel fibre.

Cured in a controlled facility @ 20±2°C, R.H. 90%+.

Firing Tests (3-day)

Single central impact, 7.62mm A.P. Bullet

Slab No.	Bullet Velocity (m/s)	Penetration Path Length (mm)	
DUO/B/ 1	806	105	
2	-	145(P)	
3	-	100	
4	-	129(P)	
5	803	116	
6	-	163(P)	
7	-	136(P)	
8	-	132	
9	808	137	
10	-	101	
11	-	106	
12	838	87	
13	830	101	
14	834	72	
15	818	Mean Value =95mm (105)	Mean Value = 84mm Standard deviation = 33.2mm
16	838	s.d. = 15.0mm (103)	
17	833	(78)	
18	816	Mean Value = 73mm (120)	
19	-	s.d. = 46.5mm (72)	
20	808	(27(R))	

P = Perforation, R = Possible Ricochet.

3-Day Compressive Strength Tests

Cube No.	Density (kg/m³)	Compressive Strength (N/mm²)
Slabs 15/16/17 (DUO/B/ 1	2460	36.8
(DUO/B/ 2	2470	27.4
(DUO/B/ 3	2460	30.5
	Mean = 2460	Mean = 31.6
Slabs 18/19/20 (DUO/B/ 4	2420	28.5
(DUO/B/ 5	2480	34.2
(DUO/B/ 6	2420	36.4
	Mean = 2440	Mean = 33.1

Statistical Analysis

Slab No. DUO/B/	Actual Penetration Depth (mm)	Predicted Penetration Depths (mm) Using 5mm Increments to Perforated Values						
		0	5	10	15	20	25	30
1	105	107	105	103	102	100	98	97
2	145(P)	136	141	146	151	155	160	165
3	100	111	111	112	113	114	114	115
4	129(P)	109	111	114	116	118	120	122
5	116	114	114	115	116	117	118	118
6	163(P)	130	132	135	137	139	141	144
7	136(P)	122	126	129	132	135	139	142
8	132	108	108	107	107	107	107	106
9	137	127	127	128	128	128	128	128
10	101	140	142	145	148	150	153	156
11	106	119	120	122	123	125	126	127
12	87	103	105	106	107	109	110	112
13	101	99	100	101	103	104	106	107
14	72	103	105	106	108	109	110	112
15	105	83	83	83	83	83	83	83
16	103	83	83	83	83	83	83	83
17	78	83	83	83	83	83	83	83
18	120	83	83	83	83	83	83	83
19	72	83	83	83	83	83	83	83
20	27(R)	83	83	83	83	83	83	83
λ^2-Test: Confidence level		<0.5%	<0.5%	<0.5%	<0.5%	<0.5%	<0.5%	<0.5%
Independent Quantitative variable Yielding minimum path length	X_1	0	0	0	0	0	0	0
	X_2	0	0	0	0	0	0	0
	X_3	0	0	0	0	0	0	0
Minimum Predicted Path Length		83.3	83.1	83.1	83.0	83.0	82.9	82.8

Using a mean value (96mm) of slabs 15-19 to compensate for unusual result (ricochet) of slab 20 gave the following result :

λ^2 - Test Confidence level; <0.5%

Minimum path length combination (X_1, X_2, X_3) = (0, 0, 0) yielding 94.8mm

Table VI.2 Statistical Analysis for DUO/B/1-20

(iii) SERIES 13K/B/1 - 13K/B/20

Concrete Cast

Quantitative Independent Variable Ranges

Variable	Coded Levels				
	$-2^{3/4}$	-1	0	1	$2^{3/4}$
X_1: Water - Cement Ratio	0.35	0.42	0.525	0.63	0.70
X_2: Agg - Cement Ratio (Fine: Coarse 2:1)	1:3.0	1:3.4	1:4.0	1:4.6	1:5.0
X_3: Fibre Content	0	0.25	0.61	0.98	1.22

Aggregate Moisture Content

Zone 2 Limestone Sand

Using Standard Siphon Can Test

V_w = 295ml, V_b 249ml, V = 500ml

$$\% \text{ Moisture Content by dry mass} = \frac{V_w - V_b}{2000-V-V_w} \times 100\%$$

$$= \underline{3.8\%}$$

10mm Single Size Basalt

Standard Siphon Can Test

V_w = 220ml, V_b = 175ml, V = 500ml

% Moisture content by dry mass = 3.5%

Actual Mix Designs

450x450x 125mm Slab No.	Ordinary Portland Cement (kg)	Free Water (kg)	10mm Single Size Basalt (kg)	Zone 2 Limestone Sand (kg)	Fibre* (kg)
13K/B/ 1	16.5	4.8	19.3	38.6	0.196
2	15.8	8.0	18.4	36.9	0.196
3	13.2	3.3	20.8	41.7	0.196
4	12.7	5.8	20.2	40.5	0.196
5	16.5	4.8	19.3	38.6	0.773
6	15.8	8.0	18.4	36.9	0.773
7	13.2	3.3	20.8	41.7	0.773
8	12.7	5.8	20.2	40.5	0.773
9	14.8	3.0	20.4	40.9	0.485
10	13.9	7.6	19.2	38.4	0.485
11	17.5	7.2	18.1	36.3	0.485
12	12.1	4.2	20.9	42.0	0.485
13	14.4	5.3	19.8	39.7	0
14	14.4	5.3	19.8	39.7	0.969
15) All 16) as 17) one mix	41.2	15.5	56.7	113.9	1.391
	Three 100 x 100x 100mm cubes (C1,C2,C3) cast also				
18) All 19) as 20) one mix	41.2	15.5	56.7	113.9	1.391
	Three 100 x 100 x 100mm cubes (C4,C5,C6) cast also				

* 13mm length KEVLAR-29 (Type 970) 12µm diameter bundled fibre cured in a controlled facility @ 20±2°C, R.H. >90%+.

Firing Tests (3-Day)

Single central impact, 7.62mm A.P. bullet, 20m range.

Slab No.	Velocity (m/s)	Penetration Path Length (mm)		
13K/B/ 1	-	112		
2	-	132(P)		
3	-	114		
4	811	149(P)		
5	810	117		
6	800	150(P)		
7	-	122		
8	-	152(P)		
9	799	141(P)		
10	-	178		
11	-	128		
12	-	128		
13	-	160(P)		
14	-	141(P)		
15	811	Mean = 143 mm s.d. = 3.8 mm	(245(P)	Mean Path Length = 139mm Standard deviation = 17.8mm
16	-		(139(P)	
17	-		(146(P)	
18	-	Mean = 134 mm s.d. = 26.6 mm	(123	
19	805		(114	
20	800		(164	

P = Perforation

Compressive Strength (3-Day) Tests

Cube No.	Density (kg/m³)	Compressive Strength (N/mm²)
Slabs 15/16/17 (13K/B/C1	2330	26.0
(13K/B/C2	2330	30.6
(13K/B/C3	2350	27.1
	Mean = 2340	Mean = 27.9
Slabs 18/19/20 (13K/B/C4	2350	28.6
(13K/B/C5	2380	31.2
(13K/B/C6	2370	30.2
	Mean = 2370	Mean = 30.0

Statistical Analysis

Slab No. 13K/B/	Actual Penetration Depth (mm)	Predicted Penetration Depths (mm) (Incremental steps of 5mm to Perforated Values)						
		0	5	10	15	20	25	30
1	112	122	124	125	127	128	129	131
2	132(P)	144	143	142	142	142	140	140
3	114	126	128	129	130	132	133	135
4	149(P)	154	153	152	152	151	150	150
5	117	124	125	126	128	129	131	132
6	150(P)	149	148	148	147	146	146	145
7	122	122	123	124	126	127	128	130
8	152(P)	153	152	152	151	150	149	149
9	141(P)	128	125	122	119	116	113	110
10	178	172	174	176	178	180	182	184
11	128	116	115	115	114	114	113	113
12	128	122	121	121	120	120	119	119
13	160(P)	141	141	140	140	139	139	138
14	141(P)	142	141	141	140	140	139	139
15	145(P)	138	136	136	131	129	126	124
16	139(P)	138	136	136	131	129	126	124
17	146(P)	138	136	136	131	129	126	124
18	123	138	136	136	131	129	126	124
19	114	138	136	136	131	129	126	124
20	164	138	136	136	131	129	126	124

λ^2-Test: Confidence Level		25%	10%	10%	5%	1%	<0.5%	<0.5%
Independent Quantitative variable combination yielding minimum path length	X_1	$-2^{3/4}$	$-2^{3/4}$	$-2^{3/4}$	$-2^{3/4}$	$-2^{3/4}$	$-2^{3/4}$	$-2^{3/4}$
	X_2	$2^{3/4}$	$2^{3/4}$	$2^{3/4}$	$2^{3/4}$	$2^{3/4}$	$2^{3/4}$	$2^{3/4}$
	X_3	$2^{3/4}$	1	1	1	1	0	0
Minimum Predicted Path Length (mm)		104	104	104	104	104	103	102

At a confidence level of 25%, minimumpredicted path length = 104mm

Actual values of coded levels are:

X_1: Water-Cement ratio = 0.35

X_2: Aggregate-Cement ratio = 1:5.0 (Fine: Coarse Aggregate 2:1)

X_3: Fibre Content = 1.22% by Concrete Weight (2.0% Concrete Volume)

Table VI.3 Statistical Analysis for 13K/B/1-20

(iv) SERIES 13K/RG/1-13K/RG/20

Concrete Cast

Quantitative Independent Variable Ranges

Variable	$-2^{3/4}$	-1	0	1	$2^{3/4}$
X_1: Water - Cement Ratio	0.35	0.42	0.525	0.63	0.70
X_2: Agg - Cement Ratio (Fine: Coarse 2:1)	1:3.0	1:3.4	1:4.0	1:4.6	1:5.0
X_3: Fibre Content % weight by concrete wt.	0	0.25	0.61	0.98	1.22

Aggregate Moisture Content

Zone 2 Limestone Sand

Using Standard Siphon Can Test

V_w = 309ml, V_b = 249ml, V = 500ml

Percentage moisture content by dry mass = $\frac{V_w - V_b}{2000-V-V_w} \times 100\%$

= 5.0%

10mm River Gravel

Using Standard Siphon Can Test

V_w = 290ml, V_b = 252ml, V = 500ml.

Percentage moisture content be dry mass = 3.1%

All aggregate moisture content assumed to be free.

Actual Mix Designs

450x450x 125mm Slab No.	Ordinary Portland Cement (kg)	Free Water (kg)	10mm Single Size River Gravel (kg)	Zone 2 Limestone Sand (kg)	Fibre* (kg)
13K/RG/ 1	16.5	4.4	19.2	39.1	0 .196
2	15.8	7.5	18.4	37.4	0 .196
3	13.2	2.9	20.7	42.2	0 .196
4	12.7	5.4	20.1	41.0	0 .196
5	16.5	4.4	19.2	39.1	0 .773
6	15.8	7.5	18.4	37.4	0 .773
7	13.2	2.9	20.7	42.2	0 .773
8	12.7	5.4	20.1	41.0	0 .773
9	14.8	2.6	20.3	41.4	0 .485
10	13.9	7.2	19.1	38.9	0 .485
11	17.5	6.9	18.0	36.8	0 .485
12	12.1	3.8	20.8	42.5	0 .485
13	14.4	5.0	19.7	40.1	0
14	14.4	5.0	19.7	40.1	0 .969
15) All					
16) as 41.2	14.4		56.5	115.2	1.391
17) one mix	Three 100 x 100 x 100mm cubes (13K/RG/C1,C2,C3) also cast				
18) All					
19) as 41.2	14.4		56.5	115.2	1.391
20) one mix	Three 100 x 100 x 100mm cubes (13K/RG/C4,C5,C6) also cast				

* 13mm length KEVLAR-29 (Type 970) 12µm diameter bundled fibre cured in a controlled facility @ 20±2°C, R.H. 90%+

Firing Tests (3-Day)

Single central impact, 7.62mm A.P. bullet, 20m range.

Slab No.	Velocity (m/s)	Penetration Path Length (mm)	
13K/RG/ 1	800	89	
2	802	65 (R)	
3	-	72	
4	-	195 (P)	
5	-	151 (P)	
6	-	107	
7	787	82	
8	804	102	
9	-	93	
10	789	112	
11	-	86	
12	-	84 (R)	
13	-	105	
14	-	123	
15	-	Mean=108mm s.d.=3.2mm (106, (112, (107	Mean Value = 107mm Standard deviation = 11.0mm
16	824		
17	-		
18	-	Mean=105mm s.d.=16.8mm (94, (124, (96	
19	-		
20	-		

P = Perforation R = Possible ricochet

Compressive Strength Tests

These tests were carried out at 4 days in error

Cube No.	Density (kg/m³)	Compressive Strength (N/mm²)
Slabs 15/16/17 (13K/RG/C1	2230	19
(13K/RG/C2	2230	19
(13K/RG/C3	2240	18
	Mean = 2230	Mean = 19
Slabs 18/19/20 (13K/RG/C4	2250	19
(13K/RG/C5	2240	21
(13K/RG/C6	2270	21
	Mean = 2250	Mean = 20

Statistical Analysis

Slab No. 13K/RG/	Actual Penetration Depth (mm)	Predicted Penetration Depths (mm) (Incremental steps of 5mm to Perforated Values)						
		0	5	10	15	20	25	30
1	89	78	77	77	75	76	75	75
2	65	71	71	70	69	69	69	68
3	72	77	76	76	75	75	74	74
4	195(P)	176	181	185	189	194	199	203
5	151(P)	163	167	172	175	181	185	190
6	107	95	94	94	93	93	92	92
7	82	68	68	67	66	66	66	65
8	102	106	106	105	104	104	104	103
9	93	93	94	95	95	96	97	97
10	112	120	120	121	121	122	123	124
11	86	84	85	86	86	87	88	89
12	84	93	94	95	95	96	97	97
13	105	112	112	113	113	114	115	116
14	123	124	125	126	126	127	128	128
15	106	106	106	106	106	106	106	106
16	112	106	106	106	106	106	106	106
17	107	106	106	106	106	106	106	106
18	94	106	106	106	106	106	106	106
19	124	106	106	106	106	106	106	106
20	96	106	106	106	106	106	106	106
λ^2-Test: Confidence Level		50%	50%	25%	25%	25%	25%	25%
Independent quantitative variable combination yielding minimum path length	x_1	$-2^{3/4}$	$-2^{3/4}$	$-2^{3/4}$	$-2^{3/4}$	$-2^{3/4}$	$-2^{3/4}$	$-2^{3/4}$
	x_2	$2^{3/4}$	$2^{3/4}$	$2^{3/4}$	$2^{3/4}$	$2^{3/4}$	$2^{3/4}$	$2^{3/4}$
	x_3	1	1	1	1	1	1	1
Minimum Predicted Path Length (mm)		1.2	-0.6	-2.5	-6.0	-6.1	-7.9	-9.7

Table VI.4 Statistical Analysis for 13K/RG/1-20

(v) SERIES 37K/RG/1-37K/RG/20

Concrete Cast

Quantitative Independent Variable Ranges

Variable	Coded Levels				
	$-2^{3/4}$	-1	0	1	$2^{3/4}$
X_1: Water - Cement Ratio	0.35	0.42	0.525	0.63	0.70
X_2: Agg - Cement Ratio (Fine: Coarse 2:1)	1:3.0	1:3.4	1:4.0	1:4.6	1:5.0
X_3: Fibre Content % wt. by concrete wt.	0	0.25	0.61	0.98	1.22

Aggregate Moisture Content

Zone 2 Limestone Sand

Using Standard Siphon Can Test . .

V_w = 308ml, V_b = 249ml, V = 500ml.

Percentage moisture content by dry mass = $\frac{V_w - V_b}{2000 - V - V_w}$ x 100%

= 5.0%

10mm Single Size River Gravel

Using Standard Siphon Can Test

V_w = 290ml, V_b = 252ml, V = 500ml.

Percentage moisture content by dry mass = 3.1%

All aggregate moisture content assumed to be free.

Actual Mix Designs

450x450x 125mm Slab No.	Ordinary Portland Cement (kg)	Free Water (kg)	10mm Single Size River Gravel (kg)	Zone 2 Limestone Sand (kg)	Fibre* (kg)
37K/RG/ 1	16.5	4.4	19.2	39.1	0.196
2	15.8	7.5	18.4	37.4	0.196
3	13.2	2.9	20.7	42.2	0.196
4	12.7	5.4	20.1	41.0	0.196
5	16.5	4.4	19.2	39.1	0.773
6	15.8	7.5	18.4	37.4	0.773
7	13.2	2.9	20.7	42.2	0.773
8	12.7	5.4	20.1	41.0	0.773
9	14.8	2.6	20.3	41.4	0.485
10	13.9	7.2	19.1	38.9	0.485
11	17.5	6.9	18.0	36.8	0.485
12	12.1	3.8	20.8	42.5	0.485
13	14.4	5.0	19.7	40.1	0
14	14.4	5.0	19.7	40.1	0.969
15) All					
16) as	41.2	14.4	56.5	115.2	1.391
17) one mix	Three 100 x 100 x 100mm cubes (C1,C2,C3) also cast				
18) All					
19) as	41.2	14.4	56.5	115.2	1.391
20) one mix	Three 100 x 100 x 100mm cubes (C4,C5,C6) also cast				

* 37mm Length KEVLAR-29 (Type 970) 12µm diameter bundled fibre (600 single filaments per bundle)

cured in a controlled facility @ 20±2°C, R.H. 90%+

Firing Tests (3-Day)

Single central impact, 7.62mm A.P. bullet, 20m range.

Slab No.	Velocity (m/s)	Penetration Path Length (mm)		
37K/RG/ 1	-	67		
2	-	141 (P)		
3	-	40 (R)		
4	-	84		
5	-	106		
6	-	89		
7	-	95		
8	-	92		
9	-	104		
10	814	81		
11	818	77		
12	815	75		
13	-	106		
14	-	79		
15	824	Mean = 92 mm s.d. = 14.6mm	(94) (76) (105)	Mean Value = 84mm Standard deviation = 15.6mm
16	-			
17	-			
18	-	Mean = 77mm s.d. = 15.0mm	(81) (60) (89)	
19	-			
20	-			

P = Perforation R = Possible ricochet.

Compressive Strength Tests

(Carried out at 7 days)

Cube No.	Density (kg/m³)	Compressive Strength (N/mm²)
Slabs 15/16/17 (37K/RG/C1	2410	48
(37K/RG/C2	2400	55
(37K/RG/C3	2410	57
	Mean = 2410	Mean = 54
Slabs 18/19/20 (37K/RG/C4	2360	47
(37K/RG/C5	2410	48
(37K/RG/C6	2380	42
	Mean = 2380	Mean = 46

Statistical Analysis

Slab No. 37K/RG/	Actual Penetration Depth (mm)	Predicted Penetration Depths (mm) (Incremental steps of 5mm to Perforated Values)						
		0	5	10	15	20	25	30
1	67	80	81	81	81	81	81	81
2	141 (P)	128	126	125	138	141	144	148
3	40	52	51	50	50	49	48	48
4	84	91	91	91	91	91	91	91
5	106	97	96	95	95	94	94	93
6	89	75	75	75	75	75	75	76
7	95	106	107	108	109	110	111	113
8	92	76	75	75	74	73	73	72
9	104	86	86	85	85	85	85	84
10	81	100	101	102	103	104	105	106
11	77	88	89	90	91	92	93	94
12	75	65	65	64	64	64	64	63
13	106	93	94	95	96	96	97	98
14	79	94	93	93	93	93	92	92
15	94	84	84	84	84	84	84	84
16	76	84	84	84	84	84	84	84
17	105	84	84	84	84	84	84	84
18	81	84	84	84	84	84	84	84
19	60	84	84	84	84	84	84	84
20	89	84	84	84	84	84	84	84

λ^2-Test: Confidence Level		<0.5%	<0.5%	<0.5%	<0.5%	<0.5%	<0.5%	<0.5%
Independent quantitative Variable	X_1	$-2^{3/4}$	$-2^{3/4}$	$-2^{3/4}$	$-2^{3/4}$	$-2^{3/4}$	$-2^{3/4}$	$-2^{3/4}$
Gombination Yielding	X_2	$2^{3/4}$	$2^{3/4}$	$2^{3/4}$	$2^{3/4}$	$2^{3/4}$	$2^{3/4}$	$2^{3/4}$
Minimum Path Length	X_3	$-2^{3/4}$	$-2^{3/4}$	$-2^{3/4}$	$-2^{3/4}$	$-2^{3/4}$	$-2^{3/4}$	$-2^{3/4}$
Minimum Path Length (mm)		7	5	4	3	2	0	-1

Table VI.5 Statistical Analysis for 37K/RG/1-20

(vi) SERIES 37K/B/1-37K/B/20

Concrete Cast

Quantitative Independent Variable Ranges

Variable	Coded Levels				
	$-2^{3/4}$	-1	0	1	$2^{3/4}$
X_1: Water - Cement Ratio	0.35	0.42	0.525	0.63	0.70
X_2: Agg : Cement Ratio (Fine: Coarse 2:1)	1:3.0	1:3.4	1:4.0	1:4.6	1:5.0
X_3: Fibre Content % wt. by concrete wt.	0	0.25	0.61	0.98	1.22

Aggregate Moisture Content

Zone 2 Limestone Sand

Using Standard Siphon Can Test

V_w = 315ml, V_b = 249ml, V = 500ml.

$$\text{Percentage Moisture Content by dry mass} = \frac{V_w - V_b}{2000 - V - V_w} \times 100\%$$

$$= \underline{\underline{5.6\%}}$$

10mm Single Size Basalt

Using Standard Siphon Can Test

V_w = 203 ml, V_b = 175ml, V = 500ml,

Percentage moisture content by dry mass = $\underline{\underline{2.2\%}}$

All aggregate moisture assumed to be free.

Actual Mix Designs

(Using Coded Level Values and taking into account moisture content)

450x450x 125mm Slab No.	Ordinary Portland Cement (kg)	Free Water (kg)	10mm single size Basalt (kg)	Zone 2 Limestone Sand (kg)	Fibre* (kg)
37K/B/ 1	16.5	4.4	19.0	39.3	0.196
2	15.8	7.5	18.2	37.6	0.196
3	13.2	2.9	20.5	42.4	0.196
4	12.7	5.4	19.9	41.2	0.196
5	16.5	4.4	19.0	39.3	0.773
6	15.8	7.5	18.2	37.6	0.773
7	13.2	2.9	20.5	42.4	0.773
8	12.7	5.4	19.9	41.2	0.773
9	14.8	2.6	20.1	41.6	0.485
10	13.9	7.2	18.9	39.1	0.485
11	17.5	6.9	17.9	36.9	0.485
12	12.1	3.7	20.6	42.8	0.485
13	14.4	5.0	19.5	40.3	0
14	14.4	5.0	19.5	40.3	0.969
15)	As				
16)	one 28.0	9.8	38.1	78.6	0.945
)	mix Three 100 x 100 x 100mm cubes (C1,C2,C3) cast also				
17)	As				
18)	one 28.0	9.8	38.1	78.6	0.945
)	mix Three 100 x 100 x 100mm cubes (C4,C5,C6) cast also				
19)	As				
20)	one 28.0	9.8	38.1	78.6	0.945
)	mix Three 100 x 100 x 100mm cubes (C7,C8,C9) cast also				

*37mm length KEVLAR-29 (Type 970) 12μm diameter bundled (600 filaments/bundle)

N.B. Due to difficulties experienced in mixing this length of KEVLAR into a concrete in the amount required to cast three slabs, the six similar slabs of this series were cast as 3 separate mixes of two slabs each. Concrete was cured in a controlled facility @ 20±2°C. R.H. 90%+.

Firing Tests (3-Day)

Single central impact, 7.62mm A.P. bullet, 20m range

Slab No.	Velocity (m/s)	Penetration Path Length (mm)
37K/B/ 1	-	111
2	830	129
3	-	92
4	-	129
5	834	70
6	-	145
7	818	140 (P)
8	-	121
9	-	123
10	-	131
11	-	82
12	-	123
13	-	104
14	819	144
15	-	(138) Mean Value = 104mm
16	-	(69) standard deviation = 48.8mm
17	-	(72) Mean Value = 99mm
18	-	(126) standard deviation = 38.2mm
19	-	(110) Mean Value = 115mm
20	809	(119) standard deviation = 6.4mm

Mean Value = 106mm
Standard deviation = 28.8mm

P = Perforation

Compressive Strength Tests (3-Day)

	Cube No.	Density (kg/m³)	Compressive Strength (N/mm²)
Slabs 15/16	(37K/B/C1	2440	33
	(37K/B/C2	2350	32
	(37K/B/C3	2390	33
		Mean = 2390	Mean = 33
Slabs 17/18	(37K/B/C4	2400	32
	(37K/B/C5	2350	27
	(37K/B/C6	2430	32
		Mean = 2390	Mean = 30
Slabs 19/20	(37K/B/C7	2290	29
	(37K/B/C8	2370	29
	(37K/B/C9	2340	29
		Mean = 2330	Mean = 29

Statistical Analysis

Slab No. 37K/B/	Actual Penetration Depth (mm)	Predicted Penetration Depths (mm) (Incremental steps of 5mm to Perforated Values)						
		0	5	10	15	20	25	30
1	111	94	93	93	92	91	91	90
2	129	131	132	133	134	135	136	138
3	92	110	111	111	111	111	111	111
4	129	110	109	108	108	107	107	106
5	70	89	90	90	90	90	90	90
6	145	127	126	125	125	124	124	123
7	140 (P)	139	142	145	149	152	155	159
8	121	138	138	138	139	139	139	139
9	123	110	111	112	113	114	115	116
10	131	141	141	140	140	140	140	139
11	82	89	89	89	89	88	88	88
12	123	113	114	115	116	117	118	119
13	104	113	112	112	112	111	111	111
14	144	133	134	135	136	137	138	139
15	138	105	105	105	105	105	105	105
16	69	105	105	105	105	105	105	105
17	72	105	105	105	105	105	105	105
18	126	105	105	105	105	105	105	105
19	110	105	105	105	105	105	105	105
20	119	105	105	105	105	105	105	105

λ^2-Test: Confidence Level		<0.5%	<0.5%	<0.5%	<0.5%	<0.5%	<0.5%	<0.5%
Independent quantitative variable combination yielding minimum path length.	X_1	$-2^{3/4}$	$-2^{3/4}$	$-2^{3/4}$	$-2^{3/4}$	$-2^{3/4}$	$-2^{3/4}$	$-2^{3/4}$
	X_2	$-2^{3/4}$	$-2^{3/4}$	$-2^{3/4}$	$-2^{3/4}$	$-2^{3/4}$	$-2^{3/4}$	$-2^{3/4}$
	X_3	1	1	1	1	0	0	0
Minimum Path Length (mm)		67	66	66	65	64	63	62

Table VI.6 Statistical Analysis for 37K/B/1-20

(vii) POL/B/1-5 and POL/B/10

The full statistical series of twenty slabs planned using this polypropylene fibre was not possible since only a small amount of fibre was received from the U.S.A., hence a part series used to investigate the mixing properties of the material, was carried out.

Concrete Cast

Quantitative Variable Ranges

Variable	Coded Levels				
	$-2^{3/4}$	-1	0	1	$2^{3/4}$
X_1: Water: Cement Ratio	0.40	0.46	0.55	0.64	0.70
X_2: Agg: Cement Ratio (Fine: Coarse 2:1)	1:3.0	1:3.4	1:4.0	1:4.6	1:5.0
X_3: Fibre Content (% wt. by concrete wt.)	0	0.235	0.580	0.925	1.160*

* Equivalent to 3.0% volume by concrete volume.

Aggregate Moisture Content

Zone 2 Limestone Sand

Using Standard Siphon Can Test

Percentage moisture content by dry mass = 4.7%

10mm Single Size Basalt

Percentage Moisture content by dry mass = 3.9%

All aggregate moisture taken as free.

Actual Mix Designs Planned

450x450x 125mm Slab No.	Ordinary Portland Cement (kg)	Free Water (kg)	10mm single size Basalt (kg)	Zone 2 Limestone Sand (kg)	Fibre* (kg)
POL/B/ 1	16.3	5.1	19.1	38.5	0.186
2	15.7	7.7	18.5	37.2	0.186
3	13.1	3.3	20.8	41.9	0.186
4	12.7	5.5	20.2	40.6	0.186
5	16.3	5.1	19.1	38.5	0.733
6	15.7	7.7	18.5	37.2	0.733
7	13.1	3.3	20.8	41.9	0.733
8	12.7	5.5	20.2	40.6	0.733
9	14.7	3.4	19.8	39.9	0.459
10	13.9	7.3	19.2	38.7	0.459
11	17.4	7.3	18.1	36.4	0.459
12	12.1	4.0	20.9	42.2	0.459
13	14.3	5.4	19.7	39.8	0
14	14.3	5.4	19.7	39.8	0.919
15) All 16) one 17) mix	40.9	16.3	56.6	114.1	1.318
18) All 19) one 20) mix	40.9	16.3	56.6	114.1	1.318

* 37mm length Forta Fibre - polypropylene lattice bundled fibre.

Ultimately, only slabs 1 - 5 and 10 were cast due to a lack of fibrous material.

Slabs cast were cured in a controlled facility at 20±2°C and a relative humidity of >90%.

Firing Tests (3-Day)

Single central impact, 7.62mm A.P. bullet, 20m range.

Slab No.	Velocity	Penetration Path Length (mm)
POL/B/ 1	-	54
2	-	129(P)
3	803	125
4	-	131
5	808	139
10	-	120

The only useful observations were that this fibrous material did not appear to improve the ballistic resistance of the basalt-based concrete

to a greater degree than any other fibre type and that the polypropylene fibre was very easily and evenly distributed through the concrete matrix by the action of a standard paddle-type concrete mixer.

APPENDIX VII

RESULTS OF LIMITED VARIABLE APPROACH PENETRATION TESTS

Limestone/Melt Extract

Typical Coding: L/ME/3/B

Where L = Limestone, 10mm single size coarse aggregate

ME = 25mm x $\overline{0.3}$mm melt extracted steel fibre

3 = 5.0% fibre content by concrete weight
[1,2,3,4,5 = 0,2.5,5.0,7.5,10% respectively]

A,B,C - Designation for each of the three specimens cast per fibre content level

Specimen Coding	Actual Path Length (mm)	Mean Actual Path Length (mm)	Actual Crater Volume ($x10^3 mm^3$)	Mean Actual Crater Volume ($x10^3 mm^3$)
L/ME/1/A	115	76 DisregardingC=95	359.3	492.0 DisregardingC=548.3
L/ME/1/B	75		737.2	
L/ME/1/C	39		379.5	
L/ME/2/A	108	92	70.1	109.8
L/ME/2/B	83		111.2	
L/ME/2/C	84		148.0	
L/ME/3/A	82	80	129.5	150.5
L/ME/3/B	94		173.2	
L/ME/3/C	63		148.8	
L/ME/4/A	64	80	71.6	73.7
L/ME/4/B	96		53.6	
L/ME/4/C	80		95.9	
L/ME/5/A	82	66 DisregardingB=85	19.9	35.3 DisregardingB=25.4
L/ME/5/B	29		55.2	
L/ME/5/C	87		30.9	

Specimen Class	7-Day Compressive Cube Strength (N/mm^2)	7-Day Density (kg/m^3)
L/ME/1	47	2360
L/ME/2	53	2398
L/ME/3	54	2452
L/ME/4	61	2514
L/ME/5	66	2574

Limestone/Duoform

Typical Coding: L/DUO/2/C

Where L = Limestone, 10mm single size coarse aggregate

DUO = 25 x 0.25mm brass-coated indented circular drawn steel fibre (DUOFORM)

2 = 2.5% fibre content by concrete weight
[1,2,3,4,5 = 0,2.5,5.0,7.5,10% respectively)

A,B,C - Designation for each of the three specimens cast per fibre content level

Specimen Coding	Actual Path Length (mm)	Mean Actual Path Length (mm)	Actual Crater Volume ($x10^3 mm^3$)	Mean Actual Crater Volume ($x10^3 mm^3$)
L/DUO/1/A	97	83	243.6	339.5
L/DUO/1/B	69		459.0	
L/DUO/1/C	82		315.9	
L/DUO/2/A	94	94	142.0	104.7
L/DUO/2/B	102		115.4	
L/DUO/2/C	85		56.6	
L/DUO/3/A	97	91	134.9	125.3
L/DUO/3/B	80		134.9	
L/DUO/3/C	95		106.0	
L/DUO/4/A	80	DisregardingC=74	56.7	DisregardingC=55.4
L/DUO/4/B	67		54.0	
L/DUO/4/C	25		52.6	
L/DUO/5/A	69	74	38.4	59.1
L/DUO/5/B	76		79.1	
L/DUO/5/C	78		59.8	

Specimen Class	7-Day Compressive Cube Stength (N/mm^2)	7-Day Density (kg/m^3)
L/DUO/1	47	2367
L/DUO/2	53	2406
L/DUO/3	45	2446
L/DUO/4	29	2245
L/DUO/5	14	1992

Limestone/Drawn

Typical Coding: L/DRA/4/A

Where L = Limestone, 10mm single size coarse aggregate

DRA = 25 x 0.25mm brass-coated circular drawn fibre

4 = 7.5% fibre content by concrete weight
[1,2,3,4,5 = 0,2.5,5.0,7.5,10% respectively]

A,B,C - Designation for each of the three specimens cast per fibre content level

Specimen Coding	Actual Path Length (mm)	Mean Actual Path Length (mm)	Actual Crater Volume ($x10^3 mm^3$)	Mean Actual Crater Volume ($x10^3 mm^3$)
L/DRA/1/A	81		256.2	
L/DRA/1/B	37	68	228.5	238.9
L/DRA/1/C	85	DisregardingB=83	232.1	DisregardingB=244.2
L/DRA/2/A	85		156.7	
L/DRA/2/B	91	87	128.1	151.3
L/DRA/2/C	85		169.0	
L/DRA/3/A	78		74.1	
L/DRA/3/B	83	83	153.1	114.2
L/DRA/3/C	87		115.3	
L/DRA/4/A	35		78.0	
L/DRA/4/B	51	60	41.9	62.2
L/DRA/4/C	94	DisregardingA=73	66.7	DisregardingA=54.3
L/DRA/5/A	92		52.3	
L/DRA/5/B	35	68	88.7	78.8
L/DRA/5/C	76	DisregardingB=84	95.5	DisregardingB=73.9

Specimen Class	7-Day compressive Cube Strength (N/mm^2)	7-day Density (kg/m^3)
L/DRA/1	56	2387
L/DRA/2	55	2428
L/DRA/3	58	2483
L/DRA/4	51	2487
L/DRA/5	30	2349

Basalt/Melt Extract

Typical Coding: B/ME/3/A

Where B = Basalt, 10mm single size coarse aggregate

ME = 25mm x $\overline{0.3}$mm melt extracted steel fibre

3 = 5.0% fibre content by concrete weight
[1,2,3,4,5 = 0,2.5,5.0,7.5,10% respectively]

A,B,C - Designation for each of the three specimens cast per fibre content level

Specimen Coding	Actual Path Length (mm)	Mean Actual Path Length (mm)	Actual Crater Volume ($x10^3 mm^3$)	Mean Actual Crater Volume ($x10^3 mm^3$)
B/ME/1/A	108	87	137.9	276.9
B/ME/1/B	80		415.9	
B/ME/1/C	73		Specimen split	
B/ME/2/A	30	62 Disregarding A=79	119.5	124.0
B/ME/2/B	108		115.7	
B/ME/2/C	49		136.8	
B/ME/3/A	103	102	62.2	83.4
B/ME/3/B	106		81.9	
B/ME/3/C	98		106.2	
B/ME/4/A	88	91	61.9	67.8
B/ME/4/B	93		71.8	
B/ME/4/C	93		69.6	
B/ME/5/A	106	101	60.3	67.2
B/ME/5/B	97		100.7	
B/ME/5/C	99		40.5	

Specimen Class	7-Day compressive Cube Strength (N/mm^2)	7-Day Density (kg/m^3)
B/ME/1	49	2397
B/ME/1	51	2431
B/ME/3	52	2466
B/ME/4	49	2529
B/ME/5	51	2528

Basalt/Duoform

Typical Coding: B/DUO/3/C

Where B = Basalt, 10mm single size coarse aggregate

DUO = 25 x 0.25mm brass-coated indented circular drawn steel fibre [DUOFORM]

3 = 5.0% fibre content by concrete weight [1,2,3,4,5 = 0,2.5,5.0,7.5,10% respectively]

A,B,C - Designation for each of the three specimens cast per fibre content level

Specimen Coding	Actual Path Length (mm)	Mean Actual Path Length (mm)	Actual Crater Volume ($x10^3 mm^3$)	Mean Actual Crater Volume ($x10^3 mm^3$)
B/DUO/1/A	101	89	157.8	185.6
B/DUO/1/B	77		234.9	
B/DUO/1/C	89		164.0	
B/DUO/2/A	96	84	193.1	147.7
B/DUO/2/B	95		126.7	
B/DUO/2/C	62		123.2	
B/DUO/3/A	67	81	62.6	63.6
B/DUO/3/B	105		75.3	
B/DUO/3/C	71		52.8	
B/DUO/4/A	82	84	40.8	56.8
B/DUO/4/B	94		5.0	
B/DUO/4/C	75		124.7	
B/DUO/5/A	86	91	31.2	31.4
B/DUO/5/B	87		31.1	
B/DUO/5/C	99		31.9	

Specimen Class	7-Day compressive Cube Strength (N/mm^2)	7-Day Density (kg/m^3)
B/DUO/1	52	2383
B/DUO/2	54	2436
B/DUO/3	50	2438
B/DUO/4	48	2508
B/DUO/5	24	2206

Basalt/Drawn

Typical Coding: B/DRA/3/B

Where B = Basalt, 10mm single size coarse aggregate

DRA = 25mm x 0.25mm brass-coated circular drawn fibre

3 = 5.0% fibre content by concrete weight
[1,2,3,4,5 = 0,2.5,5.0,7.5,10% respectively)

A,B,C - Designation for each of the three specimens cast per fibre content level

Specimen Coding	Actual Path Length (mm)	Mean Actual Path Length (mm)	Actual Crater Volume ($x10^3 mm^3$)	Mean Actual Crater Volume ($x10^3 mm^3$)
B/DRA/1/A	75	93	140.8	251.5
B/DRA/1/B	107		180.3	
B/DRA/1/C	97		433.5	
B/DRA/2/A	106	85	95.6	135.5
B/DRA/2/B	79		95.5	
B/DRA/2/C	69		215.4	
B/DRA/3/A	131 (perforation)	102 DisregardingA=88	71.0	88.9 DisregardingA=97.9
B/DRA/3/B	102		87.2	
B/DRA/3/C	73		108.5	
B/DRA/4/A	101	86	46.3	48.1
B/DRA/4/B	87		37.0	
B/DRA/4/C	71		60.9	
B/DRA/5/A	71	79	75.7	68.9
B/DRA/5/B	77		88.1	
B/DRA/5/C	78		43.0	

Specimen Class	7-Day compressive Cube Strength (N/mm^2)	7-Day Density (kg/m^3)
B/DRA/1	42	2367
B/DRA/2	47	2415
B/DRA/3	47	2457
B/DRA/4	13	2103
B/DRA/5	11	1947

River Gravel/Melt Extract

Typical Coding: RG/ME/3/B

Where RG = River Gravel, 10mm single size coarse aggregate

ME = 25mm x $\overline{0.3}$mm melt extracted steel fibre

3 = 5.0% fibre content by concrete weight
[1, 2, 3, 4, 5 = 0, 2, 5, 5, 0, 7, 5, 10% respectively]

A, B, C - Designation for each of the three specimens cast per fibre content level

Specimen Coding	Actual Path Length (mm)	Mean Actual Path Length (mm)	Actual Crater Volume ($x10^3 mm^3$)	Mean Actual Crater Volume ($x10^3 mm^3$)
RG/ME/1/A	51		307.6	
RG/ME/1/B	40	56	298.2	280.5
RG/ME/1/C	77	DisregardingB=64	235.7	DisregardingB=271.7
RG/ME/2/A	60		263.5	
RG/ME/2/B	44	50	205.3	236.3
RG/ME/2/C	46		240.1	
RG/ME/3/A	59		135.5	
RG/ME/3/B	87	86	176.7	135.2
RG/ME/3/C	112		93.3	
RG/ME/4/A	60		174.1	
RG/ME/4/B	61	80	206.5	160.7
RG/ME/4/C	118		101.5	
RG/ME/5/A	41		229.3	
RG/ME/5/B	90	68	106.7	147.7
RG/ME/5/C	74		107.2	

Specimen Class	7-Day compressive Cube Strength (N/mm^2)	7-Day Density (kg/m^3)
RG/ME/1	46	2327
RG/ME/2	43	2371
RG/ME/3	44	2427
RG/ME/4	46	2464
RG/ME/5	48	2539

River Gravel/Duoform

Typical Coding: RG/DUO/3/A

Where RG = River Gravel, 10mm single size coarse aggregate

DUO = 25 x 0.25mm brass-coated indented circular drawn steel fibre [DUOFORM]

3 = 5.0% fibre content by concrete weight
[1,2,3,4,5 = 0,2.5,5.0,7.5,10% respectively)

A,B,C - Designation for each of the three specimens cast per fibre content level

Specimen Coding	Actual Path Length (mm)	Mean Actual Path Length (mm)	Actual Crater Volume ($x10^3 mm^3$)	Mean Actual Crater Volume ($x10^3 mm^3$)
RG/DUO/1/A	93	74	551.7	346.1
RG/DUO/1/B	50		306.4	
RG/DUO/1/C	79		180.1	
RG/DUO/2/A	48	67 DisregardingA=77	193.4	181.1 DisregardingA=175.0
RG/DUO/2/B	102		183.7	
RG/DUO/2/C	51		166.3	
RG/DUO/3/A	99	93	375.7	280.5
RG/DUO/3/B	108		277.5	
RG/DUO/3/C	71		188.4	
RG/DUO/4/A	69	75	74.2	85.2
RG/DUO/4/B	69		81.2	
RG/DUO/4/C	87		100.2	
RG/DUO/5/A RG/DUO/5/B RG/DUO/5/C	Not cast due to fibre distribution difficulties			

Specimen Class	7-Day compressive Cube Strength (N/mm^2)	7-Day Density (kg/m^3)
RG/DUO/1	37	2302
RG/DUO/2	47	2418
RG/DUO/3	43	2452
RG/DUO/4	46	2476
RG/DUO/5	-	-

River Gravel/Drawn

Typical Coding: RG/DRA/3/C

Where RG = River Gravel, 10mm single size coarse aggregate

DRA = 25mm x 0.25mm brass coated circular drawn fibre

3 = 5.0% fibre content by concrete weight
[1,2,3,4,5 = 0,2.5,5.0,7.5,10% respectively]

A,B,C - Designation for each of the three specimens cast per fibre content level

Specimen Coding	Actual Path Length (mm)	Mean Actual Path Length (mm)	Actual Crater Volume (x 10^3 mm^3)	Mean Actual Crater Volume (x10^3 mm^3)
RG/DRA/1/A	93	DisregardingB=97	223.4	DisregardingB=279.5
RG/DRA/1/B	37		195.8	
RG/DRA/1/C	100		335.6	
RG/DRA/2/A	113	93	193.6	149.2
RG/DRA/2/B	76		136.5	
RG/DRA/2/C	91		117.6	
RG/DRA/3/A	30	DisregardingA=86	80.5	DisregardingA=112.6
RG/DRA/3/B	91		122.2	
RG/DRA/3/C	81		103.0	
RG/DRA/4/A	77	71	49.9	52.1
RG/DRA/4/B	76		33.5	
RG/DRA/4/C	61		72.9	
RG/DRA/5/A	93	68 DisregardingC=89	23.7	32.7
RG/DRA/5/B	85		48.2	
RG/DRA/5/C	27		26.2	

Specimen Class	7-Day compressive Cube Strength (N/mm^2)	7-Day Density (kg/m^3)
RG/DRA/1	44	2305
RG/DRA/2	46	2385
RG/DRA/3	48	2397
RG/DRA/4	27	2262
RG/DRA/5	12	1954

APPENDIX VIII

DETAILS OF TESTS TO STUDY IMPACT AND PENETRATION MECHANISMS

VIII.1 High speed rotating prism camera tests

The general arrangement for the tests is shown in Figure 5.1 whilst details of the camera and firing circuit are shown in Figure 5.2. The experimental procedure is described in Section 5.2.1.

Specimen details

The mix designs and properties of two plain concrete specimens (RP1 and RP2) and one fibre reinforced concrete specimen RP3 are given in Table VIII.1. Concrete specimens were 450 x 450 x 125mm cured in a controlled atmosphere at 20±2°C with relative humidity > 90%. All specimens were impacted centrally by a single 7.62mm A.P. projectile at a range of 20m. Details of a single plasticine target are given in Section 5.2.3.

Photographic details

Photec IV Rotating Prism camera fitted with a 45mm focal length lens; sunshade and fisheye adaptor attached.

Relative Aperture = f2.8

Camera footage trigger (firing system) set to 21.3m of film.

film - Ilford HP5 (400 ASA)

Timing lights (Internal) - 1000Hz

Lighting - four 1kw photofloods facing camera, two thicknesses of standard 90g tracing paper as diffusers.

Framing rate - set to 5500pps, half height prism in use. Effective rate = 11000pps.

Datum distance	RP1	Target front face to marker	100mm
	RP2	Target front face to marker	103mm
	RP3	Thickness of specimen	125mm
	Plasticine	Diameter of specimen	100mm

Results

The projectile mean velocity was only obtained for specimen RP1. Its value at 18m range was 822 m/s.

In all tests an adequate series of images was captured showing both the projectile before impact and the material response after impact. The actual framing rate calculated from the timing lights varied from test to test as follows:

RP1	198 frames in	18ms = 11000pps	≡	91μs interframe time
RP2	45 frames in	4ms = 11250pps	≡	78μs interframe time
RP3	55 frames in	5ms = 11000pps	≡	92μs interframe time
Plasticine	57 frames in	5ms = 11400pps	≡	88μs interframe time

VIII.2 Ultra-high speed rotating mirror camera tests

Details of the principle of operation of this camera are given in Section 5.2.2. Two methods of illumination were used - backlighting (see Figure 5.10) and frontlighting (see Figure 5.11).

Specimen details

For the backlighting test a concrete building block 450 x 210 x 100mm was used, and for the frontlighting test an instrumented plain concrete specimen 450 x 450 x 125mm was used. Details of this latter target (V2) are given in Appendix VIII.3. Both targets were impacted centrally by a single 7.62mm A.P. projectile at a range of 20m.

Photographic details

Barr & Stroud Rotating Mirror camera.

Free run time - backlighting - approximately 1.5μs interframe time.

- frontlighting - approximately 1.0μs interframe time.

Lens - 35mm focal length at f2.8 relative aperture giving a field of view approximately 125mm diameter.

Film - 35mm Ilford HP5 black and white film (400 ASA uprated during development to 1600 ASA).

Illumination - Xenon flash unit triggered using a contact switch consisting of two 0.001mm thick brass shim plates separated by a paper insulator placed 120mm ahead of the target.

backlighting - reflection from a white screen (see Figure 5.10)

frontlighting - direct lighting of projectile plus a single 1kW photoflood light used to highlight slab edge detail. An illuminated scale with 5mm intervals was placed in the plane of the projectile trajectory (see Figure 5.11).

Results

Backlighting - A series of 30 frames showing the projectile flight between detector and target were obtained. No pre-impact projectile velocity was

obtained but using an estimated velocity of 800 m/s the calculated interframe time of 0.94μs was of the expected order.

Figure VIII.1 shows the sequence of photographs obtained. The brass detector may have induced tumbling in the projectile. Since the illumination was still increasing at the time of exposure the target edge is undefined making assessment of the rate and extent of projectile inclination impossible.

The projectile perforated and fragmented the concrete building block target.

Frontlighting - A series of 30 frames showing the projectile flight between detector and target were obtained. Using the photodiode based velocity measuring system projectile velocity 2m from the target impact face was 815 m/s. In the 30 photographic frames the projectile travelled 26mm giving an interframe time of 1.1μs.

Figure VIII.2 shows the sequence of photographs whose quality is disappointing in that no projectile detail is observable, although it would appear that the projectile is travelling normal to the target impact face.

VIII.3 Tests to study deceleration of the projectile in plain concrete targets

As described in Section 5.2.9, six detectors were cast into each of four plain concrete targets. Figures 5.33 and 5.34 show the arrangement for the first two targets (V1 and V2), and Figure 5.39 shows the arrangement for the other two targets (V3 and V4).

Specimen details

The mix designs and properties of the plain concrete targets are given in Table VIII.2. Specimens 450 x 450 x 125mm were cured in a controlled atmosphere at 20 ± 2°C with relative humidity > 90%. All specimens were impacted centrally by a single 7.62mm A.P. projectile at a range of 20m.

Detector data recording details

In tests on specimens V1 and V2 the detectors were connected in series, but in tests V3 and V4 separate capacitance breakdown circuits were used for each channel. Details of the recording systems are given in Table VIII.3.

VIII.4 Tests to study front face spalling

Graphite detectors were installed in spall zones as described in Section 5.2.10.

Specimen Details

The mix designs and properties of three plain concrete and three fibre reinforced concrete specimens are given in Table VIII.4. All specimens were 450 x 450 x 125mm cured in a controlled atmosphere at 20 ± 2°C, relative humidity > 90°. All specimens were impacted centrally by a single 7.62mm AP projectile at a range of 20m.

Detector data recording details

Details of the oscilloscope settings and trigger arrangements are given in Table VIII.5.

Results

In the tests on plain concrete specimens, although graphite detectors broke, triggering problems meant that no results were obtained. These triggering problems were overcome in the fibre reinforced concrete tests, but only one spall detector broke in each of these tests so velocities of spall propagation could not be obtained. Results are summarised in Table VIII.5.

		Specimen Number		
		RP 1(V3)	RP 2(V4)	RP 3
Mix design (ratio by weight)	OPC	1.0	1.0	1.0
	Free water	0.525	0.525	0.50
	10mm single size basalt	1.33	1.33	1.33
	Zone 2 limestone sand	2.67	2.67	2.67
Duoform fibre 25 x 0.25mm	(% concrete weight)	0	0	2.5
Aggregate m/c (% dry mass)	basalt - 10mm	2.2	2.2	0.5
	sand - Zone 2	2.2	2.2	3.4
Age at testing	(days)	7	7	14
Compressive strength	(N/mm^2)	39.0	39.0	-
Density	(kg/m^3)	2370	2370	-

Table VIII.1 Details of concrete specimens prepared for rotating prism camera tests.

		Specimen Number			
		V1	V2	V3 (RP1)	V4 (RP2)
Mix design (ratio by weight)	OPC	1.0	1.0	1.0	1.0
	Free water	0.525	0.525	0.525	0.525
	10mm single size basalt	1.33	1.33	1.33	1.33
	Zone 2 limestone sand	2.67	2.67	2.67	2.67
Aggregate	basalt	1.4	1.4	2.2	2.2
m/c (% dry mass)	sand	1.5	1.5	2.2	2.2
Age at testing (days)		3	7	7	7
Compressive strength (N/mm^2)		-	-	39	39
Density (kg/m^3)		-	-	2370	2370

Table VIII.2 Details of concrete specimens prepared for projectile deceleration tests.

		Specimen number			
		V1	V2	V3	V4
Type of "make" triggering system		two 0.001mm thick brass shims held 2mm apart			2 aluminium foil sheets
Distance of trigger from target face (mm)		120			103
Recorder type *		Gould OS 4000		Ch.1/2 Gould OS4020 Ch.3/4 Gould OS4000 Ch.5/6 Biomation TR	
Recorder Setting	Voltage	0.5V/cm	1.0V/cm	10V/cm	10V/cm
	Timebase	1ms/cm	1ms/cm	0.5ms/cm	Ch 1-2 0.2ms/cm Ch 3-6 0.5ms/cm

* OS = Oscilloscope, TR - Transient recorder

Table VIII.3 Details of detector recording systems for projectile deceleration tests.

		Specimen Number	
		GR/P/1 - GR/P/3	GR/F/1 - GR/F/3
Mix Design (ratio by weight)	OPC	1.0	1.0
	Free water	0.5	0.5
	10mm single size basalt	1.33	1.33
	Zone 2 limestone sand	2.67	2.67
Drawn Fibre (% composite weight)		0	2.5
Aggregate m/c (% dry mass)	Basalt - 10mm single size	0.1	0.0
	Sand - Zone 2	2.1	2.2
Age at testing (days)		14	14
Compressive strength N/mm^2 (14 days)		56	58
Density kg/m^3		2340	2385

Table VIII.4 Details of concrete specimens prepared for graphite rod detector tests

Test No	Oscilloscope Settings						Trigger system	Distance between graphite detectors at slab surface (mm)		Detector pre impact resistance Ω				Results
	OS4000			OS4020										
	Det No	V/cm	ms/cm	Det No	V/cm	ms/cm				Det 1	Det 2	Det 3	Det 4	
GR/P/1	1,2	2.0	0.2	3,4	2.0	0.2	OS4000:breakage of Det.1 OS4020:breakage of Det.3	1→2 3→4	18 21	1	1	1	1	Scopes not triggered. Det.1,2,3 broken.
GR/P/2	1,2	2.0	0.2	1,3	2.0	0.2	OS4000:breakage of Det.1 OS4020:breakage of Det.1	1→2 1→3 2→3	31.5 70 65	1.4	1.3	0.67	∞	Scopes not triggered Det.1,2,3 broken.
GR/P/3	1,2	2.0	0.2	1,4	2.0	0.2	OS4000:breakage of Det.1 OS4020:breakage of Det.1	1→2 1→4 2→4	20 99 111	1.1	1.2	∞	1.0	Scopes not triggered. Det.1,2,4 broken.
GR/F/1	1,3	2.0	0.2	3,4	2.0	0.2	OS4000)aluminium foil OS4020)capacitance)breakdown circuit	1→3 1→4 3→4	35 57 26	1.3	∞	1.4	1.35	Both scopes triggered Only Det.3 broke
GR/F/2	1,2	2.0	0.2	3,4	2.0	0.2	OS4000)aluminium foil OS4020)capacitance)breakdown circuit	1→2 1→3 1→4 2→3 2→4 3→4	15 70 91 85 105 24	1.1	1.1	1.1	1.0	Both scopes triggered. Only Det.3 broke.
GR/F/3	1,2	2.0	0.2	3,4	2.0	0.2	OS4000)silver paint grid OS4020)breakdown circuit	1→2 1→3 1→4 2→3 2→4 3→4	25 69 90 87 104 24	1.35	92*	1.7	1.3	Both scopes triggered. No useful data recorded

* considered unlikely to be working at this resistance.

Table VIII.5 Summary of oscilloscope settings, triggering arrangements and results of front face spalling tests.

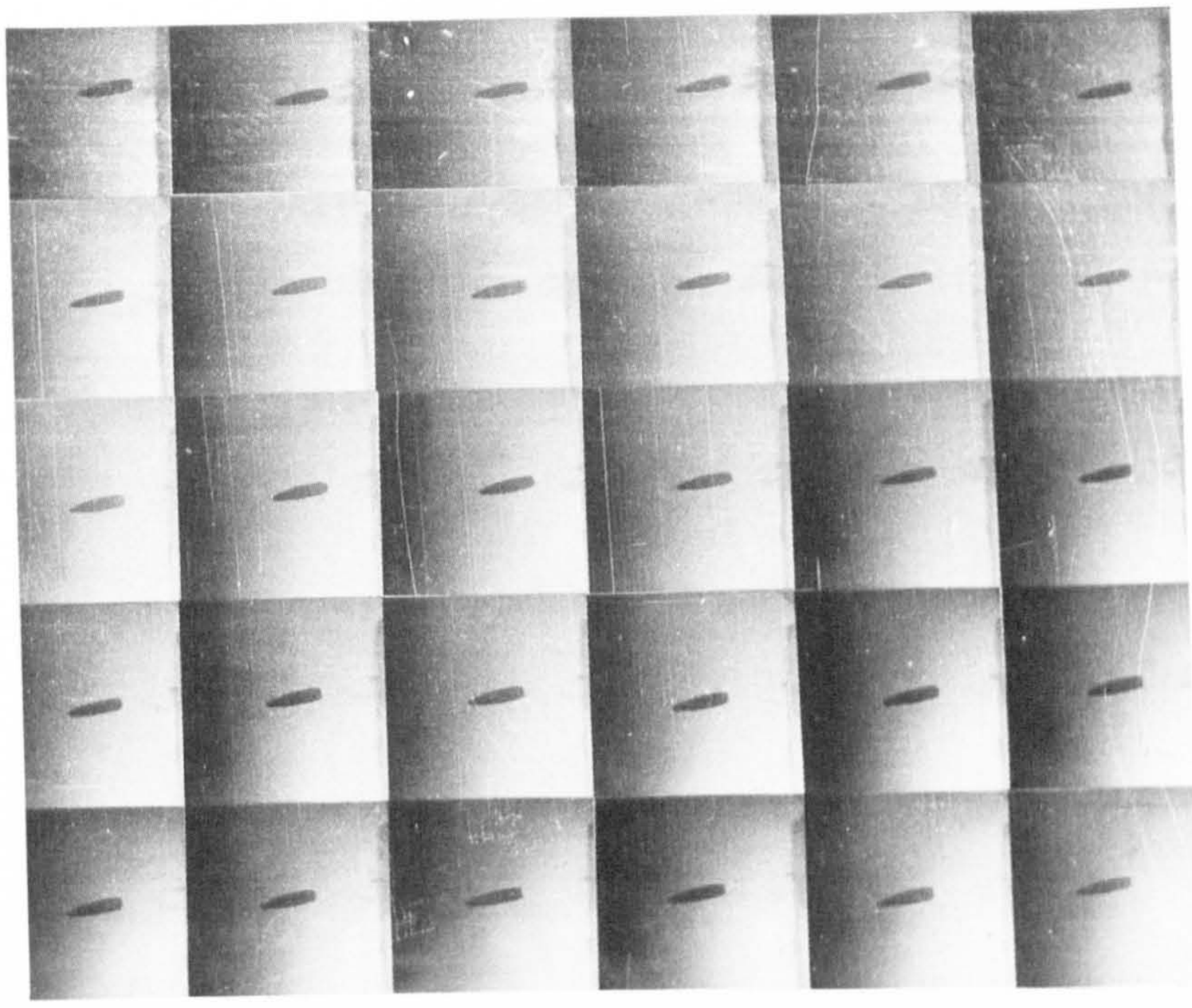

Figure VIII.1 Backlit sequence of photographs obtained using Ultra-high Speed Rotating Mirror Camera

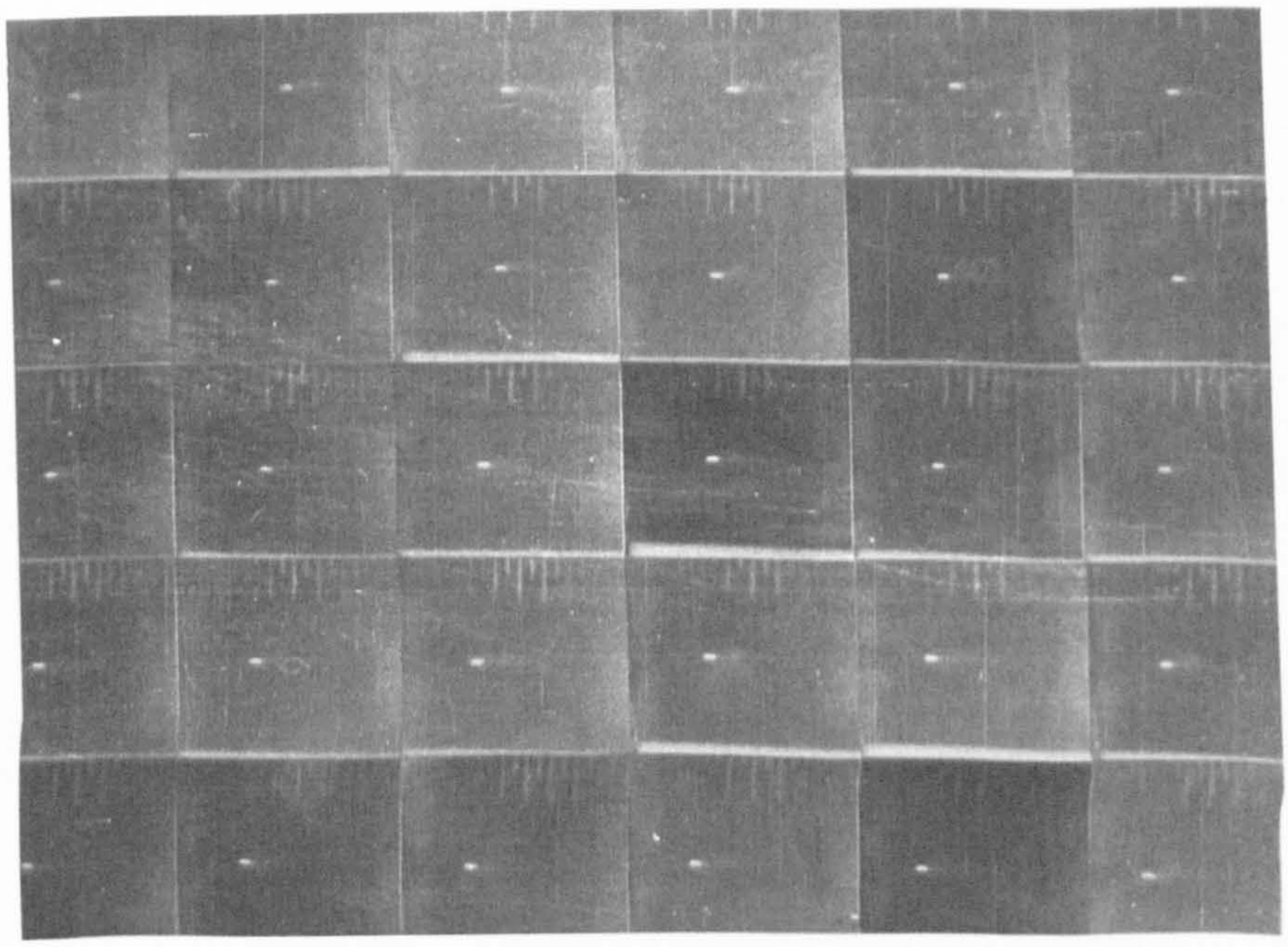

Figure VIII.2 Frontlit sequence of photographs obtained using Ultra-High Speed Rotating Mirror Camera